Old Dominion University

ODU Digital Commons

Thermo-Elasto-Plastic Behavior of Biaxially Loaded Steel Beam-Columns Inducing Those From World Trade Center Towers

Yanhong Zhao
Old Dominion University

Recommended Citation

THERMO-ELASTO-PLASTIC BEHAVIOR OF BIAXIALLY LOADED STEEL

BEAM-COLUMNS INDLUCING THOSE FROM WORLD TRADE CENTER

TOWERS

by

Yanhong Zhao
B.A. July 2000, Yantai University, Shandong, China
M.S. July 2005, Shandong Jianzhu University, Shandong, China

A Dissertation Submitted to the Faculty of
Old Dominion University in Partial Fulfillment of the
Requirements for the Degree of

DOCTOR OF PHILOSOPHY

CIVIL ENGINEERING

OLD DOMINION UNIVERSITY
December 2013

Approved by:

—————————————
Zia Razzaq (Director)

—————————————
Duc T. Nguyen (Member)

—————————————
Gene J. -W. Hou (Member)

—————————————
Mojtaba B. Sirjani (Member)

—————————————
Yunbyeong Chae (Member)

ABSTRACT

THERMO-ELASTO-PLASTIC BEHAVIOR OF BIAXIALLY LOADED STEEL BEAM-COLUMNS INCLUDING THOSE FROM WORLD TRADE CENTER TOWERS

Yanhong Zhao
Old Dominion University, 2013
Director: Dr. Zia Razzaq

An experimental and theoretical investigation into the behavior of biaxially loaded steel beam-columns is conducted including the effects of high temperature. Systems of materially nonlinear differential equations of beam-column equilibrium are first formulated for both ambient and high temperature conditions. An iterative finite integral procedure is formulated and programmed to solve the governing differential equations. To check the validity of the theoretically predicted behavior and strength of the beam-columns, a series of forty-two laboratory tests are conducted at both ambient and high temperature up to $950^{\circ}F$. Upon achieving a good agreement between the predicted beam-column behavior and that observed in the experiments, the theory developed is then applied to predicting the behavior and strength of typical beam-columns which were used in the 110-story World Trade Center (WTC) buildings. Thermo-elasto-plastic stiffness degradation and load-moment interaction curves are generated for typical WTC beam-columns which existed in the impacted area during 9/11 attacks.

This thesis is dedicated to my two lovely daughters, Lingling and Lily.

ACKNOWLEDGMENTS

NOMENCLATURE

A	Area
B	Section width
D	Section depth
dA	Elemental area
E, E_T	Modulus of elasticity at ambient and elevated temperature
$\{f\}$	Cross-sectional load vector
$\{\dot{f}\}$	Cross-sectional load rate vector
I_x, I_y	Moment of inertia about x-axis and y-axis
I_{xy}	Product of inertia relative to x-axis and y-axis
$[K]$, $[K_T]$	Member global tangent stiffness matrix at ambient and high temperature
$[k_t]$	Cross-sectional tangent stiffness matrix
k_{Ax}, k_{Bx}	End Rotational stiffness about x axis
k_{By}, k_{By}	End Rotational stiffness about y axis
L	Member length
m_{Ax}, m_{Bx}	Restraint moments at bottom and top about x axis
m_{Ay}, m_{By}	Restraint moments at bottom and top about y axis
m_x, m_y	Cross-sectional dimensionless moments
M_{Ax}, M_{Bx}	Applied moments at bottom and top about x axis
M_{Ay}, M_{By}	Applied moments at bottom and top about y axis
M_{xp}, M_{yp}	Moments due to plastification
M_{xre}, M_{yre}	Moments due to residual stress
M_{xth}, M_{yth}	Moment due to thermal deformation
F_x, F_y	Load vector in the governing equation
$\{F\}$	Load vector
$\{\Delta''\}$	Vector of the second order derivative of deflection
P	Applied axial load
P_p	Axial load due to plastification
P_r	Axial load due to residual stress

P_{th}	Axial load due to thermal expansion
R_x, R_y	Reaction force
T	Temperature
U	Total deflection in x-direction
V	Total deflection in y-direction
u	Deflection due to applied load or raised temperature in x-direction
v	Deflection due to applied load or raised temperature in y-direction
u_o	Midspan initial member crookedness in x-direction
v_o	Midspan initial member crookedness in y-direction
u_{oi}	Initial beam-column crookedness at nodal point i in x-direction
v_{oi}	Initial beam-column crookedness at nodal point i in y-direction
u''	The second order derivative of u
v''	The second order derivative of v
$\varepsilon, \varepsilon_T$	Normal strain at ambient and elevated temperature
ε_r	Residual strain
ε_0	Average axial strain
ε_{th}	Thermal strain
$\dot{\varepsilon}$	Strain rate
Φ_x, Φ_y	Bending curvatures about x and y axes
σ_Y, σ_{YT}	Yield stress at ambient and elevated temperature
σ_{rt}, σ_{rc}	Compressive and tensile residual stress
$\dot{\sigma}$	Stress rate
$\{\delta\}$	Cross-sectional deformation vector
$\{\dot{\delta}\}$	Cross-sectional deformation rate vector
$\int_A$	Cross-sectional integration
θ	End rotation

TABLE OF CONTENTS

Page

LIST OF TABLES

LIST OF FIGURES

CHAPTER

1. INTRODUCTION

1.1 Introduction

This dissertation presents the outcome of an experimental and theoretical elasto-plastic study of the behavior of biaxially loaded steel beam-columns including those from 110-story World Trade Center (WTC) buildings. The outermost vertical support structure, that is, the periphery of these buildings, was made-up of hollow rectangular section beam-columns fabricated by welding four steel plates. A number of beam-columns, which were carrying the usual service loads, were suddenly subjected to increased loads and high temperature caused by fire during and right after the terrorist attack. The study presented herein deals with predicting the behavior of beam-columns under biaxial bending, axial load, and high temperature. In addition, experiments are conducted on small-scale steel members having a hollow square cross section to verify the validity of the theoretical prediction model developed.

The study presented herein also investigates the influence of the sequence of applied axial load, biaxial bending moments, and high temperature. The theoretical analysis is based on an equilibrium approach involving formulation and a numerical solution of simultaneous ordinary differential equations. Due to the materially nonlinear or elasto-plastic nature of the problem, the numerical solution procedure developed is iterative. The experimental study is conducted at room temperature as well as at high temperatures up to about 950°F. The capability of the theoretical prediction model developed, however, is not limited to this temperature. Specifically, the theoretical analysis of the WTC beam-columns is presented with temperatures up to about 1600°F. The variation of material properties with temperature is accounted-for in the analysis.

Development of a theoretical solution algorithm is a challenge when dealing with nonlinear differential equations having coefficients which vary with the degree of inelastic action at any load level, as well as with high temperature. An iterative procedure exploiting a technique called the finite integral approach is adopted for the theoretical portion of this study. To obtain the load-, temperature-, and deformation-dependent coefficients of the ordinary nonlinear differential equations governing the overall

behavior of the beam-columns, the finite integral approach is intertwined with a cross-sectional elasto-plastic tangent stiffness procedure.

A comparison of the theoretically predicted behavior of the beam-columns is made with that observed in the laboratory at both room temperature and high temperatures. After validating the theoretical analysis procedure using the experimental results, predictions are made about the expected behavior and strength of representative WTC beam-columns at both room and high temperatures.

1.2 Literature Review

1.2.1 Studies Conducted at Ambient Temperature

In the 1960's, Galambos and Ketter (1, 2) developed the solutions for the wide-flange beam-columns under combined bending and thrust in the presence of end restraints. Galambos and Prasad (3) presented the ultimate strength tables for wide-flange beam-columns bend by end-moments about their major axis, which gave the critical combinations of length, end moments and axial force when failure occurs. In 1966, Lu and Kamalvand (4) investigated the maximum carrying capacity of steel columns subjected to combined axial thrust and lateral load.

Chen and Atsuta (5, 6) published a comprehensive literature review and summary of steel beam-column research conducted up to 1976. Reference 5 described two-dimensional beam-columns problems. Reference 6 provided a comprehensive source of information on biaxially loaded beam-columns under various load conditions. Since 1976, a vast number of papers have been published on the behavior and strength of steel beam-columns. A brief overview of a few publications have closer relevance to the present research is given below.

In 1980, Chen (7) studied the influence of end-restraints on stability of the column in the presence of initial crookedness and residua stress. It was found that end conditions had a significant influence on column behavior, which should be considered to determine the resistance design factor.

In 1983, Razzaq (8) theoretically investigated the effect of end restraint on steel column strength by dealing with the response of minor axis of the column cross section. The columns were partially restrained by linear, elastic-plastic, or nonlinear end restraints

in the presence of initial crookedness and residual stress. It was found that the presence of partial end restraints and initial imperfections have a very significant effect on the column behavior and strength.

In 1985, Razzaq and Calash (9) theoretically studied the influence of biaxial partial restraints on the response of the hollow rectangular steel nonsway columns with or without biaxial crookedness and residual stresses. Inelastic stiffness degradation and strength characteristics of the columns were predicted.

In 1986, Razzaq and McVinnie (10) performed theoretical and experimental study of the inelastic behavior of rectangular tubular steel columns subjected to nonproprotional biaxial loading. Special gimbals were developed to simulate biaxial end hinges. Test results were shown to be in good agreement with those from theoretical analysis. Additionally, it was found that twisting may be neglected for columns of hollow square or rectangular sections.

In 1990, Darbhamulla (11) conducted a theoretical study of imperfect nonsway beam-columns with nonproportional biaxial loads. Two types of sections were considered, I-section and a hollow rectangular section. It was found that the effect of nonproportional loading on the beam-column strength was quite significant. In addition, a second-order finite-difference solution was formulated to solve the nonlinear equilibrium equations.

1.2.2 Studies Conducted at High Temperature

In 1995, Poh and Bennetts (12) developed a general numerical model to analyze the nonlinear behavior of load-bearing members under elevated temperature conditions. The method took into account the combined actions of axial force and biaxial bending, external restraints, temperature variation over the cross section and along the member, material nonlinearity, geometric nonlinearity, unloading and reloading, residual stresses and initial crookedness. Poh and Bennetts (13) compared the results obtained by using this numerical procedure with the data from 18 steel I-section column tests. The model of column is shown in Figure 1. The tests were with different heating rates, axial loads, load eccentricities and end-support conditions (unrestrained, rotationally restrained, and axially restrained). It was found that a reasonable prediction of the behavior of the

columns was obtained when the Eurocode 3 stress-strain relationship was used by using this developed numerical method.

Around 1997, Franssen and Talamona et al (14, 15) studied the stability of steel columns in case of fire by means of numerical programs and experimental tests. Centrally loaded as well as eccentrically loaded H-section columns were considered. The rotation about the major axis of columns was fixed, and for minor axis is free. The buckling coefficient was proposed for predicting the maximum load of centrally loaded columns under fire. A P-M interaction formula was proposed for eccentrically loaded columns under fire.

In 1998, Ali and Shepherd et al. (16) conducted theoretical and experimental studies on the performance of axially restrained steel I-section columns during fire with three parameters: slenderness ratio (λ= 49, 75, 98), degree of axial restraint (α_k = $0, 0.1, 0.2, 0.3$) and loading ratio ($\alpha_L = 0, 0.2, 0.4, 0.6$). The slenderness ratio, λ, was defined in relation to the effective length of the column to the radius of gyration of the cross-sectional area. The axial restraint, α_k, due to the surrounding structure, was defined by expressing the structure stiffness in relation to the column axial stiffness. The load ratio, α_L , was defined in relation to the ultimate load of the particular section under test. It was found that imposing and increasing the axial restraint can reduce the fire resistance of the column, increase the value of restraint force generated and reduce the critical temperature corresponding to zero load-carrying capacity, for all values of slenderness tested. The magnitude of additional restraint force generated decreased with increasing load ratio.

In 2002, Cabita-Neves et al. (17) developed a simple mode to illustrate the possible type of behavior of heated steel columns with elastic restraint to the thermal elongation, and the reasons why the critical temperature of axially loaded slender steel columns with thermal restraint can sometimes be lower than the critical temperature of the same columns free to elongate. Also, it was found that columns having slenderness, that is greater than 80 are the most affected by thermal restraint.

In 2007, Takagi and Deierlein (18) evaluated the design equations for structural steel members at elevated temperatures through comparisons with nonlinear finite element simulations. The comparative analyses of AISC specifications and Eurocode 3 provisions

for laterally unsupported I-shaped columns, beams, and beam-columns at temperatures between ambient to 800°C was conducted. It was found that AISC provisions significantly over-estimate the nominal strength of columns, beams and beam-columns at elevated temperatures; however, a good agreement is achieved between EC3 provisions and simulations results.

In 2009, Yang and Hsu (19) conducted a series of experimental studies to examine the behavior of H-shape steel columns subjected to central loading. The influence of the width-thickness ratio, slenderness ratio, residual stress and effective column length on the structural performance in fire was investigated. It was found that the influence of the width-thickness ratio and slenderness ratio is significant for column behavior at temperatures below 1022°F (550°C); however, temperature is the dominate factor to influence column behavior at temperatures above 1022°F (550°C). Also, it was found the residual stress had been released in the fire event and its influence on column strength could be neglected.

In 2010, Kodur and Dwaikat et al. (20) reviewed high-temperature constitutive relationships for steel currently available in the American and European Standards. It was found that the Eurocode high-temperature stress strain relationship gives a more realistic fire resistance prediction than does the use of ASCE stress strain relations. Kodur and Dwaikat (21) used the finite element computer program, ANSYS, to study the fire response of steel I-section beam-columns under realistic fire, load and restraint scenarios. The parametric studies show that the fire scenario, load level, and degree of end-restraint have significant influence on the behavior of beam-columns under fire conditions.

Around 2010, Wang and Moore (22) investigated the effect of thermal restraint on column behavior in a frame. The rest of the frame is assumed to be an axial restraint on the column. It is found that the effect of thermal restraint has to be taken into consideration in the fire resistant design of steel columns. This effect generally increases the axial compressive force in the column and is particularly detrimental for slender columns.

1.2.3 The World Trade Center Disaster

FEMA (2002) (23) described the 9/11 event: "On the morning of September 11, 2001, two hijacked commercial jetliners were deliberately flown into the WTC towers." 56 minutes after the struck, the south tower collapsed. The north tower collapsed 103 minutes after the jetliner crashed into it. Building 7 of the World Trade Center also came down almost seven hours after the Twin Towers had come down. FEMA (2002) also reported that the loss of human life: "A total of 2,830 people lost their lives in the collapse of the WTC towers, including 2,270 building occupants, 157 airplane crew and passengers, and 403 firefighters, police personnel, and other emergency responders."

The National Institute of Standards and Technology (NIST) (24) initiated a formal federal building and fire safety investigation of the World Trade Center disaster in 2002. One of its main objectives was to determine why and how the WTC1 and WTC2 collapsed following the initial impact of the aircraft, and why and how the 47-story WTC7 collapsed. The most probable collapse reason and sequence for the WTC towers summarized by NIST is described below: some perimeter and core columns were damaged and out of commission, which resulted in the redistribution of column loads to adjacent perimeter columns and core columns via the hat truss and floor systems; the subsequent fires weakened column and floor systems and triggered additional local failure, which ultimately led to column instability; the global collapse ensued when redistribution loads could not accommodate any further due to the progression of initiation and horizontal column instability. "The working hypothesis for the collapse of the WTC 7 building suggests that it was a classic progressive collapse including an initiating event, a vertical progression at the east side of the building, a subsequent horizontal progression from the east to the west side of the building, and global collapse" (23). Reference 23 also developed the load-carrying capacity curves for critical columns from WTC Building 7 based on the AISC column capacity formulas.

Miamis (25) from Purdue University studied the failure mechanism of the World Trade Center Building 1 (the North Tower) through conducting a study about the effect of high temperature on the behavior of the structural steel members. The temperature-strength interaction curves for the columns from the WTC Towers were developed based

on the mathematical expression of the 1995 Eurocode 3 "buckling curves c." Three possible failure scenarios were presented in Reference 22: "

- The collapse sequence was initiated by bucking of the core columns as a result of the fires that followed the aircraft impact.

- Failure of the exterior framing system because of buckling of the exterior columns initiated the collapse.

- The initiation of the collapse sequence was caused by failure of the trusses that supported the floor system."

Abolhassan (26), a professor at the University of California at Berkeley, thought that the World Trade Center Buildings should have stood longer, even after such a catastrophic impact, and the collapse should not have been so nearly vertical. After examining the construction documents, he said: "this building was so strange, and so many violations of practice and code were introduced." His simulation models also proved that the two airliners wouldn't have breached the structure if the WTC buildings designs followed the codes and traditional systems.

To the best of author's knowledge, no research has been published in the past on a rigorous study of partially end restrained steel beam-columns under nonproportional loading and high temperature.

1.3 Problem Definition

This dissertation focuses on a rigorous study of the influence of nonproportional loads on the behavior of steel beam-columns including those from World Trade Center Buildings at ambient and high temperatures. The influence of imperfections, flexible connections, and the axial restraint to thermal expansion on the steel beam-column strength and behavior is also investigated. Figure 2 shows the imperfect and partially restrained beam-column AB, which is subjected to axial load P, and bending moments M_{Ax}, M_{Ay}, M_{Bx}, and M_{By}. Symbols k_{Ax}, k_{Ay}, k_{Bx}, and k_{By} represent the stiffness of end rotation restraints. Subscripts A and B refer to the beam-column bottom and top ends.

The theoretical analysis is based on an equilibrium approach which leads to a system of materially nonlinear ordinary differential equations with appropriate boundary equations. To obtain the load and deformation dependent coefficients of the differential

equations, a finite integral approach is used and intertwined with a cross-sectional elasto-plastic tangent stiffness procedure. A series of experiments is conducted to study the behavior of the steel beam-columns under nonproprotional loading at ambient and high temperatures in order to verify the inelastic theoretical procedure presented here.

1.4 Objectives and Scope

The principal objectives of this research are to:

1. Develop a finite integral based solution algorithm for predicting the behavior of biaxially loaded steel beam-columns at ambient and high temperatures.

2. Study the experimental behavior of small-scale steel beam-columns under nonproportional biaxial loading and with hollow square section at both ambient and high temperatures to validate the theoretical analysis procedure.

3. Investigate the influence of partial end rotational restraints on the behavior of steel beam-columns at ambient and high temperatures.

4. Determine the influence of material unloading on the beam-column inelastic response when loaded nonproportionally.

5. Quantify the influence of axial restraint to thermal expansion on the behavior of imperfect steel beam-columns at high temperature.

6. Conduct an in-depth analysis of the behavior of beam-columns which were used in the outer structure of the 110-story WTC buildings at high temperature.

The primary motivation for this research is to study the effects of high temperature on rectangular tube steel beam-columns under nonproportional loading, and then to apply the theory developed for a formal study of the WTC members used in the outer vertical support system.

1.5 Assumptions and Conditions

The following assumptions and conditions are adopted in this study:

1. Small deflection theory is applicable.

2. The beam-column material has an elastic-perfectly plastic normal stress-strain relationship at both ambient and high temperatures with material elastic unloading.

3. The compression and tension stress-strain relationships are the same.

4. Any induced torsional effects are negligible.

5. Plate local buckling does not occur in the member.

6. Member shear deformation and axial shortening are negligible.

7. Only axial and biaxial bending equilibrium conditions are considered.

8. The external loads are nonproportional in nature and are applied gradually, that is, no dynamic effects are included.

9. Plane sections remain plane including during high temperature induction.

10. The partial rotational end restraints are either linear or elasto-plastic.

11. Creep effects due to high temperature are negligible.

12. The temperature distribution over the cross section and along the member covered by the furnace used in the experimental study is uniform.

CHAPTER

2. EXPERIMENTAL INVESTIGATIN

Presented in this chapter is the outcome of an experimental study of the inelastic behavior of steel beam-columns under nonproportional loading in the presence of ambient and high temperatures.

2.1 Test Apparatus

The apparatus for the experimental study has four major components. These include a pair of gimbals, partial rotational restraints to simulate flexible beam-column end connections, a high temperature furnace, and a setup to apply biaxial bending moment. Each of these parts of the apparatus is described in the following sub-sections.

2.1.1 Gimbals

Razzaq and McVinnie (10) developed a method for testing biaxially loaded steel beam-columns. The apparatus involved the design of a pair of steel gimbals later included in a textbook by Singer et al. (27). The same type of apparatus shown in Figure 3 was designed and fabricated at Old Dominion University and used by Sanders (28) for a study of angle section columns; however, it was modified to provide partial rotational end restraint about one of the gimbal principal axes at both top and the bottom.

Sanders (28) described the fixtures as follows: "At each end, the base plate of the test specimen bolts to a machined flat on a cross shaft which serves as the first free axis, called x axis. The cross shaft is supported by a tapered conical roller bearing between two opposite faces of a four sided gimbal box. The alternate faces of the box, in turn, are bolted to spindles supported in a second set of conical tapered bearings, forming the second orthogonal free axis called y axis. The supporting bearings for y axis are attached to a fixed supporting structure for the top gimbal, and a linear slide powered by a hydraulic jack with an inline load cell at the bottom gimbal." Figure 4 shows one of the gimbals. This arrangement provides nearly frictionless rotation of the entire gimbal about the center-line of the stub shaft that corresponds to the x axis shown in Figure 4. The net effect of the arrangement described is that rotation of the specimen ends is permitted about any horizontal axis.

2.1.2 Flexible Connections

To provide the partial rotational end restraint about one of the gimbal principal axes, Lock Plate A shown near the left bottom part of Figure 3 is replaced by a 22-inch long steel flat bar shown in Figure 5, which is called Machined Arm. This process created a partial rotational restraint about the y axis identified in Figure 4. Bolt the Machined Arm with the cross shaft of the gimbal and then they can move together, as shown in Figure 6. The Cantilever Beam shown in Figure 6 was a sandwich beam and was constituted by four steel flat bars. The Machined Arm was connected with the Cantilever Beam by a moveable Link as shown in Figures 5 and 6. The function of the Cantilever Beam is to prevent the movement of the Machined Arm with the help of the link; meanwhile it provides the rotational restraints for the gimbal about y axis. The stiffness of the rotational end restrains, k, depends on the distance between the link and the center of the gimbal, L, and the stiffness of the Cantilever Beam. It is assumed that the stiffness of the Machined Arm and the Link is infinite.

Figure 6 shows the schematic of the flexible connection. The Machined Arm acts like a cantilever beam with a point load, P, at the end, but herein the stiffness of rotational end restraint is k instead of infinity. The end- rotation and moment of the Machined Arm are represented by θ and m, respectively. The deformation of the Machined Arm, Δ_{arm}, equals the deflection of the Cantilever Beam Δ_{c-beam}. The end moment m is calculated as Equation 2,

$$m = P\,L = k\,\theta \tag{1}$$

$$\Delta_{arm} = L\,\theta = \frac{PL^2}{k} \tag{2}$$

$$\Delta_{c-beam} = \frac{P\,(L-4)^3}{3E\,I} \tag{3}$$

where E and I are the Young's modulus and the moment of inertial of the Cantilever Beam. Enforce $\Delta_{arm} = \Delta_{c-beam}$, k is solved as follows:

$$k = \frac{3\,E\,I\,L^2}{(L-4)^3} \tag{4}$$

This flexible connection functions as a spring with stiffness k, providing rotational end restraint for the gimbal in y axis.

2.1.3 Furnace

To generate high temperature conditions, a furnace with a capacity of up to $1000^{\circ}F$ was developed. Figure 7 shows the inside view of the furnace. The furnace frame is built with silica refractory insulation boards and covered by the flat-thin aluminum. Four " Γ" shaped flat-thin bronze pieces as heating elements are adhered the top and bottom board. Other heating elements are four stainless steel bars which cross the bronze pieces and stand at each corner of the furnace. This homemade electronic furnace is 28.0 in. in height, 24 in. in length and 18.5in. in width. The controller shown in Figure 8 adjusts and controls the heating process. The time-temperature curves of the furnace are shown in Figure 9. The uppermost curve is the standard ASTM E119 (29) temperature-time relationship, the lower three curves up to almost $950^{\circ}F$ are based on the actual tests utilizing the furnace developed for this research. The three curves corresponding to the three different experimental runs were obtained to check the repeatability of the temperature-time data.

2.1.4 Axial Load and Biaxial Bending Devices

A 50-kip capacity electronic compression load cell mounted atop of a hydraulic jack is under the linear slide as shown in Figure 3. The hydraulic jack is mounted to the laboratory test-bed. The axial load P can be applied by manually controlling the hydraulic jack.

Biaxial moment is applied at the top end of the specimen, using a moment arm bolted to the cross-shaft center of the top gimbal as shown in Figure 10. The moment arm is made of the steel flat with dimensions $1.0 \times 2.0 \times 24.0$ in.. The angle between the moment arm and the x axis of the gimbal is adopted 45° for applying biaxial bending moments and 0° for applying uniaxial moment respectively. A moment-producing load W is applied near the end of the moment arm, providing a pair of moment components M_{Bx} and M_{By}, which are expressed as below:

$$M_{Tx} = W \, e_y \hspace{6cm} (5)$$

$$M_{Ty} = W \, e_x \hspace{6cm} (6)$$

The load W is applied through two 0.75-in. diameter tie rods, each about 75 inches long. These rods are separated at the top and bottom by 12-inch long 0.5-in. thick steel plates forming a closed ring shown in Figure 11. The top plate (A) sits on the machined arm by means of a ball and socked arrangement, shown in Figure 10. The bottom plate is attached to a 5-kip capacity compression load cell using a similar arrangement. The 5-kip capacity load cell (D) is mounted atop another hydraulic jack (C), which is bolted on the underneath of top plate (C) of a steel table. The steel table is mounted to the laboratory test-bed. Manually control the hydraulic jack, and the load W can be produced. Figure 12 shows the setup for the ambient test.

2.2 Specimens and Test Procedure

A-hot-rolled hollow tube steel with the dimensions $1.5 \times 1.5 \times 0.125$ in. is adopted for all of the experiments. The length of the specimen is 37.5 in., including the thickness of the end base plates as shown in Figure 13. Concentricity of loading is determined in the manufacture of the test specimens. Good test results require both precise and accurate work by a skilled machine shop in production of the specimens. For this investigation, the machine shop is provided with sketches which located the centroid of each section on its respective base plate relative to the holes for the base plate bolts. A jig is used during assembly to assure that the centroid of each section is centered above the intersection of the axes of the gimbal.

This is necessary to facilitate insertion of the specimen between the two gimbal boxes, which must be rotated to clear the specimen. Once the specimen is settled down, the alignment of bottom and the top gimbal should be checked. And then the specimen is covered by the furnace symmetrically to conduct high temperature tests.

There are four dial gauges installed at each corner of the linear slide assembly to make sure that there is no rotation happening on it. Two dial gauges are set up at the midpoint of the specimen to measure the deflections in x and y axes for the ambient temperature tests. Four more dial gauges are used to measure the specimen top and

bottom end-rotation about x and y axes for tests at both ambient and high temperatures. One thermal couple is mounted at midspan point to measure the temperature of the specimen for high temperature tests.

Load and moments are applied slowly, with regular stops at intervals of load to record the temperature, axial load P, moment-producing load W and dial gauge readings. The member load-carrying capacity is reached when either the deformation reading begins to increase without increasing any of load, moment and temperature, or the applied load cannot be increased anymore and start dropping, the steel member load-carrying capacity is reached.

2.3 Material Properties

2.3.1 Mechanical Properties at Ambient Temperature

To determine the material yield stress σ_y and Young's modulus E, tension coupon tests were performed in accordance with ASTM E8-04 (30), *Standard test Methods for Tension Testing of Metallic Materials.* Four sub-size specimens are cut from all four sides of the hollow tube section, shown in Figure 14. Two strain gauges are mounted on the midpoint of each side of the sample. Strain gauge values are recorded at each load level. The experimental stress-strain curves obtained from tension coupon tests are shown in Figure 15. The stub column tests were also performed following the stub-column test procedure-Technical Memorandum No.3 (31). The average σ_Y and E values found are about 58.7ksi and 29,000ksi, respectively.

In this investigation, an elastic-perfectly plastic stress-strain model including elastic unloading for the steel beam-column material used in this research at ambient temperature is adopted, shown in Figure 16, where E is the Young's modulus, σ_Y is the yield stress, and ε_Y is the yield strain. The σ- ε relationship during material loading is expressed as below:

$$\sigma = E\,\varepsilon \qquad\qquad for\ -\varepsilon_Y < \varepsilon < \varepsilon_Y \qquad\qquad (7a)$$

$$\sigma = +\sigma_Y \qquad\qquad for\ \varepsilon \geq \varepsilon_Y \qquad\qquad (7b)$$

$$\sigma = -\sigma_Y \qquad\qquad for\ \varepsilon \leq -\varepsilon_Y \qquad\qquad (7c)$$

During material unloading, the σ- ε relationship follows the path BC shown in Figure 16 is presented below:

$$\sigma = \sigma_f - E\left(\varepsilon_f - \varepsilon\right) \tag{8}$$

where ε_f and σ_f present the strain and stress values of the former load level, respectively.

2.3.2 Mechanical Properties at High Temperature

References 19, 25, 29, 32, 33, 34, 35, 36, and 37 represent some of the important investigations conducted in the past by various researchers to determine the structural steel properties at high temperature. The well-established constitutive model of 2005 Eurocode3 (35) is adopted, herein. The steel yield strength σ_{YT} and Young's modulus E_T at any temperature T are given as follows:

$$\sigma_{YT} = k_{\sigma_{Y,T}}\,\sigma_Y \tag{9}$$

$$E_T = k_{E,T}\,E \tag{10}$$

where $k_{\sigma_{Y,T}}$ and $k_{E,T}$ are reduction factors for the material yield stress and Young's modulus at high temperature T.

Reduction factor $k_{\sigma_{Y,T}}$ is defined for various temperatures ranges as follows:

For $\quad 20°C < T \leq 400°C$: $\qquad k_{\sigma_{y,T}} = 1$ $\hfill (11a)$

For $400°C \leq T \leq 500°C$: $\qquad k_{\sigma_{y,T}} = -2.2 * T/1000 + 1.88$ $\hfill (11b)$

For $500°C \leq T \leq 600°C$: $\qquad k_{\sigma_{y,T}} = -3.1 * T/1000 + 2.33$ $\hfill (11c)$

For $600°C \leq T \leq 700°C$: $\qquad k_{\sigma_{y,T}} = -2.4 * T/1000 + 1.91$ $\hfill (11d)$

For $700°C \leq T \leq 800°C$: $\qquad k_{\sigma_{y,T}} = -1.2 * T/1000 + 1.07$ $\hfill (11e)$

For $800°C \leq T \leq 900°C$: $\qquad k_{\sigma_{y,T}} = -0.5 * T/1000 + 0.51$ $\hfill (11f)$

For $900°C \leq T \leq 1200°C$: $\qquad k_{\sigma_{y,T}} = -0.2 * T/1000 + 0.24$ $\hfill (11g)$

For $1200°C \leq T$: $\qquad k_{\sigma_{y,T}} = 0.0$ $\hfill (11h)$

Reduction factor $k_{E,T}$ is defined for various temperatures ranges as follows:

$$For\ 20°C \leq T \leq 100°C: \qquad k_{E,T} = 1 \qquad\qquad (12a)$$

$$For\ 100°C \leq T \leq 500°C: \qquad k_{E,T} = -T/1000 + 1.1 \qquad\qquad (12b)$$

$$For\ 500°C \leq T \leq 600°C: \qquad k_{E,T} = -2.9 \times T/1000 + 2.05 \qquad\qquad (12c)$$

$$For\ 600°C \leq T \leq 700°C: \qquad k_{E,T} = -1.8 \times T/1000 + 1.39 \qquad\qquad (12d)$$

$$For\ 700°C \leq T \leq 800°C: \qquad k_{E,T} = -0.4 \times T/1000 + 0.41 \qquad\qquad (12e)$$

$$For\ 800°C \leq T \leq 1200°C: \qquad k_{E,T} = -0.125 \times T/1000 + 0.15 \qquad\qquad (12f)$$

$$For\ 1200°C \leq T: \qquad k_{E,T} = -0.0 \qquad\qquad (12g)$$

In this study, an elastic-perfectly-plastic material stress-strain relationship at high temperature T is adopted including material elastic unloading as shown in Figure 17. During material loading, the following expressions are applicable:

$$\sigma_T = E_T\ \varepsilon_T \qquad for\ -\varepsilon_Y < \varepsilon_T < \varepsilon_{TY} \qquad\qquad (13a)$$

$$\sigma_T = +\sigma_{YT} \qquad for\ \varepsilon_T \geq \varepsilon_{TY} \qquad\qquad (13b)$$

$$\sigma_T = -\sigma_{YT} \qquad for\ \varepsilon_T \leq -\varepsilon_{TY} \qquad\qquad (13c)$$

For the material unloading part, the σ_T- ε_T relationship follows path BC as shown in Figure 17for which:

$$\sigma_T = \sigma_{Tf} - E_T\left(\varepsilon_{Tf} - \varepsilon_T\right) \qquad\qquad (14)$$

The thermal strain mode of the 2005 Eurocode3 (35) is adopted herein and presented in Equation 15.

$$\varepsilon_{th} = \begin{cases} 1.2 \times 10^{-5}T + 0.4 \times 10^{-8}T^2 - 2.416 \times 10^{-4}, & For\ T < 750°C \\ 1.1 \times 10^{-2}, & For\ 750°C \leq T \leq 860\ °C \\ 2 \times 10^{-5}T - 6.2 \times 10^{-3}, & For\ 860°C \leq T \leq 1,200\ °C \end{cases} \qquad (15)$$

It should be noted that there is negligible difference between the thermal strain model proposed by ASCE (36) and that of EC3. The ASCE model assumes a continuously

increasing thermal strain while the Eurocode model accounts for the phase change in the temperature range of 750-850°C. Eurocode model assumes a constant thermal strain from 750°C to 850°C.

2.4 Load Paths

Referring to Figure 20, four different mechanical load paths are used for steel beam-columns tests, as described below:

LP1: The axial load P is first applied incrementally and then held constant, followed by gradually applying moment M_{By} until the load-carrying capacity of the member is reached. This corresponds to the path OAE.

LP2: The moments M_{By} is first applied and then held constant, followed by gradually increasing axial load P until maximum load is reached. This corresponds to the path OGE.

LP3: The axial load P is first applied incrementally and then held constant, followed by gradually increasing equal end moments M_{Bx} and M_{By} until the load-carrying capacity of the member is reached, which corresponds to the path OAD.

LP4: The end equal moments M_{Bx} and M_{By} are first applied and then held constant, followed by gradually increasing axial load P until the strength limit is reached. This corresponds to the path OFD.

Figure 21 shows the load-temperature sequence for designed high temperature tests. The symbols T, M and P represent the temperature, applied resultant moment and applied axial load, respectively. In this investigation, seven different load paths are adopted as described below:

OPT: The axial load is first applied incrementally and then held constant, followed by elevating the temperature until the member collapses.

OTP: The temperature, T, is firstly increased from ambient temperature and then held constant, followed by gradually applying axial load P until the member fails.

OMT: The bending moment is first applied incrementally and then held constant, followed by elevating the temperature until the member fails.

OTM: The temperature T is firstly increased and then held constant, followed by gradually applying bending moment M until the member collapses.

OTPM: The temperature T is firstly increased from ambient temperature and then held constant. Next, the axial load P is applied and held constant, followed by slowly applying moment M until collapse occurs.

OTMP: The temperature T is firstly increased and then held constant. Next, the moment M is applied and held constant, followed by axial load P until collapse occurs.

OMTP: The moment M is firstly applied gradually and held constant. Next, the temperature is increased and then held constant, followed by applying axial load P until collapse occurs.

In the above mentioned load paths, M represents either the uniaxial moment or the resultant moment creating biaxial moments M_{Bx} and M_{By} .

2.5 Boundary Conditions

Two different mechanical boundary conditions are used in the experimental study. One type is based on pinned conditions about both x and y axes, and another is a combination of partial rotational restraint about the y axis while the pinned conditions about the x axis are maintained. The rotational stiffness of the connection is calculated by using Equation 4.

In general, a member at high temperature has three different situations for the axial restraint to thermal expansion, which are unrestrained, end restrained and partial end restrained, shown in Figure 22. The setup of laboratory apparatus only allows two cases happen: unrestrained and partial end restrained. The specimen can expand freely during heating if the four screws are released, which bolt the bottom end of specimen to the gimbal. The specimen has the axial restraint to thermal expansion caused the additional compressive force if four screws are tightened during heating.

2.6 Experimental Results

The entire test results are summarized in Tables 1 through 5. All of the load-deflection and end rotation curves are presented in Figures 23 through 34. All the letters in the name of the specimen have special meaning. Herein, symbol RT represents the ambient temperature; U represents uniaxial loading; P represents the pinned boundary conditions; B represents the biaxial loading; S represents the partial boundary conditions;

HT represents the high temperature. In these figures, T_1 and T_2 represent the temperature of 500°F and 900°F, respectively. All the values used in the tables and curves are dimensionless and defined as below:

$$p = P/P_Y \tag{16}$$

$$m_x = M_x/M_{xY} \tag{17}$$

$$m_y = M_y/M_{yY} \tag{18}$$

where P_Y is the cross-sectional full plastification load; M_{xY} and M_{yY} are the yield bending moments about x and y axes.

Table 1 summarizes the biaxial loading test results at ambient temperature with pinned and partial rotational restrained boundary conditions. The maximum axial load for RTBS-7 is 0.593, which is 7.8% higher than that of RTBP-1. For RTBS-8, the maximum bending moment values for m_x and m_y are 0.858 and 0.858, respectively, which are 5.6% higher than those of RTBP-2. The boundary conditions for RTBS-7 and RTBS-8 are partial rotational end restrained boundaries, and pinned boundary conditions for RTBP-1 and RTBP-2. These two comparisons show that the end restraint can increase the member load-carrying capacity.

For the tests with specimens RTBP-3 through RTBP-6 at ambient temperature, the boundary conditions are pinned. For RTBP-3, following load path LP3, the maximum values for p, m_x and m_y are 0.334, 0.465 and 0.465 respectively. For RTBP-4, following load path LP4, the maximum values for p, m_x and m_y are 0.334, 0.465 and 0.465 respectively. The load path for RTBP-4 is exactly the reverse of RTBP-3, but their maximum loads are same. For RTBP-5, following the load path LP4, respectively, the maximum moment value for p, m_x and m_y are 0.239, 0.616 and 0.616 respectively. For RTBP-6, following the load path LP3, the maximum moment value for p, m_x and m_y are 0.239, 0.661 and 0.661, respectively. The maximum moment for RTBP-6 is about 7.3% higher than that of RTBP-5. It is found that the influence of load sequence on the behavior of steel beam-column with pinned boundary conditions is not significant.

The boundary conditions for the tests with specimens RTBS-9 and RTBS-10 at ambient temperature are partial rotational restrained in y axis and pined in x axis. The end restraint spring stiffness is 107.53in-kip/rad. For RTBP-9, following the load path LP3,

the maximum moment value for p, m_x and m_y are 0.257, 0.636 and 0.636, respectively. For RTBP-10, following the load path LP4, the maximum moment value for p, m_x and m_y are 0.268, 0.636 and 0.636, respectively. The maximum axial load for RTBP-10 is about 4.23% higher than that of RTBP-5. It is found that the influence of load sequence on the steel beam-column with pinned boundary conditions about the x axis and partially rotation restrained about the y axis is not significant.

Table 2 summarizes the uniaxially bending test results with pinned and partial rotation restrained boundary condition at ambient temperature and different load paths. The result for partial rotation restrained specimen RTUS-17 (1.620) is 27.9% higher than that of RTUP-11 (1.266) with pinned boundary conditions, which shows that the end restraint can increase the member maximum load. The maximum value p for RTUP-13(0.406), following load path LP1, is about 5.1% higher than that of RTUP-12 (0.386), following load path LP2. The maximum value m_y for RTUP-14 (0.995), following load path LP2, is about 3.6% higher than that of RTUP-15 (0.960), following load path LP1. The maximum value p for RTUS-18 (0.398), following load path LP2, is about 3.1% high than that of RTUS-17 (0.386), following load path LP1. The maximum value m_y for RTUP-20 (1.034), following load path LP1, is about 4.1% higher that of RTUP-19 (0.993), following load path LP2. The results show that the influence of load path on the steel beam-column subjected to uniaxial bending is not significant.

Table 3 summarizes the dimensionless maximum loads values for 10 uniaxial bending tests at 500°F. The load-temperature sequence for tests HTUP-1 through HTUP-5 is heating the specimen to 500°F without axial resistant to thermal expansion firstly, and then gradually starting to apply the mechanical load. For HTUPR-6, the load-temperature sequence is applying bending moment firstly, and then heating the specimen to 500°F, and lastly applying axial load p until the member fails. Obtained results show that at 500°F, the load-carrying capacity of the member is independent upon the load-temperature sequence for beam-column with pinned boundary condition and under uniaxial loading. However, for the partial boundary condition, the maximum moment m_y for HTUS-10 (0.694) is 16.6% higher than that of HTUS-9 (0.595), which shows that the member load-carrying capacity is dependent on the load sequence at partial boundary condition. By comparing the results HTUP-1 to HTUS-7, and HTUP-2 to HTUS-8, it

indicates that end restrain can increase steel beam-column failure load at high temperature.

Table 4 presents the dimensionless maximum test results for biaxial bending tests at 500°F with pinned boundaries in both x and y axes. For this group of tests, the specimens were heated firstly with or without axial resistant to thermal expansion and then different biaxial bending moments were applied. There is no axial resistant to thermal expansion for tests HTBP-11 to 13; the tests for HTBPR-1 through HTBPR-4 are with axial resistant to thermal expansion. The maximum p value for HTBPR-1 is 0.502, which is 7.5% (0.035) higher than that of HTUP-2 (0.467). The maximum m_x and m_y value for HTBPR-2 is 0.741, which is 7.1% (0.049) higher than that of HTBP-11 (0.692). The above two comparisons indicate that axial restraint to thermal expansion doesn't affect the load-carrying capacity at 500°F. By comparing the results HTBP-12 with HTBP-13 and HTBPR-3 with HTBPR-4, it shows that the load sequences do not have a significant influence on the load-carrying capacity for pinned members even at high temperature 500°F.

Table 5 collects the test results at 900°F with pinned boundary conditions. All the tests in this group are with axial resistant to thermal expansion. For HTBPR-6, the specimen was heat to 900°F firstly and then the axial load p was applied gradually until collapse occurs. For test HTBPR-7, the axial load p of the same magnitude reached in HTBPR-6 is firstly applied incrementally and held constant; then the specimen was heated until the critical temperature was reached. The axial load p value starts dropping fast when the temperature is getting around 750°F, which indicates that the collapse occurs and critical temperature is reached. For HTBPR-8, the specimen was heated to 900°F, and then the biaxial moment was applied gradually until the maximum value is reached. The peak value for m_x and m_y is 0.214. For HTBPR-9, biaxial moment of the same magnitude obtained in HTBPR-8 was firstly applied gradually, and then held constant and then the specimen was heated until the critical temperature was reached. The biaxial moment value started decreasing when the temperature is closing to 775°F. For test HTUPR-10, the specimen was heated to 900°F, and then uniaxial moment was applied gradually until the collapse occurs with the peak value, 0.402. For test HTBPR-10, uniaxial moment of the same magnitude obtained in HTBPR-10 was firstly applied

incrementally and then held constant and the specimen was heated to fail. When the temperature was near around 750°F, the moment started dropping fast which means that the load-carry capacity is reached. The critical temperature for the member with load-temperature sequence heating the member firstly and then applying mechanical load, is about 16.7% lower than that of applying mechanical load firstly and then increasing the temperature. These results show that the load-temperature sequence has a definite effect on the member strength.

Table 6 compares the maximum values obtained from ambient temperature high temperature tests. It is clear that high temperature can reduce the load-carrying capacity of steel members. Also the axial restraint to thermal expansion can significantly reduce the failure load for member at high temperatures. For example, for only applying the axial load test, the maximum axial load at ambient temperature is 0.617, at 500°F with no restraint to thermal strain is 505; at 900°F with restraint to thermal strain is 0.123. For only applying biaxial bending moments, the maximum bending moment m_x and m_y at ambient temperature is 0.811, at 500°F without axial restraint to thermal expansion is 0.761; at 500°F with axial restraint to thermal expansion is 0.0.741; for 900°F with axial restraint to thermal expansion is 0.214. Same to the uniaxial bending tests, the maximum applied load values at the ambient temperature, 500°F and 900°F are 1.266, 1.100 and 0.402, respectively.

Figures 23 and 24 show the moment versus deflection and rotation curves for uniaxial loading tests at the ambient temperature with pinned (RTUP-11, RTUP-12 and RTUP-15) and partial rotational restrained boundary conditions (RTUS-16, RTUS-17 and RTUS-20). All the curves start with linear part and then follow with plastic part until the maximum loads are reached. With the initialed applied axial load p equals to 0.0, 0.233 and 0.386, and the maximum uniaxial bending moments equal to 1.266, 0.960 and 0.648, respectively. It is clear that increasing the initial applied axial load can reduce the uniaxial moment-carrying capacity. Their corresponding deflections at failure are 0.490, 0.476 and 0.441, respectively. It is found that the maximum deflection is small if the applied axial load is relative large.

Figures 25 and 26 describe load versus midspan deflection and end rotation curves for uniaxial bending tests at ambient temperature. For tests with pinned boundaries, the

maximum axial load p values are 0.550, 0.406 and 0.233 with initially applied uniaxial moment m_y equal 0.0, 0.648 and 0.995, respectively. For tests with partial rotational end-restraints, the peak value for p reaches to 0.593, 0.398 and 0.371 having initialed applied uniaxial moment m_y, 0.0, 0.933 and 0.993, respectively. It is clear that increasing the initial applied uniaxial bending moment can reduce the axial load-carrying capacity. Also, it is found that the partial rotational end-restraints do increase the strength of steel beam-columns.

Figures 27 through 30 describe the moment- and load- deflection and end rotation curves for biaxially loading tests at ambient temperatures with pinned and partial rotational restrained boundaries. All the curves start with linear part following with plastic part, which is similar with that of uniaxial bending tests. The influence of end rotational restrain on the behaviors of steel beam-column subjected to biaxial loading is significant, which increases the member load-carrying capacity.

Figure 31 depicts the moment versus end rotation curves for the uniaxial bending test at T1= 500°F and T2= 900°F. All the curves start with elastic part following with plastic part. At last part the slope of the curve is close to zero. The slope for the moment versus end rotation curve at 900°F is smaller than that of at 500°F. The slope of the curve for the test with partial boundary condition is larger than that with pinned boundary conditions. It is clear that the rotational end-restraint increases the steel member strength limit and the high temperature reduces the steel member strength. Additionally, the initially applied axial load reduces the maximum value of the uniaxial bending moment.

Figure 32 illustrates the load versus end rotation curves for tests at 500°F with pinned or partial rotation restrained boundary conditions. The maximum rotation for the test with only applying the axial load is smaller than that of with combined loading of axial load and moments. Both the maximum load values and the slope of curves for partial boundary conditions are larger than those of with pinned boundary conditions.

Figures 33 and 34 show moment- and load- end rotation curves for tests with biaxial loading at 500°F and 900°F with pinned boundary conditions with or without axial restraint to thermal expansion. The shape of curves is the same with those of from uniaxial loading tests at high temperatures. In Figure 31, the slope of the curve for the test with specimen HTBPR-6 is even smaller because the axial restraint significant affects the

steel member load-carrying capacity. The load-temperature sequence for HTBPR-6 is that the specimen was heated to 900°F firstly with axial restraint to thermal expansion firstly and then the axial load was applied gradually until it fails. The rotation curve does not start from the zero value (around 0.004 rad.) because of the additional compressive force incurred by restrained thermal expansion. In other words, heating the steel members with axial restraint to thermal expansion is equivalent to applying an axial load.

2.7 Temperature-load Relationship

Table 7 summarizes the dimensionless maximum loads for tests at temperatures of $T_1 = 72°F$, $T_2 = 500°F$, and $T_3 = 900°F$. The value p represents the dimensionless maximum axial load values when only the axial load was applied. The symbol m_x represents the dimensionless maximum bending moment for the tests when only uniaxial bending moment about y axis was applied. The last column of Table 7 corresponds to the case only applying biaxial bending moment, which is, m_x and m_y are simultaneously applied about both x and y axes until the maximum moment values are obtained. Figure 35 describes the temperature versus applied axial load or moment curves from those three tests mentioned above. What is the critical temperature corresponding to zero load-carrying capacity? The Lagrange polynomial interpolation (38) is adopted to develop the relationship between the temperature and the maximum load. Then the relationship between the dimensionless maximum load Y and temperature T is presented as below:

$$Y = Y_1 \frac{(T - T_2)(T - T_3)}{(T_1 - T_2)(T_1 - T_3)} + Y_2 \frac{(T - T_1)(T - T_3)}{(T_2 - T_1)(T_2 - T_3)} + Y_3 \frac{(T - T_1)(T - T_2)}{(T_3 - T_1)(T_3 - T_2)} \tag{19}$$

Substitute the values $Y_1 = p_1 = 0.550$, $Y_2 = p_2 = 0.502$ and $Y_3 = p_3 = 0.123$ into Equation 19 and the relationship between the temperature and dimensionless maximum load p can be developed as shown below:

$$p(T) = (-8.819 \times 10^{-7}) T^2 + 0.00019891 T + 0.60726 \tag{20}$$

In order to determine the value of T which will result in a zero axial load capacity, $p(T)$ in Equation 20 should be set equal to zero. Thus, with $p(T) = 0.0$ in Equation 20, the following limiting temperature value is obtained:

$T_{c1} = 991.3°F$.

Substitute the values $Y_1 = m_{y1} = 1.266$, $Y_2 = m_{y2} = 1.100$ and $Y_3 = m_{y3} = 0.402$ into Equation 19 and the relationship between the temperature and dimensionless maximum bending moment m_y can be expressed as shown below:

$$m_y(T) = (1.63551E - 6)\, T^2 + 0.000545\, T + 1.236522 \tag{21}$$

In order to determine the value of T which will result in a zero uniaxial moment capacity, $m_y(T)$ in Equation 21 should be set equal to zero. Thus, with $m_y(T) = 0.0$ in Equation 20, the following limiting temperature value is obtained:

$T_{c2} = 1051.8°F$

Substitute the values $Y_1 = m_{x1} = m_{y1} = 0.811$, $Y_2 = m_{x2} = m_{y2} = 0.741$ and $Y_3 = m_{x3} = m_{y3} = 0.241$ for biaxial bending tests into Equation19 and then the relationship between the temperature and dimensionless maximum biaxial bending moment m_x and m_y can be expressed as shown below:

$$m_x(T) = m_y(T) = (-1.38878E - 6)\, T^2 + 0.006627\, T + 0.7748 \tag{22}$$

In order to determine the value of T which will result in a zero load-carrying capacity, $m_x(T) = m_y(T)$ in Equation 22 should be set equal to zero. Thus, with $m_x(T) = m_y(T) = 0.0$ in Equation 22, the following limiting temperature value is obtained:

$T_{c3} = 1005.9°F$.

The collapse temperature T_c for the member without any applying load and moments is solved by getting the average of T_{c1}, T_{c2} and T_{c3}:

$$T_c = (T_{c1} + T_{c2} + T_{c2})/3 = 1016^{\circ}\text{F}.$$

Therefore, the failure temperature is 1016°F for the steel beam-column with cross section $1.5 \times 1.5 \times 0.125in.$, yield stress 58.7ksi and Young's modulus 29000ksi and a specified axial restraint to thermal expansion.

CHAPTER

3. THEORECTICAL ANALYSIS FOR STEEL BEAM-COLUMNS

AT AMBIENT TEMPERATURE

The theoretical analysis of the behavior of nonproportionally loaded imperfect nonsway steel beam-columns at ambient temperature is presented in this chapter. The imperfections include cross-sectional residual stresses and initial member crookedness. The materially nonlinear ordinary differential equilibrium equations for nonsway imperfect beam-columns are developed. An iterative procedure exploiting a technique called the finite integral approach is formulated. To obtain the load and the deformation dependent coefficients of the differential equations, the finite integral approach is intertwined with a cross-sectional elasto-palstic tangent stiffness procedure. The modeling study of end restraints for the beam-column is conducted. The influence of load sequence on the behavior of steel beam-columns having I-section or hollow rectangular section is investigated.

3.1 Theoretical Analysis at Ambient Temperature

3.1.1 Thrust-moment-curvature Relations

Figures 36 and 37 show the discretized hollow rectangular and I-shaped sections with width B, depth D, and wall thickness t_f for the flange and t_w for the web, respectively. Each wall of the cross section is divided into subareas. The symbol A_i represents a typical elemental area. The residual stress distribution patterns for hollow rectangular section and I-section shown in Figures 18 and 19 are used. The elastic-perfectly-plastic stress-strain relationship for steel beam-column material including elastic unloading is adopted, shown in Figure 16

The normal strain ε, at a point (x, y) of the cross section subjected bending moments M_x and M_y about x and y axes and axial force P is expressed as:

$$\varepsilon = \varepsilon_0 + \Phi_x\, y - \Phi_y\, x + \varepsilon_r \tag{23}$$

in which ε_0 is the average axial strain; Φ_x and Φ_y are the bending curvatures about the x and y axes, respectively; ε_r is the residual strain. The cross sectional equilibrium equations for the axial thrust, bending moments about x-axis and y-axis can be written as:

$$P = -\int_A \sigma \, dA \tag{24}$$

$$M_x = \int_A \sigma \, y \, dA \tag{25}$$

$$M_y = -\int_A \sigma \, x dA \tag{26}$$

Substitute the elastic-perfectly plastic stress-strain relationship into Equation 17 through 19, and then the cross-sectional equilibrium equations are able to be expressed:

$$P = -\int_{Ae} \sigma_e \, dA - \int_{Ap} \sigma_Y \, dA \tag{27}$$

$$M_x = \int_{Ae} \sigma_e \, y \, dA + \int_{Ap} \sigma_Y \, y \, dA \tag{28}$$

$$M_y = -\int_{Ae} \sigma_e \, x \, dA - \int_{Ap} \sigma_Y \, x \, dA \tag{29}$$

in which dA is an elemental area of the cross section and σ is the normal stress on that area; the subscripts e and p refer to the elastic and plastic elements, respectively, of a partially plastified section; $\int_A$ represents the cross-sectional integration. Since plastic behavior is load path dependent and usually requires step by step calculations that follows the history of loading, it is only possible to establish the relationship between the infinitesimal generalized stresses increments $\dot{\sigma}$ and the infinitesimal generalized strains $\dot{\varepsilon}$. The strain rate is presented below:

$$\dot{\varepsilon} = \dot{\varepsilon}_0 + \dot{\Phi}_x y - \dot{\Phi}_y x + \dot{\varepsilon}_r \tag{30}$$

Due to the residual stress is independent of time, therefore $\dot{\varepsilon}_r = 0$. The strain rate equation can be written as

$$\dot{\varepsilon} = \dot{\varepsilon}_0 + \dot{\Phi}_x y - \dot{\Phi}_y x \tag{31}$$

The stress-strain rate relationship is given by:

$$\dot{\sigma} = E_t \, \dot{\varepsilon} \tag{32}$$

in which E_t, the tangent modulus, equals E if the material is elastic; it equals zero if the material is in plastic range. The cross-sectional load and deformation vectors, $\{f\}$ and $\{\delta\}$, are expressed as follows:

$$\{f\} = \{P \quad M_x \quad M_y \}^T \tag{33}$$

$$\{\delta\} = \{ \varepsilon_o \quad \Phi_x \quad \Phi_y \}^T \tag{34}$$

The responding cross-sectional load and deformation rate vector are expressed as:

$$\{\dot{f}\} = \{\dot{P} \quad \dot{M}_x \quad \dot{M}_y \}^T \tag{35}$$

$$\{\dot{\delta}\} = \{ \dot{\varepsilon}_o \quad \dot{\Phi}_x \quad \dot{\Phi}_y \}^T \tag{36}$$

The elements of load vector rat $\{\dot{f}\}$ are calculated as follows:

$$\dot{P} = -\int_A \dot{\sigma} \, dA = -\int_A E_t \, \dot{\varepsilon} \, dA \tag{37}$$

$$\dot{M}_x = \int_A \dot{\sigma} \, y \, dA = \int_A E_t \, \dot{\varepsilon} \, y \, dA \tag{38}$$

$$\dot{M}_y = -\int_A \dot{\sigma} \, x \, dA = \int_A E_t \, \dot{\varepsilon} \, x \, dA \tag{39}$$

The relationship between the load rate vector $\{\dot{f}\}$ and deformation rate vector $\{\dot{\delta}\}$ is expressed as follows:

$$\{\dot{f}\} = [k] \{\dot{\delta}\} \tag{40}$$

where $[k]$ is the cross-sectional tangent stiffness matrix, which is defined as below:

$$[k] = \begin{bmatrix} -\int E_t \, dA & -\int E_t \, y \, dA & \int E_t \, x \, dA \\ \int E_t \, y \, dA & \int E_t \, y^2 \, dA & -\int E_t \, xy \, dA \\ -\int E_t \, x \, dA & -\int E_t \, xy \, dA & \int E_t \, x^2 \, dA \end{bmatrix} \tag{41}$$

All the elements in the $[k]$ matrix are constant throughout the elastic range. However, in the material plastic range, the elements of $[k]$ matrix are functions of the current state of stress and strain as well as the properties of the material and cross section. Tangent stiffness E_t equal zero for the yield area, therefore, only the area of the elastic core will

contribute to the integration in Equation 41. In other words, the further increment of external forces is withstood by the remaining elastic area of the section only.

Thus, given an axial load P, and a pair of bending moments M_x and M_y, the strain distribution can be found while following Equation 40. In other words, by cross-section tangent stiffness method the compatible ϵ_o, Φ_x and Φ_y are able to be obtained, which satisfies the equilibrium for P, M_x, and M_y. Santathadaporn and Chen (41) presented the tangent stiffness method for biaxial bending. Figure 38 (41) shows the convergence of this method, which starts with a known state A and incrementally converges to the next state B for which only load vector is known. Using the solved strain distribution, the internal resisting forces are evaluated by numerical summation over the discretized cross section shown in Figures 36 and 37. This is readily done by replacing the integrals in Equations 27 through 29 by summations and dA by A_i. The maximum load-carrying capacity of the cross section is reached if the determinant of the tangent stiffness matrix $[k]$ is approaching zero.

3.1.2 Equilibrium Equations for Nonsway Beam-column

An imperfect and partially restrained nonsway beam-column AB with length L is shown in Figure 1. The origin of the longitudinal coordinate z is at A. The total deflection U and V including member initial crookedness are given by:

$$U = u + u_{oi} \tag{42}$$

$$V = v + v_{oi} \tag{43}$$

where u and v represent the deflections incurred by the applied load and moments; u_{oi} and v_{oi} represent the initial crookedness in the xz and yz planes, respectively, and given by:

$$u_{oi} = u_o \sin\left(\frac{\pi z}{L}\right) \tag{44}$$

$$v_{oi} = v_o \sin\left(\frac{\pi z}{L}\right) \tag{45}$$

In Equations 42 through 45, u_o and v_o are the mid-span initial amplitudes taken as $L/1000$ for a crooked member and as $L/100,000$ for a nearly straight one.

If the end restraint moments at ends A and B of beam-column are represented, respectively, by m_{Ax}, m_{Ay}, m_{Bx} and m_{By} then the total external moments M_x and M_y at any location z are expressed as follows:

$$M_x = P\,V - m_{Ax} + M_{Ax} + z\,R_y \tag{46}$$

$$M_y = -P\,U + m_{Ay} - M_{Ay} + z\,R_x \tag{47}$$

where R_x and R_y are given by :

$$R_x = \left(M_{Ay} - M_{By} - m_{Ay} + m_{By}\right)/L \tag{48}$$

$$R_y = \left(-M_{Ax} + M_{Bx} + m_{Ax} - m_{Bx}\right)/L \tag{49}$$

Substituting Equations 7 and 23 into the first term on the right hand side of each of Equations 27 through 29, the following materially nonlinear ordinary differential equations are obtained:

$$a_{11}\,\varepsilon_0 + a_{12}\,v'' + a_{13}\,u'' - P_{re} - P_p = P \tag{50}$$

$$a_{21}\,\varepsilon_0 + a_{22}\,v'' + a_{23}\,u'' + M_{xre} + M_{xp} = M_x \tag{51}$$

$$a_{31}\,\varepsilon_0 + a_{32}\,v'' + a_{33}\,u'' - M_{yre} - M_{yp} = M_y \tag{52}$$

in which $\Phi_x = v''$, $\Phi_y = -u''$, and the primes designate differentiation relative to z. As the quantities, a_{ij} terms are constant coefficients throughout the elastic range. However, for the partial yield section, a_{ij} terms become functions of v'' and u''. The symbols P_{re} M_{xre} and M_{yre} represent the resultant axial load, bending moment about x-axis, and bending moment about y-axis, respectively, due to the residual stress from the cross-sectional elements, which are in elastic range. Symbols P_p , M_{xp} and M_{yp} represent the summation of the axial load, the bending moment about x-axis, and the bending moment about y-axis, respectively, from the plastic areas. All the terms are defined as below:

$$a_{11} = -E\,A_e \tag{53a}$$

$$a_{12} = E\,S_{xe} \tag{53b}$$

$$a_{13} = E\, S_{ye} \tag{53c}$$

$$a_{21} = E S_{xe} \tag{53d}$$

$$a_{22} = -E\, I_{xe} \tag{53e}$$

$$a_{23} = -E\, I_{xye} \tag{53f}$$

$$a_{31} = -E\, S_{ye} \tag{53g}$$

$$a_{32} = E I_{xye} \tag{53h}$$

$$a_{33} = E\, I_{ye} \tag{53i}$$

$$A_e = \int_{Ae} dA \tag{53j}$$

$$S_{xe} = \int_{Ae} y\, dA \tag{53k}$$

$$S_{ye} = \int_{Ae} x\, dA \tag{53l}$$

$$I_{xe} = \int_{Ae} y^2\, dA \tag{53m}$$

$$I_{ye} = \int_{Ae} x^2\, dA \tag{53n}$$

$$I_{xye} = \int_{Ae} xy\, dA \tag{53o}$$

$$P_r = \int_{Ae} \sigma_r\, dA \tag{53p}$$

$$P_p = \int_{Ap} \sigma_Y\, dA \tag{53q}$$

$$M_{xre} = \int_{Ae} \sigma_r\, y\, dA \tag{53r}$$

$$M_{yre} = \int_{Ae} \sigma_r\, x\, dA \tag{53s}$$

$$M_{xp} = \int_{Ap} \sigma_Y\, y\, dA \tag{53t}$$

$$M_{yp} = \int_{Ap} \sigma_Y\, x\, dA \tag{53u}$$

$$\sigma_r = E\, \varepsilon_r \tag{53v}$$

where A_e and A_p represents the elastic area and the plastic area, respectively. At the global level, Equation 50 is enforced by first solving it for ε_0 explicitly. And then ε_0 , M_x ,

and M_y are substituted into Equation 51 and 52 utilizing Equation 46-49, which results into the following two materially nonlinear ordinary differential equations as shown below:

$$\left(-Es_{xe}s_{ye} + EA_eI_{xye}\right)u'' + \left(-Es_{xe}{}^2 + EA_eI_{xe}\right)v'' + A_eP\ v$$
$$-A_e\frac{L-z}{L}m_{Ax} - A_e\frac{z}{L}m_{Bx} = F_{xapplied} + F_{xre} + F_{xp} \tag{54}$$

$$\left(-Es_{ye}^2 + EA_eI_{ye}\right)u'' + \left(-Es_{xe}s_{ye} + EA_eI_{xye}\right)v'' + A_eP\ u$$
$$-A_e\frac{L-z}{L}m_{Ay} + A_e\frac{z}{L}m_{By} = F_{yapplied} + F_{yre} + F_{yp} \tag{55}$$

where $F_{xapplied}$ and $F_{yapplied}$ represent the moment vectors due to the applied moment and axial load; F_{xre} and F_{yre} represent the moment vector caused by the residual stress in the elastic area; F_{xp} and F_{yp} represent the moment vector due to the plastification. All the terms are defined below:

$$F_{xapplied} = -s_{xe}\ P + A_e(-P\ v_0 + \frac{(z-L)}{L}\ M_{Ax} - \frac{z}{L}M_{Bx}) \tag{56a}$$

$$F_{xre} = -s_{xe}\ P_{re} + A_e\ M_{xre} \tag{56b}$$

$$F_{xp} = -s_{xe}\ P_p + A_e\ M_{xp} \tag{56c}$$

$$F_{yapplied} = -s_{ye}\ P + A_e(-P\ u_0 + \frac{(z-L)}{L}\ M_{Ay} - \frac{z}{L}M_{By}) \tag{56d}$$

$$F_{yre} = -s_{ye}\ P_{re} + A_e\ M_{yre} \tag{56e}$$

$$F_{yp} = -s_{ye}\ P_p + A_e\ M_{xp} \tag{56f}$$

3.2 Boundary Connections

3.2.1 In-plane Inelastic Analysis of Continuous Beam

Figure 39 shows a continuous and symmetrical beam on four simple supports A, B, C and D. The plastic moment for span AB and CD is represented by m_p and M_p represents the plastic moment of span BC. The relationship between m_p and M_p depends on the cross-sectional dimension distribution along the beam, M_p might be larger, equal or smaller than m_p. Herein, it is assumed that the material properties are same along the beam AD. In Figure 39, (a) shows the case for $M_p > m_p$; (b) shows the

case for $M_p < m_p$; (c) shows the case for $M_p = m_p$.The applied moment M_o is located at the support B and C, respectively. The maximum value for the applied moment, M_o, depends on the relationship between M_p and m_p.The symbol Θ describe the slope at the support B and C. The inelastic relationship between the applied moment M_o and end rotation Θ for beam BC is able to be developed based on the moment-curvature (M-Φ) curve. Here, the symbol M represents the internal moment of cross section.

The relationship M-Φ is developed for the hollow rectangular cross section herein. Figure 40 shows the plastification pattern, stress, and strain distribution. The inelastic moment-curvature relationship can be presented as follow:

$$Elastic\ range: \qquad \frac{M}{M_Y} = \frac{\Phi}{\Phi_Y} \tag{57}$$

$$First\ inelastic\ range: \quad \frac{M}{M_Y} = \frac{BD^3}{8I_x} - \frac{BD^3}{24I_x}\left(\frac{\Phi_Y}{\Phi}\right)^2 - \frac{\Phi}{\Phi_Y} \tag{58}$$

$$Second\ inelastic\ range: \quad \frac{M}{M_Y} = \frac{BD^3}{8I_x} - \frac{D(D-2t_f)^2(B-2t_w)}{8I_x} - \frac{D^3 t_w}{12I_x}\left(\frac{\Phi_Y}{\Phi}\right)^2 \tag{59}$$

where M_Y is the yield moment about x axis; Φ_Y is the curvature responding to M_Y. The curvature Φ can be expressed explicitly from Equation 57 through 59. Then, the end rotation θ can be evaluated by using the moment area theorem, which is shown below:

$$\theta = \int_0^{L/2} \Phi\ dz \tag{60}$$

Equation 60 is also available for the inelastic range analysis. Therefore, the inelastic moment-slope relationship is able to be developed.

Inelastic analysis the beam $ABCD$ to get the relationship between M_o and Θ can be simplified to analyze the beam BC, shown in (e) of Figure 39. The beam BC is a simple support beam with the partial rotational restraints at end B and$C$. Symbols k and m represent the spring stiffness and resistant moment, respectively.

If $m_p \geq M_p$, the relationship between m and θ follows Equation 61a and 61b:

$$m = k\ \theta; \qquad 0 \leq \theta \leq (\frac{M_p}{k}) \tag{61a}$$

$$m = M_p; \qquad \theta > (\frac{M_p}{k}) \tag{61b}$$

If $m_p < M_p$, the relationship between m and θ follows Equation 61c and 6ad:

$$m = k\,\theta; \qquad 0 \leq \theta \leq \left(\frac{m_p}{k}\right) \tag{61c}$$

$$m = m_p; \qquad \theta \geq \left(\frac{m_p}{k}\right) \tag{61d}$$

The analysis presented in this sub-section is used to obtain the results presented in Section 3.7 and Section 5.3.3.

3.2.2 Boundary Conditions

Figure 41 describes three different connections m - θ relationships. Line OAB, line OAC and line OAD describe the linear model, bilinear model and elastic-plastic model, respectively. Symbols m and θ represents the resistant moment and end rotation, respectively. The relationship between m and θ for linear connection model is expressed in Equation 62 as below:

$$m = k_a\,\theta; \quad \theta \geq 0 \tag{62}$$

where k_a is the stiffness of the spring. For the bilinear model, the relationship between m and θ is expressed in Equations 63a and 63b as below:

$$m = k_a\,\theta; \quad 0 \leq \theta \leq \theta_a \tag{63a}$$

$$m = m_a + k_b(\theta - \theta_a); \quad \theta \geq \theta_a \geq 0 \tag{63b}$$

where k_a is the initial spring stiffness and is reduced to k_b if the rotations is larger than θ_a. For the elastic-plastic model, the relationship between m and θ is expressed in Equations 64a and 64b as below:

$$m = k_a\,\theta; \qquad 0 \leq \theta \leq \theta_a \tag{64a}$$

$$m = m_a; \qquad \theta \geq \theta_a \geq 0 \tag{64b}$$

where k_a is the initial spring stiffness and m_a is the plastic moment for the spring.

Symbols $\theta_{Ax}, \theta_{Bx}, \theta_{Ay}$ and θ_{By} represent the end rotations of the beam-column shown in Figure 1, which are the first derivative of deflection. The relationships are expressed as below:

$$\theta_{Ax} = v'(0); \ \theta_{Ay} = u'(0); \ \theta_{Bx} = v'(L); \theta_{By} = u'(L) \tag{65}$$

Since the column ends are not allowed to sway, the following four boundary conditions are enforced:

$$v(0) = v(L) = u(0) = u(L) = 0 \tag{66}$$

The boundary conditions prescribed in this section will be utilized in solving Equations 54 and 55.

3.3 Finite Integral Formulation

Finite integral method is a promising method of solving differential equations. It is generally of superior accuracy by comparing with the well-known finite-difference method. Finite integral method has been used successfully in the past by Brown and Trahair (40) to obtain numerical solutions of linear ordinary differential equations on sequential computers. An example of the application of this method for the nonlinear analysis of single angle columns is given by Usami and Galambos (42). Briefly, the procedure involves replacing the continuous differential equations which must be satisfied everywhere by a series of simultaneous equations which represent the differential equations at a series of discrete points. All but the highest differential coefficients in these equations are eliminated by replacing them by linear combinations of the highest differential coefficients and of the constants of integration, these combinations being determined by the method of finite integrals. The resulting simultaneous equations may be combined with the boundary conditions and solved for the highest differential coefficients. The discrete values of the dependent variables are then calculated by back-substitution into the finite integral expressions.

If the variation of a function f over an interval $z_j < z < z_{j+1}$ such that $z_{j+1} - z_j = h$ is approximated by a parabola:

$$f = a z^2 + b z + c \tag{67}$$

and fitted to three adjacent values of f, it can be shown that:

$$\int_{z_i}^{z_{i+1}} f \, dz = \frac{h}{12} (5 f_i + 8 f_{i+1} - f_{i+2}) \tag{68}$$

$$\int_{z_i}^{z_{i+2}} f \, dz = \frac{h}{12} (4 f_i + 16 f_{i+1} + 4 f_{i+2}) \tag{69}$$

For an integral defined by:

$$l_i = \int_0^{ith} f \, dz \qquad (70)$$

The matrix equation formed by single Equation 62 and 63 is written as:

$$\{l_i\} = \frac{h}{12} [N] \{f\} \qquad (71)$$

in which :

$$\{l\} = \{l_0 \ l_1 \ l_2 \ldots\ldots\ldots l_n\}^T \qquad (72)$$

$$\{f\} = \{f_0 \ f_1 \ f_2 \ldots\ldots\ldots f_n\}^T \qquad (73)$$

and N is a square matrix of size $n + 1$ defined by:

$$[N] = \begin{bmatrix} 0 & 0 & 0 & 0 & 0 & 0 & \cdot & \cdot & \cdot \\ 5 & 8 & -1 & 0 & 0 & 0 & \cdot & \cdot & \cdot \\ 4 & 16 & 4 & 0 & 0 & 0 & \cdot & \cdot & \cdot \\ 4 & 16 & 9 & 8 & -1 & 0 & \cdot & \cdot & \cdot \\ 4 & 16 & 8 & 16 & 4 & 0 & \cdot & \cdot & \cdot \\ 4 & 16 & 8 & 16 & 9 & 8 & \cdot & \cdot & \cdot \\ \cdot & \cdot & \cdot & \cdot & \cdot & \cdot & \cdot & \cdot & \cdot \\ \cdot & \cdot & \cdot & \cdot & \cdot & \cdot & \cdot & \cdot & \cdot \end{bmatrix} \qquad (74)$$

If the function l like f is approximated by a series of parabolas, the second integral m of the function f given by:

$$m_i = \int_0^{ith} l \, dz = \int_0^{ith} \int_0^{ith} f \, dz \, dz \qquad (75)$$

can be approximated by:

$$\{m\} = \left(\frac{h}{12}\right)^2 [N]^2 \{f\} \qquad (76)$$

Thus, for a function F, the integrals

$$F_i''' = \int_0^{ith} F^{IV} \, dz \qquad (77)$$

$$F_i'' = \int_0^{ith} \int_0^{ith} F^{IV} \, dz \, dz \qquad (78)$$

$$F_i' = \int_0^{ith} \int_0^{ith} \int_0^{ith} F^{IV} \, dz \, dz \, dz \qquad (79)$$

$$F_i = \int_0^{ith} \int_0^{ith} \int_0^{ith} \int_0^{ith} F^{IV} \, dz \, dz \, dz \, dz \qquad (80)$$

can be approximated, respectively, by :

$$\{F'''\} = \frac{h}{12} [N] \{F^{IV}\} \tag{81}$$

$$\{F''\} = \left(\frac{h}{12}\right)^2 [N]^2 \{F^{IV}\} \tag{82}$$

$$\{F'\} = \left(\frac{h}{12}\right)^3 [N]^3 \{F^{IV}\} \tag{83}$$

$$\{F\} = \left(\frac{h}{12}\right)^4 [N]^4 \{F^{IV}\} \tag{84}$$

Here, $[N]^2 = [N] [N]$; $[N]^3 = [N] [N] [N]$; $[N]^4 = [N] [N] [N] [N]$.

Besides u'' and v'', $u, v, u'(0), u'(L), v'(0), and\ v'(L)$, these lower order derivatives are to be expressed in terms of the respective second order derivatives of $u\ and\ v$. Thus:

$$u' = \int_0^z u'' \, dz + A_1 \tag{85}$$

$$u = \int_0^z \int_0^z u'' dz \, dz + A_1 \, z + A_2 \tag{86}$$

$$v' = \int_0^z v'' \, dz + B_1 \tag{87}$$

$$v = \int_0^z \int_0^z v'' dz \, dz + B_1 \, z + B_2 \tag{88}$$

in which A_i and B_i are constants of integration. These four constants are evaluated using boundary conditions given by Equation 57 and 58 as follows:

$$A_1 = -\frac{1}{L} \int_0^L \int_0^L u'' \, dz \, dz$$

$$A_2 = 0$$

$$B_1 = -\frac{1}{L} \int_0^L \int_0^L v'' \, dz \, dz$$

$$B_2 = 0$$

Therefore, u and v can be expressed by u'' and v'' as follows:

$$u = \int_0^z \int_0^z u'' dz\, dz - \frac{z}{L} \int_0^L \int_0^L u'' dz\, dz$$

$$v = \int_0^z \int_0^z v'' dz\, dz - \frac{z}{L} \int_0^L \int_0^L v'' dz\, dz$$

$$u = (\frac{h}{12})^2 [N]^2 \{u''\} - \left(\frac{h}{12}\right)^2 \frac{1}{L} \{z\}\left[N_n^{(2)}\right]\{u''\} \tag{89}$$

$$v = (\frac{h}{12})^2 [N]^2 \{v''\} - \left(\frac{h}{12}\right)^2 \frac{1}{L} \{z\}\left[N_n^{(2)}\right]\{v''\} \tag{90}$$

The solutions for $u'(0)$, $u'(L)$, $v'(0)$ and $v'(L)$ are shown below:

$$u'(0) = \int_0^0 u'' dz - \frac{1}{L} \int_0^L \int_0^L u'' dz\, dz = -\frac{1}{L}\int_0^L \int_0^L u'' dz\, dz$$

$$u'(0) = -\frac{1}{L}\left(\frac{h}{12}\right)^2 \left[N_n^{(2)}\right] \{u''\} \tag{91}$$

$$u'(L) = \int_0^L u'' dz - \frac{1}{L} \int_0^L \int_0^L u'' dz\, dz$$

$$u'(L) = \frac{h}{12}\left[N_n^{(1)}\right]\{u''\} - \frac{1}{L}\left(\frac{h}{12}\right)^2 \left[N_n^{(2)}\right] \{u''\} \tag{92}$$

Similarly, for $v'(0)$ and $v'(L)$:

$$v'(0) = -\frac{1}{L}\left(\frac{h}{12}\right)^2 \left[N_n^{(2)}\right] \{v''\} \tag{93}$$

$$v'(L) = \frac{h}{12}\left[N_n^{(1)}\right]\{v''\} - \frac{1}{L}\left(\frac{h}{12}\right)^2 \left[N_n^{(2)}\right] \{v''\} \tag{94}$$

where $\left[N_n^{(2)}\right]$ is the last row of the matrix product $[N]^2$ and $[N_n^{(1)}]$ is the last row of the matrix$[N]$.

Substitution u, v, $u'(0)$, $u'(L)$, $v'(0)$, $v'(L)$ into Equation 47 and 48 gives the following system of $2n$ simultaneous nonlinear equations :

$$[K]\{\Delta''\} = \{F\} \tag{95}$$

where $[K]$ is the global stiffness matrix of the order $2n \times 2n$; the vector $\{\Delta''\}$consist of the second order derivatives of u and v and is described as follows:

$$\{\Delta''\} = \{u''v''\}^T = \{u_1'' \quad u_2'' \quad u_3'' \quad \cdots\cdots u_{(n-1)}'' \quad u_n'' \quad v_1'' \quad v_2'' \quad v_3'' \quad \cdots\cdots v_{(n-1)}'' \quad v_n''\} \qquad (96)$$

The moment vector $[F]$ is expressed as below:

$$[F] = \begin{Bmatrix} \{F_{xapplied}\} + \{F_{xre}\} + \{F_{xp}\} \\ \{F_{yapplied}\} + \{F_{yre}\} + \{F_{yp}\} \end{Bmatrix} \qquad (97)$$

The problem presented in this chapter is reduced to solve Equation 95 repeatedly for various external load levels until the beam-columns reach the state of collapse. In the elastic range, F_{xp} and F_{yp} are zero vectors and the rest moment terms are able to be explicitly defined and Equation 95 can be solved directly. In the inelastic range, however, the elements in global stiffness matrix $[K]$ and the components of vector of F_{xp} and F_{yp} would be functions of u'' and v'' at each load level. When the determinant of $[K]$ matrix is coming to zero, the member load-carrying capacity is reached.

3.4 Solution for Nonsway Beam-columns at Ambient Temperature

3.4.1 Solution Procedures

Razzaq and Calash (9) presented a finite-difference based algorithm for solving nonlinear governing equations for columns with biaxial flexure. Herein, a finite integral based algorithm is developed for solving nonlinear governing equations for beam-columns with partial end-rotation restraints. The solution steps are expressed as below:

1. Evaluate the initial cross-sectional properties at n nodes along the member length and assemble the initial global nonsway beam-column stiffness matrix $[K]$ in Equation 96.

2. Specify small external loads and formulate $\{F\}_1$ following Equation 97.

3. Solve the second order derivatives vector $\{\Delta''\}$ in Equation 96 and then use Equation 89 and 90 to solve the deflection vector $\{\Delta\}$.

4. Compute the external nodal forces $\{f\}_1$ and deformations $\{\delta\}_1$ defined in Equation 33 and Equation 34, respectively, in the elastic range corresponding to $\{F\}_1$.

5. Increase $\{F\}$ to$\{F\}_2 = \{F\}_1 + \{\delta F\}$, in which $\{\delta F\}$ is the resultant load increment vector. Solve $\{\Delta''\}$ and $\{\Delta\}$ and then compute the external force vector $\{f\}_2$ corresponding to$\{F\}_2$.

6. Using$\{f\}_1$, $\{f\}_2$, $\{\delta\}_1$and ϵ_r compute $\{\delta\}_2$ using the tangent stiffness procedure as defined in Reference 41 for all cross sections.

7. Solve for an updated $\{\Delta''\}$ and $\{\Delta\}$ after assembling $[K]$ utilizing the cross-section properties obtained in step 6.

8. With the undated $\{\Delta''\}$ and$\{\Delta\}$ in step 7, formulate the load vector$\{F\}_3$. If $|\{F\}_3 - \{F\}_2| \leq \alpha$ where α is the tolerance, go to step 10.

9. Set $\{F\}_2 = \{F\}_3$; $\{f\}_2 = \{f\}_3$ and go to step 6.

10. Set $\{F\}_1 = \{F\}_3$; $\{f\}_1 = \{f\}_3$ and repeat steps 5-10 until the load-carrying.

The procedure described herein is carried out using constant load increments throughout the elastic range. In the inelastic range, the load increments are successively reduced to avoid severe imbalance between the external load and the internal forces. The maximum load is obtained within 0.0001 times the cross-sectional yield capacity.

3.5 Load Paths

Different load paths are designed for the uniaxially and biaxially loaded beam-columns, which are the same as those of Darbhamulla (11) used.

Referring to Figure 20, two different load paths are used for uniaxially loading at ambient temperature, which are described below:

NP1: The axial load P is first applied incrementally and then held constant, followed by gradually increasing equal end moments until the load-carrying capacity of the member is reached. This corresponds to the path OAE for the member minor axis analysis, or OAB for the member major axis analysis.

NP2: The equal end moments corresponding to the load-carrying capacity obtained in NP1 are applied first incrementally and held constant, followed by gradually increasing axial load P until the member collapse occurs. This corresponds to the path OGE and OCB for the member minor and major axis analyses, respectively.

Referring to Figure 20, six different load paths are used for biaxially loading at ambient temperature, which are described below:

NP3: The axial load P is first applied incrementally and then held constant, followed by gradually increasing equal end moments M_x and M_y until the load carrying capacity of the member is reached. The moment ratio is held constant and taken as follows:

$$M_x/M_y = r_x/r_y \tag{98}$$

where r_x and r_y are the major and minor axis radius of gyration. This load path corresponds to OAD.

NP4: The end equal moments M_x and M_y are first applied proportionally following Equation 90 until the peak moment values from NP3 are attained, and then P is applied until the member collapses. NP4 corresponds to the path OFD.

NP5: The axial load P of the same magnitude as in NP3 is applied first, M_x achieved in NP3 is applied next, followed by M_y until collapse occurs. NP5 corresponds to the load path OABD.

NP6: This load path is the reverse of NP5 in which M_y achieved in NP3 is applied first, followed by M_x achieved in NP3, and lastly followed by P until collapse occurs. NP6 corresponds to load path OGFD.

NP7: The axial load P of the same magnitude achieved in NP3 is applied first, M_y achieved in NP3 is applied next, followed by M_x until collapse occurs. This corresponds to load path OAED.

NP8: This load path is the reverse of NP7, in which M_x achieved in NP3 is applied first, followed by M_y achieved in NP3, and finally followed by P until the load-carrying capacity is reached. NP8 corresponds to load path OCFD.

For the double symmetrical section, NP7 and NP8 are redundant and correspond, respectively, to NP5 and NP6.

3.6 Numerical Study for Nonsway Beam-columns at Ambient Temperature

In this section, the behavior of imperfect beam-columns with I-section or hollow rectangular section subjected to different load paths noted as LP1 through LP4 are investigated. The influence of rotational end restraints, load sequence, initial crookedness and residual stress are studied.

3.6.1 Approach Corroboration

To assess the accuracy of the computational procedure, comparisons are made between some published and predicated results. Razzaq (8) theoretically studied the influence of partial end restraints on the behavior of imperfect columns. The imperfect include the initial crookedness and residual stress. Razzaq (10) also conducted experimental tests to study the inelastic behavior of biaxially loaded hollow rectangular steel columns. Tables 8 and 9 summarize the comparisons of the predicted results to those of from Reference 9 and 10 for some cases, which show that a good agreement is reached between the results from references and this investigation.

Birnstiel (43) experimentally observed the behavior of isolated steel H-columns loaded eccentrically with respect to both principal axes of the end cross sections. Sharma and Gaylord (44) theoretically studied the strength of steel columns with I-section under biaxially eccentric loading. The maximum loads predicted in this investigation are in good agreement with those in References 43 and 44; the comparisons are summarized in Tables 10 and 11, respectively.

3.6.2 Connection Modeling

In the early 1960's, Lewitt, Chesson, and Munse (45) experimentally studied the behavior of flexible riveted and bolted beam-to-column connections and the factors which influence their moment-rotation characteristics. It was found that the experimental moment-rotation curve was nonlinear. To get a better representation of the connection stiffness, or to simplify the analysis technique, a number of simplified models have been proposed, as shown in Figure 42. Rathbun (47) proposed a linear model, in which the first initial stiffness presents the behavior of connection for the entire loading range. To get a better representation, Romstad and Subramanian (48) used the bilinear model, in which the initial slope of the moment-rotational line was replaced by a shallower line at a certain transition moment. Razzaq (8) had developed the piecewise linear model, a direct extension of the bilinear model in which the nonlinear m-θ curve for the connection is represented by a series of straight line segments.

Darbhamulla (11) used a set of piecewise-linear models to study the effect of various m-θ models on the load-carrying capacity of centrally loaded I-section columns

and uniaxially loaded I-section beam-columns. It was found that the effect of the m-θ relationships on the column peak loads about minor and major axis was not significant. Six m-θ models, shown in Figure 43, were used to investigate the strength of uniaxially loaded W8 × 31 section beam-columns. The information about the beam-column is described below: length of beam-column is 15 ft; an axial load P and an end moment, M_{By}, at the member top, are applied, which are in a proportional manner such that the ratio between P and M_y is 2.25 ($P/M_{By} = 2.25$); at $z = 0$, a pinned condition is used which means $k_{Ax} = k_{Ay} = 0.0.$; whereas, a partial rotational end restraint is provided at $z = L$ to simulate the sub-assemblage used in Reference 46, which means $k_{Bx} = 0.0$ and $k_{By} \neq 0.0$. Six different kinds of models, $a2$ through $f2$, are used to find the peak load of the beam-column. It was found the peak load varied in a small range from 0.64 to 0.71. The maximum load obtained by Chen and Lui (46) was 0.64 comparing with these results. In this investigation, the m-θ model, $e2$ shown in Figure 43, is adopted and the peak load is 0.65, which is perfectly matching with those from References 11 and 46. The elastic-plastic model $e2$ was called the power model proposed by Colson (49).

3.6.3 Imperfect Beam-column Behavior

Herein, a 144-inch long hollow square section with the dimensions 7×7×0.375 steel beam-columns with E and σ_Y equal 29,000ksi and 46ksi, respectively, is adopted. The residual stresses, if present, follows the pattern shown in Figure 18, and σ_{rt} and σ_{rc} values are taken as $0.5\sigma_y$ and $-0.2\sigma_y$, respectively. For the initial out-of-straightness, the midspan amplitudes are taken as $L/100,000$ and $L/1000$ for the nearly straight and initially crooked beam-column.

Figure 44 shows the load versus deflection curves for the pinned imperfect columns with hollow square section. Symbols NS, UC and BC represent that column is nearly straight, uniaxially crooked and biaxial crooked, respectively. Symbols NR and WR represents that t the residual stress is absent and present, respectively. The dimensionless peak load p is 0.997 for the NS-NR-column; 0.935 is for the NS-WR-column; 0.907 is for UC-NR-column; 0.864 is for the UC-WR-column; 0.871 is for the BC-NR-column; 0.828 is for the BC-WR-column. It is found that residual stress and initial crookedness reduce the maximum load for the columns. The effect of initial crookedness on the load carrying

capacity is larger than that of residual stress. The corresponding bending stiffness degradation curves for these columns are shown in Figure 45. The dimensionless determinant D is defined as follows:

$$D = |[K_t]|/|[K_t]|_0 \qquad (98)$$

in which $|[K_t]|_0$= determinant for zero axial load. Razzaq (8, 9) clearly compared and summarized the effects of residual stress and initial crookedness on the behavior of the column. The curves shown in Figures 44 and 45 are same in nature to those in Reference 9.

Figures 46 and 47 show the load versus deflection curves and bending stiffness degradation curves for the imperfect beam-column with initially applied uniaxial moment equal to $0.5M_Y$. The dimensionless peak load p is 0.445 for NS-NR-beam-column; 0.472 is for NS-WR-beam-column; 0.427 is for the UC-NR-beam-column; 0.451 is for the UC-WR-beam-column; 0.425 is for the BC-NR-beam-column; 0.450 is for the BC-WR-beam-column. The influence of initial crookedness on the strength limit of beam-column is not significant when the applied moment is relatively larger. However, the influence of residual stress on the behavior of the beam-column is significant. The effect of residual stress at beginning of applying axial load is minuscule. Figure 47 shows that D-p relationship remains identical in the elastic range for those six beam-columns. Beyond the elastic range, the D-p curves follow different descending paths, depending upon the type of imperfections. A comparison of the inelastic portions of the D-p curves for beam-columns with residual stresses to those without residual stresses reveals that although the former group experience earlier stiffness degradation due to early yielding, they are still stronger that the latter group

3.6.4 Behavior of Uniaxially Loaded I-section Beam-columns

Darbhamulla (11) had studied the behavior of uniaxially loaded I-section beam-column. Four load paths LC1 through LC4 were adopted, which are described below:

LC1: Corresponding to the load path LP1, a relatively large axial load is applied first incrementally and held constant, followed by gradually increasing equal end moments until the member collapses.

LC2: The maximum end moments corresponding to the load condition LC1 are applied first incrementally and held constant, followed by a gradually increasing the axial load until the member collapses, thus following load path LP2.

LC3: Corresponding to the load path LP2, relatively large equal end moments are applied first incrementally and held constant, followed by gradually increasing the axial load until the member collapses.

LC4: The maximum axial load corresponding to the load condition LC3 is applied first incrementally and held constant, followed by gradually increasing equal end moments until the member collapses thus following the load path LP1.

It was found that the load paths had no significant effect on the member strength for the major axis, but it did affect the minor axis if the beam-column was with elastic restraints. Also, it was found that the maximum loads were not load path dependent in the presence of elastic-plastic restraints.

Herein, the same numerical study the effects of load sequence for uniaxially loaded I-section beam-columns is conducted. The chosen beam-column is described below: the cross section is W8x31and the length is 144in.; the material properties follow the stress-strain law shown in Figure 16; here E and σ_y are taken as 29,000ksi and 50ksi; the residual stress follows the type shown in Figure 20 when it is present; the elastic m-Θ model is adopted with spring stiffness $k_{a1} = 0$ in-kip/rad, $k_{a2} = 13,333$ in-kip/rad, $k_{a3} = 24,000$ in-kip/rad, individually. In addition, the behavior of the beam-column with elastic-plastic end springs is also studied; the initial spring stiffness is k_{a2} and the plastic spring moment limit value $m_a=100$ in-kips.

Table 12 summarizes the maximum dimensionless peak loads for the major and minor axis analyses using load path through LC1 to LC4 with elastic restraints. Here, $p = P/P_Y$, $m = M_{major}/M_{major-Y}$ or $m = M_{minor}/M_{minor-Y}$. By comparing the results, it is found that the load-carrying capacity is almost same for the beam-column with pinned boundary conditions; in other words, the member strength is not load path dependent for the member with pinned conditions. The maximum loads for the major axis are nearly the same, suggesting that the load paths have no significant effect on the member strength. However, the peak loads for the minor axis are load path dependent; moreover, LC1 and LC2 provide nearly same peak loads, while LC3 and LC4 exhibit a

substantial difference in the maximum loads. In the absence of initial residual stress, m for LC4 is 3.3% less than that for LC3 when the stiffness is k_{a3}. The difference is 11.1% when the initial residual stresses are included.

Table 13 collects the maximum dimension peak loads for elastic-plastic restraints and load paths through LC1 to LC4. The results indicate that the maximum loads for both the minor axis and major axis are not load path dependent in the presence of elastic-plastic restraints.

To further study the effect of load sequence on the behavior of I-section beam-column under uniaxial bending about minor axis. A analysis with 144-inch long W8×31 steel member with elastic restraints are conducted. Load paths NP1 and NP2 are adopted. Table 14 collects all the maximum dimensionless load values, which indicates that the member load-carrying capacity is load path dependent for such load combination with relative large moment and small axial load. For example, for the member with spring stiffness k_{a2} and axial load $p = 0.362$, the maximum moment is 4.500 for load path NP2, which is 23.3% larger than that of NP1 (3.649).

3.6.5 Behavior of Biaxially Loaded I-section Beam-columns

In this study, twisting is neglected for studying the biaxially loaded I-section beam-columns based on the past research from Birnstiel (43) and Sharma and Gaylord (44). Darbhamulla (11) had investigated the effects of nonproportional loading on biaxially loaded I-section beam-columns with elastic partial restraints. It was found that the load path dependency was obviously in the nonproportionally loaded I-section beam-columns. In this investigation, the same case, a 144-inch long W8×31 section member with residual stress and elastic partial restraints was adopted. The initial crookedness was taken as L/1000. The residual stress follows the type shown in Figure 19, $\sigma_{rc} = -0.3\sigma_Y$. The material properties follow the stress-strain law shown in Figure 17; here E and σ_y are 29,000ksi and 50ksi. The elastic m-Θ model is adopted with spring stiffness$k_{a2} = 13,333$ in-kip/rad.or $k_{a3} = 24,000$ in-kip/rad. Load paths NP3 and NP4 are used. The moment ratio is held constant and taken as follows: $M_x/M_y = r_x/r_y$. Here, the major axis of cross section W8×31 is called x axis; the minor axis is called y axis. Table 15 summarizes the maximum dimensionless loads for various load conditions, herein, $m_x =$

M_x/M_{xY} and $m_y^*=M_y/M_{xY}$. The results show that load path dependency is obviously present in the non-proportionally loaded I-section beam-columns when the applied moments are relative larger. Otherwise, load path independence is not significant. The interaction curve between p and m_y^*, shown in Figure 48 describes the characteristic. For the load combination with relative larger axial load, the interaction curves of NP3 and NP4 almost coincide for the range with relative larger axial load. However, when the axial load is getting small, the difference between moments from NP3 and NP4 is getting larger.

3.6.6 Behavior of Hollow Rectangular Beam-columns

Razzaq and McVinnie (10) theoretically and experimentally studied the behavior of biaxially loaded hollow rectangular columns and found that twisting could be neglected for columns with hollow-square or rectangular section. Darbhamulla (11) studied the hollow rectangular beam-columns subjected to different load paths NP3 through NP8 as defined in Section 3.5.2. It was found that the maximum loads for beam-column with pinned boundary conditions was load path independent; however, it was load path dependent for beam-columns with elastic spring restraints for certain load combinations. In this section, the same cases are investigated to further study the effect of load path on the load-carrying capacity. The details of the studied beam-columns are described below:

Hollow square sections, $7.0 \times 7.0 \times 0.375$ in. and rectangular, $8.0 \times 6.0 \times 0.375$ in. are used herein. The specimen length is 144in. long; the initial midspan amplitude is taken as $L/1000$. The residual stress distribution follows the pattern shown in Figure 19. The material stress-strain relationship follows the model shown in Figure 16. The rotational end restraints are identical for both ends about the x and y axes. The three beam-columns designated as BC1, BC2 and BC3 are studied:

BC1: hollow square section with $k = k_{a1} = 0$ k-in/rad

BC2: hollow square section with $k = k_{a3} = 24,000$k-in/rad

BC3: hollow rectangular section with $k = k_{a3} = 24,000$k-in/rad

Tables 16 through 18 summarize the dimensionless maximum load for nonproportionally loaded imperfect beam-column BC1, BC2 and BC3, respectively. Table 16 shows that the strength limits are exactly same for beam-column BC1 with load

paths through NP3 through NP6, which indicates that load path doesn't affect the load-carrying capacity of the steel member with pinned boundaries. However, in Tables 17 and 18 for the beam-columns BC2 and BC3, significant load path dependence is found for the load combinations with the relative larger bending moments. For example, the load path effect is not significant or can be ignored if p is larger than 0.25 for load path NP3 through NP8. Figures 49and 50 shows the interaction curves for hollow square beam-column BC3 with load path NP5 and NP6 ,which shows that the interaction curves for NP5 and NP6 almost coincide to the same line when the load combination has a relative small p value. The same rule can be found in the interaction curves for load path Np7 and NP8 for BC3, shown in Figures 51 and 52.

3.7 Dilemma with Large External Moment

For the member with rotational end restraints and only subjected bending moment, the maximum applied moment will be a large value when the cross section is fully plastified. There are always a few elements of cross section near the neutral axes, which are hardly getting plastified. The explanations for this appearance is that the end springs following the elastic model take over most of the applied external moment. It is found that near the range of fully plastified, the increase of the internal moment is very small. Section 3.2.1 also explains this phenomenon. The resistant moment equal the end rotation times the stiffness of the restraint, which will be large if the end rotation is large. The most part of applied moment is killed by the end restraints. Figure 53 describes the relationship between the internal moment and the end rotation, which shows that the curve is getting flat at the last part indicating that near the fully plastified the internal moment increase slowly. Using the different load-steps, the difference between the internal moment gained from the numerical analysis and cross section plastic moment is less than 3%. Figure 54 shows the load versus deflection curve for beam-column BC3, which indicates that the relative large displacements near the collapse load.

3.8 Comparisons of Theoretical and Experimental Results

The comparisons between the theoretical results and experimental results at ambient temperature are collected in Tables 19 and 20. The ratios between predicted and tested

results ranged from 0.96 to 1.14 for pinned boundary conditions. The ratios ranged from 1.08 to 1.20 for partially fixed boundary conditions except RTUS-16. The good agreement is achieved between the experimental results and theoretical results. The ratio between predicted and tested result is 1.44 for RTUS-16. The values are relatively higher than that of pinned boundary conditions. One of reasons for that is that the end spring restraints do not function properly which means there is movement between the machined arm and the gimbal shaft during testing, shown in Figure 6. For pinned boundary conditions, load path does not have a significant effect on the beam-column load carrying capacity.

Figures 55 compare the experimental and theoretical moment versus deflection curves for beam-columns under uniaxial loading and different load combination and with pinned boundary conditions. There is one thing need to be mentioned that in the symbol 'exp' and 'pre' in the figures represent the value from experimental test and predicted from theoretical analysis, respectively. For the case of only applying uniaxial bending ($p = 0.0$), at the beginning part two curves coincide. After the moment value is larger than 0.567, the deflection value from experimental tests is larger than that of from predicted results. The maximum value from experimental test is about 6.7% high than that of predicted value. For the case of $p = 0.23$, two curves coincide at the beginning part; the predicted curve is away from theoretical one with the increase of moment. The predicted maximum moment value is about 11.7% higher than that of experimental result. For the case of $p = 0.39$, the predicted deflection value is about 4.4% larger than that of experimental value at the same moment value. It is found that a good agreement is reached between the tested and predicted results.

Figure 56 compare the experimental and theoretical load versus deflection curves for beam-columns under uniaxial loading and different load combination and with pinned boundary conditions. For the case of only applying axial load ($m = 0.0$), two curves coincide until near the peak value. The predicted maximum axial load value is about 14.0% higher than that of experimental value. For the case of $m = 0.648$, two curves are perfect matching. The predicted maximum load value is almost the same with that of experimental value. For the case of $m = 0.995$, the predicted maximum load value is

about 6.0% larger than that of experimental value. It is found that a good agreement is reached between the tested and predicted results.

Figures 58 to 59 exhibit the phenomenon the material unloading for biaxially loaded imperfect beam-column RTBP-5 with load path NP3. Figure 58 shows the stiffness degradation curve D-p. Before applying the axial load, some elements of the beam-columns are plastified. Figure 47 demonstrates the distribution of the plastic area for nodes 5, 6, 7, 8 and 9. The plastified elements are shaded dark. The studies herein are based on adopting a total of 228 element areas for each of 9 nodes along the member length. Some of the plastified elements unload elastically, thereby resulting in an increase in the beam-column stiffness. Figure 59 shows the plastified elements corresponding to the state after applying the axial load.

The stiffness degradation curve in the Figure 57 for load path NP3 shows valleys in the form of near-abrupt changes (called by Darbhamulla in Reference 11) in D which indicates that the beam-column suddenly loses a considerable stiffness followed by an immediate gain with a small variation in the loads. When the member of the elemental areas was increased to 912, the number and shapes of these valleys decrease but this did not affect the peak loads, as shown Figure 57. Additionally, it was found the number and shape of these valleys could both increase and decrease, with the change of load steps. The good thing is this change doesn't affect the peak load too much: less than 3.0%.

CHAPTER

4. THEORECTICAL ANALYSIS FOR STEEL BEAM-COLUMNS

AT HIGH TEMPERTURE

The theoretical analysis of the behavior of nonproportionally loaded steel beam-columns at high temperatures is presented in this chapter. The analysis is conceptually similar to the beam-column analysis at ambient temperature. However, it is complicated by the presence of elevated temperatures on the internal forces and the material properties. There are three different axial restraints to the thermal expansion considered: rigid axial restraint, finite axial restraint and no restraint. Critical temperature corresponding to the zero load-carrying capacity is estimated and also the critical load is determined with a specified high temperature.

4.1 Total Mechanical Strain for Steel Beam-column at High Temperature

It is assumed that the initially crooked beam-column AB, shown in Figure 1 is subjected to uniform temperature T, axial load P and biaxial bending moment M_x and M_y. The responding discretized hollow rectangular and I-shaped sections are shown schematically in Figures 36 and 37. The total mechanical strain ε_T, at a point (x, y) of a cross section includes mechanical or stress-related strain, being a function of both the applied stress and the temperature, and thermal strain being a function only of temperature, T, which is expressed in Equation 97.

$$\varepsilon_T = \varepsilon_{oT} + \Phi_{xT}\, y - \Phi_{yT}\, x + \varepsilon_{th}^* \tag{99}$$

in which ε_{oT} is the average axial strain; Φ_{xT} and Φ_{yT} are the bending curvatures about the x and y axes, respectively; ε_{th}^* is the thermal strain or the part of thermal strain which will cause the stress change. Herein, one thing needs to be mentioned. The residual stress ε_r is missing in the total normal strain equation because the residual stress releasing happens with high temperature. The mechanical strain also follows the sign rule: tensile strain is positive and compressive is negative.

A heated member experiences thermal expansion due to thermal gradient. The classifications of axial restraint to thermal expansion in the US or relative to ASTM E119 are shown in Figure 22 (50). For the beam-column with free axial expansion, the thermal

strain will not change the stress state. In other words, ε_{th}^* equals zero. The cross section mechanical strain can be expressed below:

$$\varepsilon_T = \varepsilon_{oT} + \Phi_{xT}\, y - \Phi_{yT}\, x \tag{100}$$

For the beam-column with rigid axial restraint to thermal expansion, it will be hardly allowed to expand. The member deformation in length is zero throughout the elevated temperature increasing. Therefore, the mechanical strain will be equal and opposite of the thermal strain. The cross section mechanical strain related to stress state for this case can be expressed below:

$$\varepsilon_T = \varepsilon_{oT} + \Phi_{xT}\, y - \Phi_{yT}\, x - \varepsilon_{th} \tag{101}$$

The mechanical strain caused by the axial restraint to thermal expansion is compressive, which is negative.

For the beam-column with finite axial restraint, the deformation of beam-column in length is ΔL and the responding strain is $\Delta L/L$. For this case, the mechanical strain ε_{th}^* can be expressed as a part of thermal strain, shown in Equation 100.

$$\varepsilon_{th}^* = \varepsilon_{th} - \frac{\Delta L}{L} \tag{102}$$

The corresponding cross sectional normal strain at a point(x, y) can be expressed below:

$$\varepsilon_T = \varepsilon_{oT} + \Phi_{xT}\, y - \Phi_{yT}\, x - \left(\varepsilon_{th} - \frac{\Delta L}{L}\right) \tag{103}$$

If the axial restraint to thermal expansion is assumed to the axial spring, the stiffness of the spring k_{ts} is computed as follows:

$$k_{ts} = \alpha \left(\frac{EA}{L}\right) \tag{104}$$

where α is axial spring stiffness parameter, and E, A and L are elastic modulus of steel at the ambient temperature, cross-sectional area and span length, respectively. Then the developed extra compressive force, P_T , is able to be expressed as:

$$P_T = k_{ts} \left(\varepsilon_{th} - \frac{\Delta L}{L}\right) = \alpha \left(\frac{EA}{L}\right) \left(\varepsilon_{th} - \frac{\Delta L}{L}\right) \tag{105}$$

It needs to be mentioned that the axial restraint is assumed to remain at the geometrical centroid of the beam-column. In other words that the axial spring only has axial deformation.

4.2 Temperature-thrust-moment-curvature Relations

The cross sectional equilibrium equations for the beam-column shown in Figure 1subjected the axial thrust, bending moments about x and y axes, and high temperature are described as below:

$$P = -\int_A \sigma_T \, dA \tag{106}$$

$$M_x = \int_A \sigma_T \, y \, dA \tag{107}$$

$$M_y = -\int_A \sigma_T \, x dA \tag{108}$$

Substitute Equations 13a, 13b and 13c into Equations 106 through 108 and the equilibrium equations are presented below:

$$P^* = -\int_{Ae} \sigma_{eT} \, dA - \int_{Ap} \sigma_{YT} \, dA \tag{109}$$

$$M_x = \int_{Ae} \sigma_{eT} \, y \, dA + \int_{Ap} \sigma_{YT} \, y \, dA \tag{110}$$

$$M_y = -\int_{Ae} \sigma_{eT} \, x \, dA - \int_{Ap} \sigma_{YT} x \, dA \tag{111}$$

where P^* is the summation of applied axial load P and the additional compressive force caused by restrained thermal strain; dA is an elemental area of the cross section; σ_{eT} and σ_{YT} are the normal stress and the yield stress at temperature T; the subscripts e and p refer to the elastic and plastic elements, respectively, for a partial plastified section; $\int_A$ denotes cross sectional integration. Equations through 109 to 111 are expressed below:

$$P^* = -\int_{Ae} E_T \, \varepsilon_T dA - \int_{Ap} \sigma_{YT} \, dA \tag{112}$$

$$M_x = \int_{Ae} E_T \, \varepsilon_T \, y \, dA + \int_{Ap} \sigma_{YT} \, y \, dA \tag{113}$$

$$M_y = -\int_{Ae} E_T \, \varepsilon_T \, x \, dA - \int_{Ap} \sigma_{YT} x \, dA \tag{114}$$

It is same as that of the ambient temperature analysis, the relationship between the infinitesimal stress and strain increment need to be established to get the beam-column plastic behavior with high temperatures. The mechanical strain rate $\dot{\varepsilon}_T$ at high temperature is presented in Equation 115.

$$\dot{\varepsilon}_T = \dot{\varepsilon}_{0T} + \dot{\Phi}_{xT}\, y - \dot{\Phi}_{yT}\, x + \dot{\varepsilon}_{th}^* \qquad (115)$$

The stress-mechanical strain rate relationship at elevated temperatures is presented by the following Equation 116:

$$\dot{\sigma}_T = E_{Tt}\, \dot{\varepsilon}_T \qquad (116)$$

in which E_{Tt} equals E_T if the material is in the elastic range; it equals zero if the material is in the plastic range. The cross-sectional load and deformation vectors, $\{f_T\}$ and $\{\delta_T\}$, can be expressed as follows:

$$\{f_T\} = \{\, P^*\ \ M_x\ \ M_y\,\}^T \qquad (117)$$

$$\{\delta_T\} = \{\, \varepsilon_{oT} + \varepsilon_{th}^*\ \ \Phi_x\ \ \Phi_y\,\}^T \qquad (118)$$

The responding cross-sectional load and deformation rate vector are expressed as follows:

$$\{\dot{f}_T\} = \{\dot{P}^*\ \ \dot{M}_x\ \ \dot{M}_y\,\}^T \qquad (119)$$

$$\{\dot{\delta}_T\} = \{\, \dot{\varepsilon}_{0T} + \dot{\varepsilon}_{th}^*\ \ \dot{\Phi}_{xT}\ \ \dot{\Phi}_{yT}\,\}^T \qquad (120)$$

The elements of load vector rat $\{\dot{f}\}$ are able to be calculated:

$$\dot{P}^* = -\int_{Ae} E_T\, \dot{\varepsilon}_T dA \qquad (121)$$

$$\dot{M}_x = \int_{Ae} E_T\, \dot{\varepsilon}_T\, y\, dA \qquad (122)$$

$$\dot{M}_y = -\int_{Ae} E_T\, \dot{\varepsilon}_T\, x\, dA \qquad (123)$$

where $\dot{P}^*$ is the summation of the change of the applied axial load and the change of the additional axial load caused by temperature gradient. The relationship between the load rate and mechanical strain vectors at high temperature is expressed as:

$$\{\dot{f}_T\} = [k_T]\{\dot{\delta}_T\} \qquad (124)$$

where $[k_T]$ is the cross-sectional tangent stiffness matrix, which is defined below:

$$[k_T] = \begin{bmatrix} -\int E_{Tt}\, dA & -\int E_{Tt}\, y\, dA & \int E_{Tt}\, x\, dA \\ \int E_{Tt}\, y\, dA & \int E_{Tt}\, y^2\, dA & -\int E_{Tt}\, xy\, dA \\ -\int E_{Tt}\, x\, dA & -\int E_{Tt}\, xy\, dA & \int E_{Tt}\, x^2\, dA \end{bmatrix} \tag{125}$$

All the elements in the k_T matrix are constant throughout the elastic range. However, in the material plastic range, those elements are functions of the current state of stress, strain and temperature as well as the properties of the material, cross section and temperature. Thus, given an axial load P, a pair of bending moments M_x and M_y and the specified high temperature T, compatible ϵ_{oT}, Φ_{xT} and Φ_{yT} can be found following Equation 124. The solution procedure is the same with that of the ambient temperature analysis.

4.3 Equilibrium Equations for Beam-columns at High Temperature

Substitute Equation 100 into Equations 112 through 114 and the differential equilibrium equations for beam-column at high temperature are obtained below:

$$a_{11}\, \varepsilon_{0T} + a_{12}\, v_T'' + a_{13}\, u_T'' + P_{th} - P_p = P^* \tag{126}$$

$$a_{21}\, \varepsilon_{0T} + a_{22}\, v_T'' + a_{23}\, u_T'' - M_{xth} + M_{xp} = M_x \tag{127}$$

$$a_{31}\, \varepsilon_{0T} + a_{32}\, v_T'' + a_{33}\, u_T'' + M_{yth} - M_{yp} = M_y \tag{128}$$

where $v_T'' = -\Phi_{xT}$, and $u_T'' = \Phi_{yT}$; P^*, M_x and M_y are the external axial load and biaxial bending moments; P_{th}, M_{xth} and M_{yth} are the axial force and bending moments about x and y axes, respectively, due to the restrained thermal strain for the area in elastic range; P_p, M_{xp} and M_{yp} are the axial force and moment parameters for the elements which are already plastified. The coefficients a_{ij}, are defined in Section 3.1.2.

The external moments M_x and M_y at any location z can be expressed as follows:

$$M_x = M_{Ax} - m_{Ax} + P^*(v_T + v_o) - \frac{z}{L}(M_{Ax} - M_{Bx} + m_{Bx} - m_{Ax}) \tag{129}$$

$$M_y = -M_{Ay} - m_{Ay} - P^*(u_T + u_o) + \frac{z}{L}(M_{Ay} - M_{By} + m_{By} - m_{Ax}) \tag{130}$$

At the global level, ε_{0T} is solved explicitly in Equation 115 and then ε_{0T}, M_x and M_y are substituted into Equations 116 and 117. This results into the following two materially nonlinear ordinary differential equations:

$$\left(E_T A_e I_{xye} - E_T S_{xe} S_{ye}\right) u_T'' + \left(E_T A_e I_{xe} - E_T S_{xe}^2\right) v_T'' + A_e P^* \ v_T$$

$$-A_e \frac{L-z}{L} m_{Ax} - A_e \frac{z}{L} m_{Bx} = F_{xapplied,T} + F_{xp} \tag{131}$$

$$\left(E_T A_e I_{ye} - E_T S_{ye}^2\right) u_T'' + \left(E_T A_e I_{xye} - E_T S_{xe} S_{ye}\right) v_T'' + A_e P^* \ u_T$$

$$-A_e \frac{L-z}{L} m_{Ay} + A_e \frac{z}{L} m_{By} = F_{yapplied,T} + F_{yp} \tag{132}$$

where F_{xp} and F_{yp} symbolize the moment vectosr due to the plastification, following Equations 49c and 49f, respectively; $F_{xapplied,T}$ and $F_{yapplied,T}$ are the moment vectors due to restrained thermal expansion and the applied load and moments for the elastic area, which are expressed below:

$$F_{xapplied,T} = -S_{xe} \ P^* + A_e(-P^* \ v_0 + \frac{(z-L)}{L} M_{Ax} - \frac{z}{L} M_{Bx)} \tag{133}$$

$$F_{yapplied,T} = -S_{ye} \ P^* + A_e(-P^* \ u_0 + \frac{(z-L)}{L} M_{Ay} - \frac{z}{L} M_{By)} \tag{134}$$

By using the finite integral method, u_T, v_T and their first order derivatives are able to be expressed by the second order derivative, as defined in Section 3.3. If the beam-columns over $[0, L]$ are divided into (N-1) equivalent segments, the following Equation 124 will be $2N$ simultaneous nonlinear equations.

$$[K_T]\{\Delta_T''\} = \{F_T\} \tag{135}$$

where $[K_T]$ Is the global stiffness matrix of the order $2N \times 2N$; the vector $\{\Delta_T''\}$ consist of the second order derivatives of u_T and v_T is expressed as below:

$$\{\Delta_T''\} = \{u_T'' \ v_T''\}^T = \{u_{T1}'' \ u_{T2}'' \ \cdots\cdots u_{T(n-1)}'' \ u_{Tn}'' \ v_{T1}'' \ v_{T2}'' \ \cdots\cdots v_{T(n-1)}'' \ v_{Tn}''\} \tag{136}$$

The moment vector $\{F_T\}$ is described as below:

$$\{F_T\} = \left\{ \begin{array}{c} \{F_{xapplied,T}\} + \{F_{xp}\} \\ \{F_{yapplied,T}\} + \{F_{yp}\} \end{array} \right\} \qquad (137)$$

The problem of inelastic behavior and the strength of beam-column at high temperature is reduced to solving the Equation (135) for external loads and temperatures up to the collapse condition. The boundary conditions are the same as that of the ambient temperature analysis, as defined in Equations 65 and 66. In the elastic range, $\{F_{xp}\}$ and $\{F_{yp}\}$ are zero vector and other moment terms are able to be explicitly defined and Equation 135 can be solved directly. In the inelastic range, however, the elements in matrix $[K_T]$ and the components of vectors of $\{F_{xp}\}$ and $\{F_{yp}\}$ would be functions of u'', v'' and temperature T at each load level. As the determinant of $[K_T]$ matrix approaches to zero, the maximum strength of the beam-column is reached.

4.4 Solution Procedures at High Temperature

The numerical solution procedure for analysis of the elastic-plastic behavior of nonsway steel beam-columns at high temperature is basically the same as that given by Section 3.4.1 , which is described as below:

1. Specify the small external nodal loads and low temperature, P_1, M_{x1}, M_{y1} and T_1, and formulate $\{F_T\}_1$ using Equation 137.

2. Solve for the second order derivatives vector $\{\Delta_T''\}$ in Equation 135 and then use Equations 89 and 90 to solve the deflection vector $\{\Delta\}$.

3. Compute the external nodal forces $\{f_T\}_1$ and deformations $\{\delta_T\}_1$ defined in Equations 119 and 120, respectively, in the elastic range corresponding to $\{F_T\}_1$.

4. Increase $\{F_T\}$ to $\{F_T\}_2 = \{F_T\}_1 + \{\delta F_T\}$, in which $\{\delta F_T\}$ is the resultant load increment vector. Solve Equation 135 for $\{\Delta_T''\}$ and then compute the external force vector $\{f_T\}_2$ corresponding to $\{F_T\}_2$.

5. With the known $\{f_T\}_1$, $\{f_T\}_2$ and $\{\delta_T\}_1$ compute $\{\delta_T\}_2$ by using the tangent stiffness procedure in Reference 26 for all cross sections.

6. Solve for the updated $\{\Delta_T''\}$ and $\{\Delta_T\}$ after assembling $[K_T]$, utilizing the cross-sectional properties obtained in step 5.

7. With the updated $\{\Delta_T{''}\}$ in step 6, formulate the load vector $\{F_T\}_3$.

8. If $|\{F_T\}_3 - \{F_T\}_2| \leq \alpha$ where α is the tolerance taken as 0.01%, go to step 10.

9. Set $\{F_T\}_2 = \{F_T\}_3$; $\{f_T\}_2 = \{f_T\}_3$ and go to step 5.

10. Set $\{F_T\}_1 = \{F_T\}_3$; $\{f_T\}_1 = \{f_T\}_3$ and repeat steps 5-11 until the strength limit is reached.

The procedure described herein is carried out using constant load or temperature increments throughout the elastic range. In the inelastic range, the load increments are successively reduced to avoid severe imbalance between the external load and the internal forces.

4.5 Behavior of Beam-columns without Axial Restraints to Thermal Expansion

Herein, the imperfect nonsway steel beam-columns with hollow square section, 7×7×0.375in, and the length of 144 in. are adopted. Young's modulus E and yield stress σ_Y values at ambient temperature are taken as 29,000ksi and 46ksi, respectively. The stress-strain relationship at high temperature follows the elastic-perfect-plastic model, shown in Figure 17. The initial biaxial crookedness is taken as $L/1000$. It is assumed that temperature distribution along the length of the member is uniform.

4.5.1 Effects of Initial Crookedness

Table 21 summarizes the dimensionless axial load values for beam-columns with pinned boundary conditions and initially applied biaxial moment equals 0.0, 0.4 and 0.7, respectively, at different temperatures. The bending moments are only applied at the top end of the members. BC means the biaxial crookedness, which is taken as $L/1000$. NS means nearly straight, the initial crookedness is taken as $L/100,000$. The effect of initial crookedness on the strength limit of column is significant, especially at ambient temperature. The influence is lesser if the temperature rises. For the beam-columns, the effect of initial crookedness is relative small. The critical temperature of nearly straight members equals that of with initial crookedness. For the member with the relative larger moment, the influence at high temperature can be ignored. Figure 60 describes the load versus temperature curves for the member with or without initial crookedness. If the temperature is not higher than about 750°F, the member load-carrying capacity almost is

the same as that of the ambient temperature, but above 750°F, it drops quickly. Figure 61 compares the stiffness degradation curves for the initially crooked and nearly straight beam-columns with biaxial moments $m_x = m_y = 0.4$ at 68°F, 800°F, 1200°F and 2000°F, respectively. It shows that the crookedness speeds the stiffness dropping when the maximum loads is reached; the higher the temperature is, the faster the stiffness drops; and the higher the temperature is, the smaller the influence of crookedness is.

4.5.2 Effects of the Rotational End Restraints

To illustrate the influence of end rotational restraints on the behavior of steel beam-columns at high temperature, the following spring stiffness is adopted:

$kc_1 = 0.0$ kip-in/rad

$kc_2 = 13,000$ kip-in/rad

$kc_3 = 24,000$ kip-in/rad

$kc_4 = 2.4 \times 10^{12}$ kip-in/rad

Herein, $kc_1 = 0.0$ kip-in/rad represents the nearly pinned condition, $kc_2 = 13,000$ kip-in/rad and $kc_3 = 24,000$ kip-in/rad represent the partial boundary condition and $kc_4 = 2.4 \times 10^{12}$ kip-in/rad simulates a nearly fixed condition. The linear elastic model is adopted for the relationship between the resistant moment and the rotation. The beam-columns with equal end restraints and initially applied biaxial bending moments ($m_x = m_y = 0.6$) are used. The obtained results are collected in Table 22. It is clear that the rotational restraint can significantly increase the failure temperature and load-carrying capacity of steel members. For example, for pinned condition the failure temperature is about 943°F; it is about 1450°F for partial condition with the spring stiffness 24,000 kip-in/rad; the failure temperature is around 2200°F for fixed condition. Figure 62 shows the load versus temperature curves for hollow square beam-columns under biaxially loading with $m_x = m_y = 0.6$ and with different end rotation restraints. It is also clear that the end restraint can increase the ductility of the members.

4.5.3 Temperature versus Deflection Curves

The strength limit under the given temperature is calculated, and then the load versus deflection curve at a specified temperature is able to be drawn. Figure 63 describes

the load versus deflection curves for pinned columns at ambient and high temperatures. The curves are smooth line because the elastic modulus value doesn't change at the specified temperature. It is found that all the curves start with a linear part and then followed by a nonlinear part. Near the strength limit, the curves are almost flat. The flat part is long if the temperature is high. The slope of the curve of ambient temperature is larger than that of at high temperature which is reducing with the increase of temperature. At a specified high temperature, the slope might be zero.

Figure 64 shows the load versus deflection curves for the pinned beam-columns under biaxial loading with $m_x = m_y = 0.4$ at ambient and high temperatures. The characteristics for the shape and the slope of the curves are similar with those for pinned columns shown in Figure 63. There are some fuzzes shown in the curve of T= 800°F. One of reasons for that is that the beam-column suddenly loses a considerable stiffness followed by an immediate gain with a small variation in the loads, which will affect the development of the deflection. Another phenomenon corresponding it is that there are valleys in the stiffness degradation curves shown in Figure 57. The deflection may have a large increase if the beam-column loses a considerable stiffness, which will decrease after an immediate gain in the stiffness with a small variation in the loads.

The temperature versus deflection curves can be plotted after calculate the critical temperatures corresponding to zero load-carrying capacity for steel beam-columns subjected the constant service load. Table 23 summarizes the obtained critical temperatures for the pinned steel beam-columns without axial restraint to thermal expansion at different load combinations. It is found that the increase of the carrying loads reduce the critical temperature. Figure 65 shows some of corresponding temperature versus deflection curves. It is found there are "knee point" existed in the curves because of the change of elastic modulus value. The number of knee points in the curve depends on the number of changes of the elastic modulus value at the temperature range from ambient temperature to the critical temperature. The inflexion-point is appeared where the value of the elastic modulus changes. The effect of the change of the elastic modulus also can be found in the stiffness degradation curve shown in Figure 66. Below the temperature of about 212°F, there is no stiffness degradation happened. Above

that point, the stiffness starts lessening which causes the decrease of the slope of temperature versus deflection curve.

4.5.4 Beam-column Behavior at 1000°F

From the ambient temperature investigation, it is found that the member load-carrying capacity is load path dependent for the load combinations with relative larger moments. In this section, the effect of the load path on the beam-columns behavior at high temperature is studied. Figure 62 shows that the member peak loads start changing above about 750°F. Therefore, high temperature of 1000°F is chosen as the environmental temperature to investigate the behavior for nonproportional loaded initially crooked beam-columns at high temperature. The beam-column is heated to 1000°F first without axial restraint to thermal expansion and then the mechanical loading is started, which follows the load paths through NP1to NP8, as defined in Section 3.5. And it is assumed that the temperature distribution along the beam-column length is uniform.

The behavior of uniaxially loaded W8X31 beam-columns about major and minor axis is studied firstly. The dimensions and material properties at ambient temperature are defined in Section 3.6.4. The equal rotational end restraints follow the elastic model with spring stiffness $k_{a3} = 24,000$ in-kip/rad. Table 24 summarizes the maximum dimensionless peak load with load paths LC1 through LC4 for the major and minor axes. It is clear that the peak loads for the major axis are nearly the same for different load paths, suggestion that the load paths have no significant effect on the member strength limit even at high temperature. However, when the beam-column is loaded about the minor axis, it is found that the maximum load is load path dependent if the load combination with the relative larger moment. For example, LC1 and LC2 provide nearly the same maximum loads, while LC3 and LC4 exhibit a substantial difference in the maximum loads. The maximum moment value for LC4 is 24.1% greater than that for LC3 when the temperature is 1000°F.

The behavior of biaxially nonproportionally loaded W8X31 beam-columns with equal end restraints is studied with high temperature 1000°F. The end rotation restraints with stiffness ka3 (24,000 in-kip/rad.) follows the elastic model. The members are heated

to $1000°F$ without the axial restraint to thermal expansion and then the mechanical loading is started following the load paths NP3 and NP4. The results obtained are reported in Table 25. Load path dependence is obviously present for biaxially nonproportionally loaded I-section beam-columns with partial restraints at high temperature. The influence is very significant for the load combination with the relative large bending moments.

The next study is about the behavior of biaxially loaded beam-columns with hollow square section and equal end restraints. The end rotational restraints follow the elastic model with initial stiffness, $k_{a3} = 24,000$ in-kip/rad. The same steel beam-column is adopted, which is defined in Section 3.6.6. The mechanical load paths follow NP3 through NP6. The results obtained are summarized in Table 26, which indicates that the influence of the load sequence on the beam-column load-carrying capacity is significant at high temperature especially for the load combination with a relative large bending moment. Specifically, the value for the maximum biaxial bending moment m_x and m_y is 1.085 at the given axial load p= 0.25 for load path NP3, however, the maximum axial load p is 0.197 for load path NP4 instead of 0.250 in load path NP3, which is 21.2% less than that of in load path NP3. Two more examples: the maximum bending moment m_y is 0.825 for load path NP5 instead of 1.085 in NP3 and NP4, which is about 24% less than those of in load path NP3 and NP4; the maximum axial load is 0.191 in load path NP6 replacing of 0.250 in load path NP3, which is about 23.6% less than that of in load path NP3.

The last study in this section is about the behavior of biaxially nonproportionally loaded hollow rectangular beam-columns. The equal end restraints follow the elastic model with stiffness, $k_{a3} = 24,000$in-kip/rad. The same hollow rectangular steel beam-column is adopted, which is defined in Section 3.6.6. The load-temperature sequence is that the member is heated to $1000°F$ first and then the mechanical loading is started, which follows the load paths NP3 through NP8. The obtained results are summarized in Table 27. The influence of load path on the member strength limit at high temperature is significant, especially for the load combination with relative larger moments.

4.5.5 Effects of Load-temperature Sequence

The strength limits values shown in Tables 21, 22, 24, 25, 26 and 27 are evaluated by calculating the maximum load of the beam-column under a specified temperature, called "load approach". The strength limits values in Table 23 are gained by calculating the critical temperature that the member can sustain under the given loads, called "temperature approach". Are these two approaches similar to evaluate the steel beam-column strength limit? Does the load-temperature sequence affect the load carrying capacity? These problems are to be studied in this section. It needs to be mentioned that there is no axial restraint to thermal expansion when the temperature is increasing, herein.

Nine different load-temperature sequences referring to Figure 21 are used, which are defined below:

OTMP: Raise the temperature T first and hold constant, and then gradually apply m_x and m_y simultaneously and hold constant, followed by P until the member collapse.

OTPM: Raise the temperature T first and hold constant, and then incrementally apply P and hold constant, followed by applying M_x and M_y simultaneously until the member collapses.

OMTP: The biaxial bending moments M_x and M_y are applied first and hold constant, and followed by raising the temperature T gradually, and lastly apply the axial load P until the collapse occurs.

OMPT: The biaxial bending moment M_x and M_y are applied simultaneously first and hold constant, and then apply axial load P and hold constant, and lastly raise the temperature until it fails.

OPTM: The axial load P is applied firstly and held constant, followed by appling biaxial bending moment M_x and M_y simultaneously and holding them constant, which is followed by raising the temperature T gradually, and lastly apply the axial load P until the collapse occurs.

OTMMP: Raise the temperature T first and hold constant, and then apply bending moment M_x only and hold constant, and then apply M_y gradually and hold constant, and then lastly apply the axial load P until the member fails.

OTPMM: Raise the temperature T firstly and hold constant, and then apply P incrementally and hold constant, and then apply uniaxial bending moment M_x gradually and hold constant; and then lastly apply the uniaxial bending moment M_y until the member load-carrying capacity is reached.

OMMPT: The bending uniaxial moment M_x is applied firstly and held constant, and then the bending moment M_y is applied and held constant, and then axial load P is gradually applied and held constant, and lastly the temperature is raised until it fails.

OPMMT: The axial load P is gradually applied first and held constant, and then the uniaxial bending moment M_x is applied and held constant, and then uniaxial bending moment M_y is incrementally applied and held constant, which is lastly followed by raising the temperature T until the collapse occurs.

The 144-in. long steel beam-column with the hollow square section $7 \times 7 \times 0.375$ in. and biaxial initial crookedness is adopted. The values of E and σ_y at ambient temperature are taken as 29,000ksi and 46ksi. Table 28 prescribes the member load-carrying capacity including the maximum values of the axial load, bending moment and temperature with different load-temperature paths for pinned boundaries. The peak values for different load-temperature-sequence are nearly same, indicating that strength is not load-temperature sequence dependent for pinned boundary conditions.

For the partial boundary conditions, the equal rotational end restraints following the elastic model with initial stiffness $k_{a3} = 24,000$ in-kip/rad. is used. All the results obtained are summarized in Table 29. It is clear that the influence of load-temperature sequence for steel beam-column behavior with partial boundary conditions is small and can be negligible.

4.6 Beam-column Behavior with Rigid Axial Restraint

Steel beam-columns with rigid axial restraint to thermal expansion, when exposed to an environment with raising temperature, additional axial compressive forces are developed due to the restrained thermal expansion. The steel beam-columns as defined in Section 4.6.5 also are used to study the effects of the rigid axial restraint on the member behavior. It is found that the critical temperature is about 268°F if increase the temperature until the steel beam-column fails, which is particularly low. It indicates that steel beam-columns with rigid axial restraint are very susceptible to the increase of temperature and will most certainly fail prematurely.

Figures 67 describes the additional compressive force versus temperature curve for columns with rigid axial restraint to thermal expansion, which indicates that at around the temperature of 268°F the additional compressive force already equal about $0.8P_y$ and it increase linearly with the increase of temperature. Figure 68 shows the corresponding temperature versus deflection curve and Figure 69 shows the stiffness degradation curve and the temperature versus deflection curve for the steel beam-column with rigid axial restraint to thermal expansion. These curves resemble those from the case, that is, only applying axial load until the member fails at ambient temperature.

4.7 Comparing Theoretical with Experimental Results at High Temperature

The comparisons of the theoretical and the theoretical dimensionless peak load for steel beam-columns without axial restraints to thermal expansion at 500°F are given in Table 30. The load-temperature sequence for this group tests is that members are heated to 500°F first without axial restraint to thermal expansion and followed by the mechanical loadings. For HTUP-1, only applying axial load at 500°F, the ratio between the predicted and the tested maximum axial load is 1.106. For HTUP-2 only subjected to the uniaxial moments at 500°F, the ratio between the predicted and the tested maximum bending moment is 1.261. For HTUP-3 with the initial applied uniaxial moment m_y = 0.595 at 500°F, the ratio is 0.1374. For HTUP-4 and HTUP-5, the ratios are 1.478 and 1.571, respectively. For HTUS-7 through HTUS-10 with partial rotational end restraint, the ratios between the predicted and the tested maximum load value is 1.207, 1.148, 1.256

and 1.294, respectively. For specimens HTBP-11 through HTBP-13 with partial rotational end restraint, the ratios between the predicted and the tested maximum moment value is 1.207, 1.137, 1.190 and 1.190, respectively. Table 31 collects the comparisons between the experimental and the predicted maximum load values for the beam-columns with axial restraints to thermal expansion at 500°F. The ratios between the predicted and tested results range from 1.075 to 1.215.

Figure 70 compares the experimental and theoretical axial load versus end rotation curves for the members HTUP-2 and HTUP-3, respectively. Figure 71 compares the experimental and predicted bending moment versus end rotation curves for members HTUP-1 and HTUP-4. Referring to Figures 70 and 71, it is seen that shapes of the experimental and theoretical curves are very similar. Specimen HTUP-2 and HTUP-3 (Fig 71) indicates very good correlation with theory, showing slightly larger experimental rotation. The tested results and those predicted results have a good agreement. The HTUP-1 and HTUP-4, at the beginning part a good correlation is achieved between the curves. But near the peak value, for HTUP-1 the experimental peak load value is larger than the predicted one; for HTUP-4, the predicted peak values is slightly higher than the experimental one.

The comparisons for the rest specimens are similar with specimen HTUP-1 or HTUP-4. At the beginning part, the predicted and theoretical load versus rotation curves has good correlation, but near the peak load, two curves are slightly away from each other.

CHAPTER

5. INELASTIC BEHAVIOR OF WORLD TRADE CENTER BEAM-COLUMNS

The purpose of this chapter is to analyze the behavior of the steel beam-columns which were used in the outer structure of the 110-story World Trade Center buildings. Both ambient and high temperature conditions are considered. After the air plane attack, a number of beam-columns were destroyed and thus the rest of the beam-columns ended up having to carry additional loads. The high temperature due to the fire after the aircraft impact resulted in a very dramatic reduction in the load-carrying capacity of the beam-columns.

5.1 World Trade Center Towers

The World Trade Center (WTC) towers were designed and built during the period from 1966 to 1973. FEMA (2002) describes the general information about the building: "The WTC towers, also known as WTC1 and WTC2, were the primary components of the seven building World Trade Center complex. Each tower encompassed 110 stories above the plaza level and seven levels below. WTC1 (the north tower) had a roof height of 1,368 feet, briefly earning it the title of the world's tallest building. WTC2 (the south tower) was nearly as tall, with a roof height of 1,362 feet. A rectangular service core, with overall dimensions of approximately 87 feet by 137 feet, was present at the center of each building, housing 3 exit stairways, 99 elevators, and 16 escalators."

On September 11, 2001, two hijacked commercial jetliners were deliberately flown into the WTC towers. After the two aircrafts impacted the buildings, fireballs erupted and jet fuel ignited fires. Regarding the aircraft impact on the two towers, FEMA (2002) reported that: "The north tower was struck between floors 94 and 98, with impact rightly centered on the north face. The south tower was hit between floor 78 and 84 toward the east side of the south face." The south tower collapsed 56 minutes after it was struck. The north tower collapsed too after 1hour and 43 minutes the jetliner crashed into it. The Federal Emergency Management Agency (FEMA) in 2002 reported that: "A total of 2,830 people lost their lives in the collapse of the WTC towers". The FEMA report in

2002 suggested that the heat-induced failures in the buildings core columns initiated a progressive collapse.

5.2 Structural Features of WTC Towers

Generally, a skyscraper is modeled as a large cantilever vertical column and the wind load rather than the gravity load dominated the structural design. In order to make the towers capable of withstanding the wind load, the lightweight "perimeter tube" design was chosen. On each of the facades a vierendeel girder type wall was formed by 59 box-section columns which were rigidly connected to panels at each floor level, as shown in Figure 72. These walls were interconnected to transmit shear at the corner of the building; they form a torsional rigid framed tube which is fixed to the foundations and transmits all wind loads. Adjacent exterior columns were connected at each floor level by deep steel spandrel plates, as shown in Figure 73 (FEMA, 2002). There are twelve grades of steel, having yield strengths varying between 42ksi and 100ksi, being used to fabricate the perimeter column and spandrel plates as dictated by the computed gravity and wind demands. Plate thickness also varied both vertically and around the building perimeter, to accommodate the predicted loads and minimize differential shortening of columns across the floor plate. The upper floors of the buildings had less wind load and building mass to support. Thus, on higher floors, the thickness of steel plates making up the columns decreased, becoming as thin as 0.25 in. near the top down from as thick as 3.0 in at lower floors. Figure 74 shows the typical cross sections for the exterior column, which is box-shaped and welded from four plates. Section A is for the WTC beam-columns near the bottom of the building; Section B is for the WTC beam-columns near the impact area; and Section C is for the members near the tower top.

The structural core extending from its bedrock foundation to its roof supports the tower. The cores are rectangular pillars with numerous large columns and girders. There are no intermediate columns between the perimeter walls and core system. The floor diaphragms connect them, providing large expanses of uninterrupted floor space. In total, 47 columns constituted the core system only carrying the vertical loads inside the core, aligned in five rows of eight and one row of seven columns as shown in Figure 72. The core columns with box-section are continuous for their entire height, going from their

bedrock anchors in the sub-basements to near the tower top. "9-11 Research.com (51)" describes the dimension of core columns: "Like the perimeter columns, the thickness of the steel in the core columns tapered from bottom to top. Near the bottoms of the towers the steel was 4.0 in. thick, whereas near the tops it may have been as little as 0.25 in. thick. Some of these columns have outside dimensions of 36 ×16in. Others have larger dimensions, measuring 52×22 in." Figure 75 shows the typical dimensions and thickness for the core columns. Section D was used for the columns near the bottom area and Section E was used for the top area of the tower. There are two grades of steel used with yield strength 36ksi and 42ksi, respectively for the core columns.

5.3 WTC Steel Member Behavior

The stress-strain relationship for WTC beam-column material at high temperature follows the elasto-perfect plastic models as shown in Figure 17. The reduction factors for yield stress and Young's modulus at high temperature follows the EC3 (2005) model, defined in Section 2.3. The linear partial rotational end restraint with stiffness k_a equals $0, \frac{EI}{L}$ and $\frac{10EI}{L}$ respectively is used. Herein, moment of inertia, I, is the average value of I_x and I_y. Three stiffness values of axial restraint to thermal expansion are used, 0, $\frac{EA}{L}$ and $\frac{2EA}{L}$, respectively. Here, E, A, I and L are the material elastic modulus at ambient temperature, cross-sectional area, moment inertia and length for WTC member, respectively. Assume 144-inch long WTC beam-columns with biaxial initial crookedness L/1000. The residual stress is not included herein because it is released at high temperature. All the load values shown in the Tables and Figures are dimensionless.

5.3.1 Exterior WTC Column Behavior at High Temperature

The exterior column of WTC Tower 1 with Section C (located near the tower top) shown in Figure 74 is selected to investigate the behavior at high temperature. The yield stress σ_y and elastic modulus at ambient temperature is 42ksi and 29,000ksi.

Table 33 collects the obtained dimensionless maximum axial loads for the WTC columns with different end rotation restraints and axial restraints to thermal expansion. It is found that the effect of partial rotational restraints on the maximum load of the WTC

column is significantly at ambient temperature. For example, at ambient temperature the maximum load value for WTC columns near the tower top with partial rotational end restraints is 0.970, 0.982 and 0.986 for partial restraints with k_a equal $0.0, \frac{EI}{L}$ and $\frac{10\,EI}{L}$, respectively. However, it is found that the influence of partial end restraints at high temperature for WTC near the tower top is not significantly. Specifically, the maximum load value for WTC columns without axial restraint to thermal expansion at 1600°F is 0.072, 0.073 and 0.073, which are pretty close to each other, for k_a equal $0.0, \frac{EI}{L}$ and $\frac{10\,EI}{L}$, respectively. Therefore, the influence of partial rotational end restraints on the critical temperature corresponding to zero load-carrying capacity of WTC column is not significant. The effect of axial restraint to thermal expansion on the WTC columns load-carrying capacity is significant. For example, the temperature corresponding to zero load-carrying capacity is about 1600°F, 600°F and 450°F for the WTC columns for k_{ts} equal $0, \frac{EA}{L}$ and $\frac{2EA}{L}$, respectively.

Figure 76 presents the load versus temperature curves for the WTC columns near the tower top. It is clear that the influence of temperature on the strength of the WTC columns with free axial restraint to thermal expansion is small with a temperature lower than 750°F and load-carrying capacity is almost same with that of ambient temperature; while the temperature is between about 750°F and 1400°F, the strength drops linearly; above 1500°F, the dropping speed gets slower, but the load-carrying capacity is close to zero. However, for the WTC columns with axial restraint to thermal expansion, the load carrying capacity is linearly dropping with the increase of temperature.

Figure 77 shows the load versus deflection curves for WTC columns with pinned boundary conditions and free axial restraint to thermal expansion at the temperature of 68°F, 800°F and 1200°F, respectively. The slope of the load versus deflection curve is decreasing with the increase of the temperature. One of the possible reasons for that is the value of Young's modulus decrease when the temperature increases. The slope may be zero at a specified high temperature. The shape of the curve at high temperature is similar with that of at ambient temperature, which always starts with linear part and follows with inelastic part. The last part of curve is nearly flat, which means without the increase of load, the deflection continue to increase.

Figure 78 shows the stiffness degradation curves for pinned WTC columns near the tower top with or without axial restraint to thermal expansion at 68°F, 800°F and 1200°F, respectively. It shows that somewhat moderate structural stiffness degradation is observed with increasing axial load and with temperatures of up to 800°F. However, severe stiffness degradation is observed at 1200°F. It is observed that the influence of axial restraint to thermal expansion on the stiffness degradation of WTC columns is significantly. Even at the low temperature of 400°F, the severe stiffness degradation already happens. It is clear that the axial restraints reduce the member load-carrying capacity because of the additional compressive force caused by the axial restraint to thermal expansion at high temperature.

Figures 79 through 81 show the temperature versus deflection curve, the temperature versus stiffness degradation curve and the temperature versus compressive force curve for WTC column with rigid axial restraint, respectively. It is clear that the column with rigid axial restraint is almost fully plastified at 238°F. Figure 79 exhibits that the additional compressive force caused by axial restrain to thermal expansion is linearly increasing until the member load-carrying capacity is reached. Figure 80 shows the midspan deflection is almost linearly increasing with increase of temperature until bucking happens. Figure 81 shows that that e bucking happens when the column lost about 25% of stiffness. In short, the column load-carrying capacity is very sensitive to the axial restraint to thermal expansion and it fails in very low temperature.

5.3.2 Exterior WTC Beam-column Behavior at High Temperature

Table 34 summarizes the dimensionless maximum load p for WTC beam-columns near the tower top under biaxial loading with $m_y/m_x = r_y/r_x$ and $m_x = 0.7$ and with different end rotation restraints and axial restraints to thermal expansion. The linear partial rotational end restraint with stiffness k_a equals 0, $\frac{EI}{L}$ and $\frac{10\,EI}{L}$ respectively, is adopted. The axial restraint to thermal expansion with stiffness k_{ts} equal 0, $\frac{EA}{L}$ and $\frac{2EA}{L}$, respectively, is used. It is found that the influence of the partial rotational end restraint on the beam-column load-carrying capacity is significant at both ambient and high temperatures. For example, the dimensionless maximum axial load value for WTC beam-

columns without axial restraint to thermal expansion is 0.323, 0.551 and 0.814 for k_a equals $0, \frac{EI}{L}$ and $\frac{10\,EI}{L}$, respectively. The maximum load for k_a equals $\frac{10\,EI}{L}$ is more than two times increase than that of k_a equals 0. The critical temperature responding to zero load-carrying capacity for WTC beam-columns without axial restraint to thermal expansion are 1000°F, 1200°F and 1650°F for k_a equals $0, \frac{EI}{L}$ and $\frac{10\,EI}{L}$, respectively. It is also observed that the effect of axial restraint to thermal expansion on the critical temperature of WTC beam-columns is significant. Specifically, the critical temperature for pinned beam-columns is 1000°F, 500°F and 400°F for k_{ts} equal $0, \frac{EA}{L}$ and $\frac{2EA}{L}$, respectively; and the critical temperature for partially restrained beam-columns with k_a equals $\frac{EI}{L}$ is 1200°F, 500°F and 400°F for k_{ts} equal $0, \frac{EA}{L}$ and $\frac{2EA}{L}$; critical temperature for partially restrained beam-columns with k_a equals $\frac{10EI}{L}$ is 1600°F, 600°F and 400°F for k_{ts} equal $0, \frac{EA}{L}$ and $\frac{2EA}{L}$.

Figure 82 describe load versus temperature curves for WTC beam-columns from impacted area under biaxial loading ($m_y/m_x = r_y/r_x$ and $m_x = 0.7$) with different boundary conditions and axial restraint to thermal expansion. It is obvious that the end restraints increase the WTC member strength at ambient and high temperatures. It is also clear that the influence of axial restraint to thermal expansion on the WTC member strength and behavior is significant.

5.3.3 Load-moment Interaction Relationship

To study the interaction relationship between load and moment, the exterior WTC column with Section B shown in Figure 74 from the impacted area around 94-98 stories is investigated. The yield stress and elastic modulus at ambient temperature are 55ksi and 29,000ksi, individually. Assume that the beam-column is initially crooked with the value L/1000 and without residual stress. Pinned and end restrained boundaries are considered. The initial spring stiffness for linear rotational end restraint is $k_a = \frac{EI}{L}$. Herein, moment initial I is the average value of I_x and I_y. For stiffness of axial restraint to the thermal

expansion, three values, 0.0, $\frac{EA}{L}$ and $\frac{2EA}{L}$, are adopted where E, A and L is the beam-column elastic modulus, cross section area and length at ambient temperature.

Table 35 summarizes the dimensionless maximum loads for WTC beam-columns from impacted area under uniaxial loading (m_x only) for partially rotation restrained boundary conditions. It is clear that load-carrying capacity of the WTC beam-columns reduces with increases of temperature. For example, in Table 35 for the case of $k_{ts}= 0.0$ and the initially applied axial load $p = 0.25$, the maximum value m_x is 2.664 at $600°F$ but it is 1.504 at $1500°F$. Also, it is found that the strength of WTC beam-columns is very sensitive to the axial restraints to thermal expansion. For example, for the case of only applying bending moment m_x, the maximum applied external moment m_x is 1.589 for $k_{ts}=0.0$ at $1500°F$, it already drops to 0.893 at $400°F$ if $k_{ts}=\frac{EA}{L}$. Furthermore, it drops to 0.522 for $k_{ts} = 2\frac{EA}{L}$ at $400°F$. Also, it is clear that the increase of axial force reduces the moment-carrying capacity of WTC beam-columns. For example, for WTC columns under uniaxial loading with axial restraint to thermal expansion $k_{ts}=\frac{EA}{L}$ and partial rotational end restraints $k_a =\frac{EI}{L}$ and at the temperature of $400°F$, the maximum moment is 0.377 if $p = 0.0$, and it is 0.136 if $p = 0.110$ and it is zero if $p = 0.135$.

Tables 36 and 37 summarize the dimensionless maximum loads for WTC beam-columns from the impacted area under uniaxial loading (m_x only) for pinned and rotation partially restrained boundary conditions. Tables 38 through 40 summarize the dimensionless maximum loads for WTC beam-columns from the impacted area under biaxial loading with a different ratio of m_y to m_x for pinned and rotation partially restrained boundaries. Similar rules are found about the influence of temperature and axial restraint to thermal expansion on the strength of WTC beam-columns.

Figure 83 describes the interaction curves for WTC beam-columns from impacted area under uniaxial loading (m_x only) with partial rotational end restraints and without axial restraint to thermal expansion at different temperatures. It shows a dramatic reduction in strength with an increase of temperature, which also can be found in Figures 84 through 99.

5.3.3 Dilemma with Large Load-carrying Capacity at 600°F with $k_{ts}= 0.0$

It is found that the moment-carrying capacity of WTC beam-columns from the impacted area without the axial restraint to thermal expansion at the temperature of 600°F is larger than that at ambient temperature. The interaction curve of 600°F envelops that of 68°F, which can be found in Figures 83, 86, 90, 93 and 96. One of reasons for that is the way adopted to determine the yield stress and elastic modulus values at high temperature. In the temperature range of 20°C < T ≤ 400°C, the reduction factor for yield stress is less than 1.0, as defined in Equation 11. However, for elastic modulus, it is 0.784 which is less than 1.0, as defined in Equation 12. Therefore, the end rotation at 600°F is larger than that at ambient temperature which means that the resistant moment provides by rotational end restraints is large at 600°F than that at 68°F. Based on the analysis in Section 3.2.1, the large applied moment can be carried by the WTC beam-columns at 600°F. For the WTC beam-columns with axial restraint to thermal expansion, this phenomenon disappears because the additional compressive force incurred due to thermal expansion overcomes the increased applied external moment if the temperature is below 400°C (752°F).

5.4 Behavior of Beam-column from North Tower after Airplane Impact

First, it is important to discuss the initial damage on the exterior framing system of the North Tower after the air plane impact. Based on the existing photography material identifying columns that were destroyed by the impact, the damage of the exterior wall can be easily quantified. FEMA (2002) supplies the visual evidence of the damaged columns in the impressed region. Table 41(25) prescribes the number of columns that were severely damaged after the impact for each of the impacted floors. It was stated in Reference 37 that: "following the aircraft impact, the structural damage to the exterior columns of the north face was compensated by redistribution of the load to the remaining perimeter columns of the building, through the deep spandrel beams that connected the exterior columns. Because of the unique structural system of the North Tower, in which the exterior system was connected to the core by bar joists which were not designed to transfer moment, the load resisted by the perimeter columns was not redistributed to the

core." After the airplane impact, the service load and the environmental temperature were changed.

In the north side of 94th floor of the building, 21 out of 59 columns were damaged. If the load-carrying capacity of each facade is assumed as 1.0, then the total load-carrying capacity for whole floor is 4.0. Due to the fact that 21 columns were damaged in the north side, 35.6% (21/59= 0.356) of resistance ability was lost due to the aircraft impact. That also means the service load of the columns changed; the change rate η is calculated as follows:

$$\eta = \frac{4.0}{1.0+1.0+1.0+1.0-0.356} = 1.1 \tag{138}$$

Before the aircraft impact, assuming all the loads are live loads; then the largest approximated existing service loads P_0, M_{x0} and M_{y0} are calculated:

$$P_o = \frac{\Phi_c P_n}{1.6} \tag{139}$$

$$M_{xo} = \frac{\Phi_b M_{nx}}{1.6} \tag{140}$$

$$M_{yo} = \frac{\Phi_b M_{ny}}{1.6} \tag{141}$$

where: P_n, M_{nx} and M_{ny} are the nominal compressive, flexural strength about x and y axis, respectively; $\Phi_c = 0.85$, the resistance factor for compress; $\Phi_b = 0.9$, the resistance factor for flexure. After the aircraft impact, the new service load can be calculated and

$$P_{new} = \eta P_o \tag{142}$$

$$M_{xnew} = \eta M_{xo} \tag{143}$$

$$M_{ynew} = \eta M_{yo} \tag{144}$$

The yield stress and elastic modulus for the column at ambient temperature are 55ksi and 29,000ksi, individually. The column length is 144 in with cross section B. According

to the Steel Construction Manual (52), P_n, M_{nx} and M_{ny} are calculated and equal 0.497, 0.818 and 0.884, respectively.

Regarding the aircraft impact on the two towers, FEMA (2002) described that: "Each plane banked steeply as it was flown into the building, causing damage across multiple floors." FEMA (2002) also reported that: "As the two aircraft impacted the buildings, fireballs erupted ... and jet fuel spread across the impact floor and down interior shaft ways, igniting fires." Evidently, the exterior beam-columns forming the vertical support structure experienced high temperature.

After the air plane attack, the load was redistributed. Some of columns were out of commission and the rest of columns needed to carry the entire floor load. The incurred fire after the air plane attack increased the building temperature. Table 42 compares the critical temperature, which corresponds to a zero load-carrying capacity, of WTC beam-columns from the impacted area with existed and new service loads responding to before and after airplane impact. It is assumed that the service load does not change during the increase of temperature. The critical temperatures were 1086°F and 1056°F for WTC columns from the impacted area with service load of 0.497(existed) and 0.547(new), respectively, which are about 2.8% differences. The critical temperature are 1058°F and 1025°F for WTC beams from impacted area with service moment m_x of 0.818 (existed) and 0.911 (new), respectively, which are about 3.2% differences. However, the critical temperature are 815°F and 658°F for WTC beam-columns under biaxial loading from impacted area with existed and new service load, which are about 23.8% differences. It is clear that the change of the critical temperature for the WTC beam-columns from the impacted area under biaxial loading after airplane impact is significant.

The British Standard (BS) (53) temperature-time curve is adopted to develop the time versus deflection curve for WTC columns, herein, which is expressed in Equation 145 below:

$$T = T_0 + 345 \log(0.133t + 1) \tag{145}$$

where t represents the time in second; T represents the temperature in Celsius; T_0 represents the temperature at the start of the fire and usually $T_0 = 20\ °C$. It is stated in

Reference 54 that the standard fire curve for ASTM E119 is prescribed by a series of points rather than an equation but is almost identical to the BS curve.

Figure 99 presents the temperature versus deflection curves for WTC columns near the impacted area and under a service load of 0.547 with different end. It is found that the WTC column from the impacted area with a dimensionless axial service load of 0.547 became unstable at about 1000°F. Figure 100 shows the time versus deflection curves, which show the same characteristics with the temperature versus deflection curves. It shows that the critical temperature of the WTC columns from the impacted area and under a service load of 0.547 will be reached in about five minutes after airplance impact.

CHAPTER

6. CONCLUSIONS AND RUTURE RESEARCH

6.1 Conclusions

Within the range of parameters considered in this dissertation, the experimental and theoretical study conducted on the behavior of biaxially loaded steel beam-columns resulted in the following main conclusions:

1. The finite integral approach for solving the materially nonlinear system of differential equations predicted the experimentally observed behavior of steel beam-columns quite accurately.

2. The predicted beam-column load-deflection relationships were in good agreement with those based on the experiments for both ambient and high temperature conditions.

3. Both at ambient and high temperatures, the strength of hollow rectangular and I-section beam-columns loaded about the minor axis is found to be load path dependent when the applied moment plays a dominant role compared to the axial load. Similar influence of load path was observed for the beam-columns with biaxial loading.

4. At high temperature, the strength of biaxially loaded beam-columns has significant dependence on the load versus temperature sequence.

5. The strength of beam-columns is reduced due to initial member crookedness at both ambient and high temperatures.

6. Axial restraint to thermal expansion significantly decreases the strength of both uniaxially and biaxially loaded beam-columns which were used in the impacted area of the World Trade Center (WTC) towers.

7. The strength of beam-columns is reduced drastically at temperatures above $750^{\circ}F$. This type of effect was also observed for the strength of the WTC beam-columns.

8. For the WTC columns analyzed, somewhat moderate structural stiffness degradation is observed with increasing axial load and with a temperature of up to $800^{\circ}F$. However, severe stiffness degradation is observed at $1200^{\circ}F$.

9. The WTC columns which were used in the impacted area became unstable at about $1000^{\circ}F$ in the presence of a dimensionless axial service load of 0.547.

10. The WTC columns with rigid axial restraint to thermal expansion reached nearly full plastic condition at a temperature of 238°F.

11. The load-moment interaction curves developed for the WTC beam-columns loaded uniaxially or biaxially show a dramatic reduction in strength with an increase in temperature.

6.2 Future Research

The combined effects of biaxial loading, applied torsion and high temperature on the behavior and strength of steel members need to be investigated in the future. Reliable and practical analysis and design procedures for conducting collapse analysis of steel building structures should also be developed.

REFERENCES

1. Galambos, T. V., & Ketter, R. L.. "Further Studies on the Strength of columns under Combined Bending and Thrust," *Fritz Engineering Laboratory Report*, No. 205 A.19, Lehigh University Institute of Research, June 1957.

2. Galambos, T. V., and Ketter, R. L., "Columns Under Combined Bending and Thrust," *Fritz Engineering Laboratory Report*, No. 205 A.21, Lehigh University Institute of Research, April 1958.

3. Galambos, T. V. and Prasad, J., "Ultimate Strength Tables for Beam-columns," *Fritz Engineering Laboratory Report*, No. 287 3, Lehigh University Institute of Research, January 1962.

4. Lu, L. W. and Kamlvant, H., "Ultimate Strength of Laterally Loaded Columns," Fritz Engineering Laboratory Report, No. 273.52, Lehigh University Institute of Research, Nov. 1966.

5. Chen, W. F., and Atsuta, T., *Theory of Beam-Columns*, Vol.1, McGraw-Hill, Inc., New York, 1977.

6. Chen, W. F., and Atsuta, T., *Theory of Beam-Columns*, Vol. 2, McGraw-Hill, Inc., New York, 1977

7. Chen, W. F., "End Restraint and Column Stability," *Journal of the Structural Division*, ASCE, Vol, 106 No. ST11, November, 1980.

8. Razzaq, Z., "End Restraint Effect on Steel Column Strength," *Journal of Structural Engineering*, ASCE, Vol. 109, No. 2, February, 1983, pp. 314-334.

9. Razzaq, Z., and Calash, A. Y., "Imperfect Columns with Biaxial Partial Restraints", *Journal of Structural Engineering*, ASCE, Vol. 111, No. 4, April, 1985, pp. 758-776.

10. Razzaq, Z., and McVinnie, W. W., "Theoretical and Experimental Behavior of Biaxially Loaded Inelastic Columns," *Journal of Structural Mechanics*, Vol. 14, No. 3, March, 1986.

11. Darbhamulla, S. P., *Nonproportionally Loaded Steel Beam-Column and Flexibly-Connected Nonsway Frames* (Doctoral dissertation). Old Dominion University, May, 1990.

12. Poh, K.W. and Bennetts, I.D., "Analysis of Structural Members under Elevated Temperature Conditions," *Journal of Structural Engineering*, Vol. 121, No. 4, April 1995, pp. 664-675.

13. Poh, K.W. and Bennetts, I.D., "Behavior of Steel Columns at Elevated Temperatures," *Journal of Structural Engineering*, Vol. 121, No. 4, April 1995, pp. 676-684.

14. Talamona, D., Franssen, J.M., Schleich, J. B, and Kruppa, J., "Stability of Steel of Column in Case of Fire: Numerical Modeling," *Journal of Structural Engineering*, Vol. 123, No. 6, pp 713-720, 1997.

15. Franssen, J.M., Talamona, D, Kruppa, J. and Cajot, L.G., "Stability of Steel of Column in Case of Fire: Experimental Evaluation," *Journal of Structural Engineering*, Vol. 124, No. 2, pp 158-163, 1998.

16. Ali, F. and Shepherd, P. et al, "The Effect of Axial Restraint on the Fire Resistance of Steel Columns," *Journal of Constructional Steel Research*, 1998.

17. Cabrita-Neves, I., Valente, J. C. and Correia-Rodrigues, J. P., "Thermal Restraint and Fire Resistance of Columns," *Fire Safety Journal*, Vol. 37, May 2002, pp753-771.

18. Takagi, J. and Deierlein, G. G., "Strength Design Criteria for Steel Members at Elevated Temperatures," *Journal of Constructional Steel Research*, Vol.63, pp1036-1050, 2007.

19. Kodur, V., and Dwaikat, M. M. S., etc., "High Temperature Properties of Steel for Fire Resistance Modeling of Structures," *Journal of Material in Civil Engineering, ASCE*, May 2010.

20. Kodur, V. and Dwaikat, M. M. S, "Response of Steel Beam-Column Exposed to Fire," *Engineering Structures* 31 (2009) 369-379.

21. Yang, K. C. and Hsu, R., "Structural Behavior of Centrally Loaded Steel Columns at Elevated Temperature," *Journal of Constructional Steel Research*, 2009, pp 2062-2068.

22. Wang, Y.C. and Moore, D. B., "Effect of Thermal Restraint on Column Behavior in a Frame," *Fire Safety Science-Proceeding of the Fourth International Symposium*, pp.1055-1066.

23. Federal Emergency Management Agency (FEMA). (2002). World Trade Center Building Performance Study: Data Collection, Perliminary Observations and Recommendations. FEMA Report 403, Washington, D.C..

24. "June 2004 Progress Report on the Federal Building and Fire Safety Investigation of the World Trade Center Disaster," NIST Special Publication 1000-5.

25. Miamis, K, "A Study of the Effects of High Temperature on Structural Steel Framing," Ph. D Dissertation, Purdue University, December 2007.

26. http://911-engineers.blogspot.com/2007/06/berkeley-engineer-searches-for-truth.htm.

27. Singer, J., Arbocz, J., and Weller, T., *Bucking Experiments: Experimental Methods in Buckling of Thin-walled Structures*, Vol. 2, John Wiley & Sons, Inc., New York, 2002, pp.1370-1371.

28. Sanders, E. C., *Experimental Investigation of Steel Angle Column Buckling and Comparison to Seven International Design Specifications* (Master report). Old Dominion University, 2009.

29. ASTM E119-98, "Fire Tests of Building Construction and Material," Project No. 16410-108710, May 2, 2001.

30. American Association State Highway and Transportation Officials Standard, "Standard Test Method for Tension Testing of Metallic Materials," AASHTO No. T68, May, 2004.

31. Galambos, T. V., *Stability Design Criteria for Metal Structures*, Fifth Edition, John Wiley & Sons, Inc., New York, 1998.

32. Arita, F. and Miyamoto, K. (2004). "Mechanical Properties of High Strength Steel at High Temperatures," Kajima Technical Research Institute, pp. 41-42.

33. Kirby, B.R., and Preston, R.R. (1988), "High Temperature Properties of Hot-rolled, Structural Steels for Use in Fire Engineering Design Studies," *Fire Safety Journal*, Vol. 13, pp. 27-37.

34. Poh, K. W., "Stress-Strain-Temperature Relationship for Structural Steel," *Journal of Material in Civil Engineering*, Vol. 13, Issue 5, Oct. 2001.

35. European Committee for Standardization, (2005), "General rules- Structural Fire Design, En 1993-1-2," *Eurocode 3*, Brussels.

36. ASCE. (1992), "Structural Fire Protection," *ASCE Committee on Fire Protection,* Manual No. 78, ASCE, Reston. Va.

37. Society of Fire Protection Engineers and National Fire Protection Association, *The SFPE Handbook of Fire Protection Engineering,* 2nd Edition, 1995, published by the National Fire Protection Association, Quincy, MA

38. Hildebrand, F. B., *Introduction to Numerical Analysis,* Mcgraw-Hill Book Company 1956.

39. Ballio, G. and Campanini, G., "Equivalent Bending Moments for Beam-Columns," *Journal of Constructional Steel Research,* Vol. 1, No. 3, May 1981.

40. Brown, P. T., and Trahair, N. S., "Finite Integral Solution of Differential Equation," *Civil Engineering Transactions,* Institution of Engineers, Australia, Vol. CE10, No. 2, October 1969.

41. Santathadaporn, S. and Chen, W. F., "Tangent Stiffness for Biaxial Bending," *Journal of Structural Division,* January, 1972.

42. Usami, T., and Galambos, T. V., "Eccentrically Loaded Single Angle Columns," *Publications, International Association for Bridge and Structural Engineering.* Vol.31-II, Zurich, 1971

43. Birnstiel, C. "Experiments on H-Columns under Biaxal Bending," *Journal of Structural Divison,* October, 1968.

44. Sharma, S. S., and Gaylord, E. H. "Strength of Steel Columns with Biaxially Eccentric Load," *Journal of Structural Divison,* ASCE, Vol. 95, No. ST 12, December, 1969, pp. 2797-2812.

45. Lewitt, C. S., Chesson, E., and Munse, W. H., "Restraint Characteristics of Flexible Riveted and Bolted Beam-to-Column Connections," *Engineering Experiment Station Bulletin,* No. 296. University of Illinois at Urbana-Champaign, March 1966.

46. Chen, W. F. and Lui, E. M., "Columns with End Restraint and Bending in Load and Resistance Design Factor," *Engineering Journal,* Third Quarter/ 1985, Page 105-133.

47. Rathbun, J.C., "Elastic Properties of Riveted Connections," *Transactions of the American Society of Civil Engineers,* Vol. 101, 1936, pp. 524-563.

48. Romstad, K.M. and Subramanian, C. V., "Analysis of Frames with Partial Connection Rigidity," *ASCE Journal of Structural Division*, Vol. 96, No. ST11, November 1970, pp. 2,283-2,300.

49. Colson, A. and J.M. Louveau, "Connection Incidence on the Inelastic Behavior of Steel Structures," Euromech *Colloquium* 174, October 1983.

50. Iwankiw, N., Beylier, C. and Beitel, J., "Testing needs for Advancement of Structural Fire Engineering," *Proceeding of the Fifth International Conference on Structural in Fire*, Sydney, Australia, 2008.

51. http://911research.wtc7.net/index.html

52. American Institute of Steel Construction Inc., *Steel Construction Manual*, 5th Edition, 2005, ISBN I-56424-055-X

53. Eurocode 1: Actions on Structures, Part 1-2; General Actions on Structures Exposed to Fire, 2002

54. Blagojevic, M.D. and Pesic, D., "A New Curve for Temperature-time Relationship in Compartment Fire," *Thermal Science*, 2011, Vol. 15. No. 2, pp.339-352

APPENDICES

APPENDIX A: TABLES

Table 1. Dimensionless maximum loads for beam-columns under biaxial loading at ambient temperature

Specimen No.	Load Path	Boundary Conditions	Dimensionless Maximum Loads	
RTBP-1	OA, P	x-pinned, y-pinned	p	0.550
			m_x	---
			m_y	---
RTBP-2	OF, M	x-pinned, y-pinned	p	---
			m_x	0.812
			m_y	0.812
RTBP-3	OAD, P+M	x-pinned, y-pinned	p	0.334
			m_x	0.465
			m_y	0.465
RTBP-4	OFD, M+P	x-pinned, y-pinned	p	0.334
			m_x	0.465
			m_y	0.465
RTBP-5	OFD, M+P	x-pinned, y-pinned	p	0.239
			m_x	0.616
			m_y	0.616
RTBP-6	OAD, P+M	x-pinned, y-pinned	p	0.239
			m_x	0.661
			m_y	0.661
RTBS-7	OA, P	x-pinned, y-partially fixed	p	0.593
			m_x	---
			m_y	---
RTBS-8	OF, M	x-pinned, y-partially fixed	p	---
			m_x	0.858
			m_y	0.858
RTBS-9	OAD, P+M	x-pinned, y-partially fixed	p	0.257
			m_x	0.636
			m_y	0.636
RTBS-10	OFD, M+P	x-pinned, y-partially fixed	p	0.268
			m_x	0.636
			m_y	0.636

Table 2. Dimensionless maximum loads for beam-columns under uniaxial loading at ambient temperature

Specimen No.	Load Path	Boundary Conditions	Dimensionless Maximum Loads	
RTUP-11	OG,M	x-pinned; y-pinned	p	0.000
			m_y	1.266
RTUP-12	OAE,P+M	x-pinned; y-pinned	p	0.386
			m_y	0.648
RTUP-13	OGE,M+P	x-pinned; y-pinned	p	0.406
			m_y	0.648
RTUP-14	OGE,M+P	x-pinned; y-pinned	p	0.233
			m_y	0.995
RTUP-15	OAE,P+M	x-pinned; y-pinned	p	0.233
			m_y	0.960
RTUS-16	OG,M	x-pinned; y-partially fixed	p	0.000
			m_y	1.620
RTUS-17	OAE,P+M	x-pinned; y-partially fixed	p	0.386
			m_y	0.932
RTUS-18	OGE,M+P	x-pinned; y-partially fixed	p	0.398
			m_y	0.932
RTUS-19	OGE,M+P	x-pinned; y-partially fixed	p	0.371
			m_y	0.993
RTUS-20	OAE,P+M	x-pinned; y-partially fixed	p	0.371
			m_y	1.034

Table 3. Dimensionless maximum loads for beam-columns uniaxial loading at 500°F
with or without axial restraint to thermal expansion

Specimen No.	Load Path	Boundary Conditions	Dimensionless Maximum Loads	
HTUP-1	OTM	x-pinned, y-pinned	p	---
			m_y	1.100
HTUP-2	OTP	x-pinned, y-pinned	p	0.467
			m_y	---
HTUP-3	OTMP	x-pinned, y-pinned	p	0.270
			m_y	0.595
HTUP-4	OTPM	x-pinned, y-pinned	p	0.270
			m_y	0.601
HTUP-5	OTPM	x-pinned, y-pinned	p	0.257
			m_y	0.590
HTUPR-6	OMTP	x-pinned, y-pinned	p	0.268
			m_y	0.595
HTUS-7	OTM	x-pinned, y-partially fixed	p	---
			m_y	1.270
HTUS-8	OTP	x-pinned, y-partially fixed	p	0.534
			m_y	---
HTUS-9	OTMP	x-pinned, y-partially fixed	p	0.352
			m_y	0.595
HTUS-10	OTPM	x-pinned, y-partially fixed	p	0.352
			m_y	0.694

Table 4. Dimensionless maximum loads for beam-columns under biaxial loading at 500°F with or without axial restraints to thermal expansion and pinned boundaries

Specimen No.	Load Path	Boundary condition	Dimensionless Maximum Loads	
HTBP-11	OTM	x-pinned, y-pinned	p	---
			m_y	0.761
			m_x	0.761
HTBP-12	OTMP	x-pinned, y-pinned	p	0.233
			m_y	0.460
			m_x	0.460
HTBP-13	OTPM	x-pinned, y-pinned	p	0.233
			m_y	0.426
			m_x	0.426
HTBPR-1	OTP	x-pinned, y-pinned	P	0.502
			m_y	---
			m_x	---
HTBPR-2	OTM	x-pinned, y-pinned	P	---
			m_y	0.741
			m_x	0.741
HTBPR-3	OTMP	x-pinned, y-pinned	P	0.156
			m_y	0.460
			m_x	0.460
HTBPR-4	OTPM	x-pinned, y-pinned	P	0.156
			m_y	0.470
			m_x	0.470

Table 5. Dimensionless maximum load for beam-columns with different load-temperature sequences

Specimen No.	Load Path	Boundary Condition	Maximum Loads or Temperature	
HTBPR-6	OTP	x-pinned, y-pinned	P	0.123
			m_y	---
			m_x	---
			T	900°F
HTBPR-7	OPT	x-pinned, y-pinned	P	0.123
			m_y	---
			m_x	---
			T	758°F
HTBPR-8	OTM	x-pinned, y-pinned	P	---
			m_y	0.214
			m_x	0.214
			T	900°F
HTBPR-9	OMT	x-pinned, y-pinned	P	---
			m_y	0.214
			m_x	0.214
			T	775°F
HTUPR-10	OTM	x-pinned, y-pinned	P	---
			m_y	0.402
			T	900°F
HTUPR-11	OMT	x-pinned, y-pinned	P	---
			m_y	0.402
			T	750°F

Table 6. Comparisons of dimensionless maximum loads for tests with or without axial restraints to thermal expansion at different temperature

Applied Load	Load Path	Temperature and Boundary Conditions	Dimensionless Maximum Value
p	OTP	72°F	0.617
		500°F, unrestrained	0.505
		500°F, moderately restrained	0.502
		900°F, moderately restrained	0.123
$m_x = m_y$	OTM	72°F	0.811
		500°F, unrestrained	0.761
		500°F, moderately restrained	0.741
		900°F, moderately restrained	0.214
m_y	OTM	72°F	1.266
		500°F, moderately restrained	1.100
		900°F, moderately restrained	0.402

Table 7. Summary the dimensionless maximum loads with pinned-pinned boundary conditions

i	Temperature, T_i °F	Dimensionless Maximum Load		
		p	m_y	$m_x = m_y$
1	72.0	0.550	1.266	0.811
2	500.0	0.502	1.100	0.741
3	900.0	0.123	0.402	0.214

Table 8. Comparisons of predicted and previously published results for imperfect beam-columns

Case No in Ref. 9	L/r_x	k (in-kip/rad.)	u_o	v_o	Dimensionless p_{max}	
					Ref. 9	Predicted
49	53.73	0	L/100,000	L/1000	0.855	0.858
52	53.73	5397.22	L/100,000	L/1000	0.890	0.885
55	53.73	15506.94	L/100,000	L/1000	0.928	0.922
73	53.73	0	L/1000	L/1000	0.81	0.824
76	53.73	5397.22	L/1000	L/1000	0.858	0.862
79	53.73	15506.94	L/1000	L/1000	0.908	0.901
105	48.65	0	L/100,000	L/1000	0.869	0.856
107	48.65	5397.22	L/100,000	L/1000	0.91	0.906
109	48.65	15506.94	L/100,000	L/1000	0.942	0.942
121	48.65	0	L/1000	L/1000	0.799	0.800
123	48.65	5397.22	L/1000	L/1000	0.844	0.844
125	48.65	15506.94	L/1000	L/1000	0.894	0.890

Table 9. Comparisons of predicted and preciously published dimensionless maximum load for pinned beam-column with nonproportional loading

Case No. in Ref. 10	Cross-sectional dimensions	L (in.)	E $(10^3 ksi)$	p	m_{max}	
					Ref. 10	Predicted
3	1.5×2.0×0.1238	53.475	26.4	0.326	0.715	0.695
4	1.5×2.0×0.1238	53.775	27.0	0.187	0.958	0.923

Table 10. Comparison of predicted and previously published dimensionless maximum load for pinned beam-columns with biaxially eccentric load

Section	Length in.	Area. in^2	Eccen. e_x (in)	Eccen. e_y (in)	Dimensionless Maximum Load p Tested in Ref. 33	Dimensionless Maximum Load p Computed in Ref. 43	Dimensionless Maximum Load p Predicted
H 6×6	96	9.67	1.61	2.78	0.329	0.329	0.328
H 5×5	120	6.76	2.38	2.51	0.189	0.195	0.194

Table 11. Comparison of predicted and preciously published dimensionless maximum load for pinned-end beam-columns with biaxially eccentric load

Section	Length in.	Area. in^2	e_x (in.)	e_y (in.)	Dimensionless Maximum Load p Ref. 44	Dimensionless Maximum Load p Predicted
W12×65	180	19.1	18.4	3.76	0.199	0.185
W12×65	270	19.1	18.4	3.76	0.169	0.167
W12×65	360	19.1	18.4	3.76	0.144	0.149

Table 12. Maximum dimensionless loads for uniaxially loaded beam-columns with linear partial rotational end restraints and load paths LC1 through LC4 (W8x31, L=12ft)

σ_{rc}	Spring stiffness	load	Major axis LC1	Major axis LC2	Minor axis LC1	Minor axis LC2	Major axis LC3	Major axis LC4	Minor axis LC3	Minor axis LC4
0	k_{a3}	p	0.950	0.950	0.935	0.935	0.436	0.436	0.140	0.140
		m	0.067	0.067	0.178	0.178	1.00	0.999	4.000	3.870
-0.3	k_{a1}	p	0.710	0.710	0.625	0.625	0.154	0.154	0.260	0.261
		m	0.190	0.190	0.087	0.087	0.900	0.898	0.850	0.850
-0.3	k_{a2}	p	0.750	0.751	0.800	0.800	0.380	0.380	0.025	0.025
		m	0.271	0.271	0.178	0.178	1.050	1.050	3.400	4.160
-0.3	k_{a3}	p	0.800	0.804	0.850	0.853	0.417	0.417	0.108	0.108
		m	0.320	0.320	0.244	0.244	1.00	1.020	4.000	4.445

Table 13. Maximum dimensionless loads for beam-columns with load paths through LC1 to LC4 and elastic-plastic partial rotational end restraints (ka2; $m_{plastic}$ =100 in-kips; W8x31, L=12ft)

Bending axis	Load	LC1	LC2	LC3	LC4
Major Axis	p	0.800	0.801	0.138	0.138
	m	0.186	0.186	1.000	1.000
Minor Axis	p	0.800	0.796	0.090	0.090
	m	0.130	0.130	1.400	1.400

Table 14. Maximum dimensionless loads for uniaxially loaded beam-columns with linear partial rotational end restraints (W8x31, L=12ft)

Spring Stiffness	Load Path	Maximum External Loads				
k_{a2}	NP2	P	0.000	0.242	0.493	0.860	0.862
		m_y	3.800	3.000	1.500	0.001	0.000
	NP1	p	0.000	0.242	0.493	0.860	0.862
		m_y	3.800	3.709	1.500	0.035	0.000
k_{a3}	NP2	P	0.000	0.362	0.458	0.663	0.894
		m_y	5.114	4.500	3.000	1.500	0.000
	NP1	p	0.000	0.362	0.458	0.663	0.894
		m_y	5.114	3.649	2.894	1.496	0.000

Table 15. Maximum dimensionless loads for biaxially loaded beam-columns with linear partial rotational end-restraints and load paths NP3 and NP4 (L=12 ft.; W8x31)

Sping Stiffness	Load Path	Maximum External Loads					
k_{a2}	NP3	p	0.000	0.250	0.500	0.750	0.810
		m_x	3.520	0.925	0.531	0.109	0.000
		$m_y{}^*$	2.063	0.542	0.311	0.064	0.000
	NP4	p	0.000	0.302	0.501	0.750	0.810
		m_x	3.520	0.925	0.531	0.109	0.000
		$m_y{}^*$	2.063	0.542	0.311	0.064	0.000
k_{a3}	NP3	p	0.000	0.250	0.500	0.750	0.854
		m_x	3.456	1.127	0.815	0.303	0.000
		$m_y{}^*$	2.020	0.660	0.478	0.177	0.000
	NP4	p	0.000	0.339	0.486	0.750	0.854
		m_x	3.456	1.127	0.815	0.303	0.000
		$m_y{}^*$	2.020	0.660	0.478	0.177	0.000

Note: $m_y{}^*=m_y/m_{xY}$, m_y is dimensionless applied external moment and m_{xY} is dimensionless yield moment about x axis.

Table 16. Maximum external loads for pinned beam-column BC1 with hollow square section and different load paths

Load Path	Maximum Dimensionless Loads					
NP3	p	0.00	0.25	0.50	0.75	0.87
	m_x	0.78	0.55	0.30	0.11	0.00
	m_y	0.78	0.55	0.30	0.11	0.00
NP4	p	0.00	0.25	0.50	0.75	---
	m_x	0.78	0.55	0.30	0.11	---
	m_y	0.78	0.55	0.30	0.11	---
NP5	p	0.00	0.25	0.50	0.75	---
	m_x	0.78	0.55	0.30	0.11	---
	m_y	0.78	0.55	0.30	0.11	---
NP6	p	0.00	0.25	0.50	0.75	---
	m_x	0.78	0.55	0.30	0.11	---
	m_y	0.78	0.55	0.30	0.11	---

Table 17. Maximum external loads for partially restrained imperfect beam-column BC3 with hollow square section (k= k_{a3}) and different load paths

Load Path		Dimensionless Maximum Loads					
NP3	p	0.00	0.10	0.25	0.50	0.75	0.93
	m_x	2.01	1.70	1.24	0.83	0.37	0.00
	m_y	2.01	1.70	1.24	0.83	0.37	0.00
NP4	m_x	2.01	1.70	1.24	0.83	0.37	---
	m_y	2.01	1.70	1.24	0.83	0.37	---
	p	0.00	0.01	0.18	0.51	0.75	---
NP5	p	0.00	0.10	0.25	0.50	0.75	---
	m_x	2.01	1.70	1.24	0.83	0.37	---
	m_y	0.39	0.85	1.12	0.84	0.37	---
NP6	m_y	2.01	1.70	1.24	0.83	0.37	---
	m_x	0.39	0.97	1.24	0.83	0.37	---
	P	0.00	0.00	0.19	0.51	0.75	---

Table 18. Dimensionless maximum loads for beam-column BC5 with rectangular section and linear rotational restraint ($k= k_{a3}$) and different load paths

Load Path		Dimensionless Maximum Loads						
NP3	p	0.0	0.05	0.10	0.25	0.50	0.75	0.92
	m_x	2.05	1.99	1.70	1.18	0.82	0.37	0.0
	m_y	2.18	2.05	1.81	1.25	0.87	0.39	0.0
NP4	m_x	2.05	1.99	1.70	1.18	0.82	0.37	---
	m_y	2.18	2.05	1.81	1.25	0.87	0.39	---
	p	0.0	0.01	0.01	0.22	0.50	0.76	---
NP5	p	0.0	0.05	0.10	0.25	0.50	0.75	---
	m_x	2.05	1.99	1.70	1.18	0.82	0.37	---
	m_y	0.7	0.75	0.98	1.20	0.86	0.41	---
NP6	m_y	2.18	2.05	1.81	1.25	0.87	0.39	---
	m_x	0.0	0.01	0.66	1.18	0.82	0.37	---
	p	0.0	0.0	0.0	0.23	0.50	0.76	---
NP7	p	0.0	0.05	0.10	0.25	0.50	0.75	---
	m_y	2.18	2.05	1.81	1.25	0.87	0.39	---
	m_x	0.0	0.0	0.37	1.13	0.81	0.40	---
NP8	m_x	2.05	1.99	1.70	1.18	0.82	0.37	---
	m_y	0.70	0.79	1.13	1.25	0.87	0.39	---
	p	0.0	0.0	0.0	0.23	0.50	0.76	---

Table 19. Comparisons between experimental and predicted dimensionless results for biaxial loading beam-columns at ambient temperature

Specimen No.	Load Path	Boundary Conditions	Maximum Dimensionless Loads			Predicted/Tested
			Load	Tested	Predicted	
RTBP-1	OA	pinned	p	0.550	0.624	1.13
			m_x	---	---	---
			m_y	---	---	---
RTBP-2	OF	pinned	p	---	---	---
			m_x	0.812	0.811	1.00
			m_y	0.812	0.811	1.00
RTBP-3	OAD	pinned	p	0.334	---	---
			m_x	0.465	0.486	1.05
			m_y	0.465	0.486	1.05
RTBP-4	OFD	pinned	p	0.326	0.334	1.02
			m_x	0.486	---	---
			m_y	0.486	---	---
RTBP-5	OFD	pinned	p	0.239	0.257	1.08
			m_x	0.616	---	---
			m_y	0.616	---	---
RTBP-6	OAD	pinned	p	0.239	---	---
			m_x	0.661	0.645	0.98
			m_y	0.661	0.645	0.98
RTBS-7	OA	partially fixed	p	0.593	0.641	1.08
			m_x	---	---	---
			m_y	---	---	---
RTBS-8	OF	partially fixed	p	---	---	---
			m_x	0.858	1.012	1.18
			m_y	0.858	1.012	1.18
RTBS-9	OAD	partially fixed	p	0.257	---	---
			m_x	0.636	0.765	1.20
			m_y	0.636	0.765	1.20
RTBS-10	OFD	partially fixed	p	0.268	0.317	1.18
			m_x	0.636	---	---
			m_y	0.636	---	---

Note: Partially fixed: x-axis is pinned and y-axis is partially fixed.

Table 20. Comparisons between experimental and predicted dimensionless maximum loads for uniaxial loading at ambient temperature

Specimen No.	Load Path	Boundary Conditions	Dimensionless Maximum Loads			Predicted/Tested
			Load	Tested	Predicted	
RTUP-11	OG	pinned	p	---	---	---
			m_y	1.266	1.216	0.96
RTUP-12	OAE	pinned	p	0.386	0.386	---
			m_y	0.648	0.681	1.05
RTUP-13	OGE	pinned	p	0.416	0.398	0.96
			m_y	0.648	0.648	---
RTUP-14	OGE	pinned	p	0.233	0.266	1.14
			m_y	0.995	0.995	---
RTUP-15	OAE	pinned	p	0.233	0.233	---
			my	0.96	1.07	1.11
RTUS-16	OG	partially fixed	p	---	---	---
			m_y	1.62	2.34	1.44
RTUS-17	OAE	partially fixed	p	0.386	0.386	---
			m_y	0.932	1.09	1.17
RTUS-18	OGE	partially fixed	p	0.398	0.429	1.08
			m_y	0.932	0.932	---
RTUS-19	OGE	partially fixed	p	0.371	0.412	1.11
			m_y	0.993	0.993	---
RTUS-20	OAE	partially fixed	p	0.371	0.371	---
			m_y	1.034	1.148	1.11

Table 21. Dimensionless axial load for imperfect pinned beam-columns with initially applied biaxial moment and different high temperatures

$m_x=m_y=0.0$			$m_x=m_y=0.4$			$m_x=m_y=0.7$		
Temp. ^oF	BC	NS	Temp. ^oF	BC	NS	Temp. ^oF	BC	NS
68	0.872	1.000	68	0.544	0.577	68	0.307	0.321
300	0.867	1.000	300	0.537	0.569	300	0.304	0.316
600	0.844	1.000	600	0.505	0.536	600	0.283	0.295
750	0.827	1.000	700	0.491	0.522	750	0.270	0.270
800	0.782	0.941	800	0.444	0.471	800	0.208	0.214
900	0.687	0.819	900	0.362	0.362	810	0.192	0.195
1050	0.479	0.576	1050	0.160	0.167	840	0.072	0.072
1200	0.285	0.352	1085	0.069	0.069	---	---	---
1500	0.088	0.102	---	---	---	---	---	---
1800	0.039	0.043	---	---	---	---	---	---
2100	0.009	0.010	---	---	---	---	---	---

Note: BC means biaxially crooked; NS means nearly straight.

Table 22. Maximum dimensionless load p for biaxial loading pinned beam-columns under biaxial loading with $m_x = m_y = 0.6$ at different temperatures

Temp. °F	Maximum Axial Load p k equal to (kip-in/rad.)			
	0	13300	24000	infinity
68	0.406	0.643	0.707	0.964
300	0.399	0.637	0.704	0.963
500	0.382	0.636	0.712	0.962
600	0.373	0.635	0.716	0.962
700	0.362	0.633	0.718	0.961
750	0.353	0.633	0.719	0.961
800	0.310	0.575	0.660	0.904
850	0.258	0.545	0.623	0.846
900	0.198	0.496	0.572	0.788
940	0.067	0.465	0.528	0.737
943	0.034	0.457	0.524	0.732
1000	---	0.389	0.449	0.637
1100	---	0.233	0.321	0.471
1200	---	0.089	0.220	0.339
1220	---	0.000	0.185	0.312
1300	---	---	0.122	0.215
1350	---	---	0.102	0.184
1400	---	---	0.050	0.152
1450	---	---	0.000	0.120
1500	---	---	---	0.098
1550	---	---	---	0.085
1600	---	---	---	0.072
1700	---	---	---	0.053
1800	---	---	---	0.042
1900	---	---	---	0.032
2000	---	---	---	0.021
2050	---	---	---	0.015
2100	---	---	---	0.010
2150	---	---	---	0.005
2180	---	---	---	0.001
2200	---	---	---	0.000

Table 23. Critical temperatures for hollow square pinned steel beam-columns under biaxial loading with different load combinations

p	Critical Temperature (°F) and Biaxial Moments	
	$m_x = m_y = 0.2$	$m_x = m_y = 0.5$
0.05	1265	977
0.1	1226	971
0.2	1130	938
0.3	1052	854
0.4	983	674
0.5	899	---
0.6	788	---
0.68	365	---

Table 24. Dimensionless maximum loads for uniaxially loaded beam-columns with load paths LC1 through LC4 and elastic rotational restraints at 1000°F (W8×31)

Load	Major axis		Minor axis		Major axis		Minor axis	
	LC1	LC2	LC1	LC2	LC3	LC4	LC3	LC4
p	0.600	0.600	0.600	0.600	0.171	0.171	0.044	0.044
m	0.127	0.127	0.105	0.105	1.200	1.300	4.000	4.964

Table 25. Maximum loads for biaxially loaded imperfect beam-columns with elastic rotational restraints and various load paths at 1000°F (W8×31; k_{a3}=24,000 in-kip/rad.)

Load Path	Maximum External Loads						
	p	0.000	0.050	0.100	0.250	0.400	0.619
NP3	m_x	2.280	1.256	1.085	0.866	0.621	0.000
	m_y*	1.337	0.735	0.635	0.506	0.364	0.000
	m_x	2.280	1.256	1.085	0.866	0.621	0.000
NP4	m_y*	1.337	0.735	0.635	0.506	0.364	0.000
	p	0.000	0.001	0.004	0.237	0.370	0.619

Note: m_y*=m_y/m_{xY}; m_y is dimensionless applied external moment and m_{xY} is dimensionless yield moment about x axis.

Table 26. Maximum external loads for biaxially loaded imperfect beam-columns with elastic rotational restraints and various load paths at 1000°F (7×7×0.375 in.; k_{a3}=24,000 in-kip/rad.)

Load path	Dimensionless Maximum Loads					
	p	0.050	0.100	0.250	0.400	0.628
NP3	m_x	1.824	1.483	1.085	0.615	0.000
	m_y	1.824	1.483	1.085	0.615	0.000
	m_x	1.824	1.483	1.085	0.615	---
NP4	m_y	1.824	1.483	1.085	0.615	---
	p	0.001	0.002	0.197	0.401	---
	p	0.050	0.100	0.250	0.400	---
NP5	m_x	1.824	1.483	1.085	0.615	---
	m_y	0.546	0.965	0.825	0.613	---
	m_y	1.824	1.483	1.085	0.615	---
NP6	m_x	0.707	1.483	1.085	0.615	---
	P	0.000	0.001	0.191	0.400	---

Table 27. Maximum loads for biaxially loaded beam-columns with elastic rotational restraints and various load paths at 1000°F (8×6×0.375 in.; k_{a3}=24,000 in-kip/rad.)

Load path	Dimensionless Maximum Loads						
NP3	p	0.050	0.100	0.250	0.350	0.500	0.625
	m_x	1.615	1.410	1.041	0.723	0.342	0.000
	m_y	1.714	1.496	1.105	0.767	0.363	0.000
NP4	m_x	1.615	1.410	1.041	0.723	0.342	---
	m_y	1.714	1.496	1.105	0.767	0.363	---
	p	0.001	0.005	0.200	0.352	0.500	---
NP5	p	0.050	0.100	0.250	0.350	0.500	---
	m_x	1.615	1.410	1.041	0.723	0.342	---
	m_y	1.513	1.321	0.985	0.761	0.363	---
NP6	m_y	1.714	1.496	1.105	0.767	0.363	---
	m_x	0.563	1.410	1.041	0.723	0.342	---
	p	0.000	0.001	0.200	0.348	0.500	---
NP7	p	0.050	0.100	0.250	0.350	0.500	---
	m_y	1.714	1.496	1.105	0.767	0.363	---
	m_x	0.387	0.776	0.720	0.693	0.344	---
NP8	m_x	1.615	1.410	1.041	0.723	0.342	---
	m_y	1.714	1.496	1.105	0.767	0.363	---
	p	0.001	0.001	0.196	0.348	0.501	---

Table 28. Dimensionless maximum loads for biaxially loaded beam-columns with different load-temperature sequences at pinned boundary conditions (7×7×0.375 in.)

Load Path	Load/Temp.	Maximum Values for Load and Temperature					
OTMP	$T(°F)$	600	600	900	900	1200	1200
	m_x/m_y	0.650	0.100	0.550	0.100	0.220	0.050
	P	0.109	0.724	0.069	0.556	0.040	0.213
OTPM	$T(°F)$	600	600	900	900	1200	1200
	P	0.109	0.724	0.069	0.556	0.04	0.213
	m_x/m_y	0.650	0.100	0.550	0.100	0.220	0.050
OMTP	m_x/m_y	0.650	0.100	0.550	0.100	0.220	0.050
	$T(°F)$	600	600	900	900	1200	1200
	P	0.109	0.725	0.069	0.556	0.040	0.213
OMPT	m_x/m_y	0.650	0.100	0.550	0.100	0.220	0.050
	P	0.109	0.724	0.069	0.556	0.040	0.213
	$T(°F)$	602	604	902	900	1200	1200
OPTM	P	0.109	0.724	0.069	0.556	0.04	0.213
	$T(°F)$	600	600	900	900	1200	1200
	m_x/m_y	0.650	0.100	0.069	0.100	0.220	0.050
OTMMP	$T(°F)$	600	600	900	900	1200	1200
	m_x	0.650	0.100	0.550	0.100	0.220	0.050
	m_y	0.650	0.100	0.550	0.100	0.220	0.050
	p	0.109	0.724	0.069	0.556	0.040	0.213
OTPMM	$T(°F)$	600	600	900	900	1200	1200
	p	0.109	0.724	0.069	0.556	0.040	0.213
	m_x	0.650	0.100	0.550	0.100	0.220	0.050
	m_y	0.650	0.100	0.549	0.100	0.220	0.049
OMMPT	m_x	0.650	0.100	0.550	0.100	0.220	0.050
	m_y	0.650	0.100	0.550	0.100	0.220	0.050
	p	0.109	0.724	0.069	0.557	0.040	0.213
	$T(°F)$	600	602	900	900	1196	1200
OPMMT	P	0.109	0.724	0.069	0.556	0.040	0.213
	m_x	0.650	0.100	0.550	0.100	0.220	0.050
	m_y	0.650	0.100	0.550	0.100	0.220	0.050
	$T(°F)$	604	604	900	900	1200	1200

Table 29. Dimensionless maximum loads for biaxially loaded beam-columns with different load-temperature sequences and partial boundaries and without axial restraint to thermal expansion (7×7×0.375 in.)

Load Path	Load/Temp.	Maximum Values for Load or Temperature					
OTMP	T(°F)	600	600	900	900	1200	1200
	m_x/m_y	1.500	0.500	1.400	0.500	1.200	0.500
	P	0.072	0.689	0.059	0.559	0.031	0.233
OTPM	T (°F)	600	600	900	900	1200	1200
	P	0.072	0.689	0.059	0.559	0.031	0.233
	m_x/m_y	1.851	0.496	1.747	0.496	1.607	0.522
OMTP	m_x/m_y	1.500	0.500	1.400	0.500	1.200	0.500
	T(°F)	212	600	752	900	1200	1200
	P	0.000	0.686	0.000	0.557	0.023	0.232
OMPT	m_x/m_y	1.500	0.500	1.400	0.500	1.200	0.500
	P	0.001	0.680	0.003	0.559	0.031	0.233
	T(°F)	68	68	68	922	1208	1202
OPTM	P	0.072	0.689	0.059	0.559	0.031	0.233
	T(°F)	600	600	900	900	1200	1200
	m_x/m_y	1.851	0.494	1.714	0.496	1.607	0.491
OTMMP	T(°F)	600	600	900	900	1200	1200
	m_x	1.500	0.500	1.400	0.500	1.200	0.500
	m_y	1.500	0.500	1.400	0.500	1.200	0.500
	p	0.066	0.688	0.057	0.559	0.028	0.232
OTPMM	T(°F)	600	600	900	900	1200	1200
	p	0.072	0.689	0.059	0.559	0.031	0.233
	m_x	1.500	0.500	1.400	0.500	1.200	0.500
	m_y	1.958	0.493	1.843	0.492	1.569	0.488
OMMPT	m_x	1.500	0.500	1.400	0.500	1.200	0.500
	m_y	1.500	0.500	1.400	0.500	1.200	0.500
	p	0.000	0.682	0.003	0.559	0.031	0.233
	T(°F)	68	68	68	922	1202	1198
OPMMT	P	0.072	0.689	0.059	0.559	0.031	0.233
	m_x	1.500	0.500	1.400	0.500	1.200	0.500
	m_y	1.500	0.474	1.400	0.500	1.200	0.500
	T(°F)	212	68	212	922	1202	1200

Table 30. Comparisons between the experimental and predicted results for beam-columns at 500°F without axial restraints to thermal expansion

Specimen No.	Load Path	Load	Dimensionless Maximum Values		Predicted/Tested
			Tested	Predicted	
HTUP-1	OTM	m_y	1.100	1.217	1.106
HTUP-2	OTP	p	0.467	0.589	1.261
HTUP-3	OTMP	p	0.270	0.371	1.374
		m_y	0.595	---	---
HTUP-4	OTPM	p	0.270	---	---
		m_y	0.601	0.888	1.478
HTUP-5	OTPM	p	0.257	---	---
		m_y	0.590	0.927	1.571
HTUS-7	OTM	m_y	1.270	1.533	1.207
HTUS-8	OTP	p	0.534	0.613	1.148
HTUS-9	OTMP	p	0.352	0.442	1.256
		m_y	0.595	---	---
HTUS-10	OTPM	p	0.352	---	---
		m_y	0.694	0.898	1.294
HTBP-11	OTM	m_y	0.761	0.886	1.164
		m_x	0.761	0.886	1.164
HTBP-12	OTMP	p	0.233	0.265	1.137
		m_y	0.460	---	---
		m_x	0.460	---	---
HTBP-13	OTPM	p	0.233	---	---
		m_y	0.426	0.507	1.190
		m_x	0.426	0.507	1.190

Table 31. Comparisons between the experimental and predicted results for beam-columns with axial restraints to thermal expansion at 500°F

Specimen No.	Load Path	Load	Dimensionless Maximum Value		Predicted/Tested
			Tested	Predicted	
HTBPR-1	OTP	P	0.502	0.548	1.092
HTBPR-2	OTM	m_y	0.741	0.797	1.076
		m_x	0.741	0.797	1.076
HTBPR-3	OTMP	P	0.156	0.244	1.564
		m_y	0.46	---	---
		m_x	0.46	---	---
HTBPR-4	OTPM	P	0.156	---	---
		m_y	0.47	0.571	1.215
		m_x	0.47	0.571	1.215
HTUPR-5	OMTP	p	0.268	0.288	1.075
		m_y	0.595	---	---

Table 32. Comparisons between the experimental and predicted results for tests at 500°F with axial resistant to thermal expansion and different load-path sequences

Specimen No.	Load Path	Maximum Dimensionless Value			Predicted/Tested
			Tested	Predicted	
HTBPR-6	OTP	T	900°F	---	---
		P	0.123	0.297	2.415
HTBPR-7	OPT	P	0.123	---	
		T	758°F	1061 °F	1.400
HTBPR-8	OTM	T	900°F	---	---
		m_y	0.214	0.327	1.528
		m_x	0.214	0.327	1.528
HTBPR-9	OMT	m_y	0.214	---	---
		m_x	0.214	---	---
		T	775°F	1007 °F	1.299
HTUPR-10	OTM	T	900°F	---	---
		m_y	0.402	0.474	1.179
HTUPR-11	OMT	m_y	0.402	---	---
		T	750°F	1043 °F	1.391

Table 33. Dimensionless maximum axial load p for WTC columns with different end rotational restraints and axial restraint to thermal expansion at different temperatures

Temp. °F	Dimensionless Maximum Axial Loads for End Rotation Stiffness Equal to								
	0.0 for k_{ts} equal to			EI/L for k_{ts} equal to			10EI/L for k_{ts} equal to		
	0.0	EA/L	2EA/L	0.0	EA/L	2EA/L	0.0	EA/L	2EA/L
68	0.970	0.970	0.970	0.982	0.982	0.982	0.986	0.986	0.986
200	0.970	0.715	0.644	0.982	0.717	0.649	0.986	0.725	0.651
300	0.968	0.533	0.417	0.982	0.536	0.419	0.985	0.544	0.413
400	0.968	0.362	0.202	0.982	0.365	0.197	0.985	0.369	0.192
450	0.968	0.278	0.097	0.982	0.284	0.094	0.985	0.286	0.088
600	0.967	0.046	---	0.982	0.051	---	0.985	0.052	---
800	0.909	---	---	0.925	---	---	0.927	---	---
1000	0.640	---	---	0.651	---	---	0.652	---	---
1200	0.340	---	---	0.346	---	---	0.346	---	---
1400	0.151	---	---	0.155	---	---	0.154	---	---
1600	0.072	---	---	0.073	---	---	0.073	---	---

Table 34. Dimensionless maximum axial load p for WTC beam-columns under biaxial loading ($m_y/m_x = r_y/r_x$, $m_x = 0.7$) with different end rotational restraints, axial restraint to thermal expansion and temperatures

Temp. °F	Dimensionless Maximum Axial Loads for End Rotation Stiffness Equal to								
	0.0 for k_{ts} equal to			EI/L for k_{ts} equal to			10EI/L for k_{ts} equal to		
	0.0	EA/L	2EA/L	0.0	EA/L	2EA/L	0.0	EA/L	2EA/L
68	0.360	0.360	0.360	0.552	0.552	0.552	0.810	0.810	0.810
200	0.360	0.249	0.304	0.552	0.442	0.354	0.810	0.591	0.437
300	0.357	0.123	0.034	0.552	0.284	0.145	0.810	0.397	0.156
400	0.335	0.033	0.0	0.554	0.100	0.0	0.811	0.131	0.0
500	0.323	0.0	---	0.551	0.0	---	0.814	0.031	---
600	0.319	---	---	0.546	---	---	0.818	0.0	---
800	0.239	---	---	0.496	---	---	0.770	---	---
900	0.109	---	---	0.288	---	---	0.666	---	---
950	0.019	---	---	0.285	---	---	0.606	---	---
1000	0.00	---	---	0.194	---	---	0.535		
1050	---	---	---	0.096	---	---	0.463		
1200	---	---	---	0.0	---	---	0.284		
1400	---	---	---	---	---	---	0.125		
1600	---	---	---	---	---	---	0.055		

Table 35. Dimensionless maximum external loads for partial rotational restrained beam-columns from WTC building under uniaxial loading (m_x only) at different temperatures and axial restrains to thermal expansion $k_a = EI/L$)

k_{ts}	Temp. (°F)		Dimensionless Load for $m_y/m_x=0.0$				
0	68	p	0.000	0.250	0.500	0.750	0.983
		m_x	2.750	2.426	1.426	0.621	0.000
	600	p	0.000	0.250	0.500	0.750	0.983
		m_x	3.104	2.664	1.489	0.649	0.000
	900	p	0.000	0.250	0.500	0.750	0.804
		m_x	2.788	2.213	0.993	0.191	0.000
	1200	p	0.000	0.100	0.200	0.300	0.345
		m_x	2.452	1.956	0.935	0.284	0.000
	1500	p	0.000	0.025	0.050	0.075	0.100
		m_x	1.589	1.504	0.877	0.372	0.000
EA/L	200	p	0.000	0.200	0.400	0.600	0.733
		m_x	1.736	1.115	0.700	0.291	0.000
	300	p	0.000	0.200	0.350	0.500	0.552
		m_x	1.203	0.769	0.454	0.147	0.000
	400	p	0.000	0.100	0.200	0.300	0.379
		m_x	0.893	0.643	0.427	0.219	0.000
	550	p	0.000	0.050	0.080	0.110	0.135
		m_x	0.377	0.252	0.193	0.136	0.000
2EA/L	200	p	0.000	0.200	0.400	0.600	0.652
		m_x	1.448	0.960	0.541	0.134	0.000
	300	p	0.000	0.100	0.200	0.300	0.416
		m_x	0.962	0.709	0.498	0.289	0.000
	400	p	0.000	0.050	0.100	0.150	0.196
		m_x	0.522	0.374	0.258	0.165	0.000

Table 36. Dimensionless maximum external loads for pinned beam-columns from WTC building under uniaxial loading (m_x only) at different temperatures and axial restrains to thermal expansion $k_a = 0.0$)

k_{ts}	Temp. (°F)		Dimensionless Maximum Loads				
0	68	p	0.000	0.250	0.500	0.750	0.971
		m_x	1.454	1.181	0.719	0.328	0.000
	600	p	0.000	0.250	0.500	0.750	0.969
		m_x	1.454	1.152	0.686	0.314	0.000
	900	p	0.000	0.200	0.400	0.600	0.794
		m_x	1.191	0.948	0.573	0.273	0.000
	1200	p	0.000	0.100	0.200	0.300	0.341
		m_x	0.513	0.371	0.192	0.056	0.000
	1400	p	0.000	0.050	0.100	0.153	---
		m_x	0.230	0.157	0.072	0.000	---
EA/L	200	p	0.000	0.200	0.400	0.600	0.734
		m_x	1.303	0.922	0.670	0.343	0.000
	300	p	0.000	0.150	0.300	0.450	0.557
		m_x	1.000	0.807	0.468	0.199	0.000
	400	p	0.000	0.100	0.200	0.300	0.383
		m_x	0.598	0.453	0.304	0.164	0.000
	550	p	0.000	0.050	0.100	0.136	---
		m_x	0.255	0.190	0.116	0.000	---
2EA/L	200	p	0.000	0.200	0.400	0.600	0.654
		m_x	1.178	0.814	0.555	0.119	0.000
	300	p	0.000	0.150	0.300	0.400	0.418
		m_x	0.753	0.430	0.216	0.066	0.000
	400	p	0.000	0.050	0.100	0.150	0.198
		m_x	0.345	0.273	0.203	0.122	0.000

Table 37. Dimensionless maximum external loads for partially restrained exterior beam-columns from WTC building under uniaxial loading (m_y only) at different temperatures and axial restraints to thermal expansion ($k_a = EI/L$)

k_{ts}	Temp. (°F)		Dimensionless Maximum Loads				
0	68	p	0.000	0.250	0.500	0.750	0.983
		m_y	3.038	2.669	1.586	0.660	0.000
	600	p	0.000	0.250	0.500	0.750	0.983
		m_y	2.977	2.445	1.523	0.654	0.000
	900	p	0.000	0.250	0.500	0.750	0.804
		m_y	2.876	2.380	1.050	0.169	0.000
	1200	p	0.000	0.100	0.200	0.300	0.345
		m_y	2.425	2.069	0.977	0.285	0.000
	1500	p	0.000	0.025	0.050	0.075	0.100
		m_y	1.694	1.445	0.913	0.386	0.000
EA/L	200	p	0.000	0.200	0.400	0.600	0.733
		m_y	1.830	1.165	0.669	0.262	0.000
	300	p	0.000	0.200	0.350	0.500	0.552
		m_y	1.167	0.723	0.410	0.107	0.000
	400	p	0.000	0.100	0.200	0.300	0.379
		m_y	0.803	0.585	0.374	0.164	0.000
	550	p	0.000	0.050	0.110	0.135	---
		m_y	0.283	0.173	0.053	0.000	---
2EA/L	200	p	0.000	0.200	0.400	0.600	0.652
		m_y	1.524	0.924	0.502	0.107	0.000
	300	p	0.000	0.100	0.200	0.300	0.416
		m_y	0.870	0.656	0.445	0.236	0.000
	400	p	0.000	0.050	0.100	0.150	0.196
		m_y	0.414	0.305	0.196	0.092	0.000

Table 38. Maximum external nonproportional loads for pinned exterior WTC beam-columns at different temperatures and axial restraints to thermal expansion ($m_y/m_x = r_y/r_x$ and $k_a = EI/L$)

k_{ts}	Temp. (°F)		Dimensionless Load for $m_y/m_x = r_y/r_x$				
0	68	p	0.000	0.250	0.500	0.750	0.983
		m_x	1.749	1.528	1.140	0.522	0.000
	600	p	0.000	0.250	0.500	0.750	0.983
		m_x	1.994	1.648	1.216	0.533	0.000
	900	p	0.000	0.250	0.500	0.750	0.804
		m_x	1.871	1.453	0.857	0.149	0.000
	1200	p	0.000	0.100	0.200	0.300	0.345
		m_x	1.675	1.236	0.827	0.239	0.000
	1500	p	0.000	0.025	0.050	0.075	0.100
		m_x	1.106	0.895	0.708	0.351	0.000
EA/L	200	p	0.000	0.200	0.400	0.600	0.733
		m_x	1.367	1.006	0.578	0.179	0.000
	300	p	0.000	0.200	0.350	0.500	0.552
		m_x	1.026	0.511	0.249	0.070	0.000
	400	p	0.000	0.100	0.200	0.300	0.379
		m_x	0.498	0.336	0.212	0.106	0.000
	500	p	0.000	0.050	0.080	0.110	0.135
		m_x	0.262	0.204	0.173	0.141	0.000
2EA/L	200	p	0.000	0.200	0.400	0.600	0.652
		m_x	1.342	0.851	0.423	0.072	0.000
	300	p	0.000	0.100	0.200	0.300	0.416
		m_x	0.702	0.440	0.268	0.142	0.000
	400	p	0.000	0.050	0.100	0.150	0.196
		m_x	0.245	0.181	0.132	0.084	0.000

Table 39. Dimensionless maximum external loads for pinned exterior WTC beam-columns under biaxial loading at different temperatures and axial restraints to thermal expansion (m_y/m_x=0.5 and k_a =EI/L)

k_{ts}	Temp. (°F)		Dimensionless Load for m_y/m_x=0.5				
0	68	p	0.000	0.250	0.500	0.750	0.983
		m_x	2.726	2.036	1.428	0.612	0.000
	600	p	0.000	0.250	0.500	0.750	0.983
		m_x	3.073	2.197	1.507	0.630	0.000
	900	p	0.000	0.250	0.500	0.750	0.804
		m_x	2.942	1.916	1.009	0.186	0.000
	1200	p	0.000	0.100	0.200	0.300	0.345
		m_x	2.542	1.670	0.977	0.283	0.000
	1500	p	0.000	0.025	0.050	0.075	0.100
		m_x	1.494	1.223	0.911	0.402	0.000
EA/L	200	p	0.000	0.200	0.400	0.600	0.733
		m_x	1.822	1.143	0.682	0.247	0.000
	300	p	0.000	0.200	0.350	0.500	0.552
		m_x	1.142	0.660	0.345	0.100	0.000
	400	p	0.000	0.100	0.200	0.300	0.379
		m_x	0.677	0.466	0.298	0.150	0.000
	500	p	0.000	0.050	0.080	0.110	0.135
		m_x	0.368	0.293	0.251	0.196	0.000
2EA/L	200	p	0.000	0.200	0.400	0.600	0.652
		m_x	1.653	0.967	0.514	0.093	0.000
	300	p	0.000	0.100	0.200	0.300	0.416
		m_x	0.817	0.588	0.372	0.202	0.000
	400	p	0.000	0.050	0.100	0.150	0.196
		m_x	0.347	0.266	0.195	0.115	0.000

Table 40. Dimensionless maximum external loads for pinned exterior WTC beam-columns under biaxial loading with different temperatures and axial restraints to thermal expansion (m_y/m_x=2 and k_a =EI/L)

k_{ts}	Temp. (°F)		Dimensionless Load for m_y/m_x=2				
0	68	p	0.000	0.250	0.500	0.750	0.983
		m_x	1.443	1.035	0.738	0.325	0.000
	600	p	0.000	0.250	0.500	0.750	0.983
		m_x	1.668	1.110	0.777	0.323	0.000
	900	p	0.000	0.250	0.500	0.750	0.804
		m_x	1.564	0.969	0.524	0.088	0.000
	1200	p	0.000	0.100	0.200	0.300	0.345
		m_x	1.369	0.830	0.498	0.141	0.000
	1500	p	0.000	0.025	0.050	0.075	0.100
		m_x	0.862	0.615	0.456	0.202	0.000
EA/L	200	p	0.000	0.200	0.400	0.600	0.733
		m_x	0.895	0.573	0.338	0.120	0.000
	300	p	0.000	0.200	0.350	0.500	0.552
		m_x	0.574	0.327	0.170	0.048	0.000
	400	p	0.000	0.100	0.200	0.300	0.379
		m_x	0.335	0.231	0.148	0.074	0.000
	500	p	0.000	0.080	0.110	0.135	---
		m_x	0.180	0.142	0.102	0.000	---
2EA/L	200	p	0.000	0.200	0.400	0.600	0.652
		m_x	0.809	0.483	0.254	0.045	0.000
	300	p	0.000	0.100	0.200	0.300	0.416
		m_x	0.404	0.292	0.182	0.099	0.000
	400	p	0.000	0.050	0.100	0.150	0.196
		m_x	0.165	0.130	0.095	0.060	0.000

Table 41. Number of exterior columns damaged in each of the impacted floors for the North Tower of WTC (Ref. 25)

Floor No.	Number of Columns out of commission
94	21
95	15
96	15
97	13
98	4

Table 42. Temperature corresponding to zero load-carrying capacity for WTC beam-columns at service load

Dimensionless Service Load		Critical Temp. °F
p_o	0.497	1086
p_{new}	0.547	1056
m_{xo}	0.818	1058
m_{xnew}	0.911	1025
m_{yo}	0.884	1058
m_{ynew}	0.972	1025
p_o-0.5 m_{xo}	0.497-0.404	901
p_{new}-0.5m_{xnew}	0.547-0.455	827
p_o-0.5(m_{xo}+m_{yo})	0.497-0.404-0.442	815
p_{new}-0.5(m_{xnew}+m_{ynew})	0.547-0.455-0.486	658

APPENDIX B: FIGURES
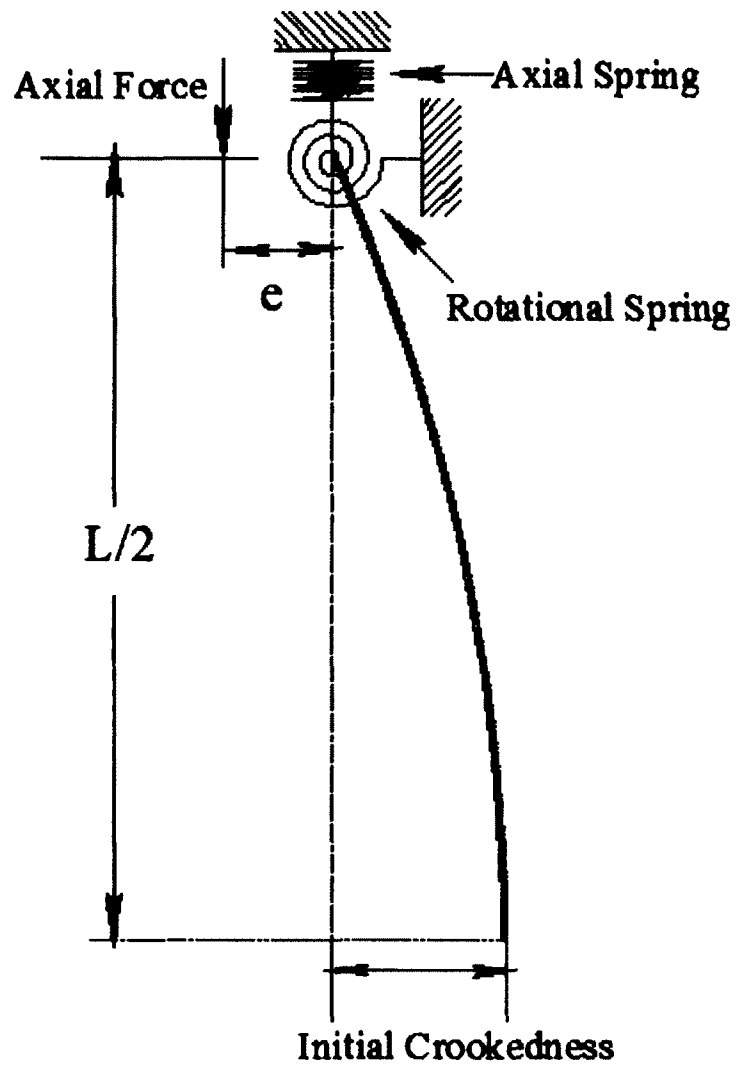
Figure 1. Model of beam-column under high temperature (13)
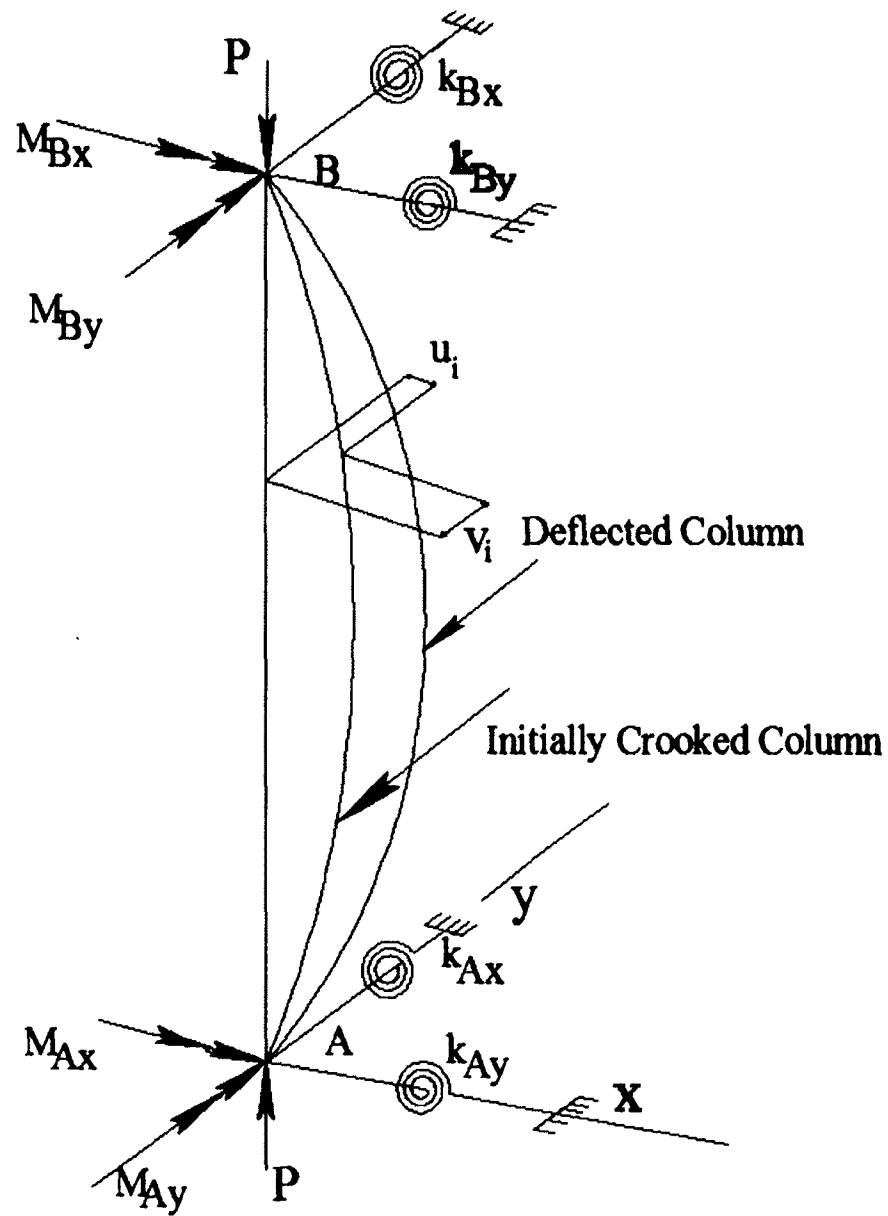
Figure 2. Biaxially loaded imperfect beam-column with partial rotational end restraints and high temperature
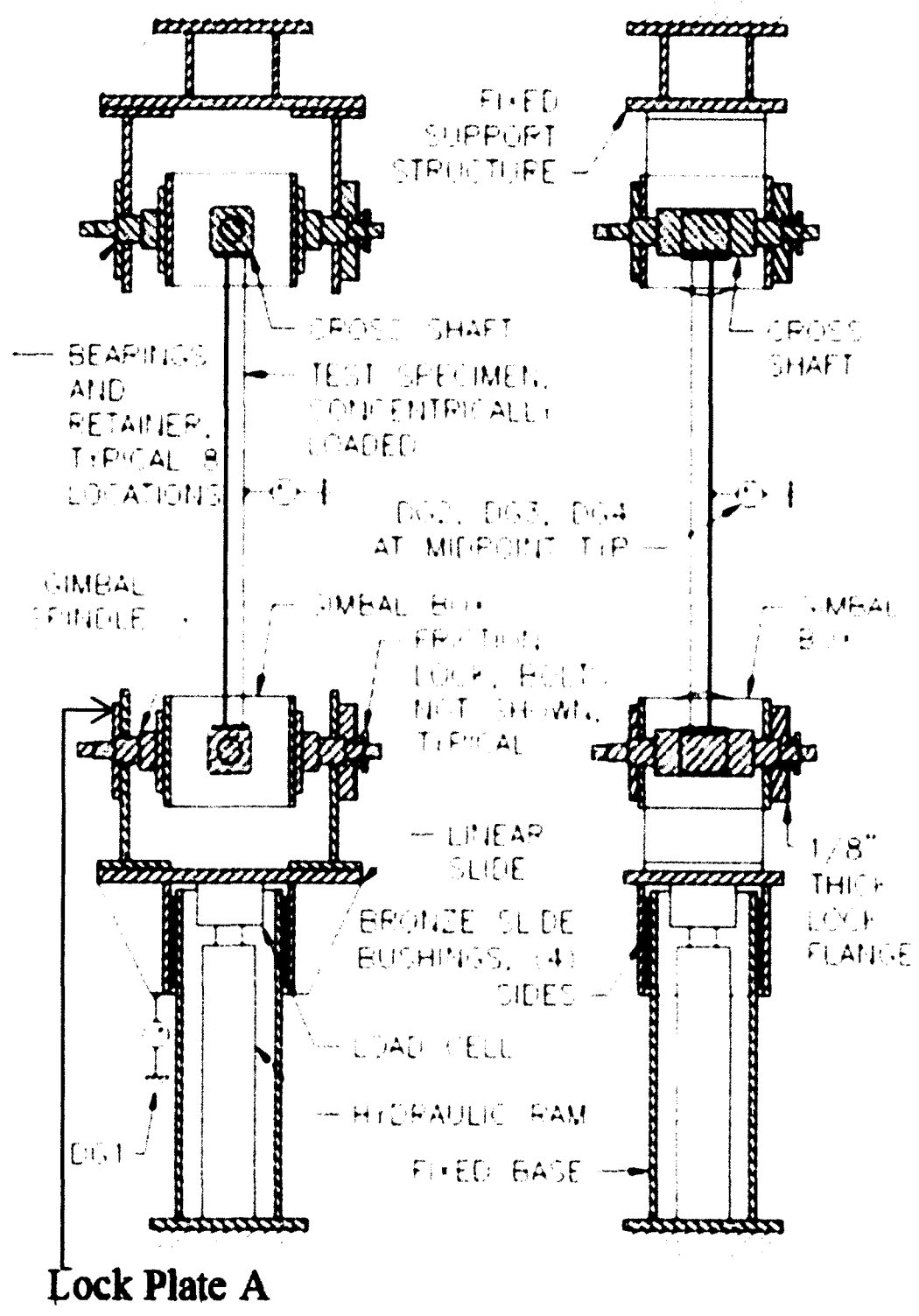
Figure 3. Schematic of test machine from (28)
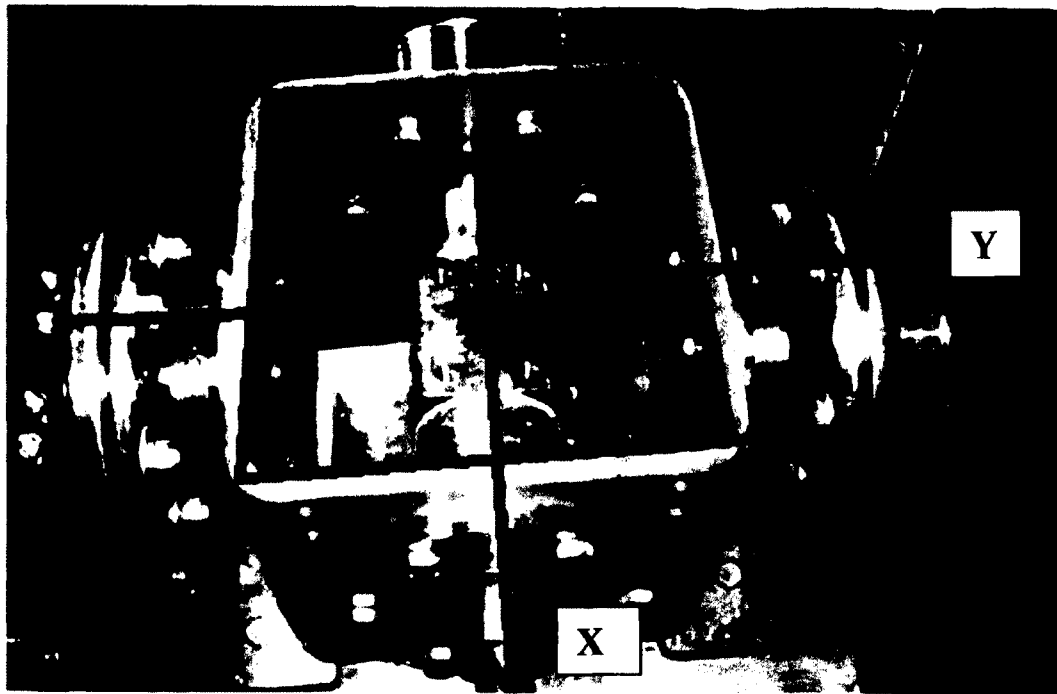
Figure 4. End fixtures simulating biaxial hinge
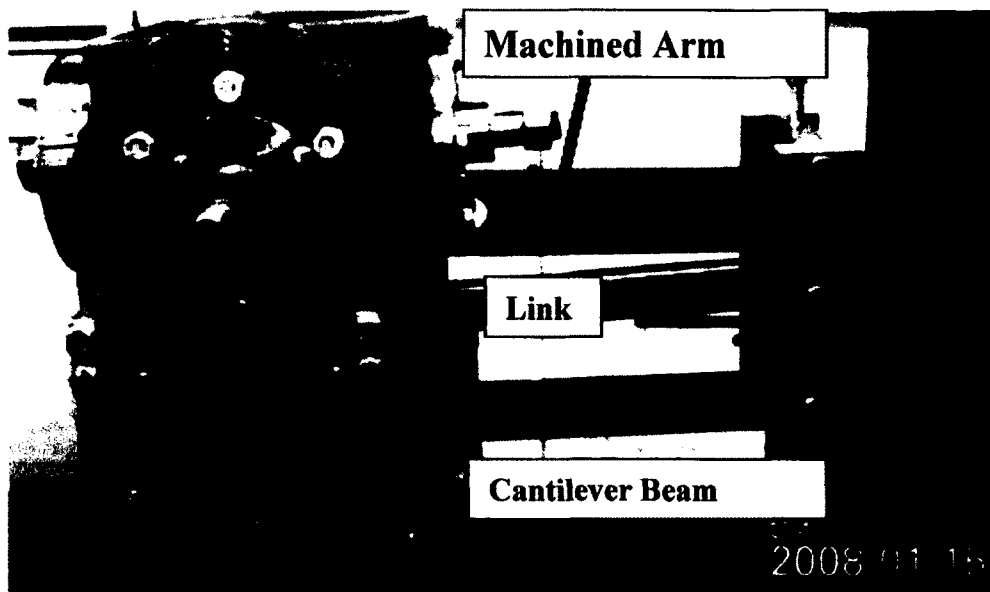
Figure 5. Flexible connection in one axis
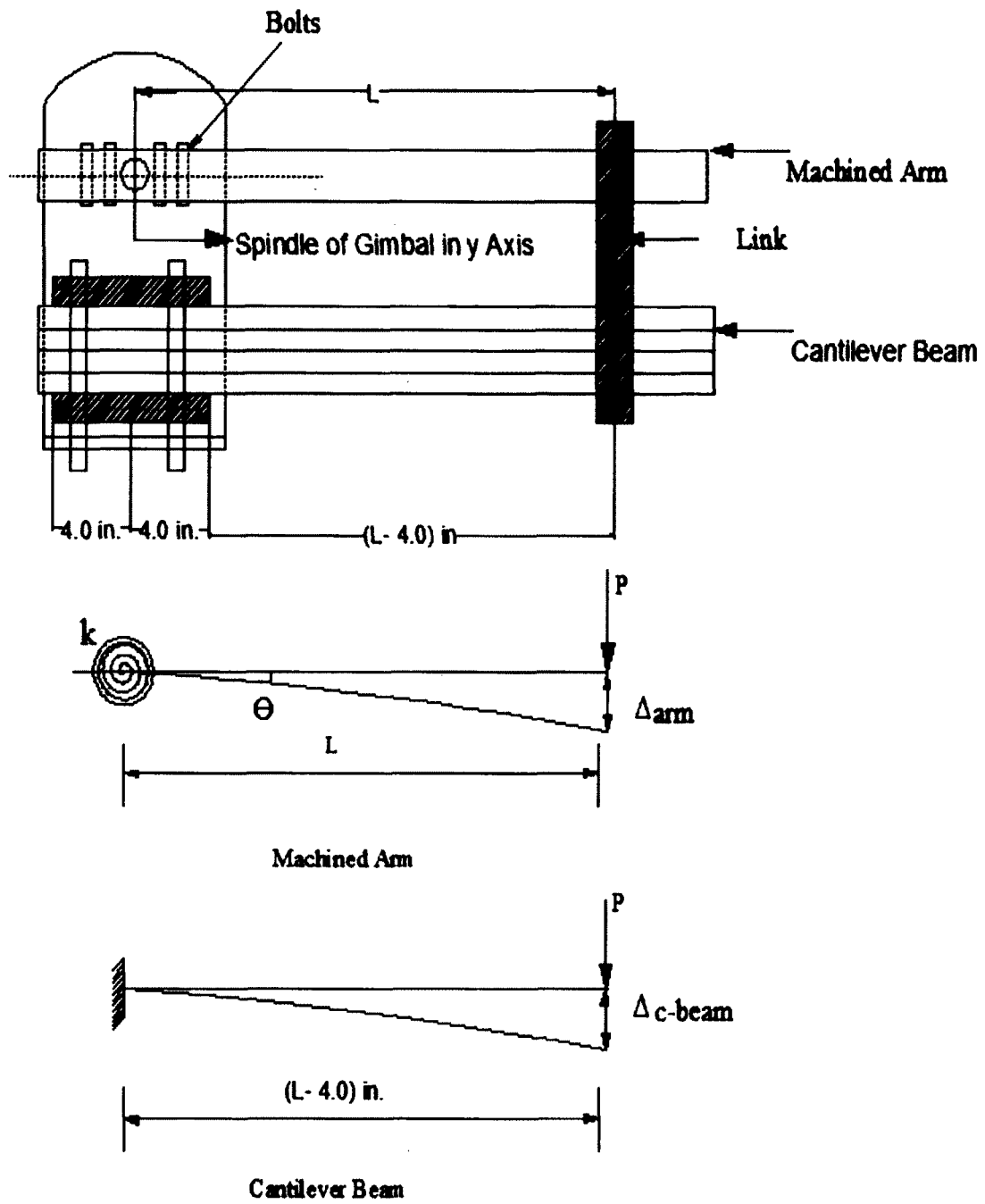
Figure 6. Schematic of flexible connection
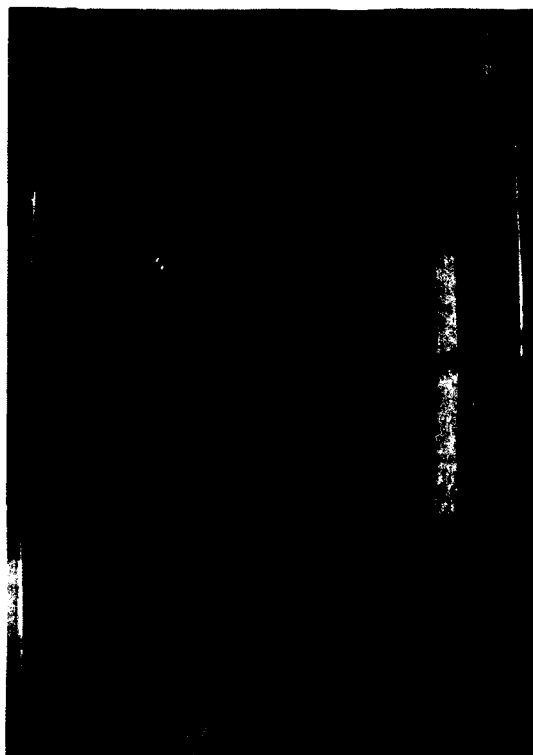
Figure 7. Furnace inside view
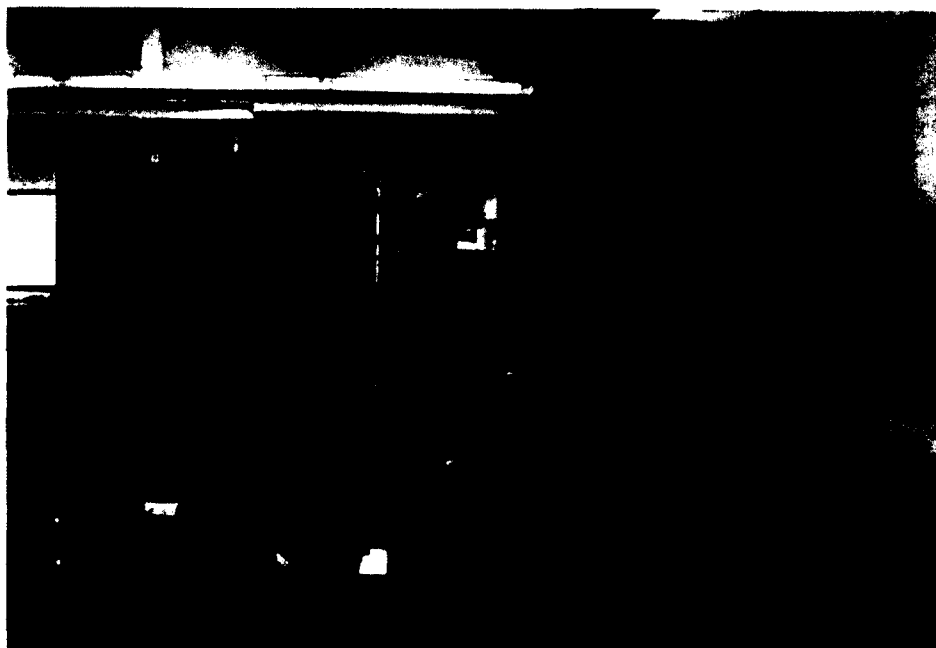
Figure 8. Heating furnace and controller
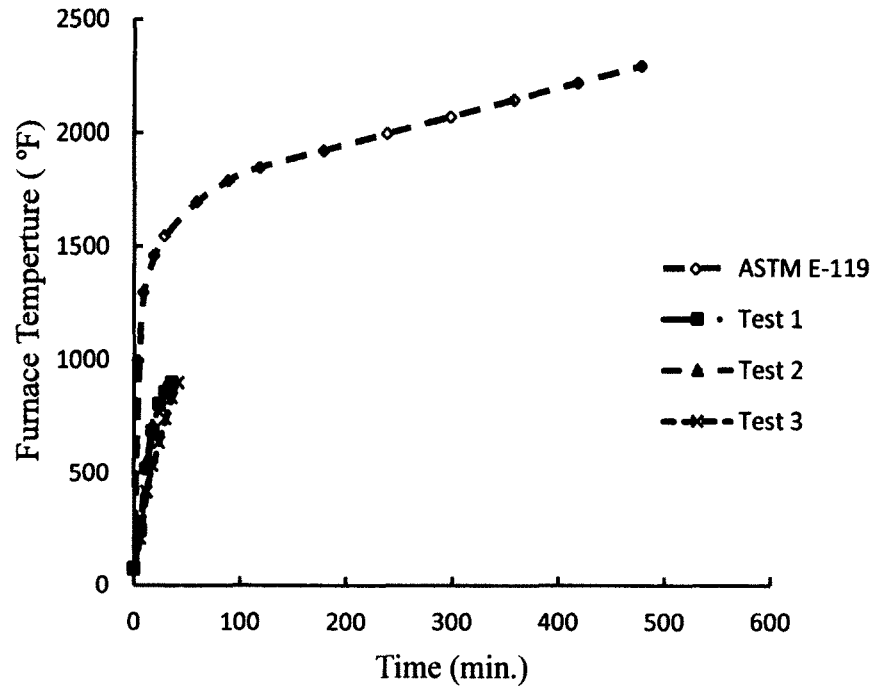
Figure 9. Furnace time-temperature exposure curve
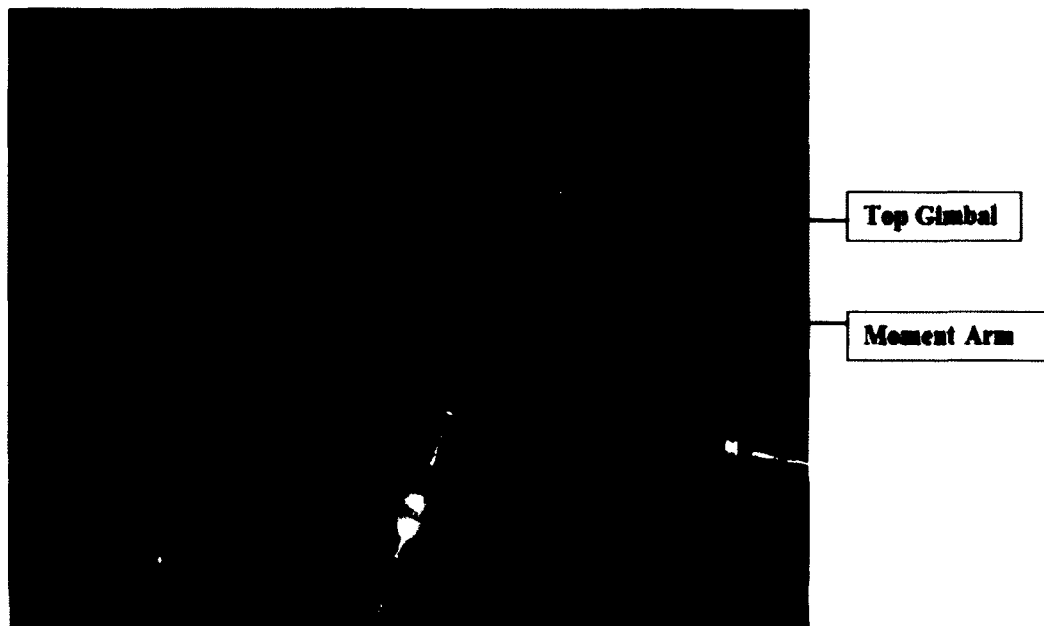
Figure 10. Connection between the moment arm and top gimbal

Top Plate A

Moment Arm

Tie Rod

Top Plate B of Steel Table

Hydraulic Jack C

Load Cell D

Bottom Plate E
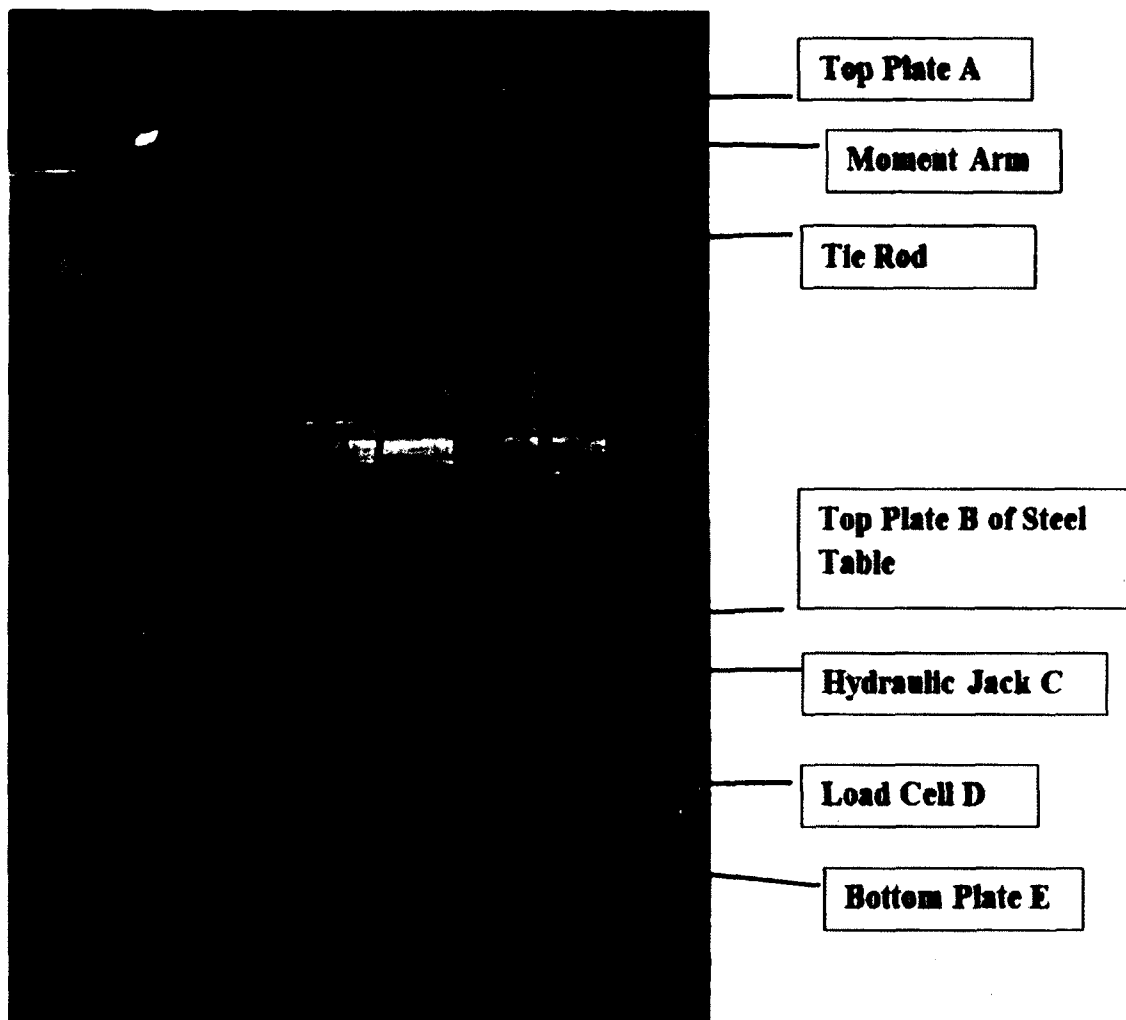
Figure 11. Picture for the moment device

Figure 12. Setup for ambient temperature test
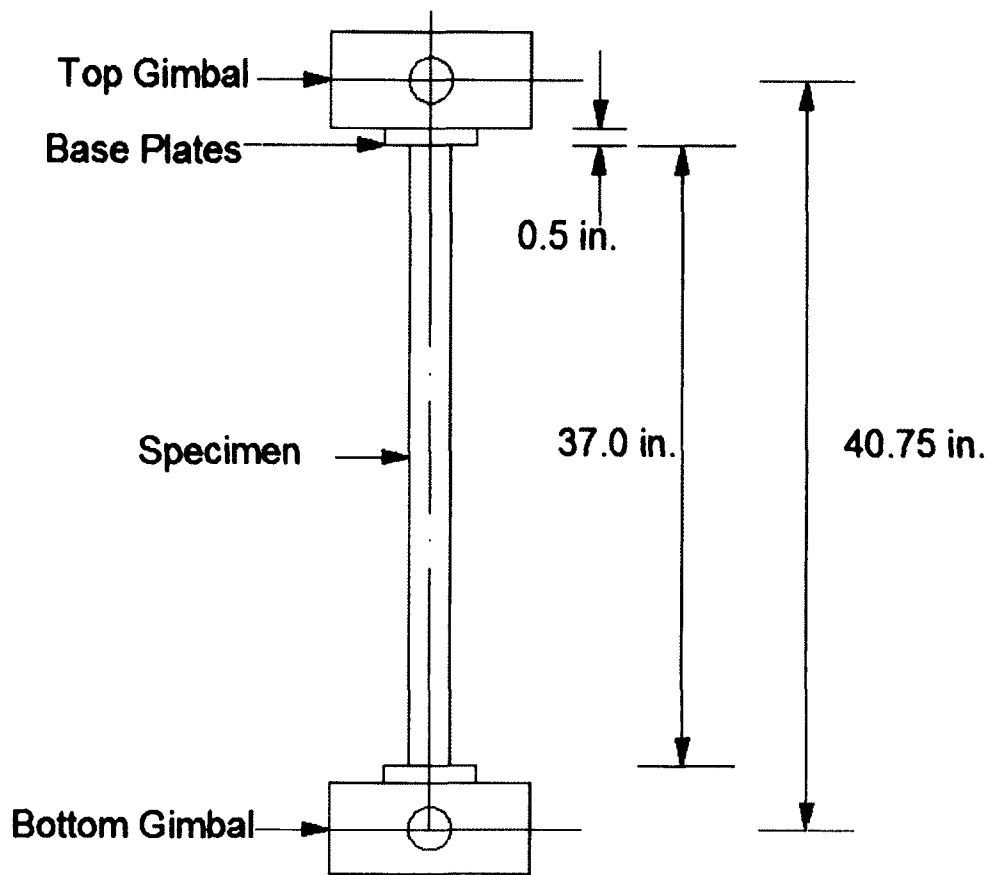
Figure 13. Schematic of test specimen including inner part of the gimbals
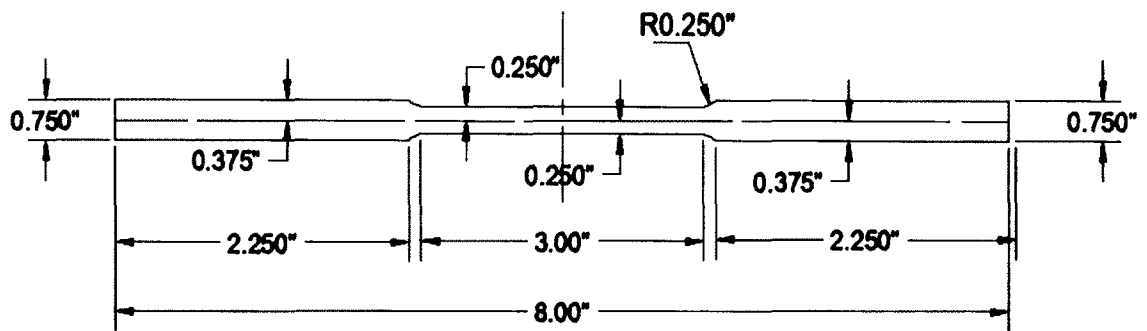
Figure 14. Typical tensile coupon
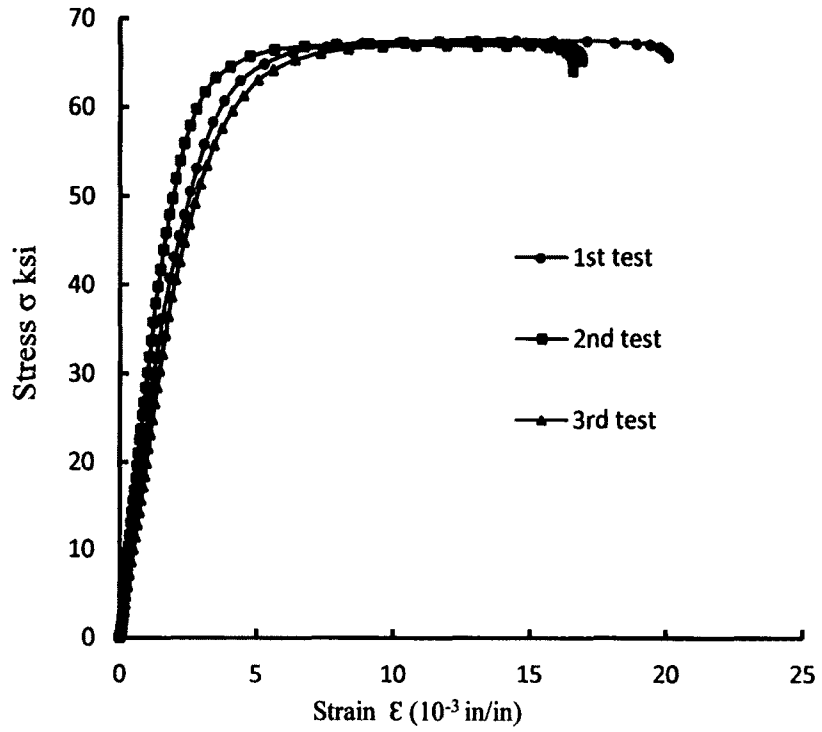
Figure 15. Stress-strain curves for tensile coupon tests
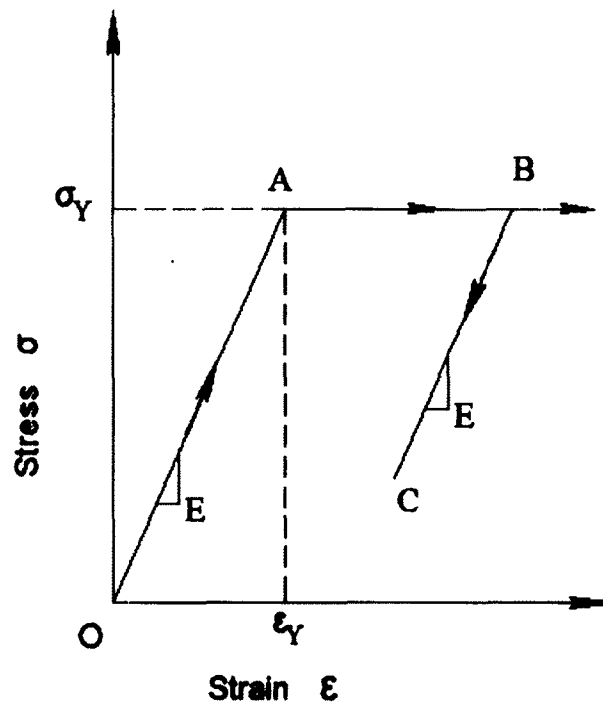
Figure 16. Material stress-strain relationship at ambient temperature
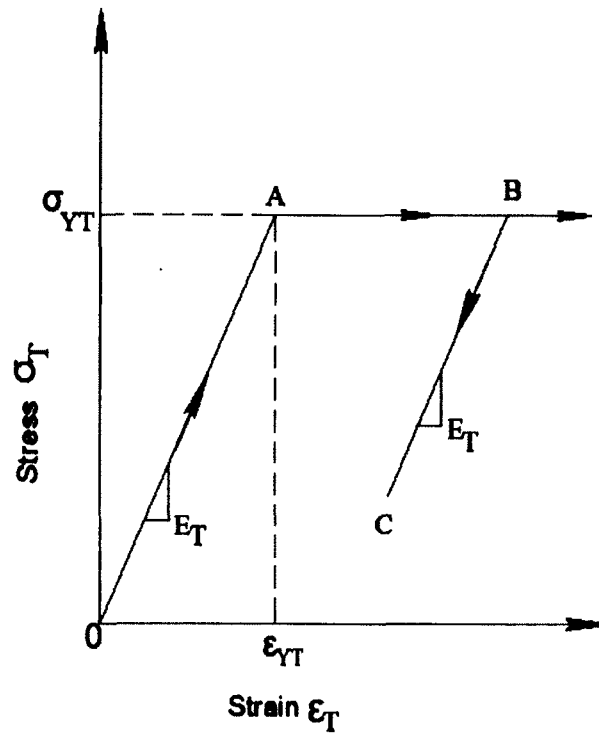
Figure 17. Material stress-strain relationship at high temperature
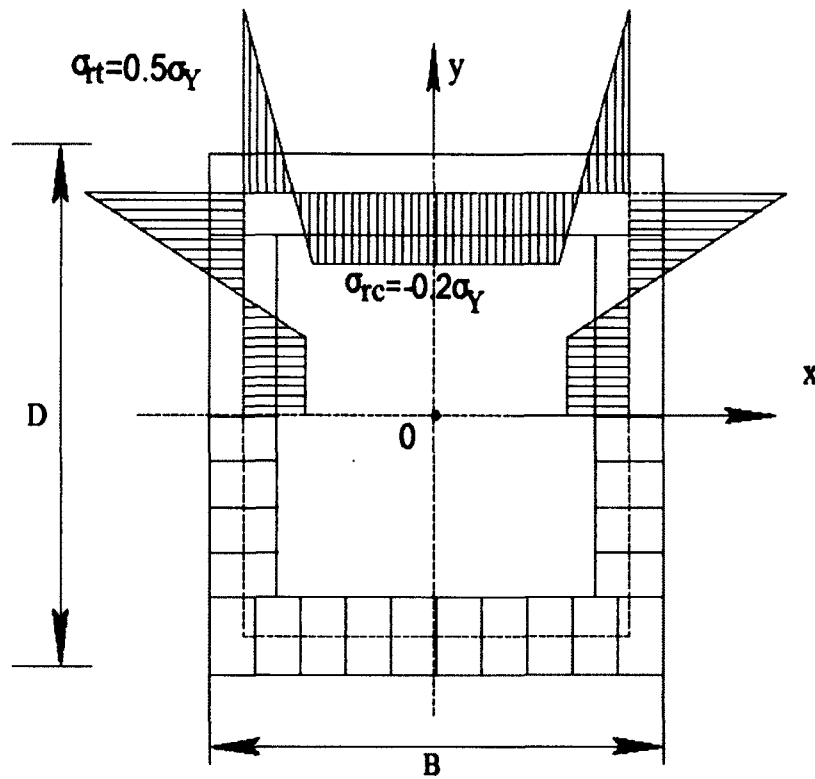
Figure 18. Typical residual stress distribution pattern for the rectangular section
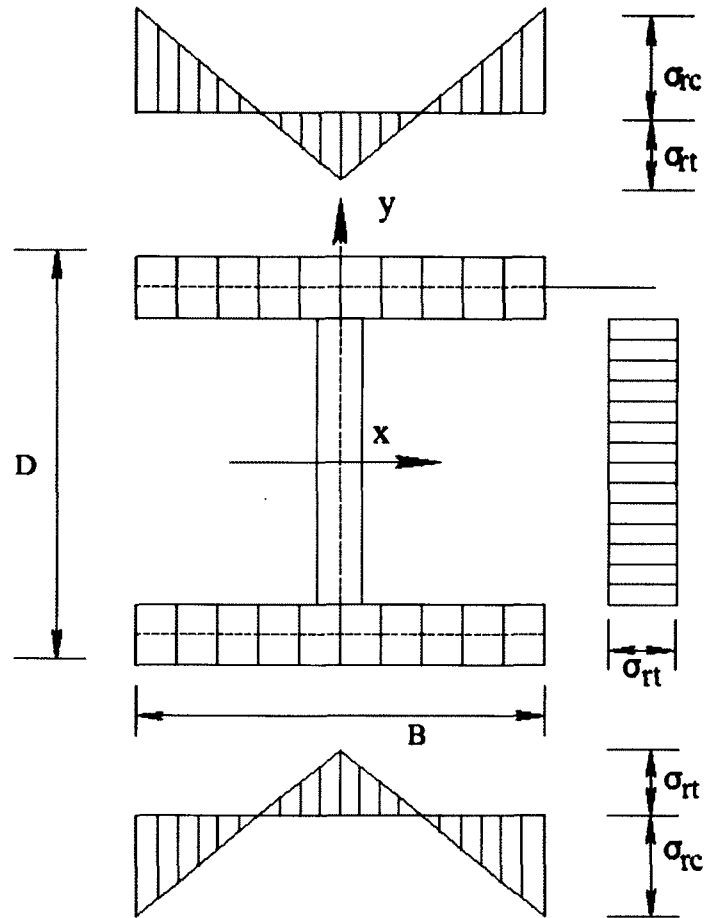
Figure 19. Typical residual stress distribution pattern for the I-section
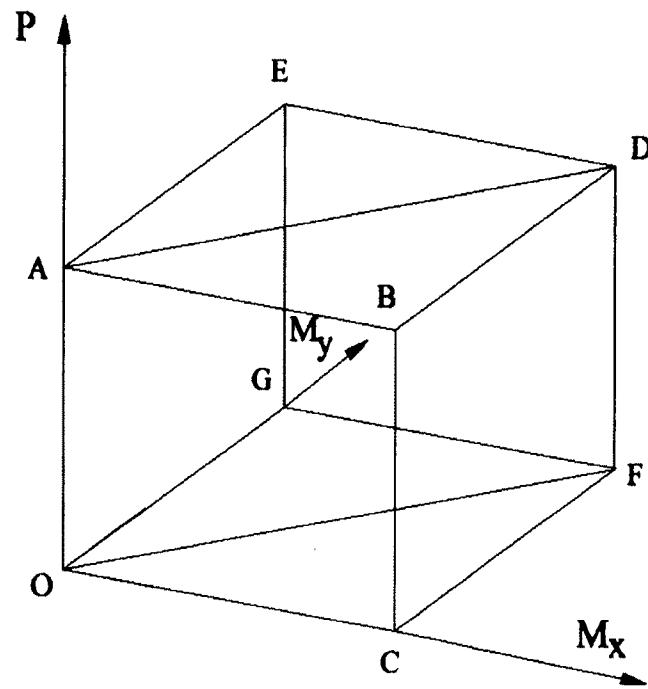
Figure 20. Loading paths for nonproportional loading at ambient temperature
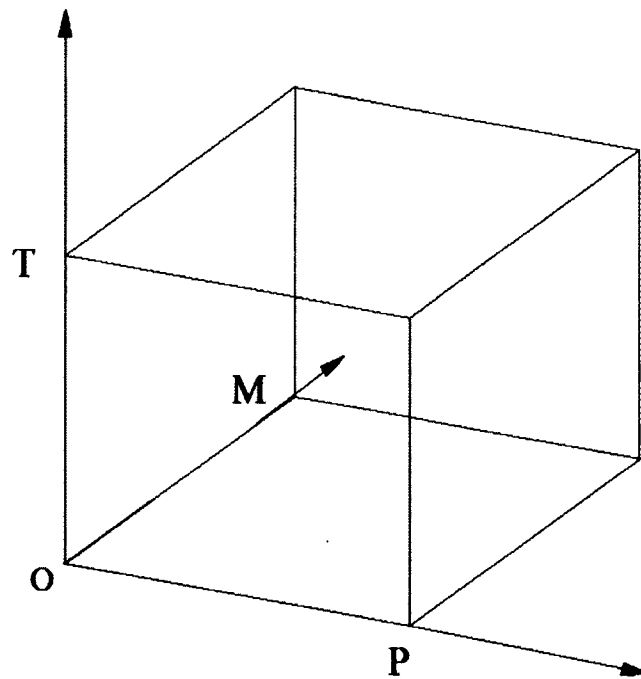
Figure 21. Loading paths for nonproportional loading at high temperature
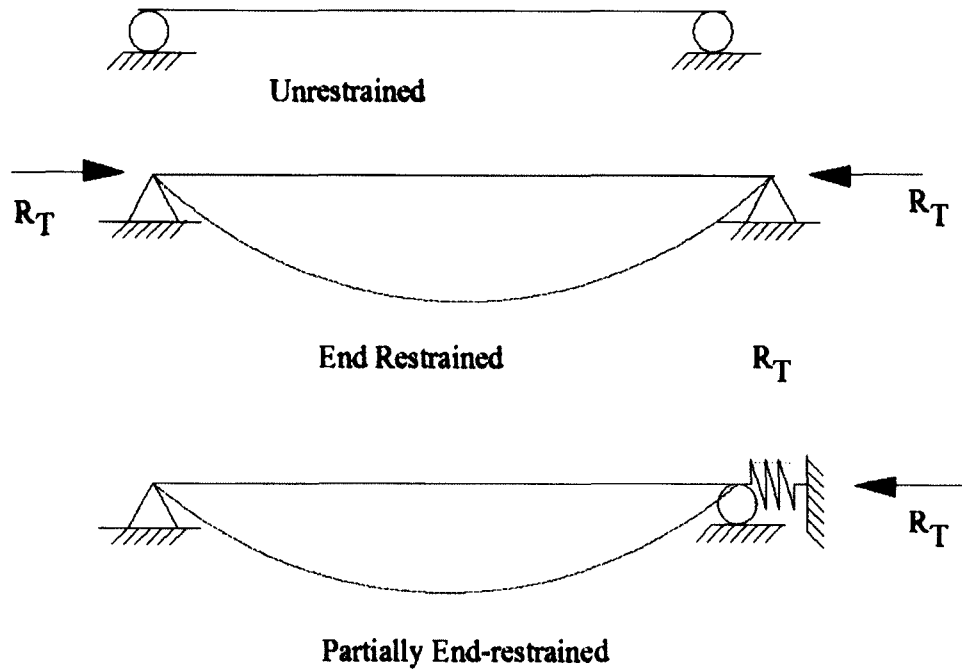
Figure 22. Various types of end restraints for thermal expansion
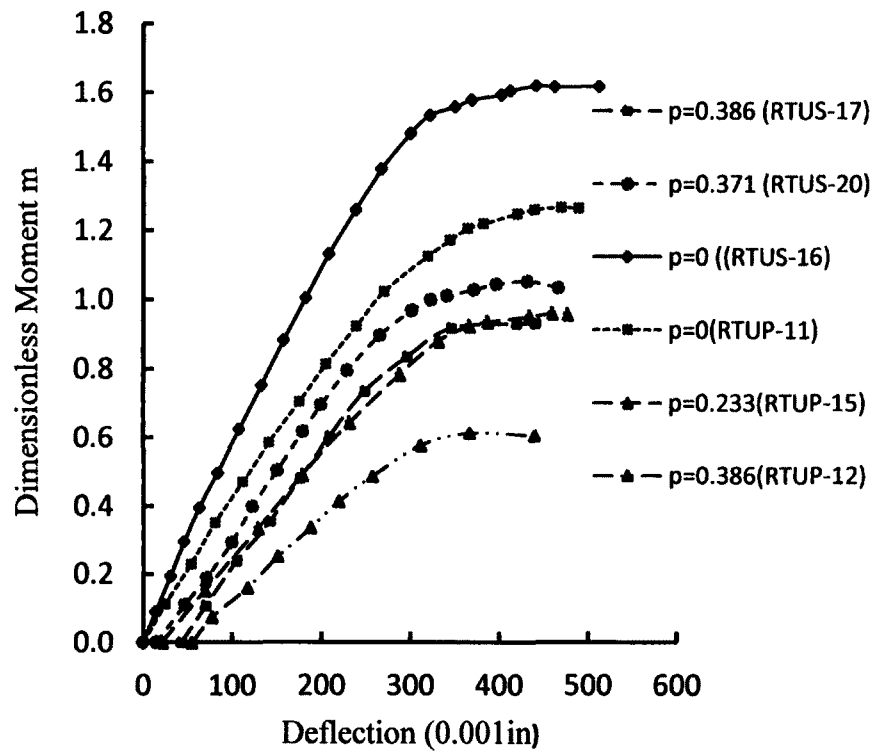
Figure 23. Moment versus deflection curves for uniaxial loading tests at ambient
temperature
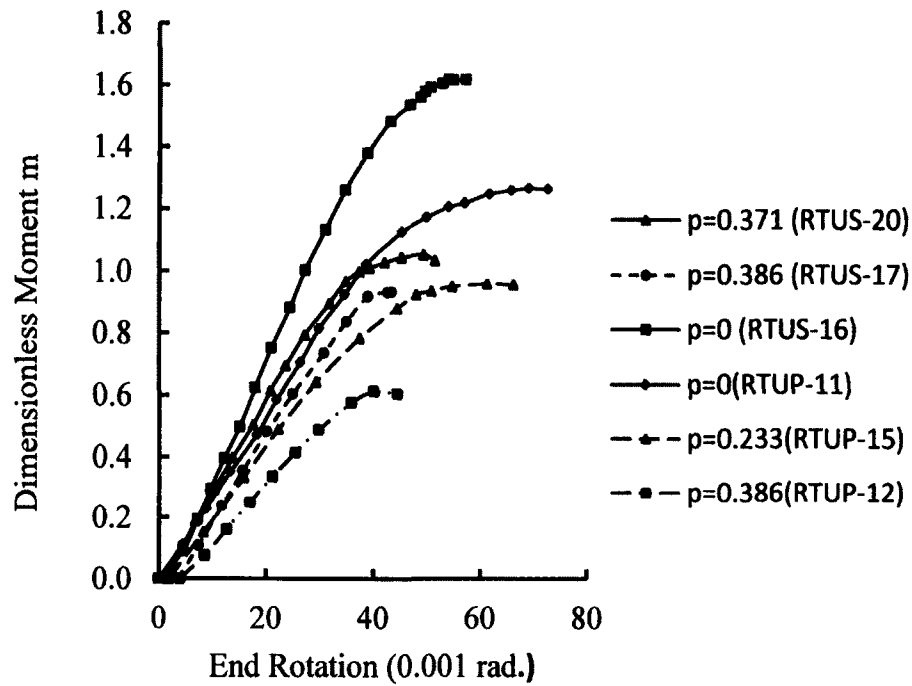
Figure 24. Moment versus end rotation curves for uniaxial loading tests at ambient temperature
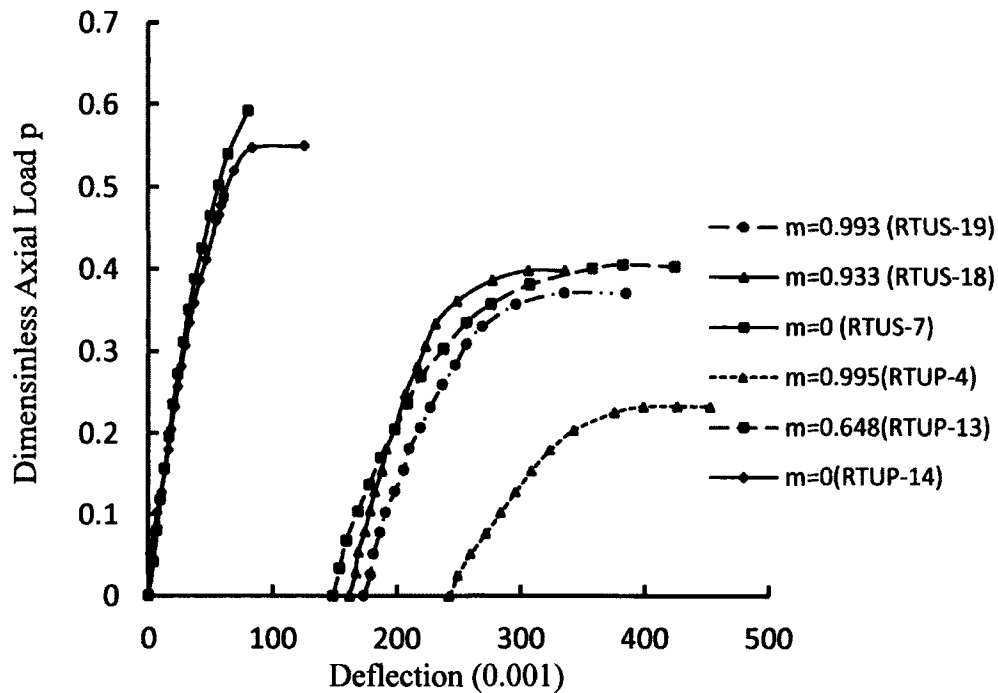
Figure 25. Load versus deflection curves for uniaxial loading tests at ambient temperature
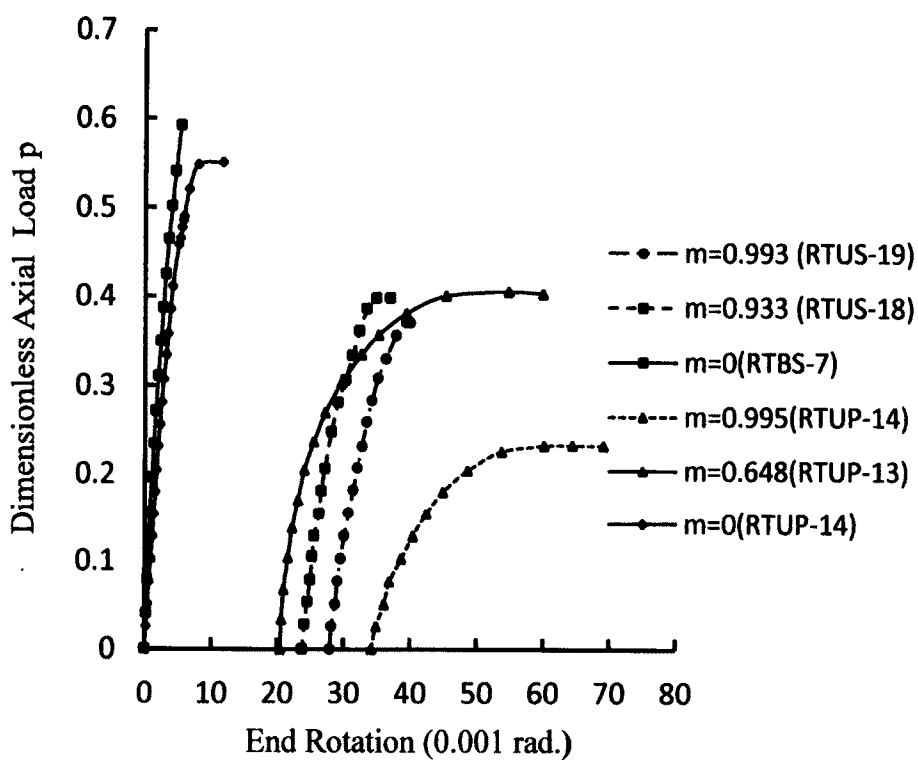
Figure 26. Load versus end rotation curves for uniaxial loading tests at ambient temperature
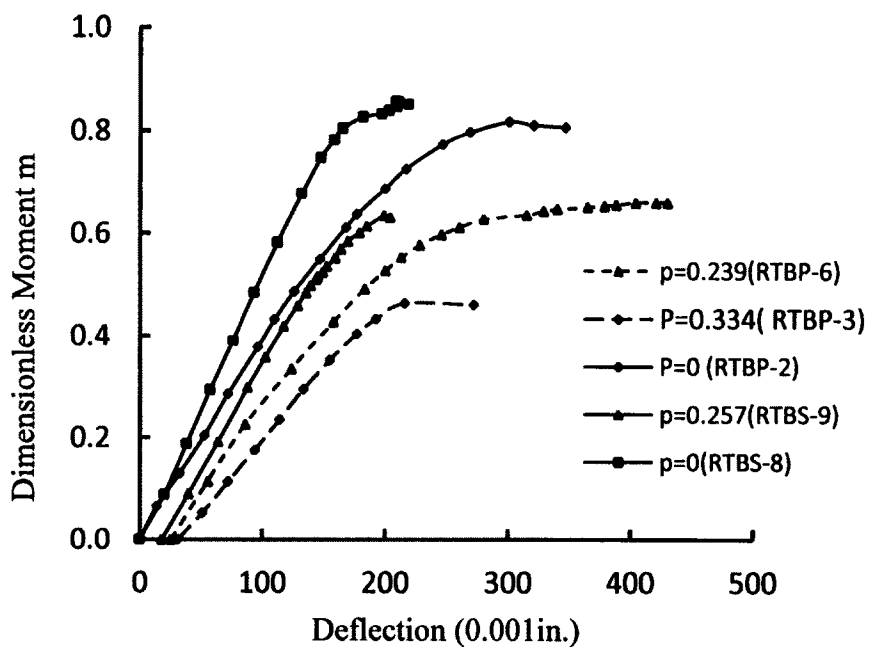
Figure 27. Moment versus deflection curves for biaxial bending tests at ambient temperature
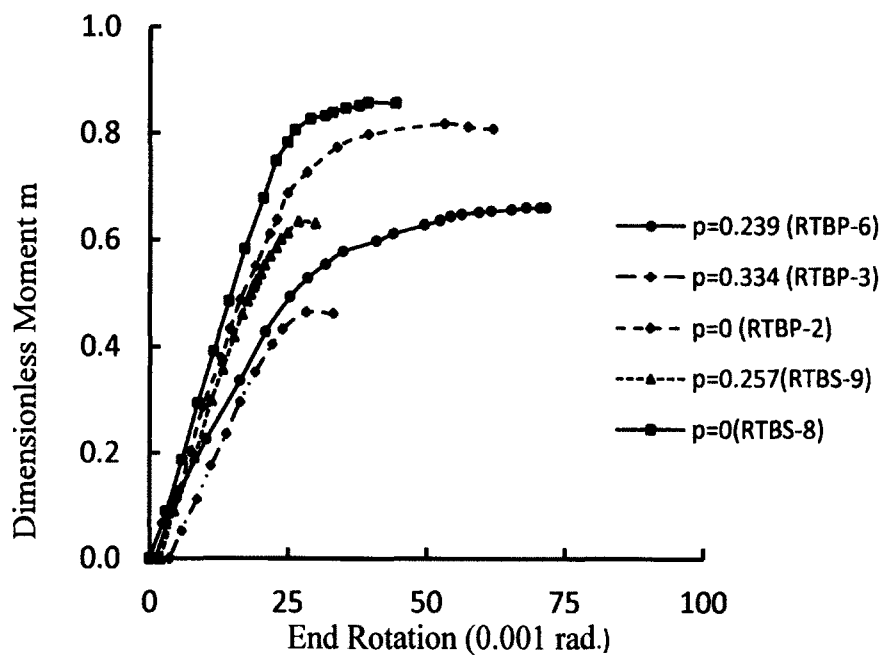
Figure 28. Moment versus end rotation curves for biaxial loading tests at ambient temperature
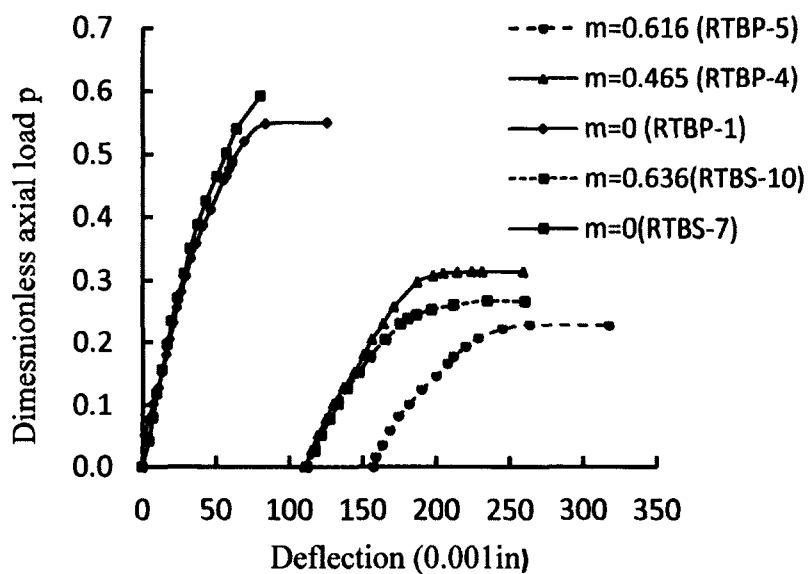
Figure 29. Load versus deflection curves for biaxial loading tests at ambient temperature
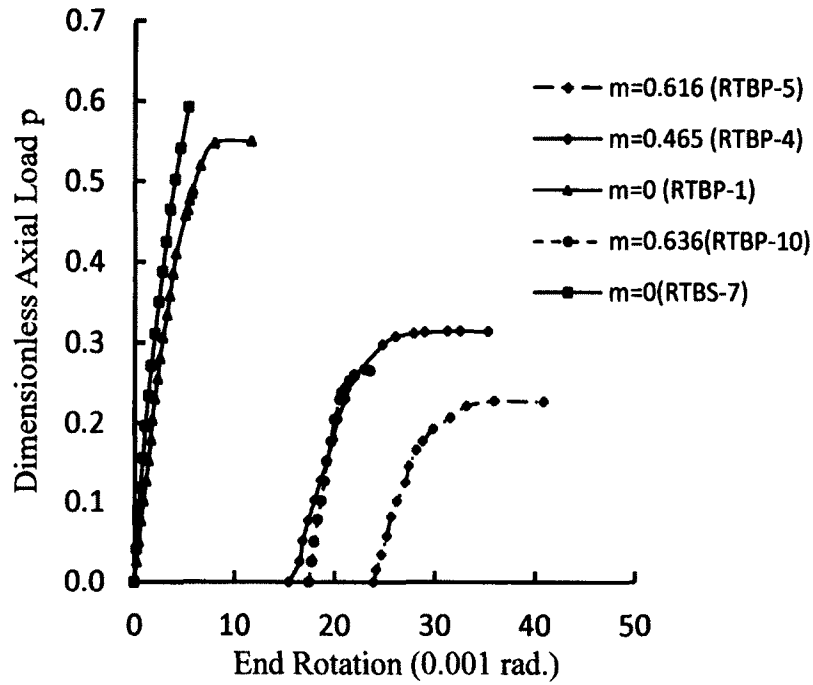
Figure 30. Load versus end rotation curves for biaxial bending tests at ambient temperature
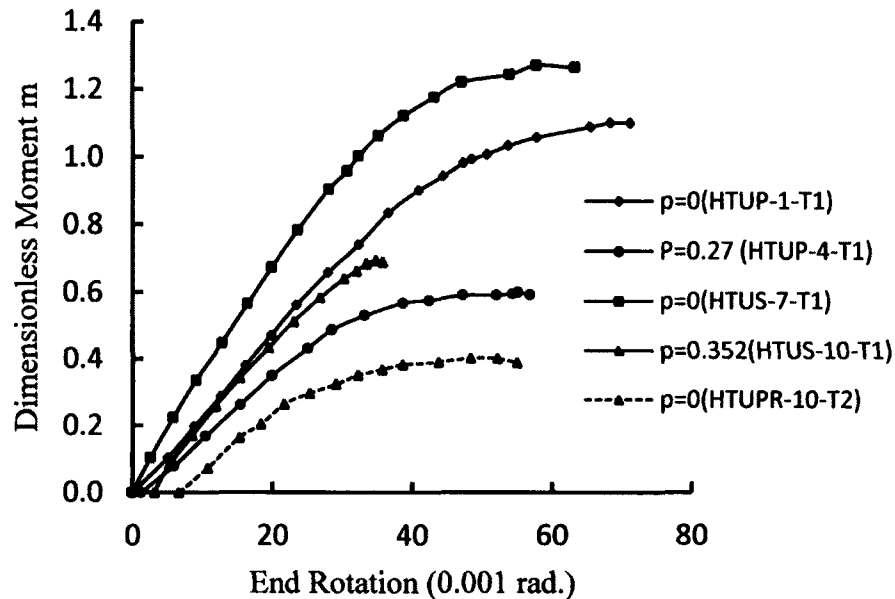
Figure 31. Moment versus end rotation curves for uniaxial loading tests at high temperatures: T1=500°F, T2=900°F
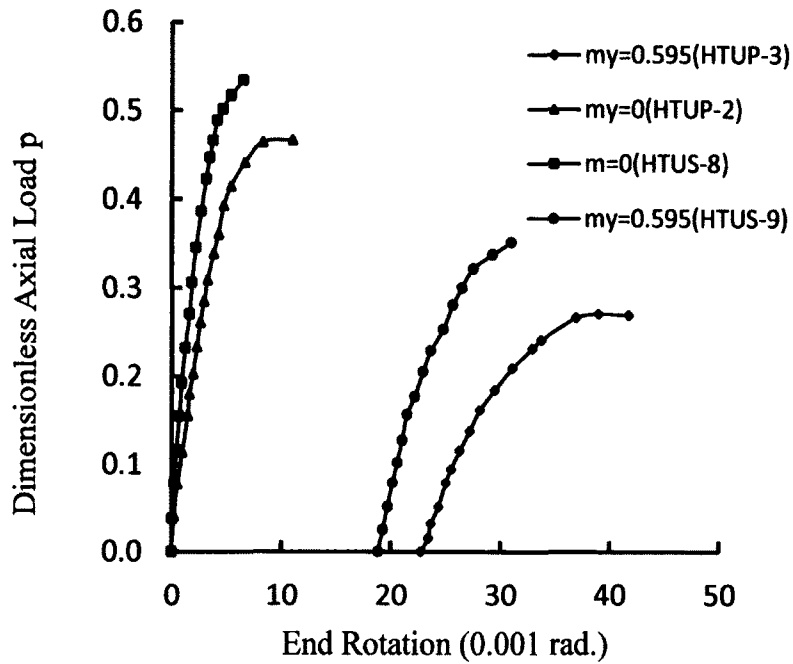
Figure 32. Load versus end rotation curves for uniaxial bending tests at the high temperature of 500°F without axial restraint to thermal expansion
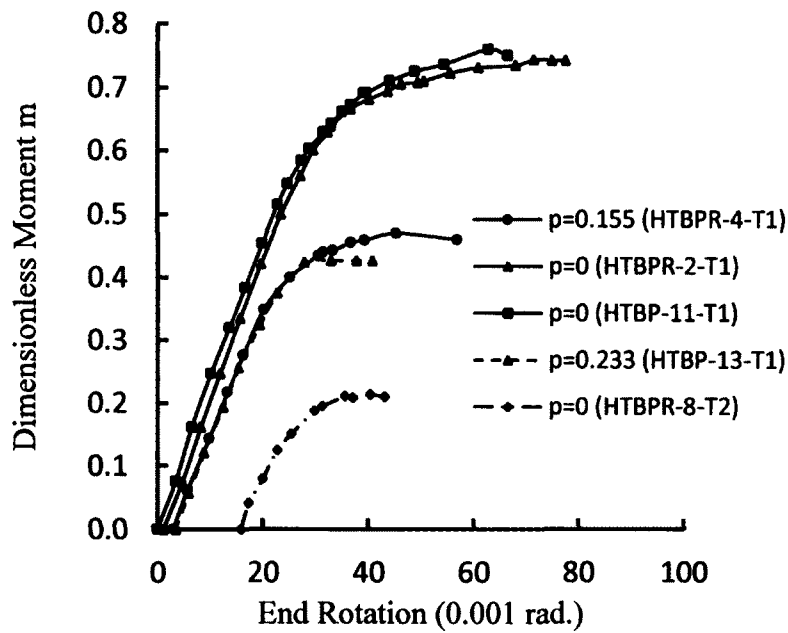
Figure 33. Moment versus end rotation curves for beam-columns under biaxial loading at T1=500°F and T2=900°F
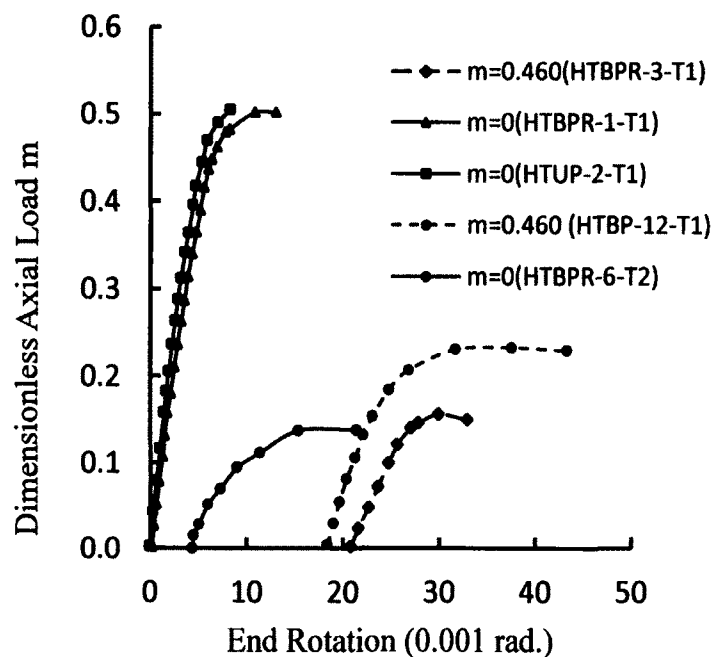
Figure 34. Load versus end rotation curves for beam-columns under biaxial loading at
T1=500°F and T2=900°F
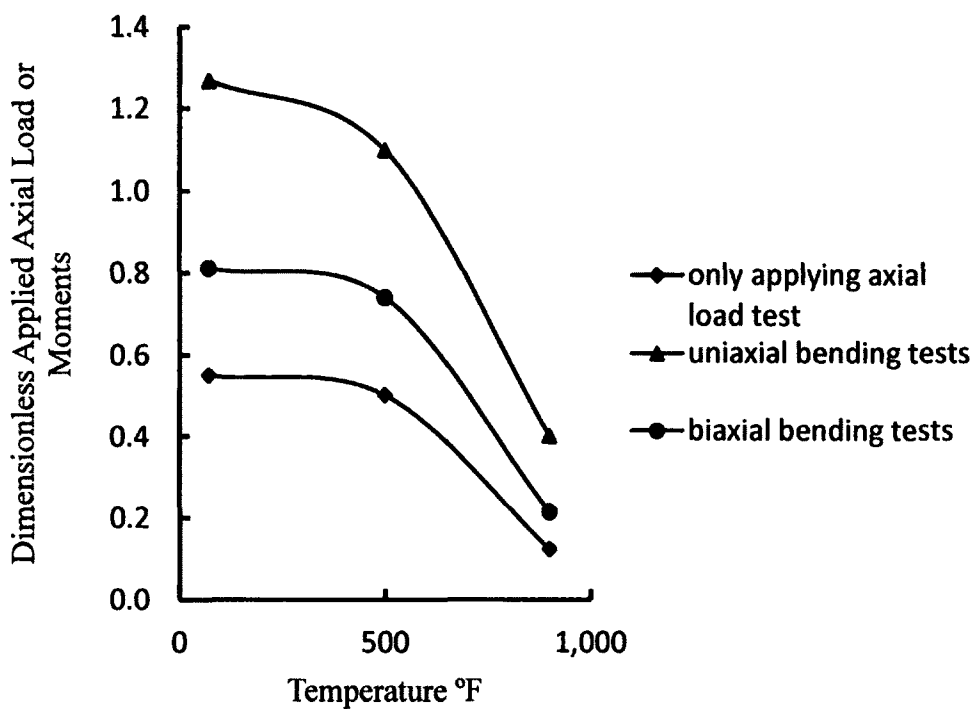
Figure 35. Temperature versus applied axial load or moments curve
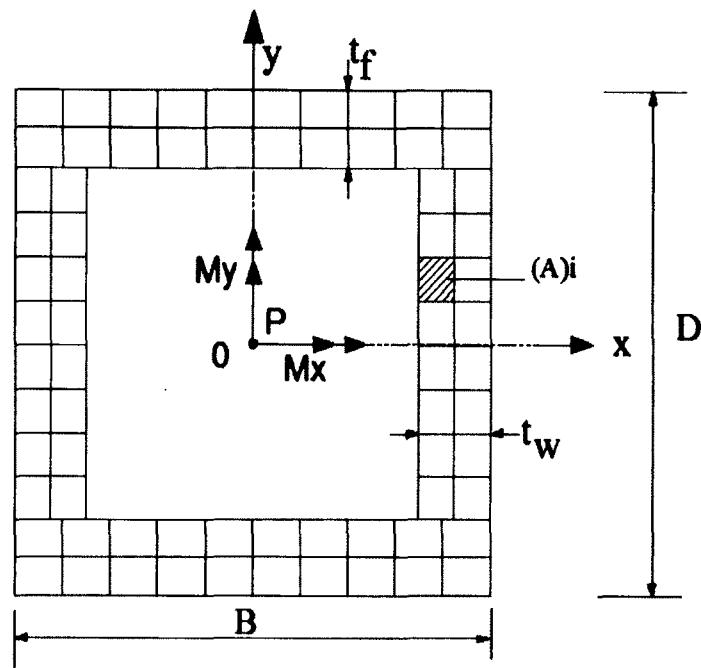
Figure 36. Discretized hollow sections subjected to axial load and biaxial bending moments
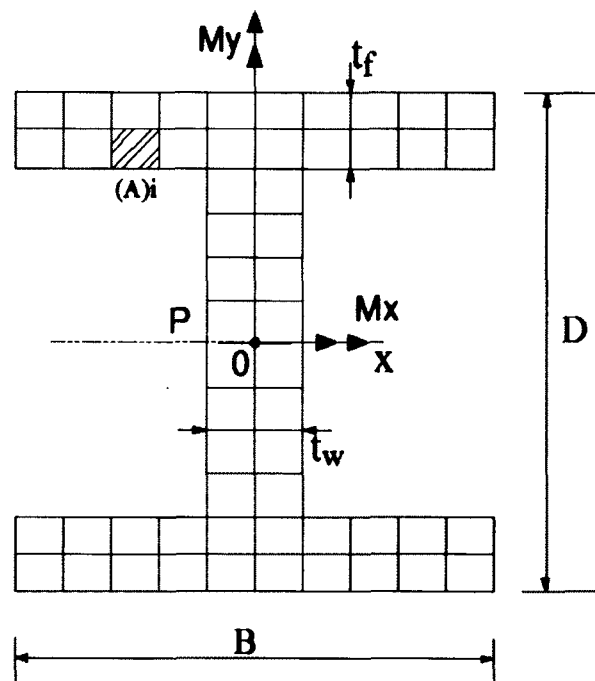
Figure 37. Discretized I-shaped sections subjected to axial load and biaxial bending moments
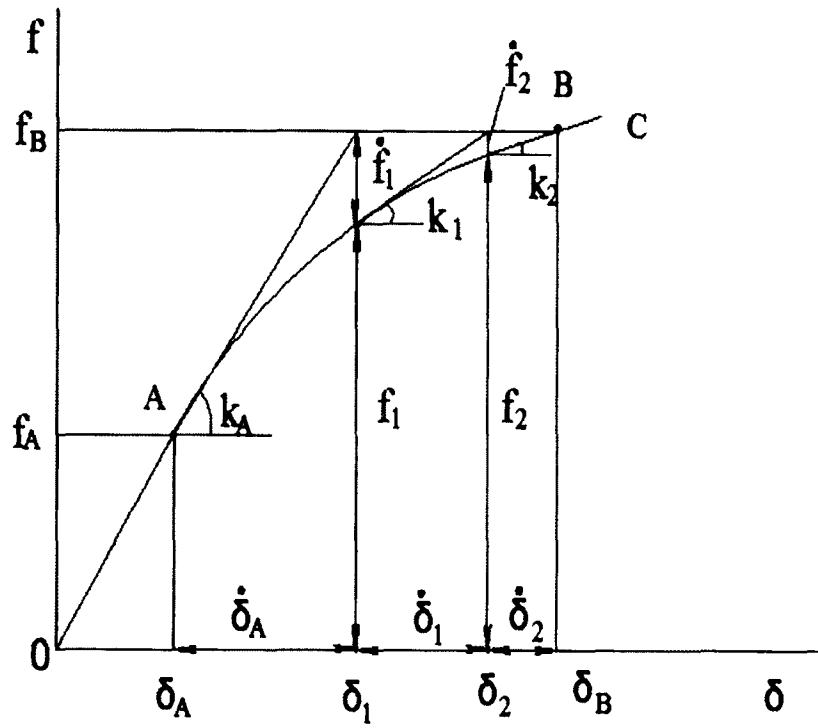
Figure 38. Procedure in tangent stiffness method (41)
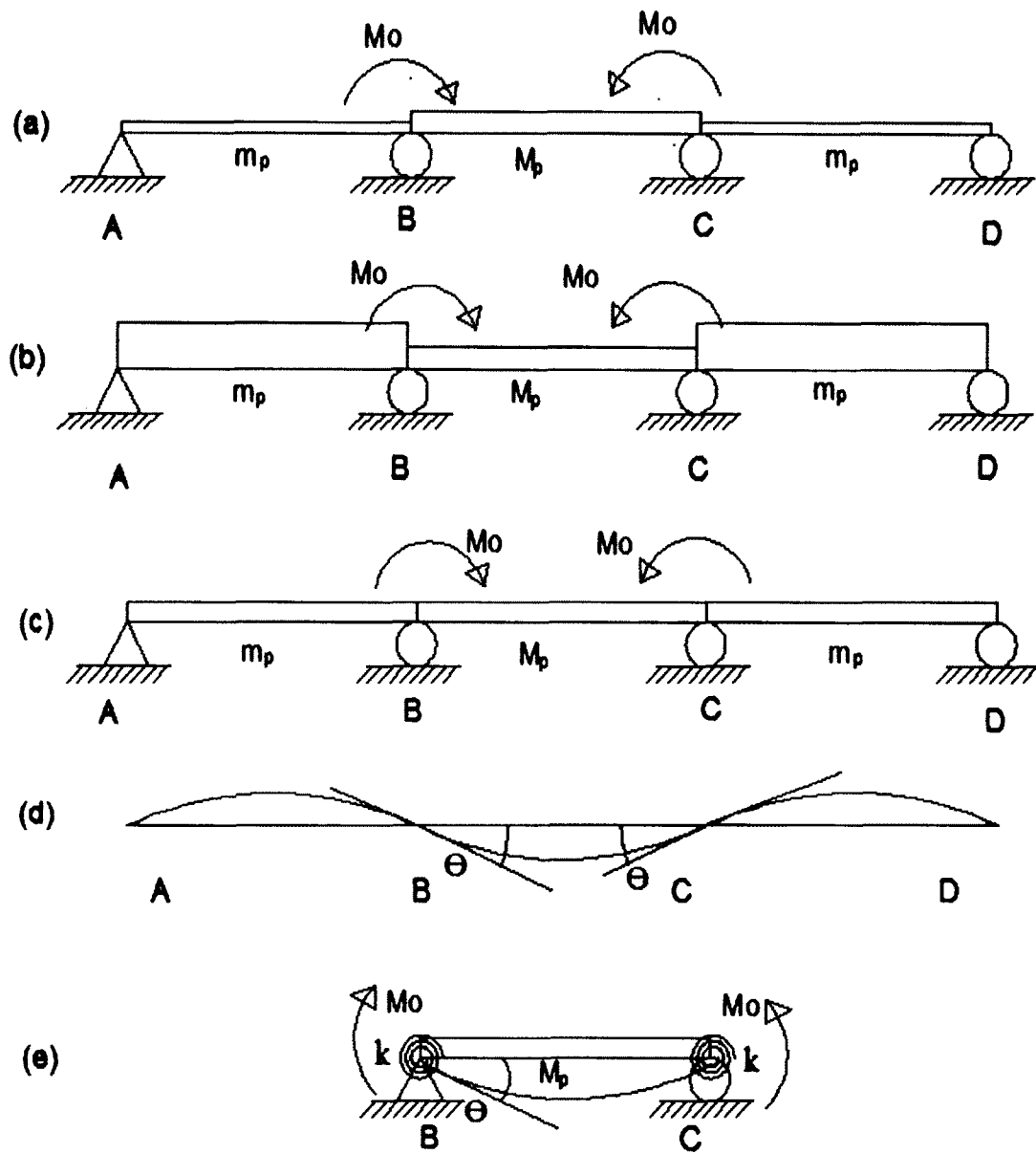
Figure 39. Three-span-beam
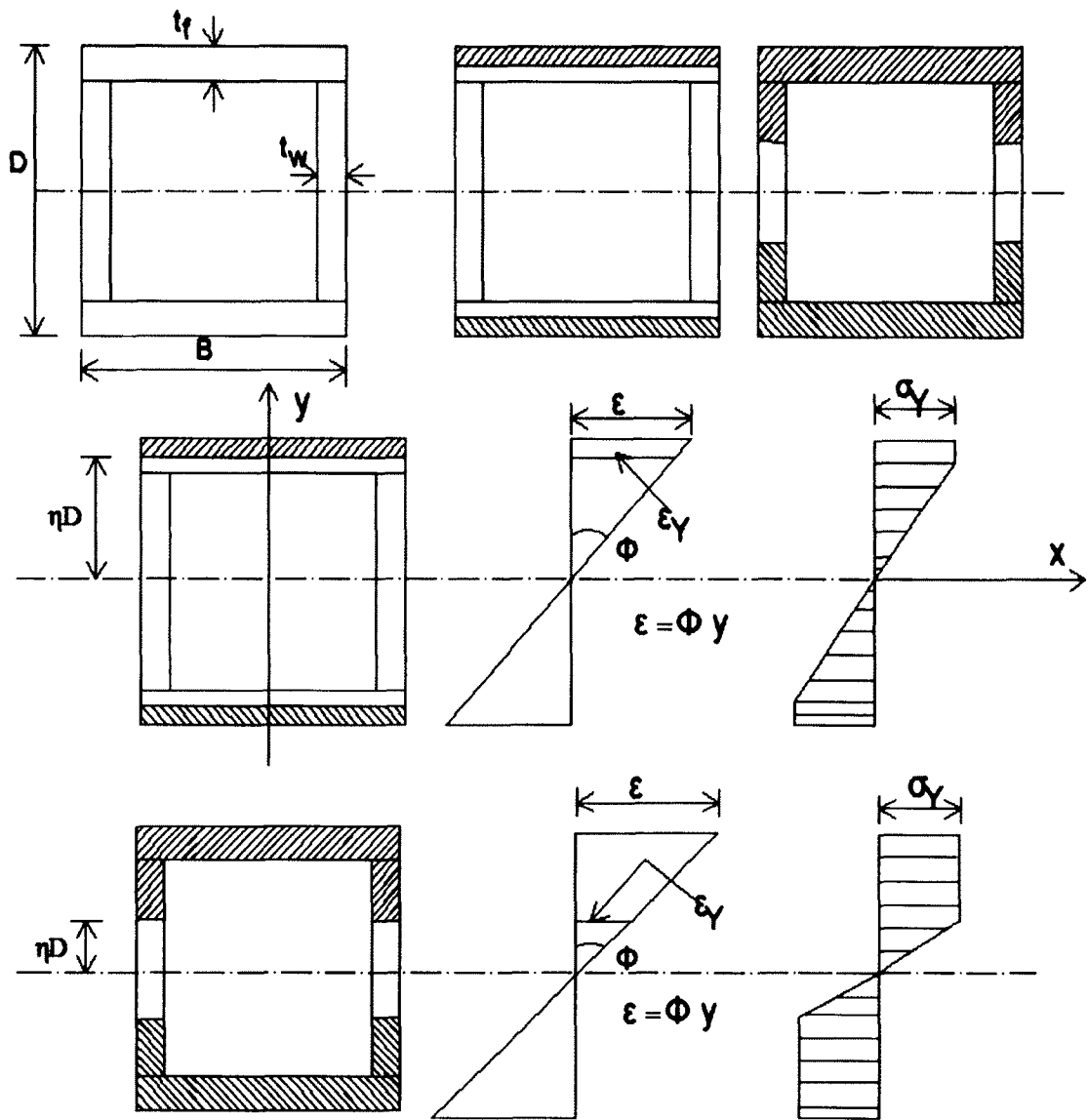
Figure 40. Plastification patterns and stress-strain distributions for span BC of three-span beam
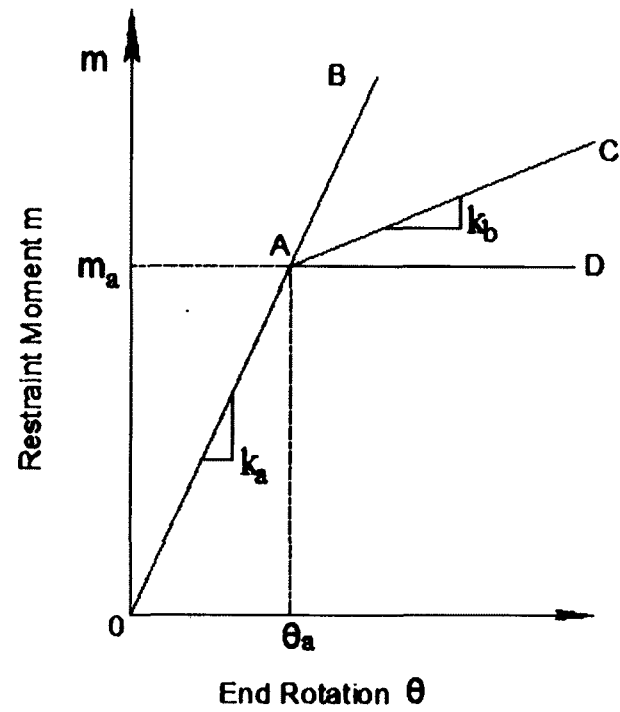
Figure 41. Moment-rotation relationships for partial rotational end restraints
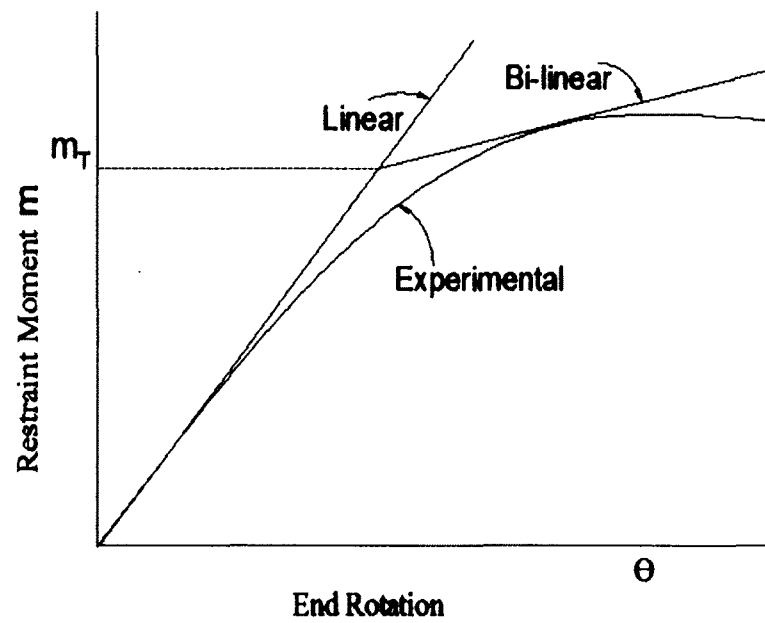
Figure 42. Idealized and actual models for partial end rotation restraints
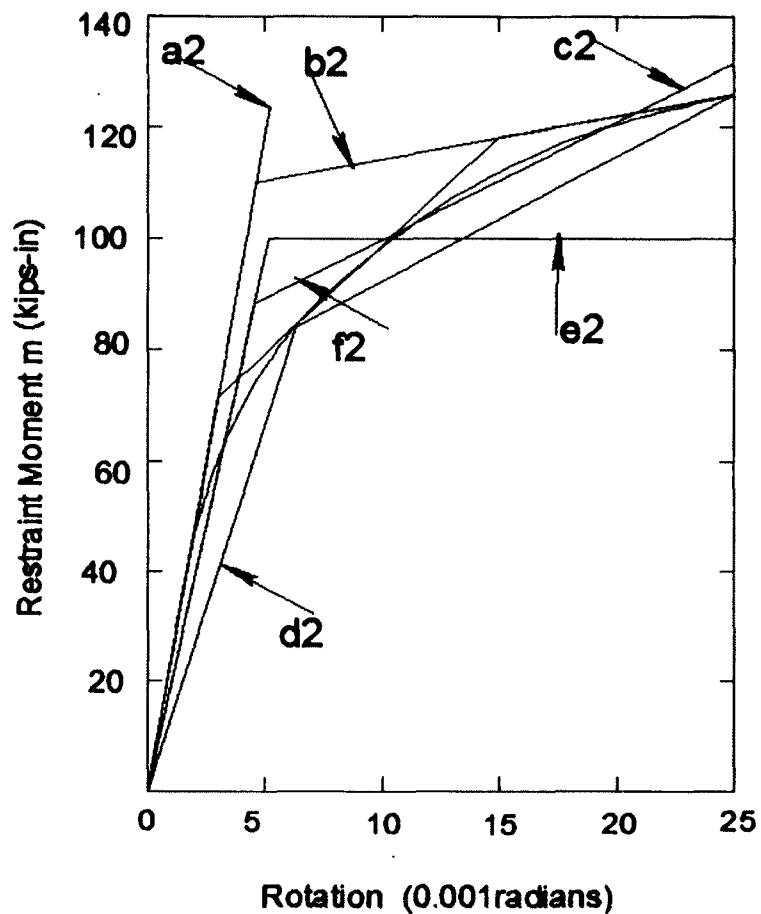
Figure 43. Linear and bilinear approximations of restraint moment and rotation curve for beam-column (11)
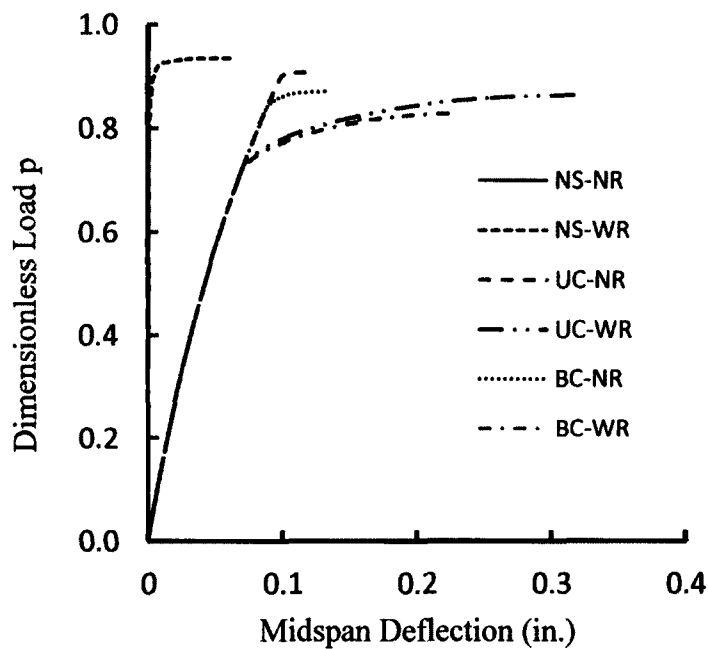
Figure 44. Load versus deflection curves for pinned imperfect hollow square columns
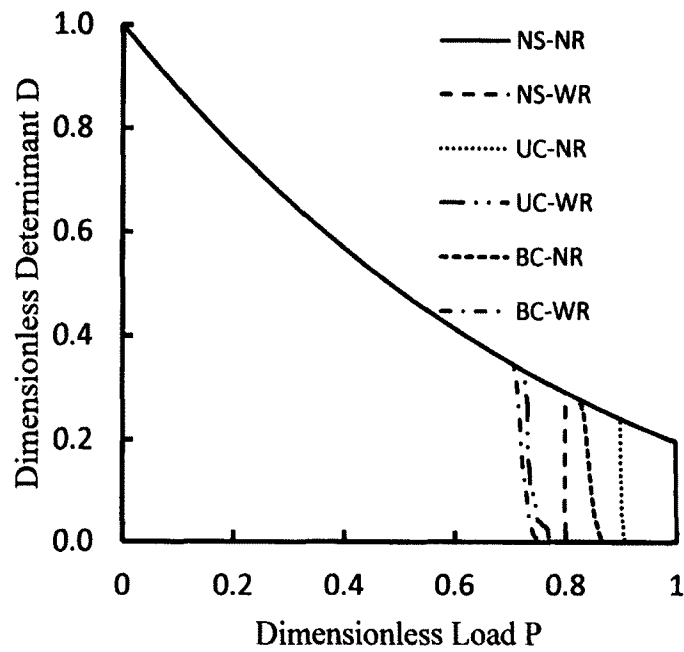
Figure 45. Stiffness degradation curves for pinned imperfect hollow square columns
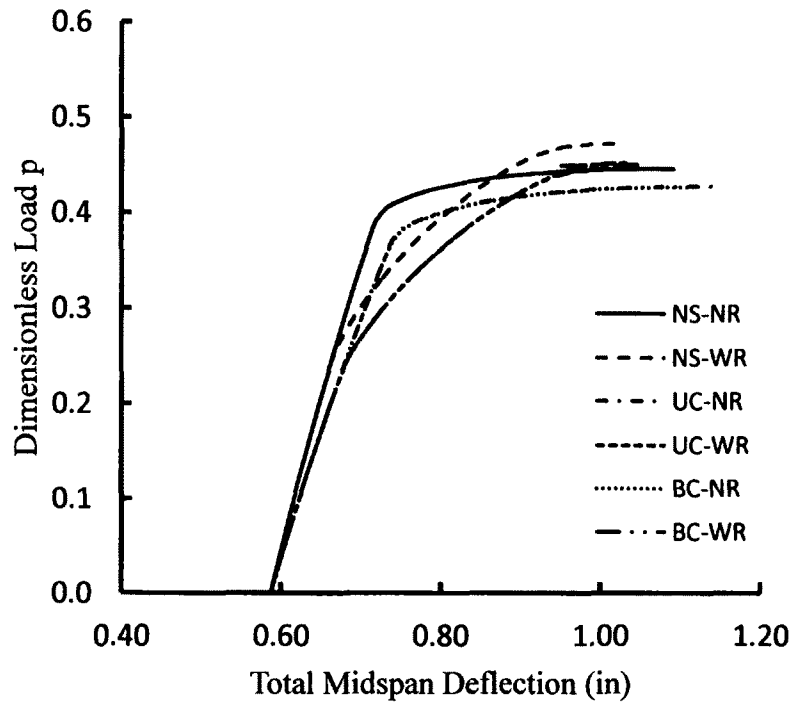
Figure 46. Load versus deflection curves for pinned imperfect
hollow square beam-columns with $m_y = 0.5M_Y$
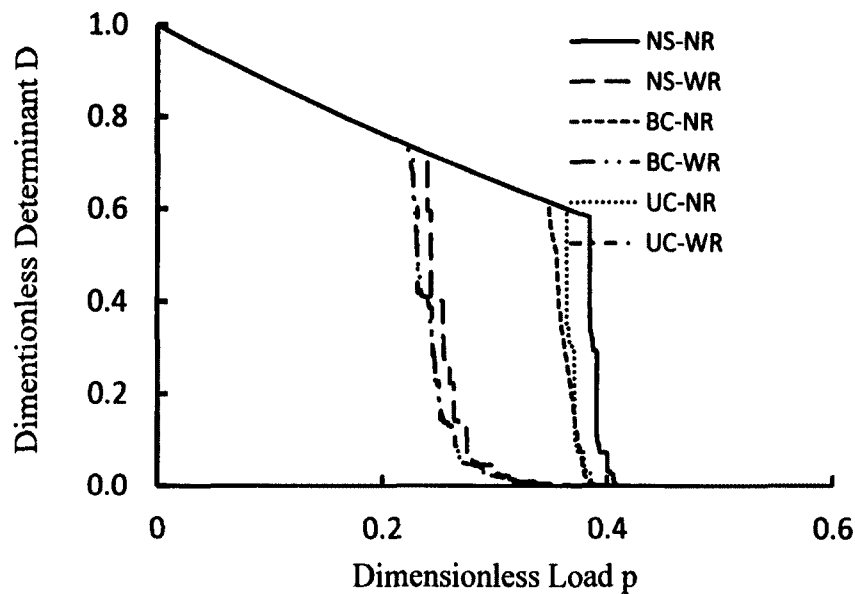
Figure 47. Bending stiffness degradation curves for pinned hollow square imperfect beam-columns under uniaxial bending with $m_y = 0.5M_Y$
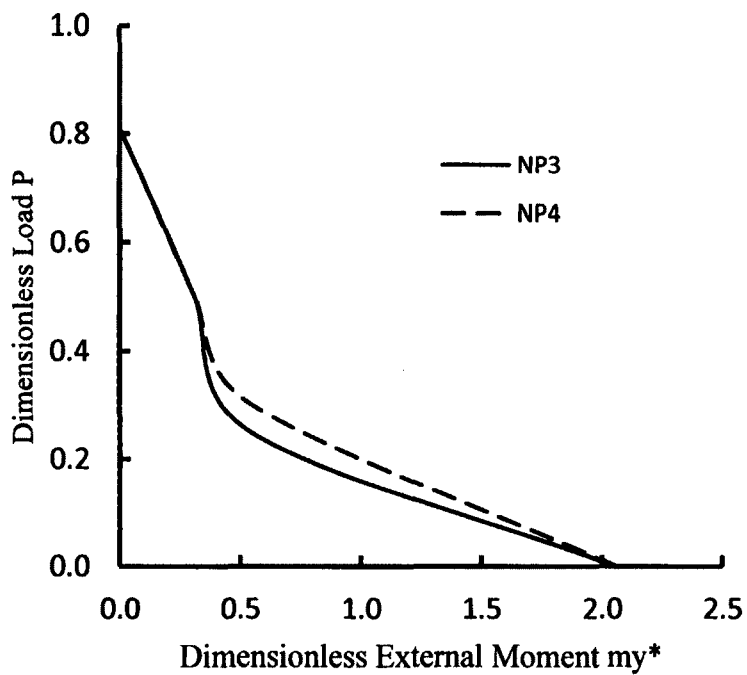
Figure 48. Interaction curves for biaxial loaded partially restrained W8x31 section beam-column with $k = k_{a2}$
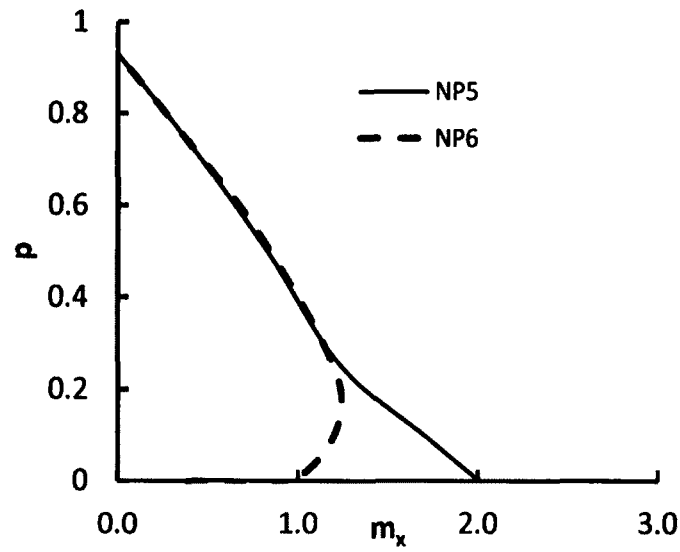
Figure 49. Interaction curves for biaxially loaded partially restrained imperfect hollow square beam-column BC2 for load paths NP5 and NP6
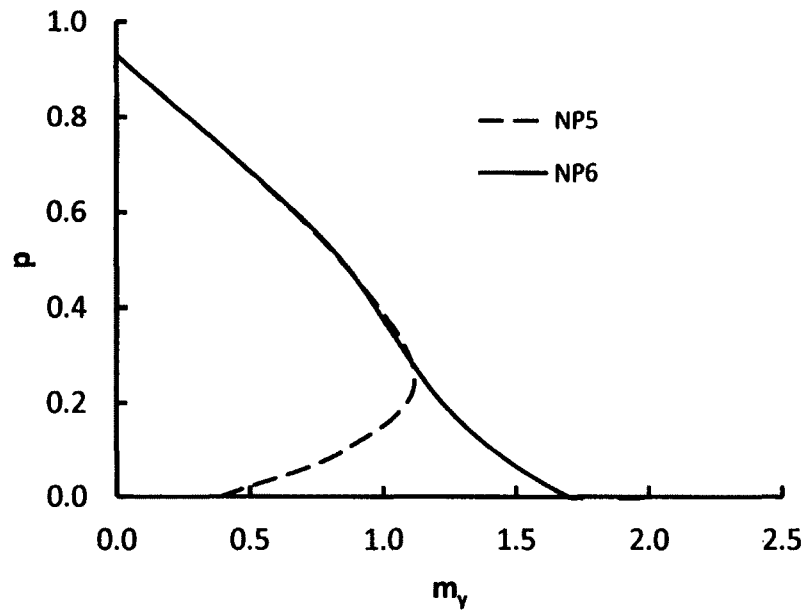
Figure 50. Interaction curves for biaxially loaded partially restrained imperfect hollow square beam-column BC2 for load paths NP5 and NP6
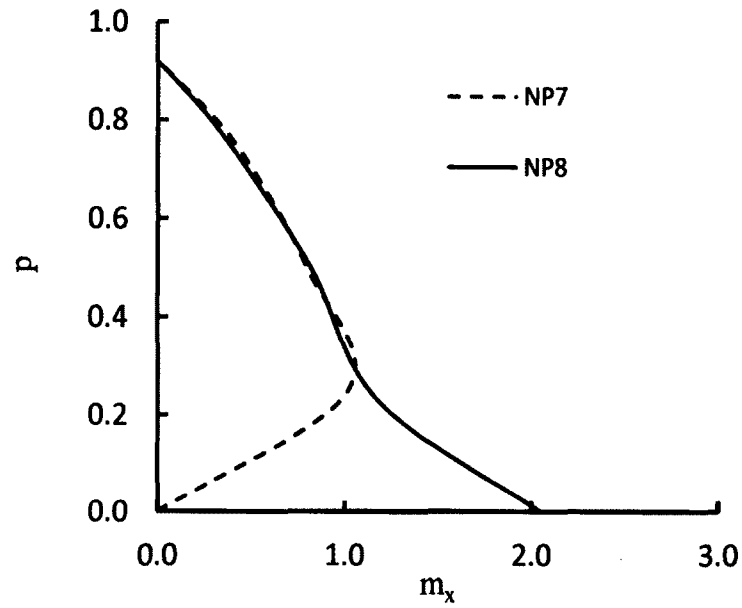
Figure 51. Interaction curves for biaxially loaded hollow rectangular beam-column BC3 with linear partial rotational restrains for load paths NP7 and NP8
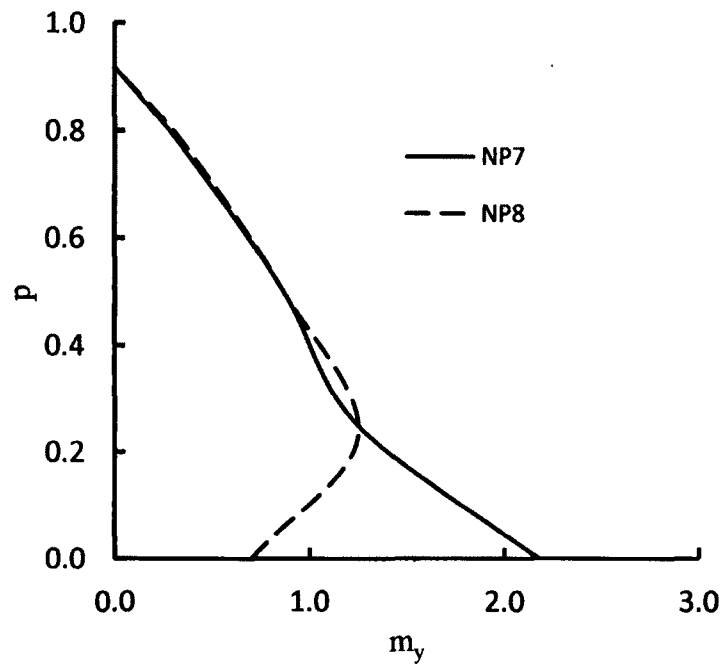
Figure 52. Interaction curves for biaxially loaded hollow rectangular beam-column BC3 with linear partial rotational restrains for load paths NP7 and NP8
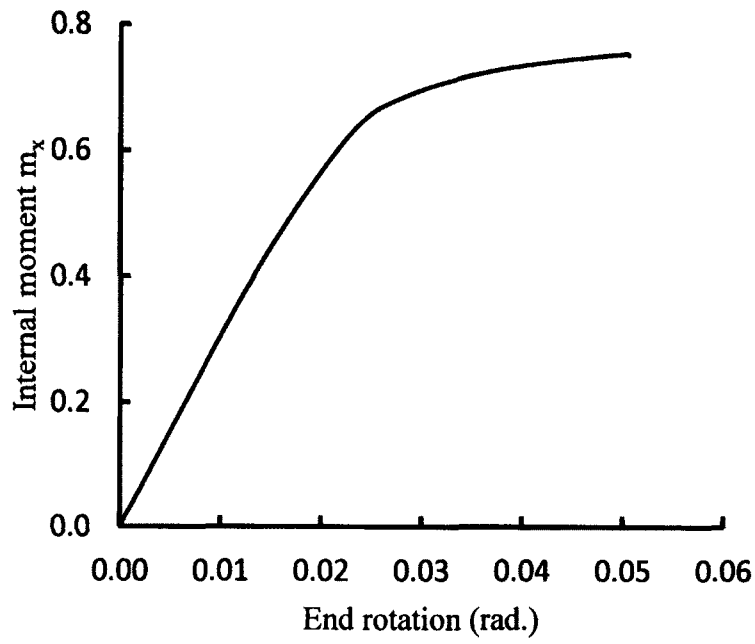
Figure 53. Internal moment m_x versus rotation relationship for BC2
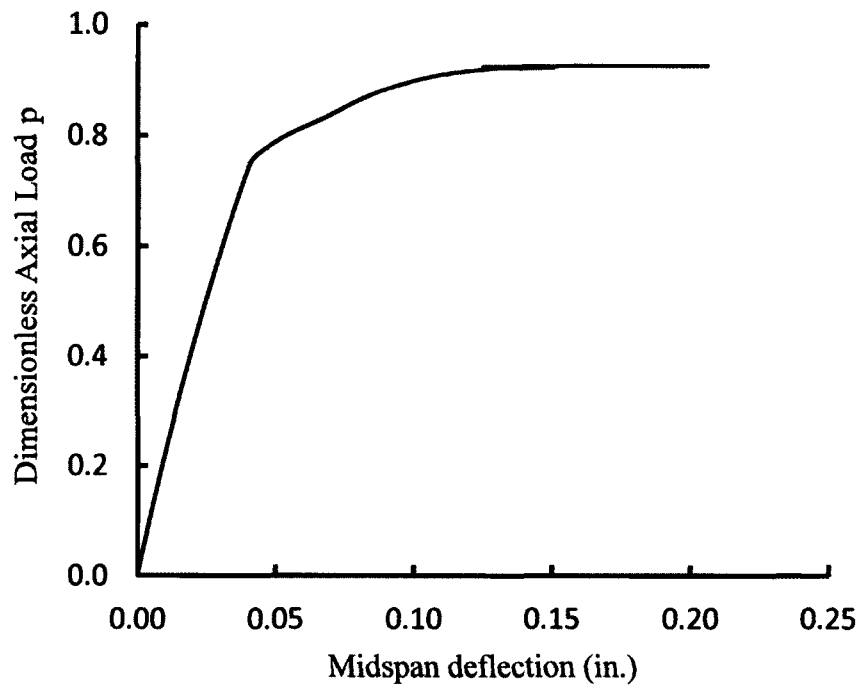
Figure 54. Axial load versus midspan deflection for BC2
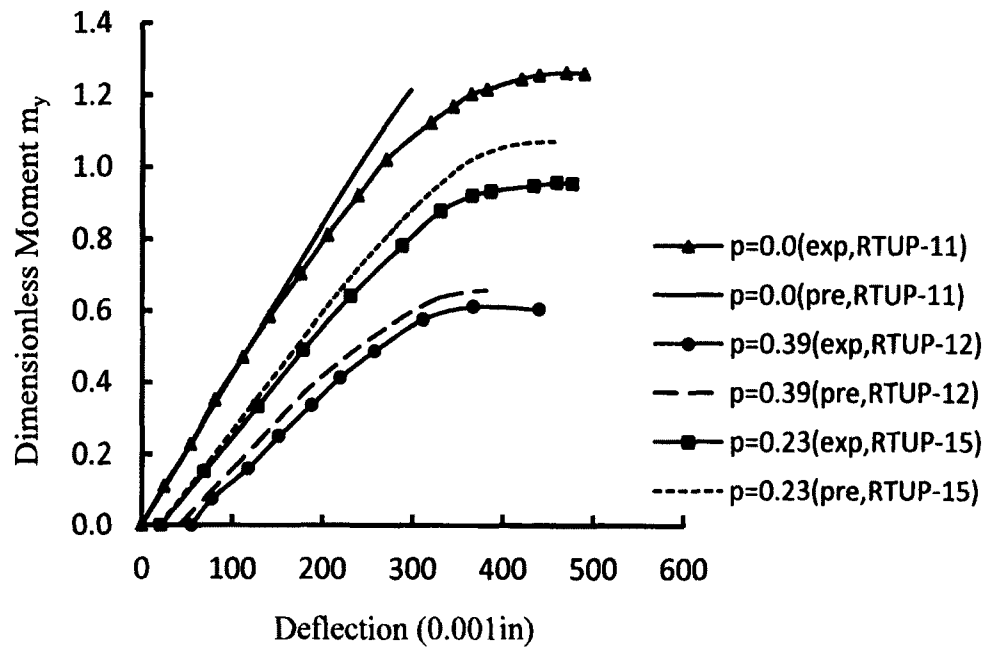
Figure 55. Comparisons between predicted and experimental moment versus deflection
curves for beam-columns with pinned boundary conditions
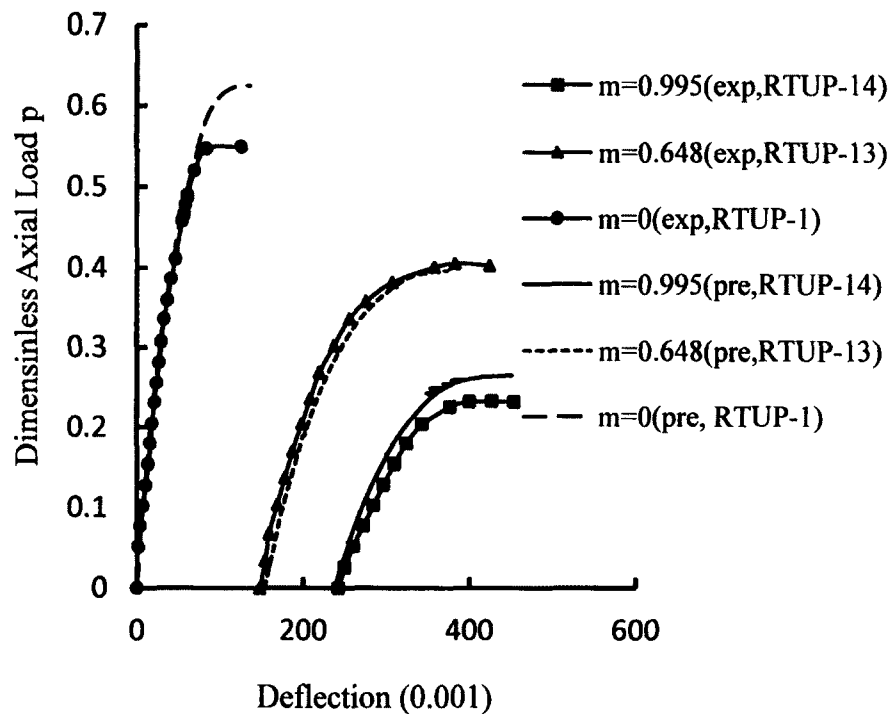
Figure 56. Comparisons between predicted and experimental load versus deflection
curves for beam-column with pinned boundary conditions
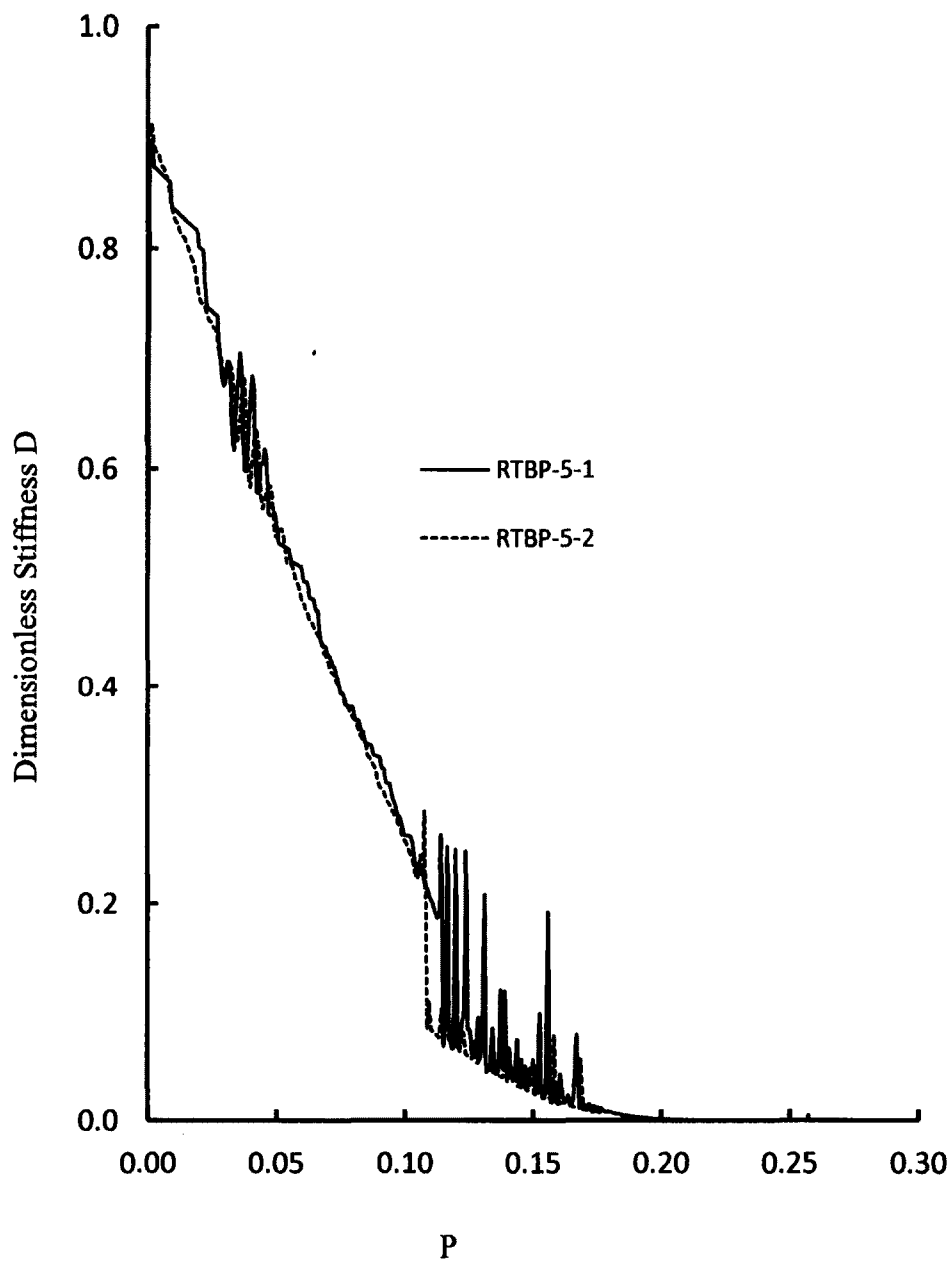
Figure 57. Stiffness degradation curves for RTBP-5 with 228 and 912 elemental areas for each of 9 nodes along the member length
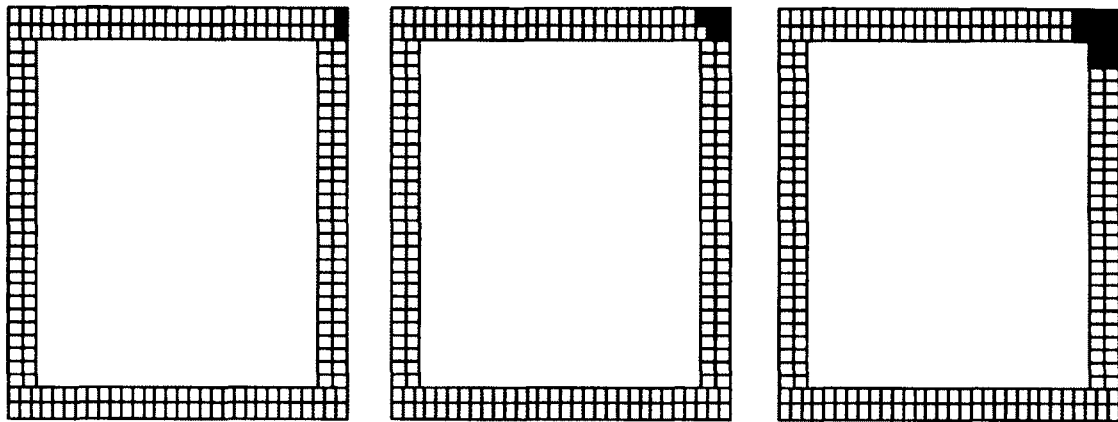
Node 5   Node 6   Node 7

Node 8   Node 9

Figure 58. Spread of plasticity in the cross sections
before axial load is applied for RTBP-5
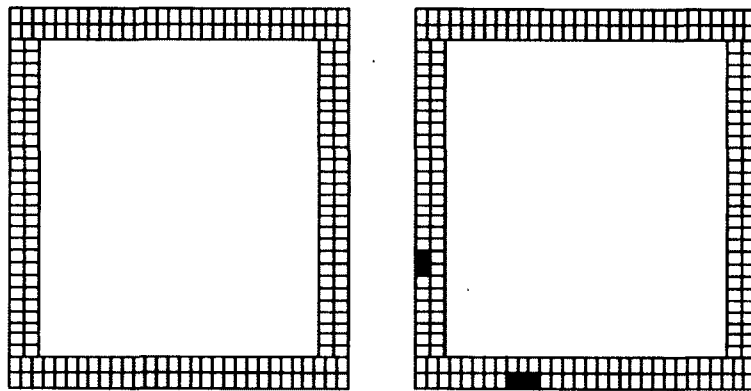
Figure 59. Spread of plasticity in the cross sections
after axial load is applied for RTBP-5
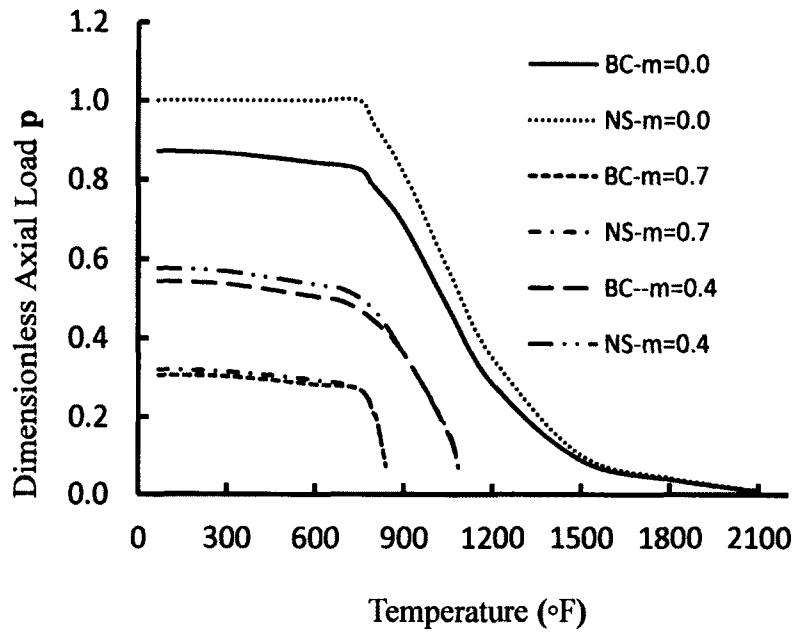
Figure 60. Load versus temperature curves for beam-columns without axial restraints to thermal expansion
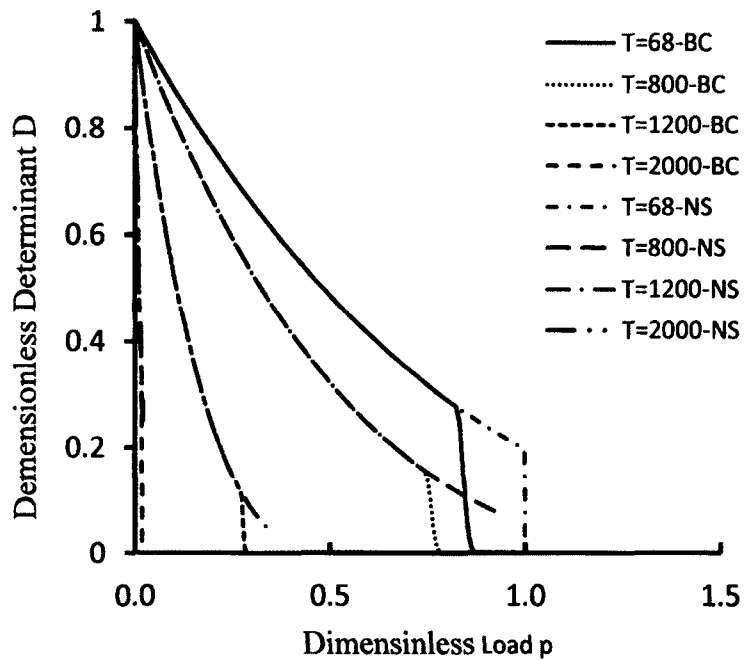
Figure 61. Stiffness degradation curves for pinned beam-columns with $m_x = m_y = 0.4$ and without axial restraints to thermal expansion at different temperatures
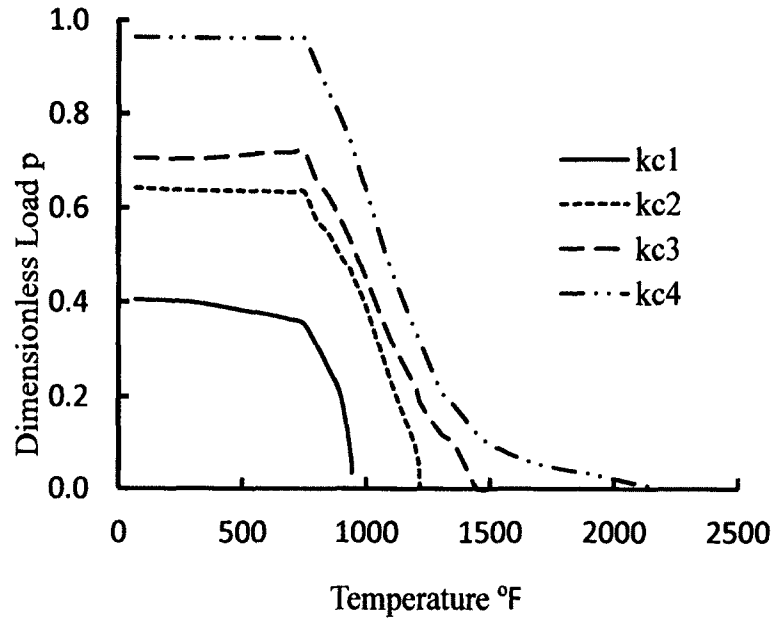
Figure 62. Load versus temperature curves for biaxially loaded beam-columns with $m_x=m_y=0.6$ and different end rotation restraints without axial restraints to thermal expansion
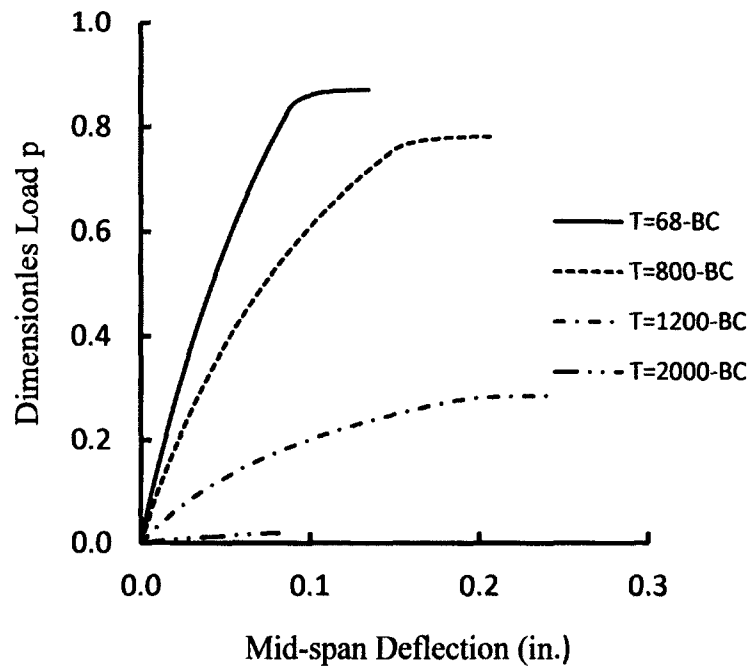
Figure 63. Load versus deflection curves for pinned columns without axial restraints to thermal expansion at different temperatures
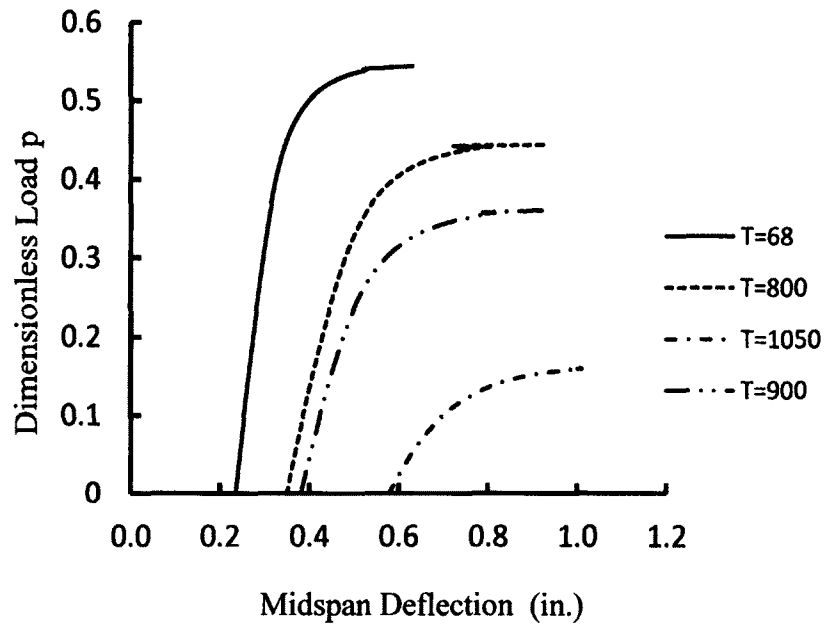
Figure 64. Load versus deflection curves for pinned beam-columns under biaxial loading with $m_x = m_y = 0.4$ and without axial restraints to thermal expansion at different temperatures
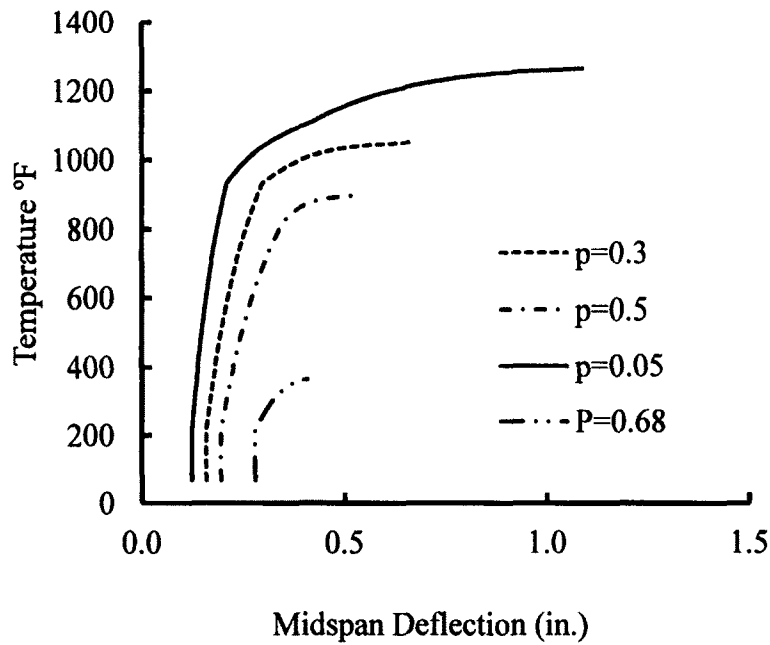
Figure 65. Temperature versus deflection curves for pinned beam-columns with $m_x = m_y = 0.2$ without axial restraints to thermal expansion
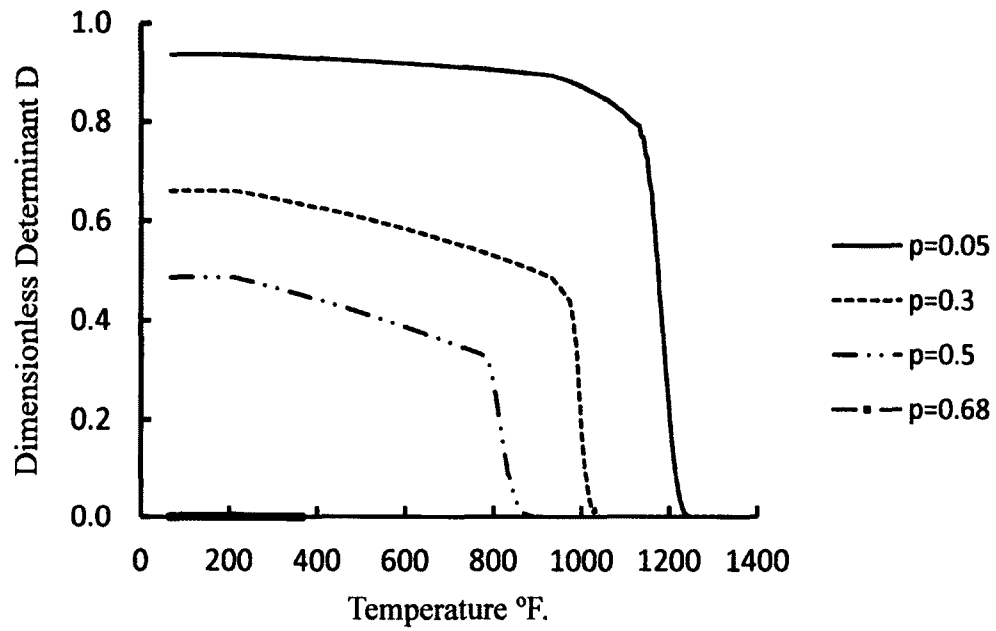
Figure 66. Stiffness degradation curves for pinned beam-columns with $m_x = m_y = 0.2$ without axial restraints to thermal expansion
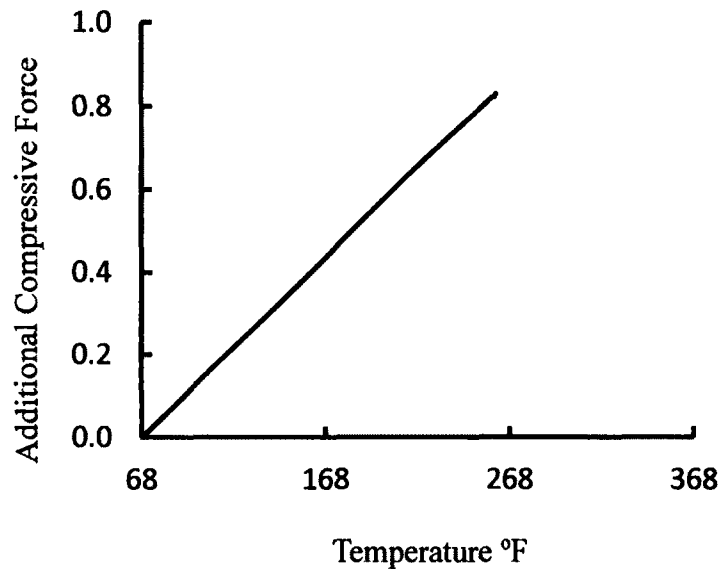
Figure 67. Additional compressive force versus temperature curve for columns with rigid axial restraint to thermal expansion
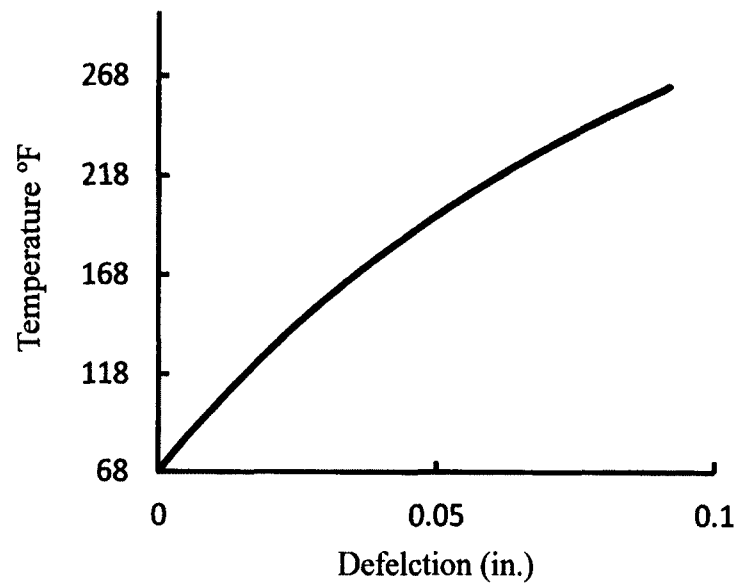
Figure 68. Temperature versus deflection curve for columns with
rigid axial restraint to thermal expansion
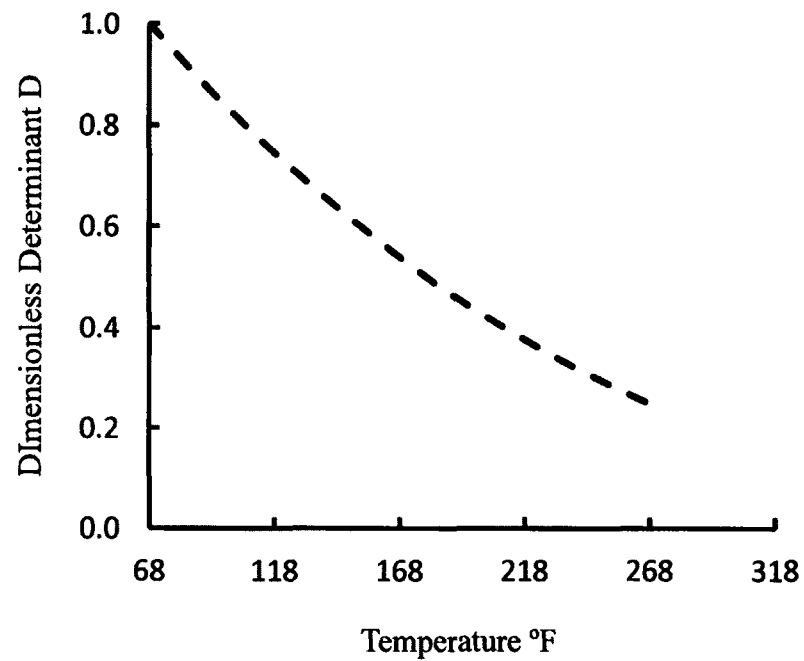
Figure 69. Dimensionless determinant versus temperature curve for columns with
rigid axial restraint to thermal expansion
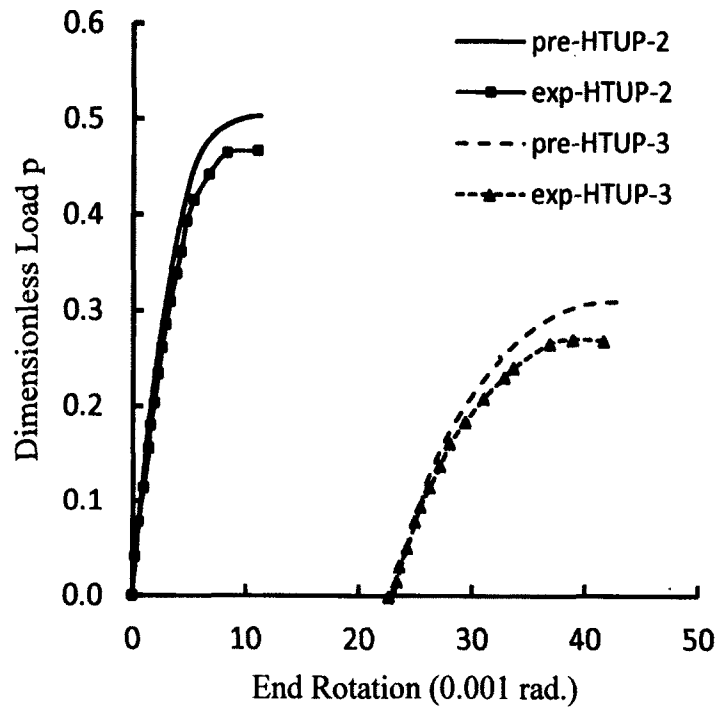
Figure 70. Load versus rotation curves for experimental and predicted results
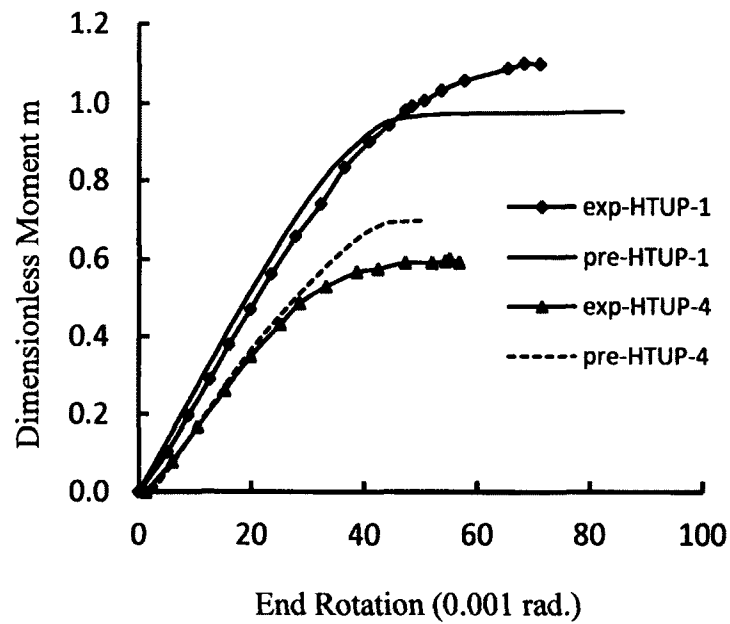
Figure 71. Comparison the experimental and predicted moment versus
end rotation curves
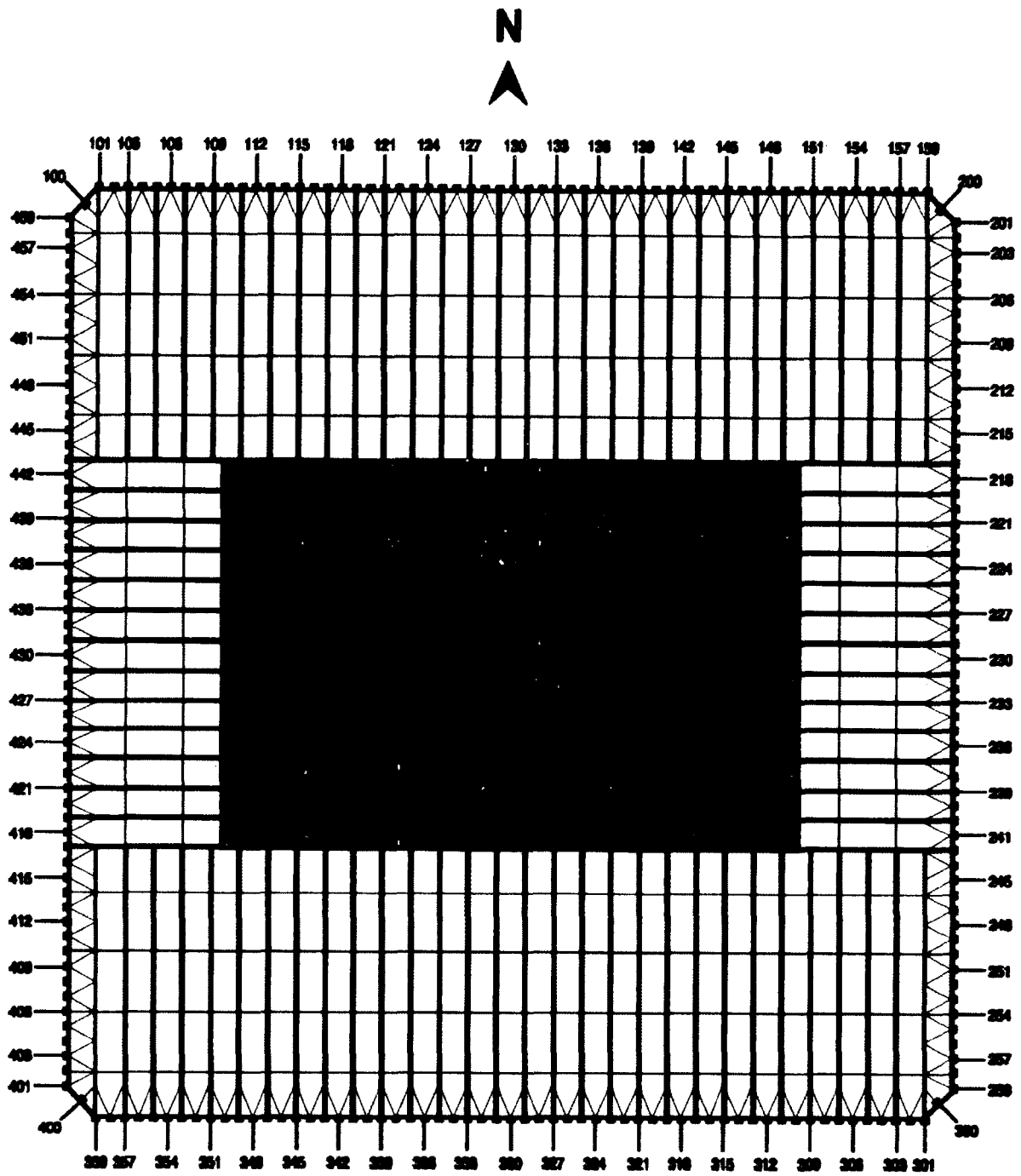
Figure 72. Typical floor plan of WTC Towers (Reference 23)
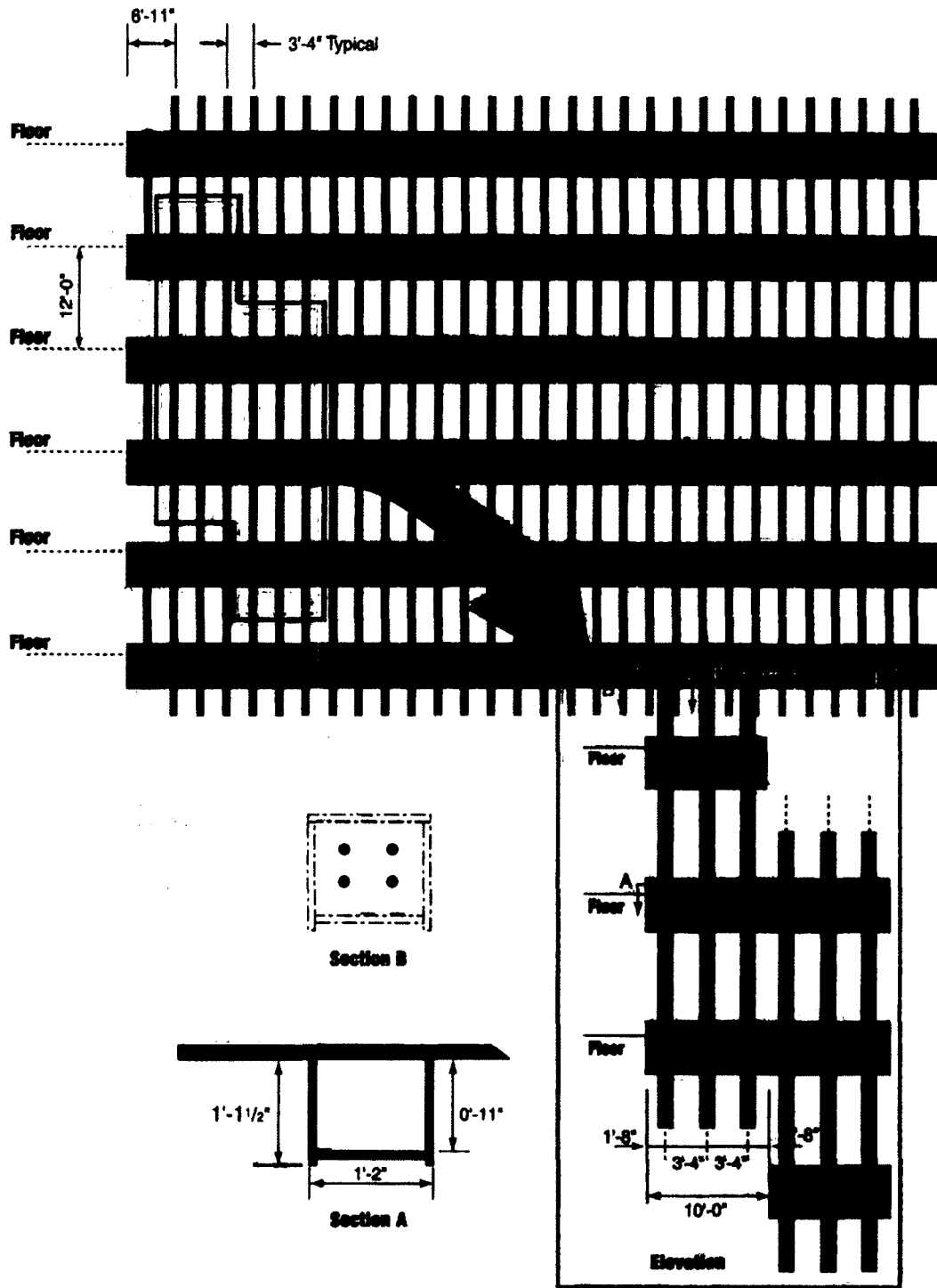
Figure 73. Partial elevation of exterior wall-frame system (23)
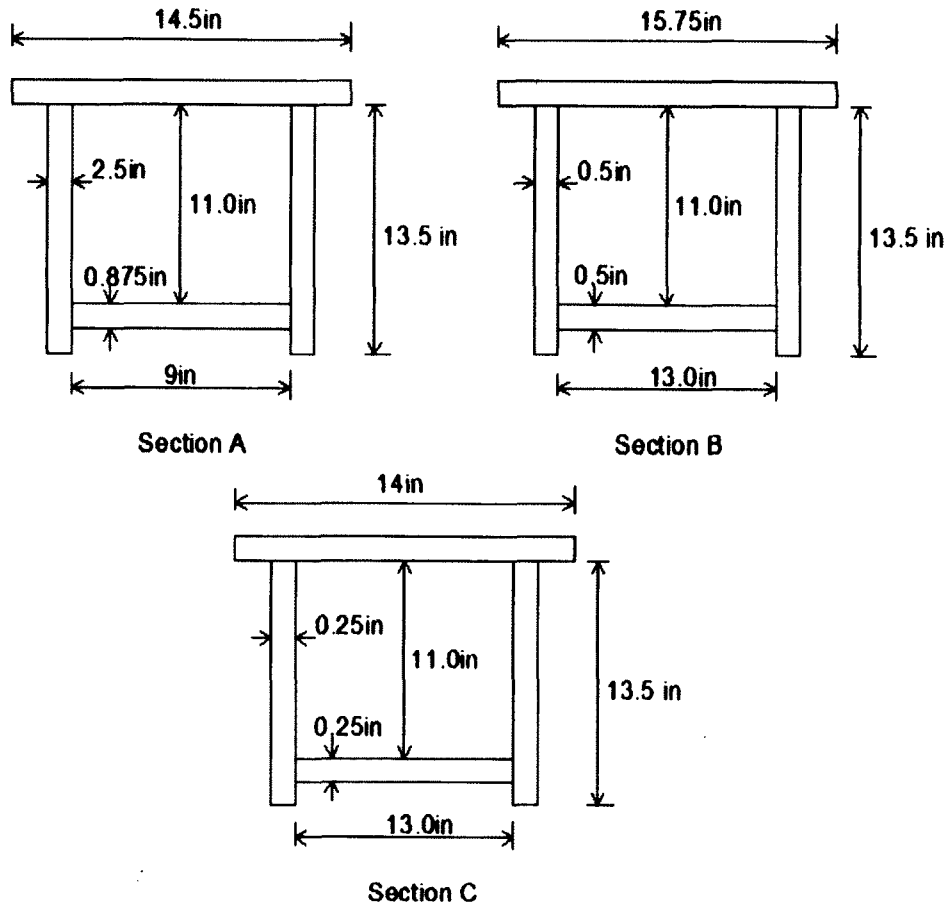
Figure 74. Typical cross sections for exterior columns
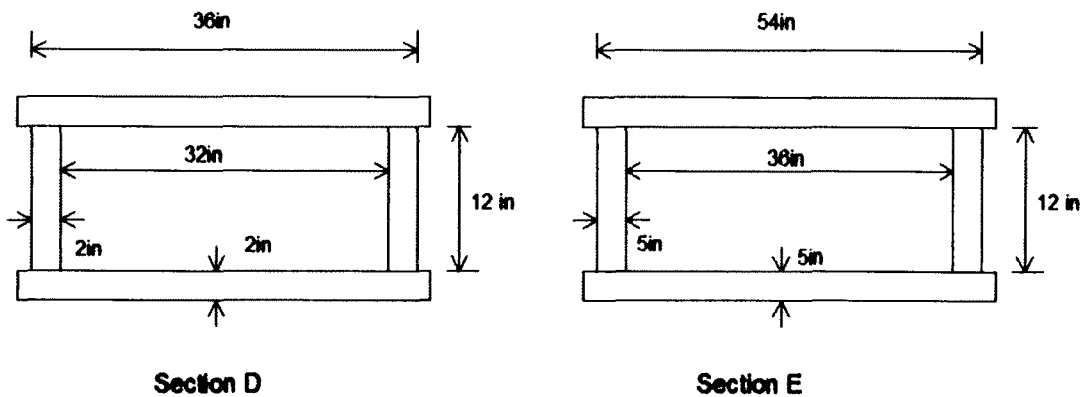
Figure 75. Typical cross sections of core columns
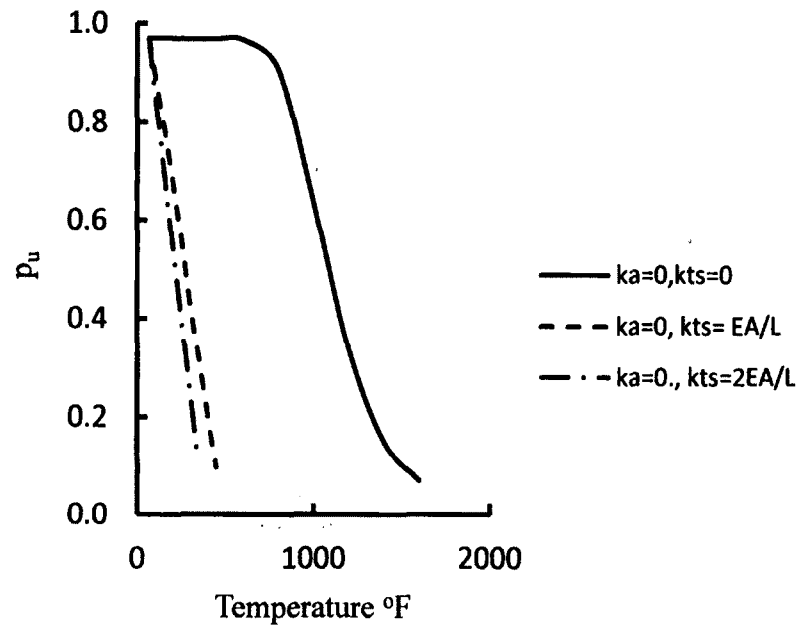
Figure 76. Load versus temperature curves for WTC columns near the tower top
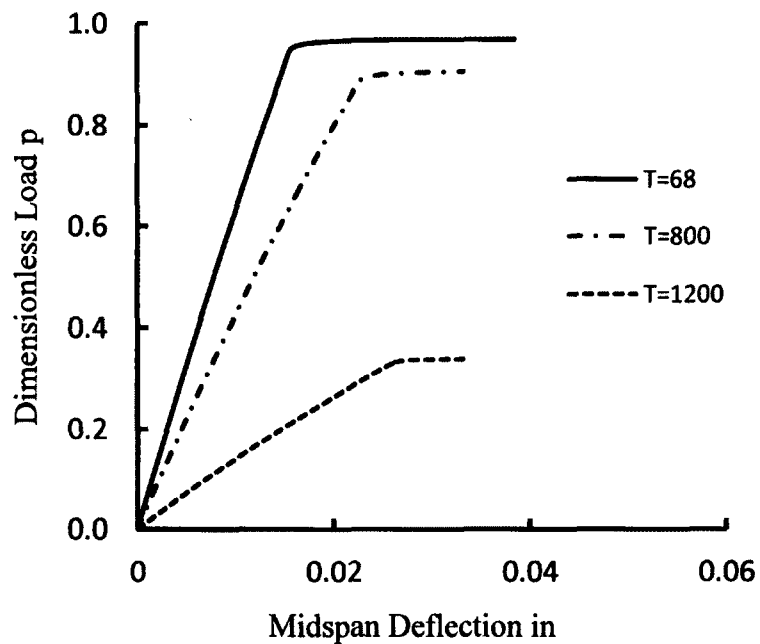
Figure 77. Axial load p versus mid-span deflection curves at different temperature for WTC columns with pinned end conditions and free axial restraint to thermal expansion
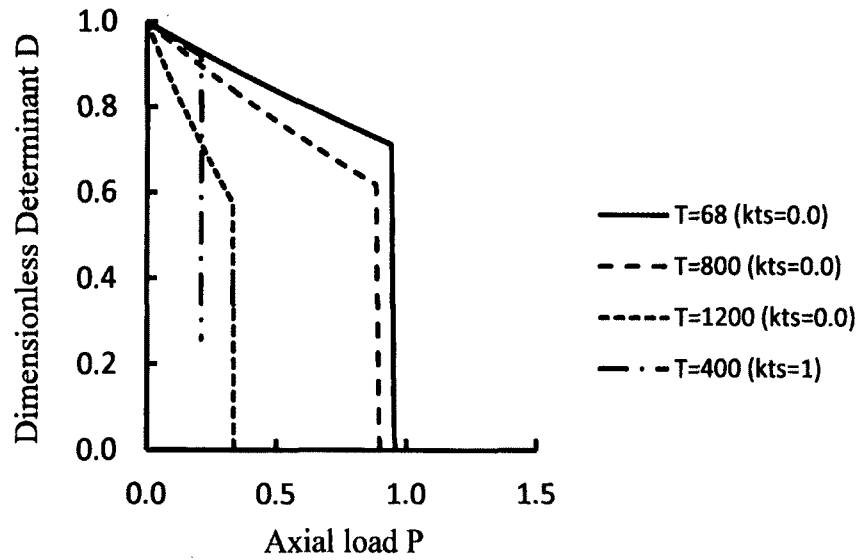
Figure 78. Stiffness degradation curves for WTC columns near the tower top with pinned conditions at different temperatures

Additonal Compressive Force Cuased by Axial Restraint to Thermal Expansion
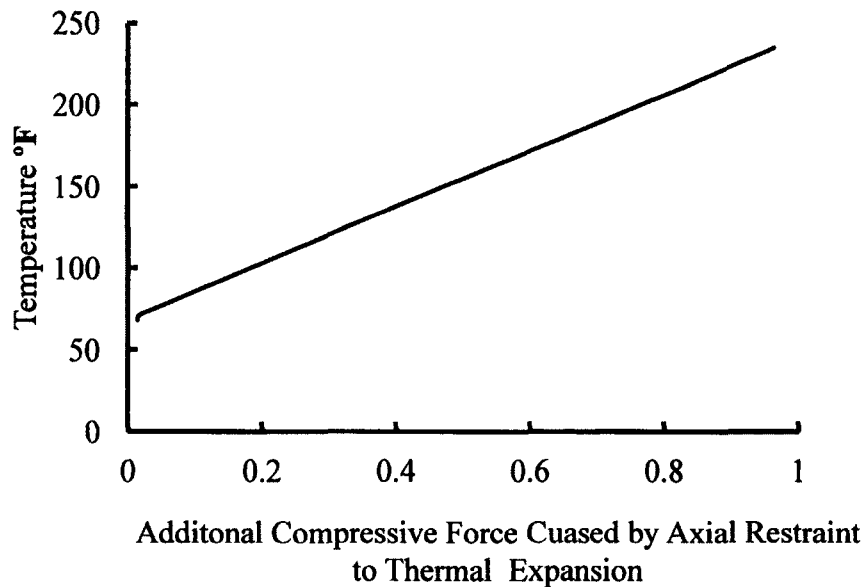
Figure 79. Additional compressive force versus temperature curve for WTC columns near the tower top with rigid axial restraint to thermal expansion
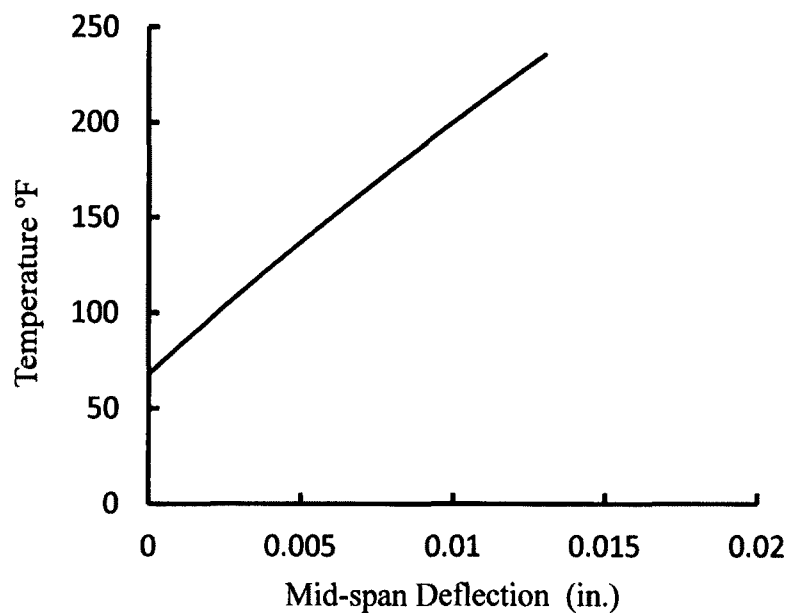
Figure 80. Mid-span deflection versus temperature curve for WTC columns near the tower top with rigid axial restraint to thermal expansion
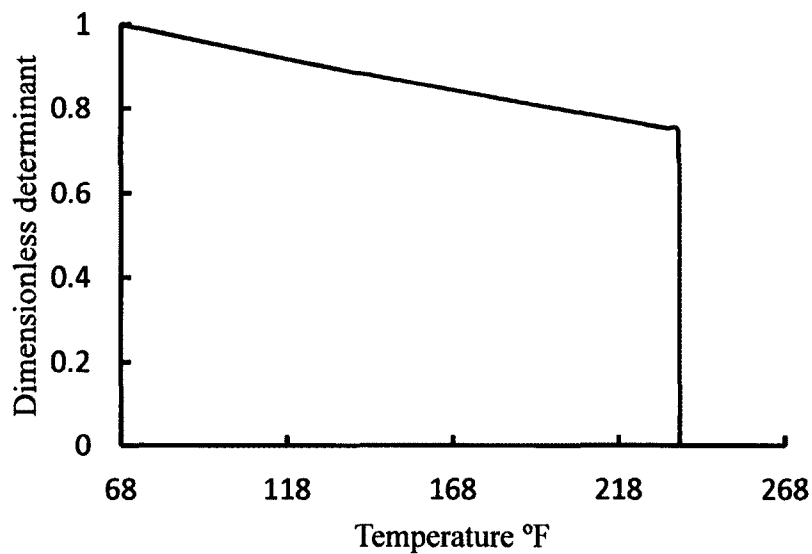
Figure 81. Stiffness degradation curves for WTC columns near the tower top with rigid axial restraint to thermal expansion
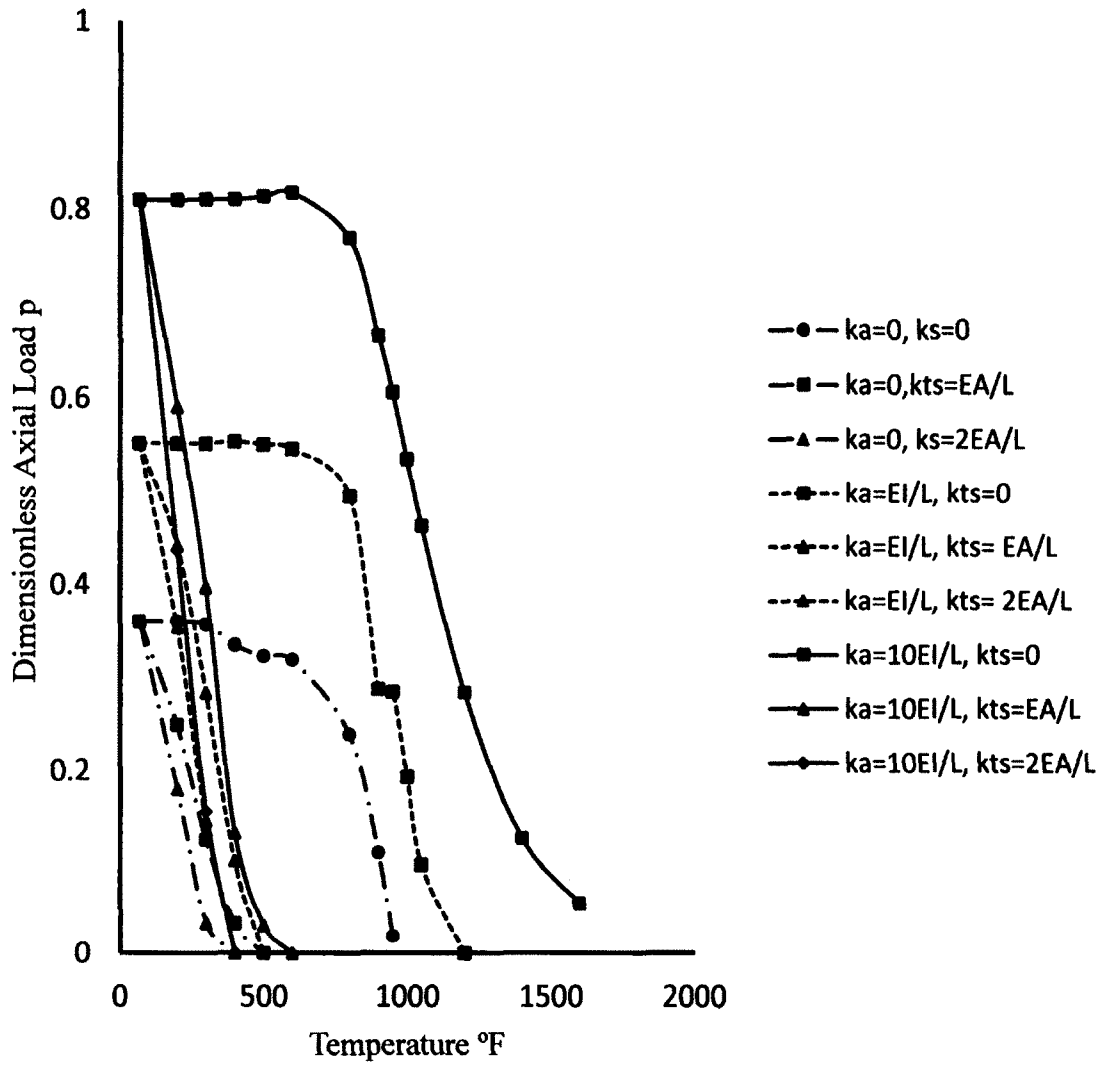
Figure 82. Load versus temperature curves for WTC beam-columns near the tower top under biaxial loading ($m_y/m_x = r_y/r_x$ and $m_x = 0.7$) with different end restraints and axial restraints to thermal expansion
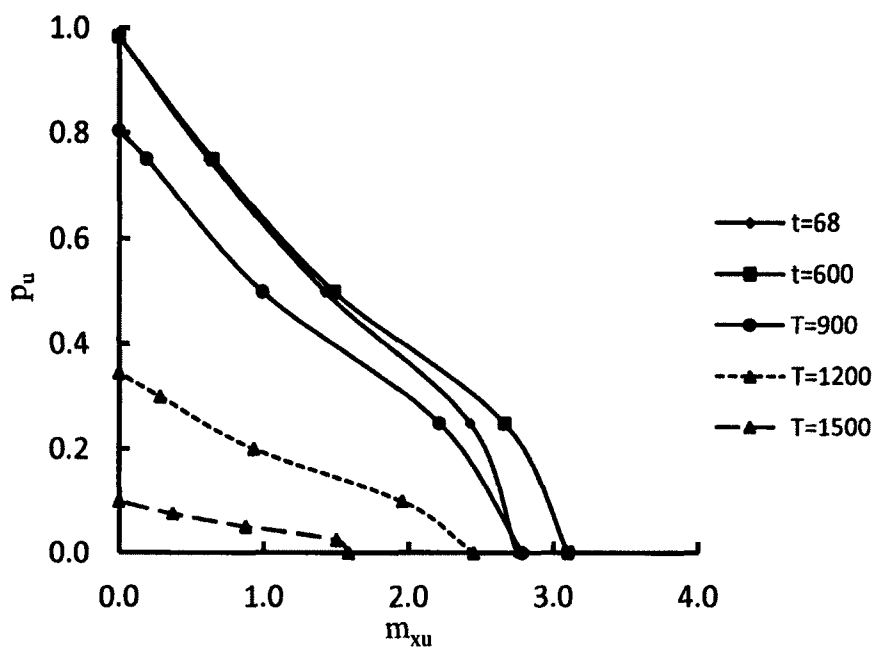
Figure 83. Interaction curves for WTC beam-columns from impacted area under uniaxial
loading (m_x only) with k_{ts}= 0 and partial rotational end restraints
at different temperatures
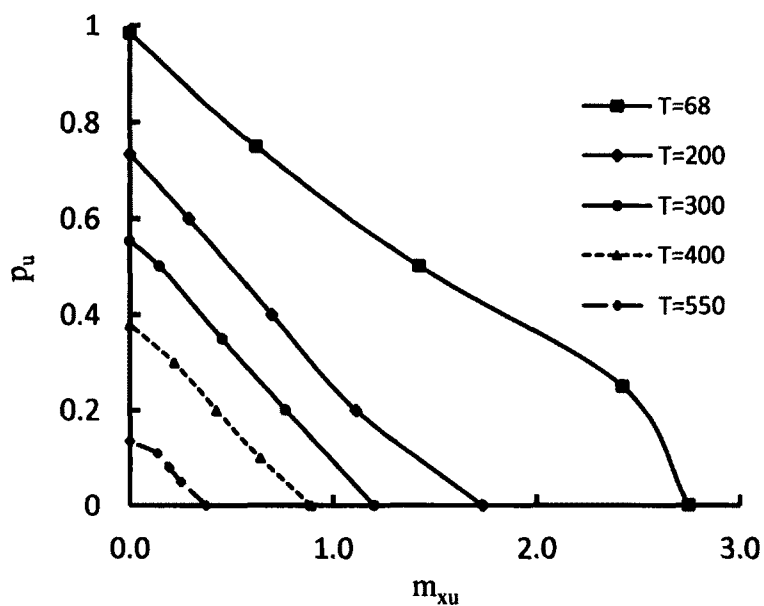
Figure 84. Interaction curves for WTC beam-columns from impacted area under uniaxial
loading (m_x only) with k_{ts}= $\frac{EA}{L}$ and partial rotational end restraints
at different temperatures
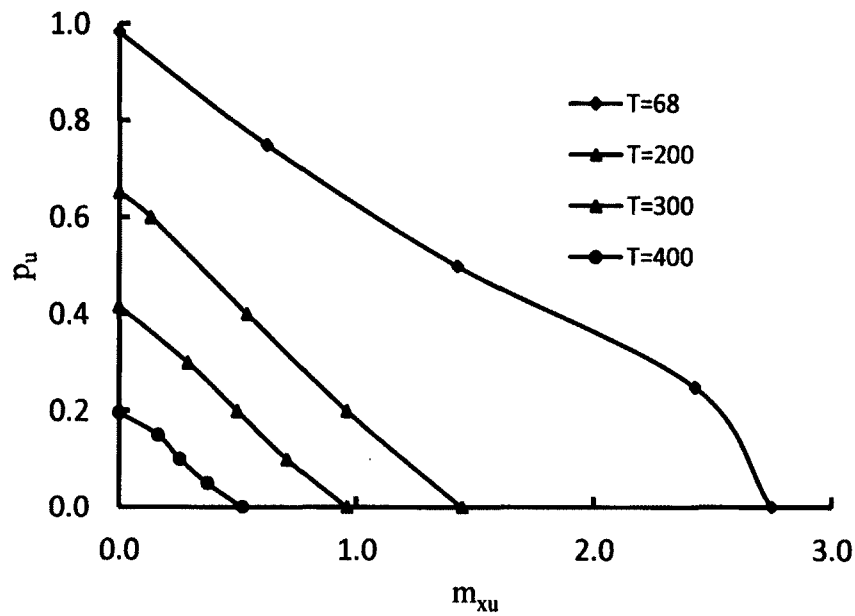
Figure 85. Interaction curves for WTC beam-columns from impacted area under uniaxial loading (m_x only) with $k_{ts} = \frac{EA}{L}$ and partial rotational end restrained at different temperatures
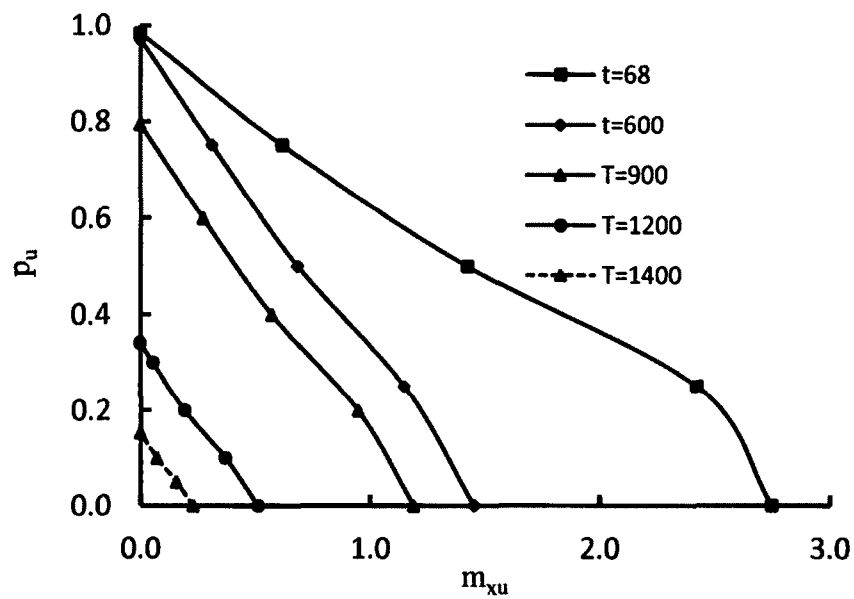
Figure 86. Interaction curves for WTC beam-columns from impacted area under uniaxial loading (m_x only) with $k_{ts} = 0.0$ and pinned boundaries at different temperatures
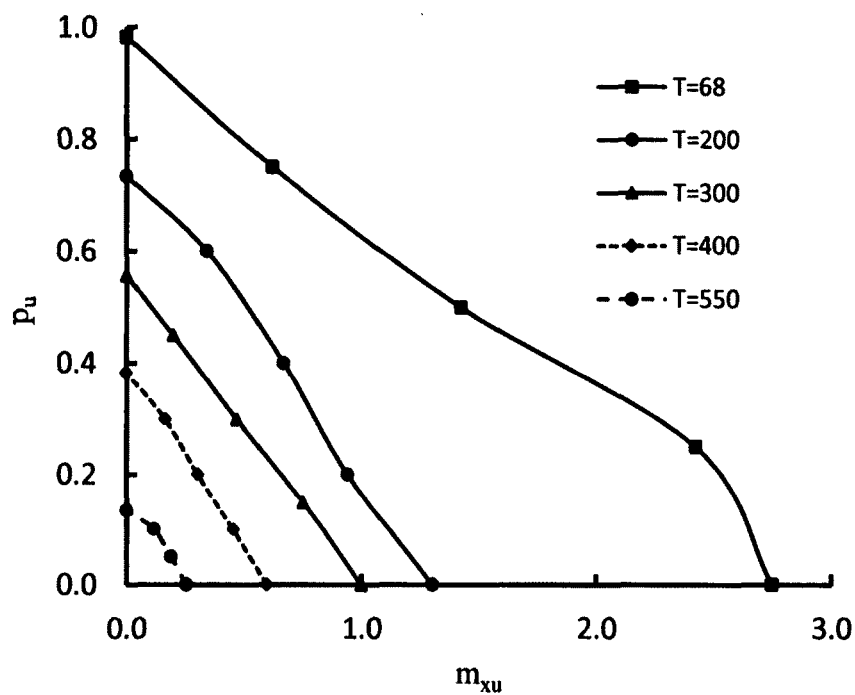
Figure 87. Interaction curves for WTC beam-column from impacted area under uniaxial loading (m_x only) with $k_{ts} = \frac{EA}{L}$ and pinned boundaries at different temperatures
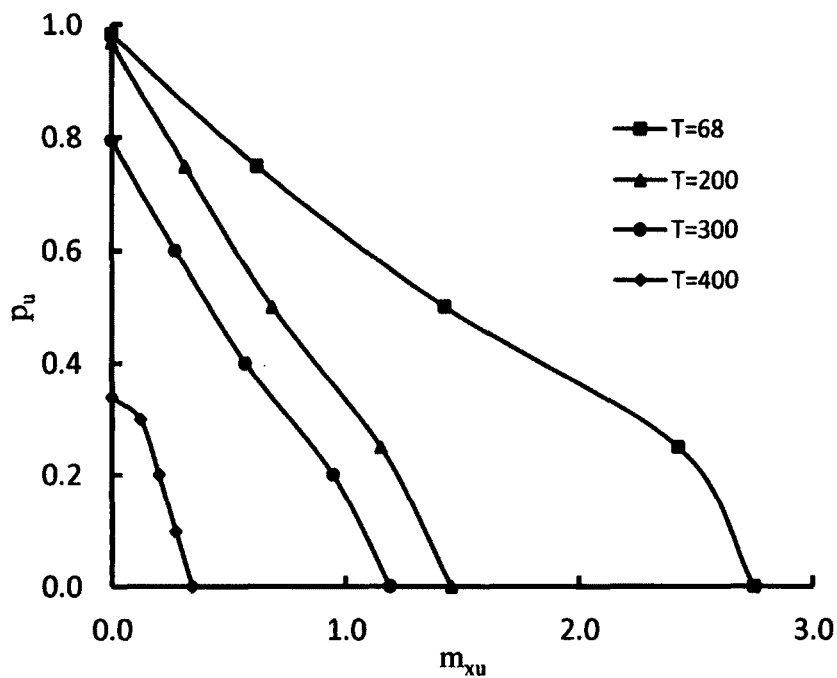
Figure 85. Interaction curves for WTC beam-column from impacted area under uniaxial loading (m_x only) with $k_{ts} = 2\frac{EA}{L}$ and pinned boundaries at different temperatures
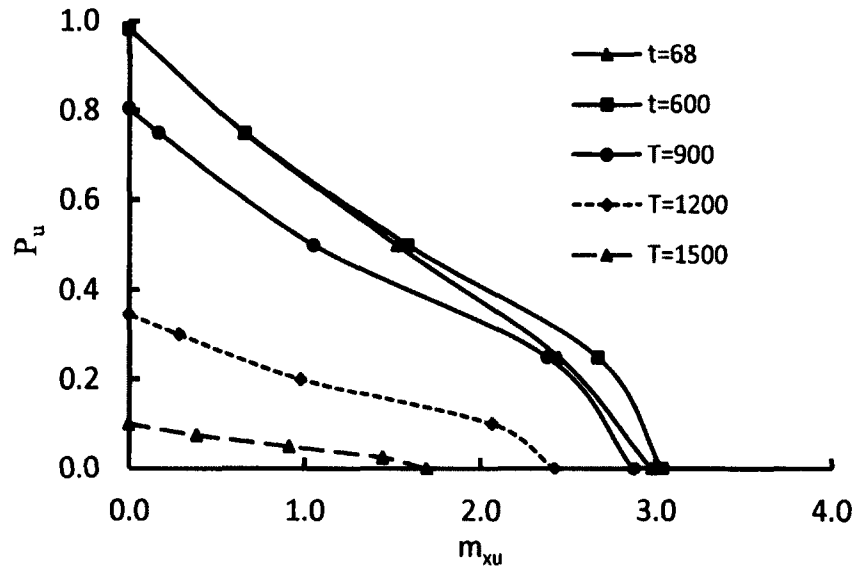
Figure 86. Interaction curves for WTC beam-column from impacted area under uniaxial loading (m_x only) with $k_{ts} = 0$ and fixed boundaries at different temperatures
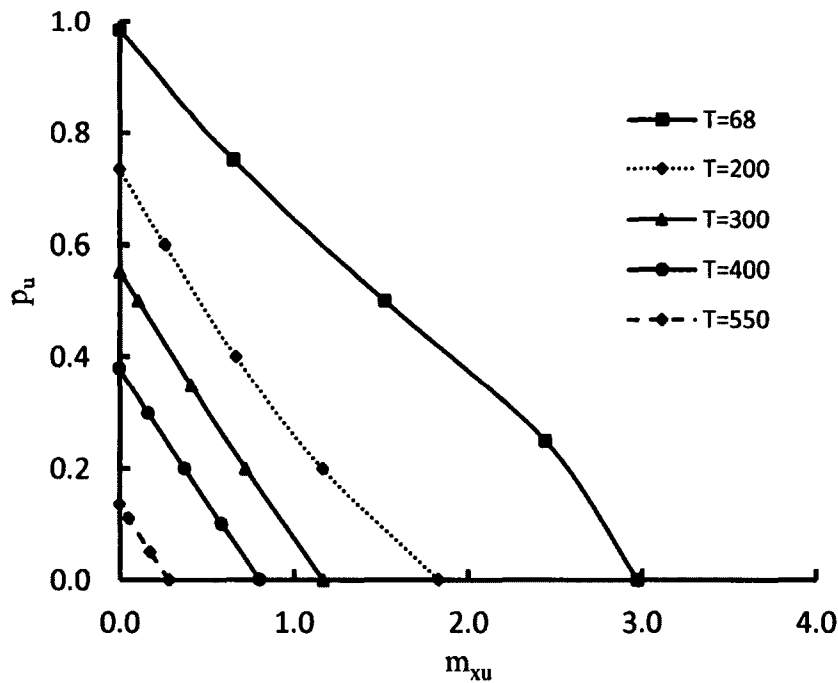
Figure 88. Interaction curves for WTC beam-column from impacted area under uniaxial loading (m_y only) with $k_{ts} = \frac{EA}{L}$ and fixed boundaries at different temperatures
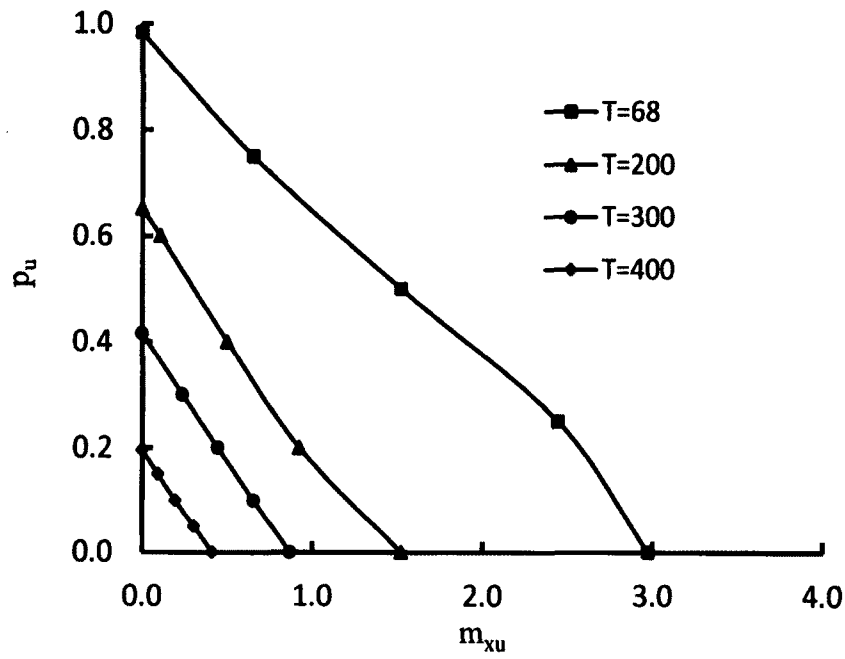
Figure 89. Interaction curves for WTC beam-column from impacted area under uniaxial loading (m_y only) with $k_{ts} = 2\frac{EA}{L}$ and partial rotational end restraints at different temperatures
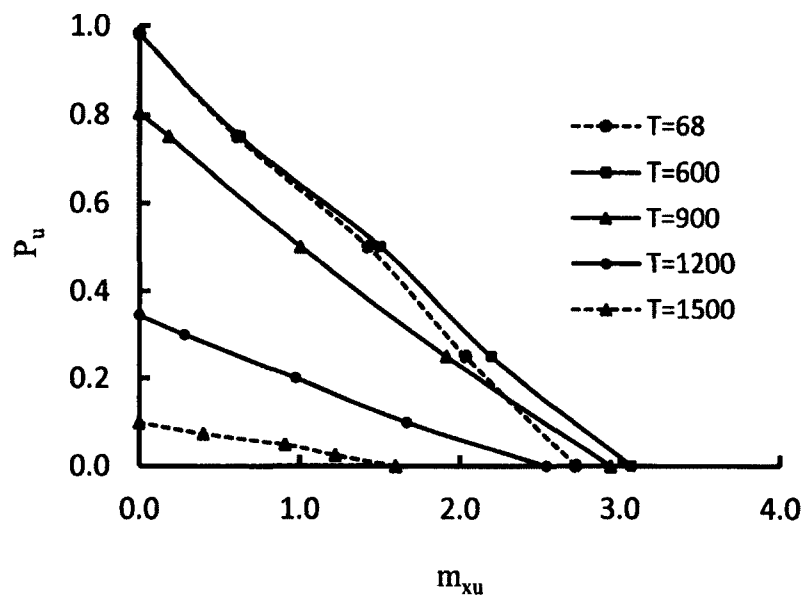
Figure 90. Interaction curves for WTC beam-column from impacted area under biaxial loading (m_y /m_x = 0.5) with $k_{ts} = 0$ and partial rotational end restraints at different temperatures
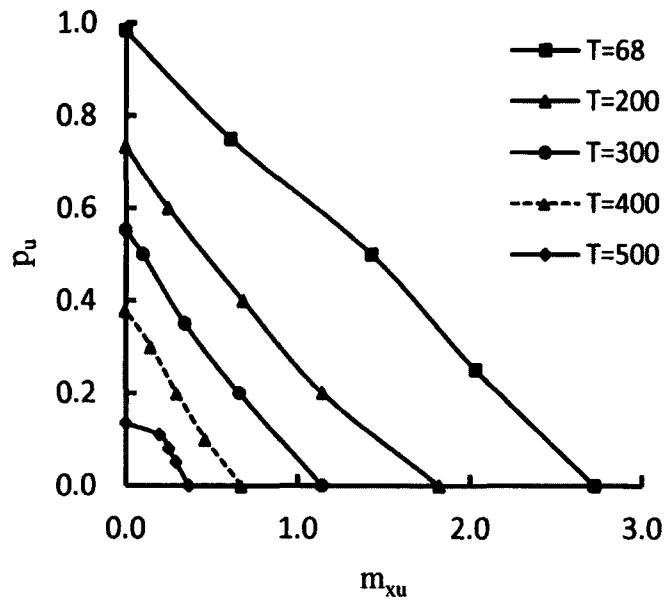
Figure 91. Interaction curves for WTC beam-column from impacted area under biaxial loading (m_y /m_x = 0.5) with k_{ts} = $\frac{EA}{L}$ and partial rotational end restraints at different temperatures
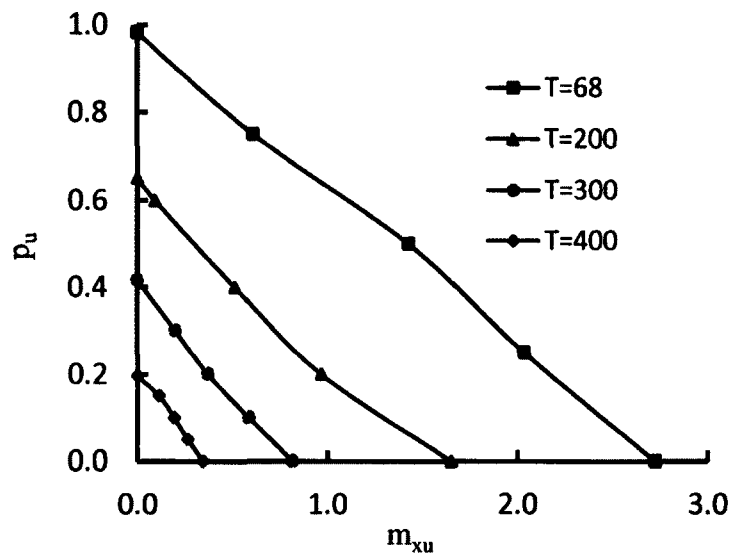
Figure 92. Interaction curves for WTC beam-column from impacted area under biaxial loading (m_y /m_x = 0.5) with k_{ts} = $2\frac{EA}{L}$ and partial rotational end restraints at different temperatures
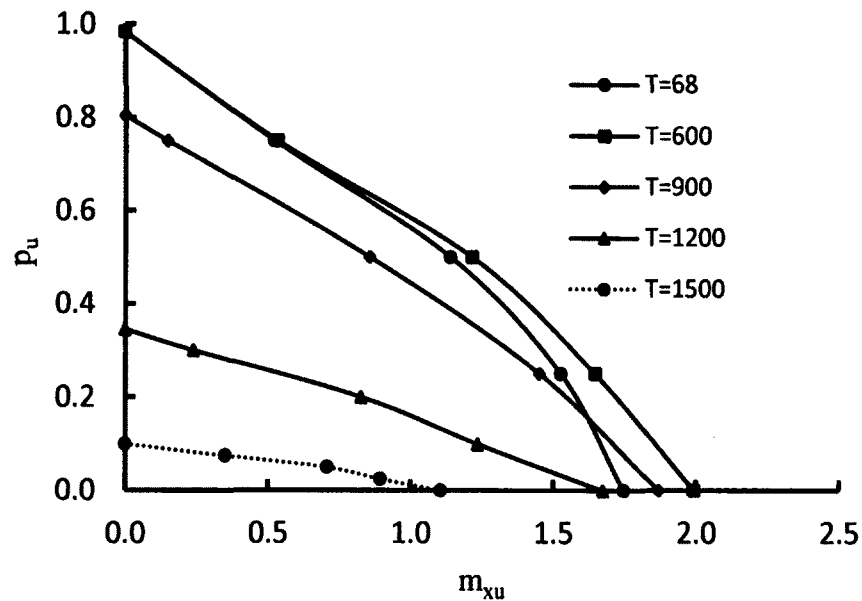
Figure 93. Interaction curves for WTC beam-column from impacted area under biaxial
loading (m_y /m_x = r_y/r_x) with k_{ts} = 0 and partial rotational end restraints
at different temperatures
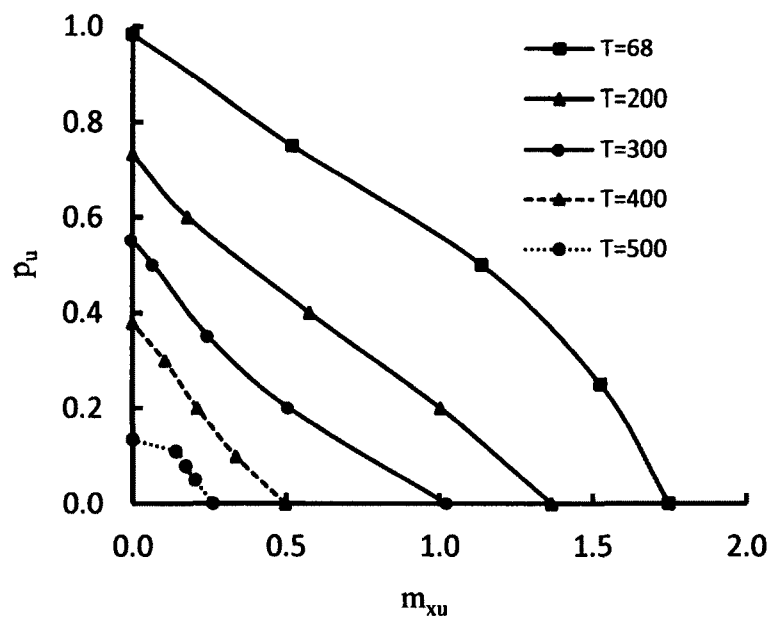
Figure 94. Interaction curves for WTC beam-column from impacted area under biaxial
loading (m_y /m_x = r_y/r_x) with k_{ts} = $\frac{EA}{L}$and partial rotational end restraints
at different temperatures
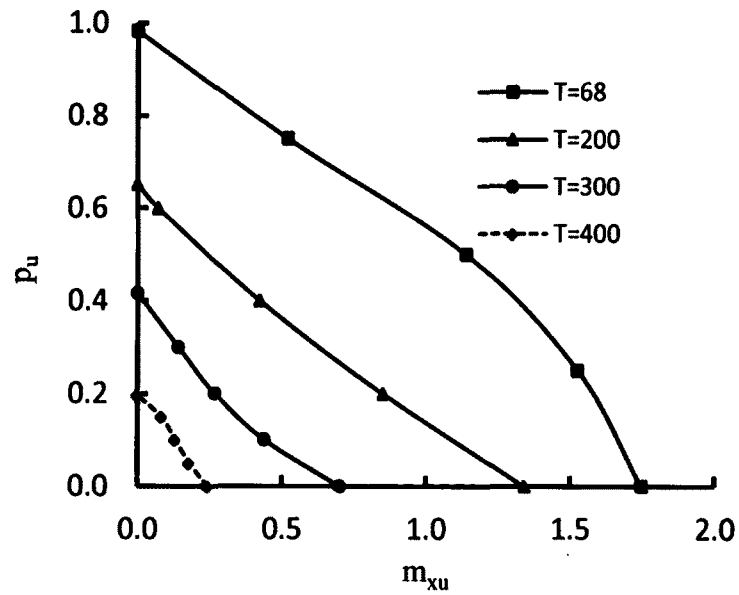
Figure 95. Interaction curves for WTC beam-column from impacted area under biaxial loading ($m_y /m_x = r_y/r_x$) with $k_{ts} = 2\frac{EA}{L}$ and partial rotational end restraints at different temperatures
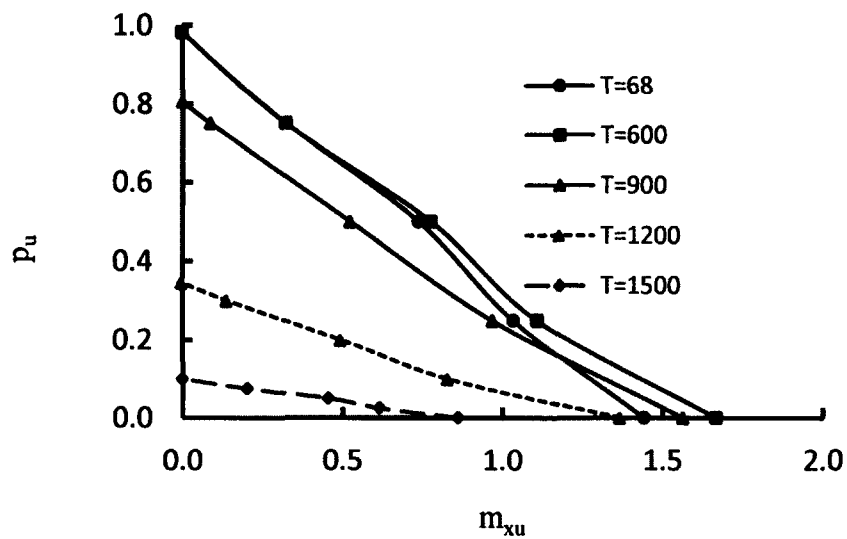
Figure 96. Interaction curves for WTC beam-column from impacted area under biaxial loading ($m_y /m_x = 2$) with $k_{ts} = 0$ and partial rotational end restraints at different temperatures
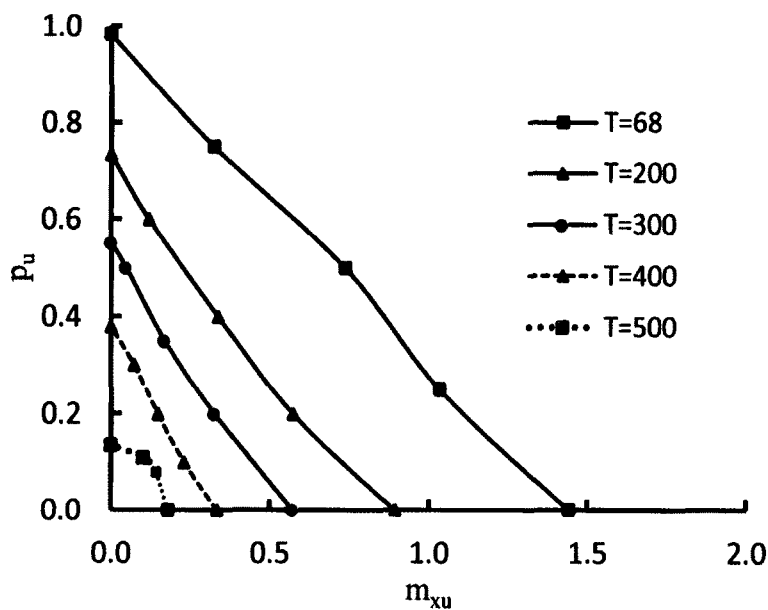
Figure 97. Interaction curves for WTC beam-column from impacted area under biaxial loading (m_y /m_x = 2) with k_{ts} = $\frac{EA}{L}$ and partial rotational end restraints at different temperatures
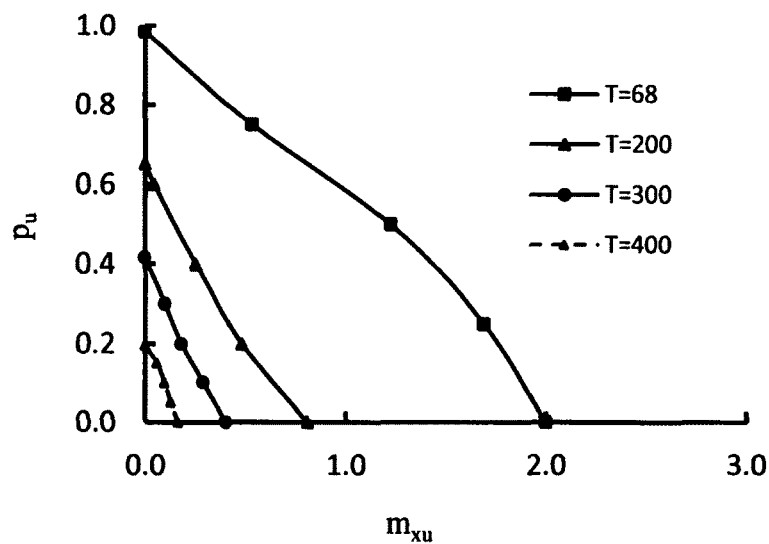
Figure 98. Interaction curves for WTC beam-column from impacted area under biaxial loading (m_y /m_x = 2) with k_{ts} = $2\frac{EA}{L}$ and partial rotational end restraints at different temperatures
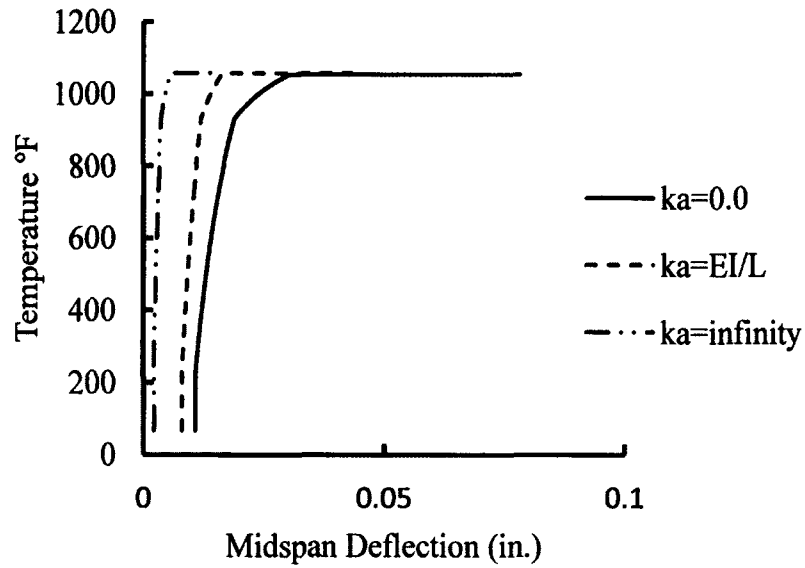
Figure 99. Temperature versus deflection curve for WTC columns from impacted area with service load of p = 0.547 and different boundaries
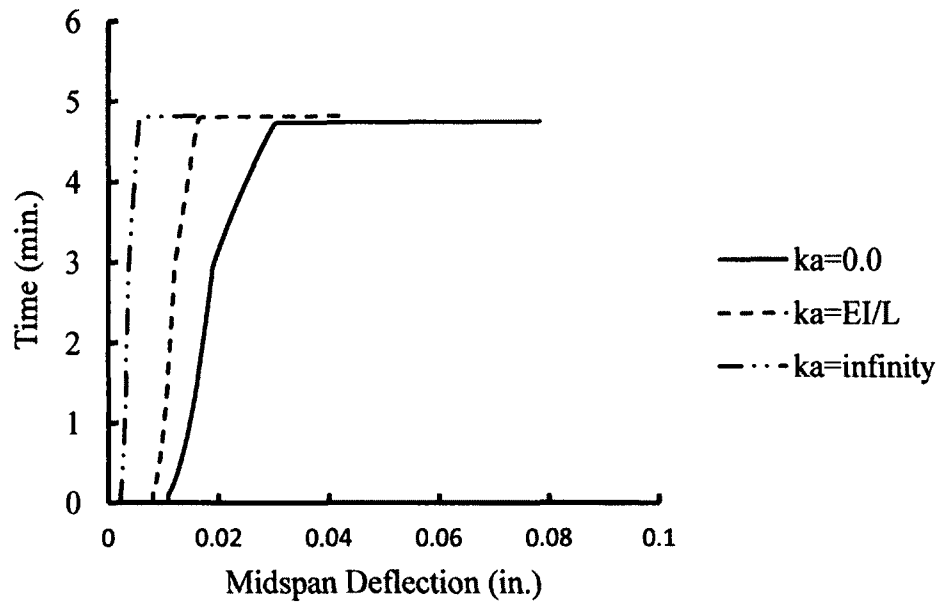
Figure 100. Time versus deflection curve for WTC columns from impacted area with service load of p= 0.547 and different boundaries

APPENDIX C: COMPUTER PROGRAM

This appendix presents the complete computer program based on the theory presented in this dissertation. It consists of one maim program, fourteen subroutine programs and two input date files. The program can be used to analyze the behavior and the strength of beam-columns with partial rotational end restraints and with box section, I-section or hollow rectangular section at ambient and high temperatures. The input parameters for the program are defined below:

W1	Width of top flange of cross section
T1	Thickness of top flange
D2	Depth of web plate
T2	Thickness of web plate
W4	Width of bottom flange of cross section
T4	Thickness of bottom flange
YB	Distance between the top and bottom flange
INPT	Number of nodes along the beam-column length
NH1	Number of layers in the top flange
NV1	Number of elements across the top flange
NH2	Number of elements across the web plate
NV2	Number of layers in the web plate
NH4	Number of layers in the bottom flange
NV4	Number of elements across the bottom flange
RTYE	Young's modulus of the material at ambient temperature
RTSIGMAY	Yield strength of the material at ambient temperature
LP	Load path
NPVALUE	Applied constant axial load
NMXVALUE	Applied constant moment about x axis
NMYVALUE	Applied constant moment about y axis
NTVALUE	Constant temperature
EL	Beam-column length
KBX	Rotational restraint about x axis at end A

KBY   Rotational restraint about y axis at end A

KTX   Rotational restraint about x axis at end B

KTY   Rotational restraint about y axis at end B

DELX   Initial crookedness in the x direction

DELY   Initial crookedness in the y direction

SIGMARC   Residual stress

BCT   BCT=1 that means there is no axial restraint to thermal expansion

                BCT=2 that means there is rigid axial restraint to thermal expansion

                BCT=3 that means there is fine axial restraint to thermal expansion

CS   Stiffness for the axial restraint to thermal expansion

TEMPD1   Temperature

One sample output is presented below, where symbol M_{By} represents the applied moment at end B; symbol U_x represents the midspan deflection in x direction; symbol Y_A represents the rotation about y axis of end A; symbol D represents the dimensionless determinant.

Temp. (°F)	P	M_{BY}	U_x	Y_A	D
800	0.000	0.000	0.000	0.000	1.000
800	0.000	0.000	0.001	0.000	1.000
800	0.000	0.001	0.006	0.000	1.000
800	0.000	0.008	0.011	0.000	1.000
800	0.000	0.015	0.016	0.000	1.000
800	0.000	0.022	0.021	0.001	1.000
800	0.000	0.029	0.026	0.001	1.000
800	0.000	0.036	0.031	0.001	1.000
800	0.000	0.043	0.036	0.001	1.000
800	0.000	0.050	0.041	0.001	1.000
800	0.000	0.057	0.046	0.001	1.000
800	0.000	0.064	0.051	0.001	1.000
800	0.000	0.071	0.056	0.002	1.000
800	0.000	0.078	0.061	0.002	1.000
800	0.000	0.086	0.066	0.002	1.000
800	0.000	0.093	0.071	0.002	1.000
800	0.000	0.100	0.076	0.002	1.000
800	0.003	0.107	0.076	0.002	0.998
800	0.005	0.107	0.077	0.002	0.996
800	0.008	0.107	0.077	0.002	0.995
800	0.010	0.107	0.077	0.002	0.993

The programs are attached below.

```
PROGRAM MAINPROGRAM
IMPLICIT NONE
INTEGER INPT,NH1,NV1,NH2,NV2,NH4,NV4,NE1,NE2,NE4,TOT
REAL*8 YBAR1,YBAR2,YBAR3,IX1,IX23,IX4
INTEGER DD,DK,DE,DG,L,I,J
REAL*8 W1,T1,D2,T2,W4,T4,YB,B1,EL,H,PYE,DELX,DELY,HB
PARAMETER(DD=42,DK=42,DE=1000,DG=100000)
REAL*8 A,IX,IY,IXY,SX,SY,KBX,KBY,KTX,KTY
REAL*8 YE,PY,MXYY,MYYY,SIGMAY,SIGMARC,SIGMART
REAL*8 AE(DD),SXE(DD),SYE(DD),IXE(DD),IYE(DD),IXYE(DD,U0(DD),V0(DD)
REAL*8 X(DE),Y(DE),AD(DE),STR(DE),Z(DD)
REAL*8 N1(DD,DD),N2(DD,DD),N3(DD,DD),N4(DD,DD),N5(DD,DD),N6(DD,DD)
REAL*8 ELD1(6),ELD2(6),FLD1(DD,5),FLD2(DD,5)
REAL*8 U1(DD),V1(DD),U2(DD),V2(DD),U3(DD),V3(DD)
REAL*8 DELTAU1(DD),DELTAV1(DD),DELTAU2(DD), DELTAV2(DD),USLOP(DD),VSLOP(DD)
REAL*8 EXMX1(DD),EXMY1(DD),EXMX2(DD),EXMY2(DD)
INTEGER GLOBLEN, TANGENTN,ICRAMER,JJ
INTEGER   ALPHAP,ALPHAMX,ALPHAMY,LP,COMBP,COMBMX,COMBMY,DPMXY
REAL*8 DP1,DMX1,DMY1,DP2,DMX2,DMY2
REAL*8 MIDU(3),MIDV(3),RATIO1,RATIO2,RATIO
REAL*8 AP(DG),AMBX(DG),AMTX(DG),AMBY(DG),AMTY(DG)
REAL*8 MDFU(DG),MDFV(DG),ITER(DG),ABMAXUSTRN(DG)
REAL*8 THETABX(DG),THETATX(DG),THETABY(DG),THETATY(DG)
REAL*8 PSPECIAL,MXSPECIAL,MYSPECIAL,MPSPECIAL,
REAL*8 NPVALUE,NMXVALUE,NMYVALUE,CONVERGE,BELTA1,BELTA2
REAL*8 PHIXY,PHIYY,PHIXBAR(DD),PHIYBAR(DD)
REAL*8 THETAP,LOADPP,MAXS(DD,2),GLMAXU (DG,DD,2)
 REAL*8 GSN(DD,DE),GSS(DD,DE),GSN1(DD,DE),GSS1(DD,DE),GSN2(DD,DE)
REAL*8 GSS2(DD,DE),GSN3(DD,DE),GSS3(DD,DE))
INTEGER NPE(DD),MAXNP,K,BCT,UPDATEN,ALPHAT, COMBT,DT
REAL*8 RTYE,RTSIGMAY,GR,SR,TVECTOR
REAL*8 SIGMAP,SIGMAU,STRNTH,EPSILONY,PATH(DD),APATH(DG),PTOT(DD)
REAL*8 BUSTRN(DD,DE), BUSJJ(DD),GBUS,UEJJ(DD,4),MDUE(DG,4)
REAL*8 JURN(DD,DE),JSTRESS(DD,DE),DM,WA0(DK,DK)
INTEGER JITE(DD,DE),JITP(DD,DE),JITE2(DD,DE),JITP2(DD,DE),JITE1(DD,DE),JITP1(DD,DE)
REAL*8 DVR1(DD,3),DVR2(DD,3),DVR3(DD,3),DVR(DD,3),CURVATURE(DG)
REAL*8 CV1,CV2,CV3,CV4,CV5,CV6,PEPSILON1,PEPSILON2,MAXLOAD,MPP
REAL *8 DETT1, DETTN, DETERMINANT(DG),DETRATIO(DG)
REAL*8 EXTMX(DG),EXTMY(DG),GDVR1(DG),GDVR2(DG),GDVR3(DG)
REAL*8 TEMPERATURE(DG),TEMPD,TEMPD1,TEMPD2,TEMPD3, SUMRESI
REAL*8 GSTRESS(DG,DE),GSTRAIN(DG,DE),PTMR,DELTAT,EPSILONYO, NTVALUE
REAL*8 AINTERMXO(DG),AINTERMXMID(DG),AINTERMYO(DG),AINTERMYMID(DG),CS
COMMON/M1/ W1,T1,D2,T2,W4,T4,YB,NH1,NV1,NH2,NV2,NH4,NV4
COMMON/M2/ RTYE,SIGMARC,RTSIGMAY
COMMON/M3/ KBX,KBY,KTX,KTY,DELX,DELY
COMMON/M4/ INPT,EL,HB
COMMON/M5/ THETAP
COMMON/M6/ BCT,PTMR, CS
OPEN(1,FILE="WTCSECTION-EC3.DAT")
READ (1,*) W1,T1,D2,T2,W4,T4,YB,INPT,NH1,NV1,NH2,NV2,NH4,NV4,RTYE,RTSIGMAY
CLOSE(1)
OPEN(2,FILE="WTCLOAD-2013.DAT")
READ (2,*) LP,NPVALUE,NMXVALUE,NMYVALUE,NTVALUE,EL,KBX,KTX,KBY,KTY &
   &,DELX,DELY,SIGMARC,THETAP,BCT,CS,PTMR,TEMPD1    CLOSE(2)
CV1=0.001D0
CV3=0.005D0
CV6=0.001D0
CV2=0.5D0
CV4=0.1D0
CV5=0.05D0
PEPSILON1=1.0D0
PEPSILON2=2.0D0
DELTAT=1
NE1=NH1*NV1
NE2=NH2*NV2*2
NE4=NH4*NV4
TOT=NE1+NE2+NE4
YBAR1=(W1*T1*T1/2+D2*T2*(T1+D2/2)*2+W4*T4*(T1+YB+T4/2))/(W1*T1+D2*T2*2+W4*T4)
YBAR2=YB+T1-YBAR1
YBAR3=T1+D2-YBAR1
A=W1*T1+D2*T2*2+W4*T4
IX1=W1*T1**3/12+W1*T1*(YBAR1-T1/2)**2
IX23=(T2*D2**3/12+D2*T2*(D2/2+T1-YBAR1)**2)
IX4=W4*T4**3/12+W4*T4*(YB+T1-YBAR1+T4/2)**2
IX=IX1+2*IX23+IX4
IY=T1*W1**3/12+T4*W4**3/12+(D2*T2**3/12+D2*T2*(W4/2+T2/2)**2)*2
```

```
IXY=SQRT(IX*IY)
TEMPD=68
CALL TEMP(TEMPD,SIGMAY,YE,STRNTH,EPSILONYO)
PY=SIGMAY*A
MXYY=(SIGMAY*IX)/MAX(YBAR1,YBAR3)
MYYY=(2*SIGMAY*IY)/W1
PHIXY=SIGMAY/YE/MAX(YBAR1,YBAR3)
PHIYY=2*SIGMAY/YE/W1
GR=SQRT(IX/A)
SR=EL/GR
H=EL/(INPT-1)
!LP=1,only apply axial load until it fail at temperature TEMPD1.
!LP=2, only apply My until it fail at temperature TEMPD1.
!LP=23, ONLY APPLY Mx UNTILE IT FAILat temperature TEMPD1
!LP=22, apply Mx and My simutaneously until it fail at temperature TEMPD1 .
!LP=3, apply axial load P firsity and then keep it as constant and then apply My until it failat temperature TEMPD1 .
!LP=32, apply axial load P firsity and then keep it as constant and then apply MX until it failat temperature TEMPD1 .
!LP=4, apply My firstly and then keep it as constant and then apply P until it fail at temperature TEMPD1 .
!LP=42,apply MX firstly and then keep it as constant and then apply P until it fail at temperature TEMPD1.
!LP=5, apply axial load P firstly and then keep it constant and then apply Mx and My simutaneously until it failat temperature  TEMPD1 .
!LP=6, apply axial load Mx and My simutaneously firstly and then keep them as constant, and then apply P until it failat temperature  TEMPD1 .
!LP=8, aly P firstly, and then apply Mx, finally ppapply My until it failat temperature TEMPD1 .
!LP=9, apply MY firstly, and then apply Mx, finally apply P until it fail at temperature TEMPD1.
!LP=10, apply Mx firstly and then apply My until it fail at temperature TEMPD1.
!LP=11, apply My firstly and then apply Mx until it failat temperature TEMPD1 .
!LP=12, apply P and My simutaneously until it failat temperature TEMPD1.
!LP=90, only increase the temperature only until it fail with rigid thermal restraint.
!LP=91, apply axial load first and keep it constantly and then increase the temperature untile it fail.
!LP=96, apply  Mx and My simutaneously firstly and thena pply P; keep them as constant and raise the temperture until it fail
!LP=97, apply mx and my firstly, and increase temperature and keep them constantly and apply axial load
!LP=98, apply p and  then apply mx and my firstly; keep them constantly and increase the temperature
!LP=922, apply mx and my firstly at the temperature TEMPD1 and then increase the temperature until it fail
!LP=93, apply mx firstly and then increase the temperature until it fail
        PSPECIAL=NPVALUE*PY
   MXSPECIAL=NMXVALUE*MXYY
   MYSPECIAL=NMYVALUE*MYYY
   ELD1(1)=0.000D0
   ELD1(2)=0.0D0
   ELD1(3)=0.0D0
   ELD1(4)=0.0D0
   ELD1(5)=0.0D0
   ELD1(6)=TEMPD1
   IF (LP.EQ.1.OR.LP.EQ.3) THEN
   ALPHAP=1
   ALPHAMX=0
   ALPHAMY=1
   ALPHAT=0
   ELSE IF(LP.EQ.2.OR.LP.EQ.4) THEN
   ALPHAP=1
   ALPHAMX=0
   ALPHAMY=1
   ALPHAT=0
   ELSE IF(LP.EQ.23) THEN
   ALPHAP=1
   ALPHAMX=1
   ALPHAMY=0
   ALPHAT=0
   ELSE IF(LP.EQ.32) THEN
   ALPHAP=1
   ALPHAMX=1
   ALPHAMY=0
   ALPHAT=0
   ELSE IF(LP.EQ.42) THEN
   ALPHAP=1
   ALPHAMX=1
   ALPHAMY=0
   ALPHAT=0
   ELSE IF(LP.EQ.5) THEN
   ALPHAP=1
   ALPHAMX=1
   ALPHAMY=1
   ALPHAT=0
   ELSE IF(LP.EQ.6) THEN
   ALPHAP=1
   ALPHAMX=1
   ALPHAMY=1
   ALPHAT=0
   ELSEIF (LP.EQ.22) THEN
```

```
        ALPHAP=0
        ALPHAMX=1
        ALPHAMY=1
        ALPHAT=0
        ELSE IF(LP.EQ.7) THEN
         ALPHAP=0
        ALPHAMX=0
        ALPHAMY=1
        ALPHAT=0
        ELSEIF(LP.EQ.8)THEN
         ALPHAP=1
        ALPHAMX=1
        ALPHAMY=1
         ALPHAT=0
        ELSEIF(LP.EQ.9)THEN
         ALPHAP=1
        ALPHAMX=1
        ALPHAMY=1
         ALPHAT=0
        ELSEIF(LP.EQ.10)THEN
         ALPHAP=0
        ALPHAMX=1
        ALPHAMY=1
         ALPHAT=0
  .     ELSEIF(LP.EQ.11)THEN
         ALPHAP=0
        ALPHAMX=1
        ALPHAMY=1
        ALPHAT=0
        ELSEIF(LP.EQ.12)THEN
         ALPHAP=1
        ALPHAMX=0
        ALPHAMY=1
        ALPHAT=0
        ELSE IF(LP.EQ.90) THEN
        ALPHAP=0
        ALPHAMX=0
        ALPHAMY=0
        ALPHAT=1
         ELSEIF (LP.EQ.91)THEN
         ALPHAP=1
         ALPHAMX=0
        ALPHAMY=0
        ALPHAT=1
        ELSEIF (LP.EQ.96.OR. LP.EQ.97.OR. LP.EQ.98.OR.LP.EQ.922.OR.LP.EQ.93)THEN
        ALPHAP=1
        ALPHAMX=1
        ALPHAMY=1
        ALPHAT=1
        ELSEIF (LP.EQ.92)THEN
        ALPHAP=0
        ALPHAMX=0
        ALPHAMY=1
        ALPHAT=1
        ELSE
        ENDIF
        CALL SEC(X,Y,AD)
        CALL RESIDUALSTRESS(STR)
        SUMRESI=0.0
        DO 0421 I=1, TOT
        SUMRESI=SUMRESI+STR(I)*AD(I)
0421  CONTINUE
        GLOBLEN=1
        DO 701 I=1,INPT
         DO 707 J=1,TOT
         GSN(I,J)=STR(J)/SIGMAY
         GSS(I,J)=STR(J)/SIGMAY
         JITE(I,J)=1
         JITP(I,J)=0
707 CONTINUE
        DVR(I,1)=0.0
        DVR(I,2)=0.0
        DVR(I,3)=0.0
701 CONTINUE
        CALL GLOB(ELD1,GSN,GSS,DVR,JITE,JITP,DVR1,EXMX1,EXMY1,MAXS,GSN1,GSS1,JITE1,JITP1,UEJJ,DETT1,WA0)
        CALL TEMP(ELD1(6),SIGMAY,YE,STRNTH,EPSILONY)
        DO 0721 I=1,INPT
        PTOT(I)=0.0
```

```
      DO 0722 J=1,TOT
      PTOT(I)=PTOT(I)+GSS1(I,J)*AD(J)*SIGMAY
0722  CONTINUE
      PATH(I)=PTOT(I)+ELD1(1)
0721  CONTINUE
      DETERMINANT(GLOBLEN)=DETT1
      DETRATIO(GLOBLEN)=DETT1/DETT1
      DO 407 I=1,INPT
      GLMAXU(GLOBLEN,I,1)=MAXS(I,1)
      GLMAXU(GLOBLEN,I,2)=MAXS(I,2)
407   CONTINUE
      GBUS=0.0
      DO 442 I=1,INPT
      BUSJJ(I)=0.0
      DO 443 J=1,TOT
      BUSTRN(I,J)=ABS(JURN(I,J))
      BUSJJ(I)=MAX(BUSJJ(I),BUSTRN(I,J))
443   CONTINUE
      GBUS=MAX(GBUS,BUSJJ(I))
442   CONTINUE
      ABMAXUSTRN(GLOBLEN)=GBUS
      DO 905 I=1,INPT
      FLD1(I,1)=ELD1(1)
      FLD1(I,2)=EXMX1(I)
      FLD1(I,3)=EXMY1(I)
      FLD1(I,4)=-PTOT(I)
      FLD1(I,5)=ELD1(6)
905   CONTINUE
      DO 902 I=1,INPT
      DELTAV1(I)=-DVR1(I,2)
      DELTAU1(I)=DVR1(I,3)
902   CONTINUE
      CALL INTEGRALCOEFFICIENT (N1,N2,N3,N4,N5,N6)
      CALL MULTIPLICATION (N6,DELTAV1,INPT,INPT,1,VSLOP)
      CALL MULTIPLICATION (N6,DELTAU1,INPT,INPT,1,USLOP)
      CALL MULTIPLICATION (N3,DELTAU1,INPT,INPT,1,U1)
      CALL MULTIPLICATION (N3,DELTAV1,INPT,INPT,1,V1)
      MIDU(1)=U1((INPT+1)/2)
      MIDV(1)=V1((INPT+1)/2)
      MAXLOAD=MAX(ABS(ELD1(1)),ABS(ELD1(2)),ABS(ELD1(4)))
      THETABX(GLOBLEN)=VSLOP(1)
      THETATX(GLOBLEN)=VSLOP(INPT)
      THETABY(GLOBLEN)=USLOP(1)
      THETATY(GLOBLEN)=USLOP(INPT)
      DETERMINANT(GLOBLEN)=DETT1
      AP(GLOBLEN)=ELD1(1)/PY
      AMBX(GLOBLEN)=ELD1(2)/MXYY
      AMTX(GLOBLEN)=ELD1(3)/MXYY
      AMBY(GLOBLEN)=ELD1(4)/MYYY
      AMTY(GLOBLEN)=ELD1(5)/MYYY
      APATH(GLOBLEN)=-PATH(5)/PY
      AINTERMXO(GLOBLEN)=EXMX1(1)
      AINTERMXMID(GLOBLEN)=EXMX1(6)
      AINTERMYO(GLOBLEN)=EXMX1(1)
      AINTERMYMID(GLOBLEN)=EXMX1(6)
      GDVR1(GLOBLEN)=DVR1(1,1)
      GDVR2(GLOBLEN)=DVR1(1,2)
      GDVR3(GLOBLEN)=DVR1(1,3)
      MDFU(GLOBLEN)=MIDU(1)
      MDFV(GLOBLEN)=MIDV(1)
      MDUE(GLOBLEN,1)=UEJJ((INPT+1)/2,1)
      MDUE(GLOBLEN,2)=UEJJ((INPT+1)/2,2)
      MDUE(GLOBLEN,3)=UEJJ((INPT+1)/2,3)
      MDUE(GLOBLEN,4)=UEJJ((INPT+1)/2,4)
      CURVATURE(GLOBLEN)=DVR1((INPT+1)/2,3)
      TEMPERATURE(GLOBLEN)=ELD1(6)
      DO 04307 I=1,INPT
      IF(I.EQ.(INPT+1)/2)THEN
      DO 04301 J=1,TOT
      GSTRESS(GLOBLEN,J)=GSS1(I,J)
      GSTRAIN(GLOBLEN,J)=GSN1(I,J)
04301 CONTINUE
      ELSE
      ENDIF
04307 CONTINUE
      GLOBLEN=2
99    IF (ABS(ABMAXUSTRN(GLOBLEN-1)).LT.PEPSILON1)THEN
      BELTA2=CV2
```

```
ELSEIF(ABS(ABMAXUSTRN(GLOBLEN-1)).GE.PEPSILON1.AND.ABS(ABMAXUSTRN(GLOBLEN-1)).LE.PEPSILON2)THEN
BELTA2=CV4
ELSEIF(ABS(ABMAXUSTRN(GLOBLEN-1)).GT.PEPSILON2)THEN
BELTA2=CV5
ELSE
ENDIF
IF(ABS(THETABX(GLOBLEN-1)).GE.0.5.OR.ABS(THETABY(GLOBLEN-1)).GE.5.0) THEN
GOTO 1000
ELSE
ENDIF
IF(LP.EQ.5)THEN
IF(ELD2(1).LT.PSPECIAL)THEN
COMBP=1
COMBMX=0
COMBMY=0
COMBT=0
BELTA1=CV1
ELSE
COMBP=0
COMBMX=1
COMBMY=1
COMBT=0
BELTA1=CV3
ENDIF
ELSEIF(LP.EQ.6)THEN
TEMPD=TEMPD2
IF(ELD2(2).LE.MXSPECIAL)THEN
COMBP=0.0
COMBMX=1
COMBMY=1
COMBT=0
BELTA1=CV1
ELSEIF(ELD2(3).GT.MXSPECIAL)THEN
COMBP=1
COMBMX=0
COMBMY=0
COMBT=0
BELTA1=CV3
ELSE
ENDIF
ELSEIF(LP.EQ.32)THEN
TEMPD=TEMPD2
IF(ELD2(1).LT.PSPECIAL)THEN
COMBP=1
COMBMX=0
COMBMY=0
COMBT=0
BELTA1=CV1
ELSE
COMBP=0
COMBMX=1
COMBMY=0
COMBT=0
BELTA1=CV3
ENDIF
ELSEIF(LP.EQ.42)THEN
TEMPD=TEMPD2
IF(ELD2(3).LT.MXSPECIAL)THEN
COMBP=0
COMBMX=1
COMBMY=0
COMBT=0
BELTA1=CV1
ELSE
COMBP=1
COMBMX=0
COMBMY=0
COMBT=0
BELTA1=CV3
ENDIF
ELSEIF(LP.EQ.22)THEN
COMBP=0
COMBMX=1
COMBMY=1
COMBT=0
BELTA1=CV1
TEMPD=TEMPD2
ELSEIF(LP.EQ.1)THEN
```

```
COMBP=1
COMBMX=0
COMBMY=0
COMBT=0
BELTA1=CV1
BELTA2=CV2
ELSEIF(LP.EQ.91)THEN
IF(ELD2(1).LE.PSPECIAL)THEN
COMBP=1
COMBMX=0
COMBMY=0
COMBT=0
BELTA1=CV1
ELSE
COMBP=0
COMBMX=0
COMBMY=0
COMBT=1
BELTA1=CV1
ENDIF
ELSEIF(LP.EQ.2)THEN
COMBP=0
COMBMX=0
COMBMY=1
COMBT=0
BELTA1=CV1
ELSEIF(LP.EQ.23)THEN
COMBP=0
COMBMX=1
COMBMY=0
COMBT=0
BELTA1=CV1
ELSEIF(LP.EQ.7)THEN
IF(ELD1(4).LT.MPSPECIAL)THEN
PRINT*, 'MPSPECIAL IS NOT REACHED YET AND LOADING NEED CONTINUE'
GOTO 9
ELSE
PRINT*, 'THE SPECIAL MEOMENT IS REACHED AND THEN GO TO UNLOADING PART'
GOTO 9999
ENDIF
ELSEIF(LP.EQ.3)THEN
IF(ELD1(1).LT.PSPECIAL)THEN
COMBP=1
COMBMX=0
COMBMY=0
COMBT=0
BELTA1=CV1
ELSE
COMBP=0
COMBMX=0
COMBMY=1
BELTA1=CV3
ENDIF
ELSEIF(LP.EQ.4)THEN
IF(ELD1(5).LT.MYSPECIAL)THEN
COMBP=0
COMBMX=0
COMBMY=1
COMBT=0
BELTA1=CV1
ELSE
COMBP=1
COMBMX=0
COMBMY=0
COMBT=0
BELTA1=CV3
ENDIF
ELSEIF(LP.EQ.8)THEN
IF(ELD1(1).LT.PSPECIAL)THEN
COMBP=1
COMBMX=0
COMBMY=0
COMBT=0
BELTA1=CV1
ELSE
IF(ELD1(2).LT.MXSPECIAL)THEN
COMBP=0
COMBMX=1
```

```
COMBMY=0
COMBT=0
BELTA1=CV3
ELSE
COMBP=0
COMBMX=0
COMBMY=1.0D0
COMBT=0
BELTA1=CV6
ENDIF
ENDIF
ELSEIF(LP.EQ.9)THEN
IF(ELD1(4).LT.MYSPECIAL)THEN
COMBP=0
COMBMX=0
COMBMY=1.0D0
COMBT=0
BELTA1=CV1
ELSE
IF(ELD1(2).LT.MXSPECIAL)THEN
COMBP=0
COMBMX=11.0D0
COMBMY=0
COMBT=0
BELTA1=CV3
ELSE
COMBP=1.0D0
COMBMX=0
COMBMY=0
COMBT=0
BELTA1=CV6
ENDIF
ENDIF
ELSEIF(LP.EQ.10)THEN
IF(ELD1(2).LT.MXSPECIAL)THEN
COMBP=0
COMBMX=1
COMBMY=0
COMBT=0
BELTA1=CV1
ELSE
COMBP=0
COMBMX=0
COMBMY=1.0D0
COMBT=0
BELTA1=CV3
ENDIF
ELSEIF(LP.EQ.11)THEN
IF(ELD1(4).LT.MYSPECIAL)THEN
COMBP=0
COMBMX=0
COMBMY=1
COMBT=0
BELTA1=CV1
ELSE
COMBP=0
COMBMX=1
COMBMY=0
COMBT=0
BELTA1=CV3
ENDIF
ELSEIF(LP.EQ.12)THEN
COMBP=1
COMBMX=0
COMBMY=1
BELTA1=CV1
COMBT=0
TEMPD=TEMPD2
ELSEIF(LP.EQ.90) THEN
COMBP=0
COMBMX=0
COMBMY=0
COMBT=1
BELTA1=CV1
ELSEIF (LP.EQ.96)THEN
IF(ELD1(5).GE.MYSPECIAL.AND.ELD1(1).GE.PSPECIAL)THEN
COMBP=0
COMBMX=0
```

```
COMBMY=0
COMBT=1
BELTA1=CV1
ELSEIF(ELD1(5).GT.MYSPECIAL.AND.ELD1(1).LT.PSPECIAL)THEN
COMBP=1
COMBMX=0
COMBMY=0
COMBT=0
BELTA1=CV1
ELSEIF(ELD1(5).LE.MYSPECIAL.AND.ELD1(1).LE.PSPECIAL)THEN
COMBP=0
COMBMX=1
COMBMY=1
COMBT=0
BELTA1=CV1
 ELSE
ENDIF
ELSEIF(LP.EQ.97)THEN
IF(ELD1(5).GE.MYSPECIAL.AND.ELD1(6).GE.NTVALUE)THEN
COMBP=1
COMBMX=0
COMBMY=0
COMBT=0
BELTA1=CV1
ELSEIF(ELD1(5).GT.MYSPECIAL.AND.ELD1(6).LT.NTVALUE)THEN
COMBP=0
COMBMX=0
COMBMY=0
COMBT=1
BELTA1=CV1
ELSEIF(ELD1(5).LE.MYSPECIAL.AND.ELD1(6).LE.NTVALUE)THEN
COMBP=0
COMBMX=1
COMBMY=1
COMBT=0
BELTA1=CV1
ELSE
ENDIF
ELSEIF(LP.EQ.98)THEN
IF(ELD1(1).GE.PSPECIAL.AND.ELD1(2).GE.MXSPECIAL)THEN
COMBP=0
COMBMX=0
COMBMY=0
COMBT=1
BELTA1=CV1
ELSEIF(ELD1(1).GT.PSPECIAL.AND.ELD1(2).LT.MXSPECIAL)THEN
COMBP=0
COMBMX=1
COMBMY=1
COMBT=0
BELTA1=CV1
ELSEIF(ELD1(1).LE.PSPECIAL.AND.ELD1(2).LE.MXSPECIAL)THEN
COMBP=1
COMBMX=0
COMBMY=0
COMBT=0
BELTA1=CV1
ELSE
ENDIF
ELSEIF(LP.EQ.922)THEN
IF(ELD1(5).GT.MYSPECIAL)THEN
COMBP=0
COMBMX=0
COMBMY=0
COMBT=1
BELTA1=CV1
ELSEIF(ELD1(5).LE.MYSPECIAL)THEN
COMBP=0
COMBMX=1
COMBMY=1
COMBT=0
BELTA1=CV1
ELSE
ENDIF
ELSEIF(LP.EQ.92)THEN
IF(ELD1(5).GT.MYSPECIAL)THEN
COMBP=0
COMBMX=0
```

```
        COMBMY=0
        COMBT=1
        BELTA1=CV1
        ELSEIF(ELD1(5).LE.MYSPECIAL)THEN
        COMBP=0
        COMBMX=0
        COMBMY=1
        COMBT=0
        BELTA1=CV1
        ELSE
        ENDIF
        ELSEIF(LP.EQ.91)THEN
        IF(ELD1(1).GT.PSPECIAL)THEN
        COMBP=0
        COMBMX=0
        COMBMY=0
        COMBT=1
        BELTA1=CV1
        ELSEIF(ELD1(5).LE.PSPECIAL)THEN
        COMBP=1
        COMBMX=0
        COMBMY=0
        COMBT=0
        BELTA1=CV1
        ELSE
        ENDIF
        ELSEIF(LP.EQ.93)THEN
        IF(ELD1(2).GT.MXSPECIAL)THEN
        COMBP=0
        COMBMX=0
        COMBMY=0
        COMBT=1
        BELTA1=CV1
        ELSEIF(ELD1(2).LE.MXSPECIAL)THEN
        COMBP=0
        COMBMX=1
        COMBMY=0
        COMBT=0
        BELTA1=CV1
        ELSE
        ENDIF
        ELSE
        ENDIF
    9   DP1=BELTA2*BELTA1*PY*ALPHAP*COMBP
        DMX1=BELTA2*BELTA1*MXYY*ALPHAMX*COMBMX
        IF(LP.EQ.22.OR.LP.EQ.5.OR.LP.EQ.6.OR.LP.EQ.97.OR.LP.EQ.98)THEN
        DMY1=DMX1*SQRT(IY/IX)
        ELSE
        DMY1=BELTA2*BELTA1*MYYY*ALPHAMY*COMBMY
        ENDIF
        DT=ALPHAT*COMBT*DELTAT
        ELD2(1)=ELD1(1)+DP1
        ELD2(2)=ELD1(2)+DMX1
        ELD2(3)=ELD1(3)+DMX1
        ELD2(4)=ELD1(4)+DMY1
        ELD2(5)=ELD1(5)+DMY1
        ELD2(6)=ELD1(6)+DT
        CALL BMP(ELD2,GSN1,GSS1,FLD1,DVR1,JITE1,JITP1,DVR2,EXMX2,EXMY2,ICRAMER,NPE,MAXS,GSN2,GSS2,JITE2,JITP2,UEJJ,DETTN,&
            &UPDATEN)
        PRINT*, 'UPDATEN=', UPDATEN
        ITER(GLOBLEN)=UPDATEN
        IF (ICRAMER.EQ.1) THEN
        DETTN=0.0
        GOTO 1000
        ELSE
        ENDIF
        GBUS=0.0
        DO 942 I=1,INPT
        BUSJJ(I)=0.0
        DO 943 J=1,TOT
        BUSTRN(I,J)=ABS(GSN2(I,J))
        BUSJJ(I)=MAX(BUSJJ(I),BUSTRN(I,J))
    943 CONTINUE
        GBUS=MAX(GBUS,BUSJJ(I))
    942 CONTINUE
        CALL TEMP(ELD2(6),SIGMAY,YE,STRNTH,EPSILONY)
        DO 0719 I=1,INPT
        PTOT(I)=0.0
```

```
      DO 0720 J=1,TOT
      PTOT(I)=PTOT(I)+GSS2(I,J)*AD(J)*SIGMAY
0720  CONTINUE
      PATH(I)=PTOT(I)+ELD2(1)
0719  CONTINUE
      MAXNP=NPE(1)
      DO 917 I=1,INPT
      MAXNP=MAX(MAXNP,NPE(I))
917   CONTINUE
      DO 602 I=1,INPT
      DELTAV2(I)=-DVR2(I,2)
      DELTAU2(I)=DVR2(I,3)
602   CONTINUE
      CALL INTEGRALCOEFFICIENT (N1,N2,N3,N4,N5,N6)
      CALL MULTIPLICATION (N6,DELTAV2,INPT,INPT,1,VSLOP)
      CALL MULTIPLICATION (N6,DELTAU2,INPT,INPT,1,USLOP)
      CALL MULTIPLICATION (N3,DELTAU2,INPT,INPT,1,U2)
      CALL MULTIPLICATION (N3,DELTAV2,INPT,INPT,1,V2)
      MIDU(2)=U2((INPT+1)/2)
      MIDV(2)=V2((INPT+1)/2)
      AP(GLOBLEN)=ELD2(1)/PY
      AMBX(GLOBLEN)=ELD2(2)/MXYY
      AMTX(GLOBLEN)=ELD2(3)/MXYY
      APATH(GLOBLEN)=-PATH(5)/PY
      AMBY(GLOBLEN)=ELD1(4)/MXYY
      AMTY(GLOBLEN)=ELD1(5)/MXYY
      EXTMX(GLOBLEN)=EXMX2(1)
      EXTMY(GLOBLEN)=EXMY2(1)
      MDFU(GLOBLEN)=MIDU(2)
      MDFV(GLOBLEN)=MIDV(2)
      DETERMINANT(GLOBLEN)=DETTN
      DETRATIO(GLOBLEN)=DETTN/DETT1
      THETABX(GLOBLEN)=VSLOP(1)
      THETATX(GLOBLEN)=VSLOP(INPT)
      THETABY(GLOBLEN)=USLOP(1)
      THETATY(GLOBLEN)=USLOP(INPT)
      ABMAXUSTRN(GLOBLEN)=GBUS
      MDUE(GLOBLEN,1)=UEJJ((INPT+1)/2,1)
      MDUE(GLOBLEN,2)=UEJJ((INPT+1)/2,2)
      MDUE(GLOBLEN,3)=UEJJ((INPT+1)/2,3)
      MDUE(GLOBLEN,4)=UEJJ((INPT+1)/2,4)
      CURVATURE(GLOBLEN)=DVR2((INPT+1)/2,3)
      AINTERMXO(GLOBLEN)=EXMX2(1)
      AINTERMXMID(GLOBLEN)=EXMX2(6)
      AINTERMYO(GLOBLEN)=EXMY2(1)
      AINTERMYMID(GLOBLEN)=EXMY2(6)
      TEMPERATURE(GLOBLEN)=ELD2(6)
      DO 04308 I=1,INPT
      IF(I.EQ.(INPT+1)/2)THEN
      DO 04302 J=1,TOT
      GSTRESS(GLOBLEN,J)=GSS2(I,J)
      GSTRAIN(GLOBLEN,J)=GSN2(I,J)
04302 CONTINUE
      ELSE
      ENDIF
04308 CONTINUE
      DO 918 I=1,INPT
      GLMAXU(GLOBLEN,I,1)=MAXS(I,1)
      GLMAXU(GLOBLEN,I,2)=MAXS(I,2)
918   CONTINUE
      DPMXY=MAX(DP1,DMX1,DMY1)
      IF(DETRATIO(GLOBLEN).LE.0.0)THEN
      GOTO 1000
      ELSE
      MIDU(1)=MIDU(2)
      ELD1(1)=ELD2(1)
      ELD1(2)=ELD2(2)
      ELD1(3)=ELD2(3)
      ELD1(4)=ELD2(4)
      ELD1(5)=ELD2(5)
      ELD1(6)=ELD2(6)
      DO 703 I=1,INPT
      DVR1(I,1)=DVR2(I,1)
      DVR1(I,2)=DVR2(I,2)
      DVR1(I,3)=DVR2(I,3)
      FLD1(I,1)=ELD2(1)
      FLD1(I,2)=EXMX2(I)
      FLD1(I,3)=EXMY2(I)
```

```
        FLD1(I,4)=-PTOT(I)
        FLD1(I,5)=ELD2(6)
703 CONTINUE
    DO 705 I=1,INPT
    DO 704 J=1,TOT
    GSN1(I,J)=GSN2(I,J)
    GSS1(I,J)=GSS2(I,J)
    JITE1(I,J)=JITE2(I,J)
    JITP1(I,J)=JITP2(I,J)
704 CONTINUE
705 CONTINUE
    GLOBLEN=GLOBLEN+1
    GOTO 99
    ENDIF
1000   PRINT*,'********'
    DO 201 I =1,GLOBLEN
    PRINT*,I,'TF=',TEMPERATURE(I),' P=',AP(I),' MY=',AMBY(I),AMTY(I),' MX=',AMBX(I),AMTX(I),' U=',MDFU(I),' V=',&
        &MDFV(I),' ','BX=',THETABX(I),' ','TX',THETATX(I),'BY=',THETABY(I),' ','TY',THETATY(I)
201 CONTINUE
888   END
!*****************************************
    SUBROUTINE BMP(ELD2,GSN1,GSS1,FLD,DVR1,JITE1,JITP1,DVR2,EXMX2,EXMY2,ICRAMER,NPE,MAXS,GSN2,GSS2,JITE2,JITP2,UEJJ,&
        &DETT,UPDATEN)
! This subrotine program is to solve external moment/stress/strain responding to ELD2.
    IMPLICIT NONE
    INTEGER INPT,NR,TOT,DD,DK,DE
    INTEGER NH1,NV1,NH2,NV2,NH4,NV4,NE1,NE2,NE4
    REAL*8 YBAR1,YBAR2,YBAR3
    INTEGER L,I,J,K
    REAL*8 W1,T1,D2,T2,W4,T4,YB,B1,EL,H,PYE,DELX,DELY,HB
    PARAMETER(DD=42,DK=42,DE=2000)
    REAL*8 A,IX,IY,IXY,SX,SY,IX1,IX23,IX4
    REAL*8 YE,PY,MXYY,MYYY,SIGMAY,SIGMARC,SIGMART
    REAL*8 KBX,KBY,KTX,KTY
    REAL*8 X(DE),Y(DE),AD(DE),Z(DD)
    REAL*8 N1(DD,DD),N2(DD,DD),N3(DD,DD),N4(DD,DD),N5(DD,DD),N6(DD,DD)
    REAL*8 ELD2(6),ELD1(6),FLD(DD,5),TLOADA(3),TLOADB(3),FT(3),UPLOAD(3),FDT(3),PATH1(DD)
    REAL*8 EXMX1(DD),EXMY1(DD),EXMX2(DD),EXMY2(DD),EXMX3(DD),EXMY3(DD),DEXMX(DD),DEXMY(DD)
    REAL*8 MAXEMX,MAXEMY,CONVERP,CONVERMX,CONVERMY
    REAL*8 PHIXY,PHIYY,PHIXBAR(DD),PHIYBAR(DD),MAXS(DD,2)
    REAL*8 GSN0(DD,DE),GSS0(DD,DE),GSN1(DD,DE),GSN2(DD,DE),GSS2(DD,DE),BSTRN(DE),BSTRES(DE)
    REAL*8 GLOBK1(DK,DK),GLOBK2(DK,DK)
    REAL*8 TEMPD,RTYE,RTSIGMAY,PTMR,CS,KS,CSTIFNESS(DD)
    REAL*8 JURN(DD,DE),JSTRESS(DD,DE),BUSTRN(DD,DE),GBUS
    REAL*8 DVR0(DD,3),DVR1(DD,3),DVR2(DD,3),DVR3(DD,3),TDVR(DD,3),BVR1JJ(3),TDVRJJ(3)
    REAL*8 UEJJ(DD,4),FUEJ(DD,4),DETT
    REAL*8 STRESS(DE),USTRN(DE),GSN3(DD,DE),GSS3(DD,DE)
    REAL*8 DELTAP(DD), STRNTH,STRNTHA,STRNTHB,DSTRNTHB,EPSILONY
    INTEGER GLOBLEN,TANGENTN,ICRAMER,JJ,UPDATEN,NPE(DD),BCT,NPE1(DD),NPLASTIC
    INTEGER JITE0(DD,DE),JITP0(DD,DE),JITE1(DD,DE),JITP1(DD,DE),JITE2(DD,DE),JITP2(DD,DE),JITE3(DD,DE),JITP3(DD,DE)
    INTEGER ITE(DE),ITP(DE),BITE(DE),BITP(DE)
    COMMON/M1/ W1,T1,D2,T2,W4,T4,YB,NH1,NV1,NH2,NV2,NH4,NV4
    COMMON/M2/ RTYE,SIGMARC,RTSIGMAY
    COMMON/M3/ KBX,KBY,KTX,KTY,DELX,DELY
    COMMON/M4/ INPT,EL,HB
    COMMON/M6/ BCT,PTMR,CS
    CALL SEC(X,Y,AD)
    NR=2*INPT
    NE1=NH1*NV1
    NE2=NH2*NV2*2
    NE4=NH4*NV4
    TOT=NE1+NE2+NE4
    YBAR1=(W1*T1*T1/2+D2*T2*(T1+D2/2)*2+W4*T4*(T1+YB+T4/2))/(W1*T1+D2*T2*2+W4*T4)
    YBAR2=YB+T1-YBAR1
    YBAR3=T1+D2-YBAR1
    A=W1*T1+D2*T2*2+W4*T4
    IX1=W1*T1**3/12+W1*T1*(YBAR1-T1/2)**2
    IX23=(T2*D2**3/12+D2*T2*(D2/2+T1-YBAR1)**2)
    IX4=W4*T4**3+W4*T4*(YB+T1-YBAR1+T4/2)**2
    IX=IX1+2*IX23+IX4
    IY=T1*W1**3/12+T4*W4**3/12+(D2*T2**3/12+D2*T2*(W4/2+T2/2)**2)*2
    IXY=SQRT(IX*IY)
    TEMPD=68
    CALL TEMP(TEMPD,SIGMAY,YE,STRNTH,EPSILONY)
    KS=CS*A*YE/EL
    CALL TEMP(ELD2(6),SIGMAY,YE,STRNTH,EPSILONY)
    PY=SIGMAY*A
    MXYY=(SIGMAY*IX)/MAX(YBAR1,YBAR3)
```

```
      MYYY=(2*SIGMAY*IY)/W1
      PHIXY=SIGMAY/YE/MAX(YBAR1,YBAR3)
      PHIYY=2*SIGMAY/YE/W1
      CONVERP=0.0001*PY
      CONVERMX=0.0001*MXYY
      CONVERMY=0.0001*MYYY
      CALL GLOB(ELD2,GSN1,GSS1,DVR1,JITE1,JITP1,DVR2,EXMX2,EXMY2,MAXS,GSN0,GSS0,JITE0,JITP0,UEJJ,DETT,GLOBK1)
      DO 904 I=1,INPT
      ELD1(1)=FLD(I,1)
      EXMX1(I)=FLD(I,2)
      EXMY1(I)=FLD(I,3)
904   CONTINUE
      UPDATEN=1
699   PRINT*,'******update the external moments vector=',UPDATEN
      JJ=1
799   TANGENTN=1
      TLOADA(1)=FLD(JJ,4)
      TLOADA(2)=EXMX1(JJ)
      TLOADA(3)=EXMY1(JJ)
      DO 611 I=1,TOT
      BSTRN(I)=GSN1(JJ,I)
      BSTRES(I)=GSS1(JJ,I)
611   CONTINUE
      CALL TEMP(FLD(JJ,5),SIGMAY,YE,STRNTHA,EPSILONY)
      CALL TEMP(ELD2(6),SIGMAY,YE,STRNTHB,EPSILONY)
899   CSTIFNESS(JJ)=0.0
      DO 0724 I=1,TOT
      CSTIFNESS(JJ)=CSTIFNESS(JJ)+AD(I)*YE*JITE1(JJ,I)
0724  CONTINUE
      IF(BCT.EQ.1)THEN
      DELTAP(JJ)=0.0
      ELSEIF(BCT.EQ.2)THEN
      DELTAP(JJ)=STRNTHB*CSTIFNESS(JJ)
      ELSEIF(BCT.EQ.3)THEN
      DELTAP(JJ)=STRNTHB*CSTIFNESS(JJ)*KS*EL/(KS*EL+CSTIFNESS(JJ))
      ELSE
      ENDIF
      TLOADB(1)=ELD2(1)+DELTAP(JJ)
      TLOADB(2)=EXMX2(JJ)
      TLOADB(3)=EXMY2(JJ)
      FT(1)=TLOADB(1)-TLOADA(1)
      FT(2)=TLOADB(2)-TLOADA(2)
      FT(3)=TLOADB(3)-TLOADA(3)
      IF(BCT.EQ.1)THEN
      BVR1JJ(1)=DVR1(JJ,1)
      ELSEIF (BCT.EQ.2)THEN
      BVR1JJ(1)=DVR1(JJ,1)
      ELSE
      BVR1JJ(1)=DVR1(JJ,1)
      ENDIF
      BVR1JJ(2)=DVR1(JJ,2)
      BVR1JJ(3)=DVR1(JJ,3))
      DO 1030 I=1,TOT
      BITE(I)=JITE1(JJ,I)
      BITP(I)=JITP1(JJ,I)
1030  CONTINUE
      CALL TANGENTSIFF(ELD2(6),BVR1JJ,BITE,BITP,FT,TDVRJJ,ICRAMER)
      TDVR(JJ,1)=TDVRJJ(1)
      TDVR(JJ,2)=TDVRJJ(2)
      TDVR(JJ,3)=TDVRJJ(3)
      IF(ICRAMER.EQ.1)THEN
      PRINT*, 'ICRAMER=', ICRAMER
      GOTO 999
      ELSE
      ENDIF
      CALL INTERLOAD(ELD2(6),BSTRN,BSTRES,TDVRJJ,UPLOAD,ITE,ITP,USTRN,STRESS,NPLASTIC)
      FDT(1)=ABS(TLOADB(1)-UPLOAD(1))
      FDT(2)=ABS(TLOADB(2)-UPLOAD(2))
      FDT(3)=ABS(TLOADB(3)-UPLOAD(3))
      IF (FDT(1).LE.CONVERP.AND.FDT(2).LE.CONVERMX.AND.FDT(3).LE.CONVERMY.OR.TANGENTN.GE.30) THEN
      NPE(JJ)=NPLASTIC
      DO 508 I=1,TOT
      GSN2(JJ,I)=USTRN(I)
      GSS2(JJ,I)=STRESS(I)
      JITE2(JJ,I)=ITE(I)
      JITP2(JJ,I)=ITP(I)
508   CONTINUE
      GOTO 99
```

```
         ELSE
         TLOADA(1)=UPLOAD(1)
         TLOADA(2)=UPLOAD(2)
         TLOADA(3)=UPLOAD(3)
         DVR1(JJ,1)=TDVR(JJ,1)
         DVR1(JJ,2)=TDVR(JJ,2)
         DVR1(JJ,3)=TDVR(JJ,3)
         DO 1061 I=1,TOT
         JITE1(JJ,I)=ITE(I)
         JITP1(JJ,I)=ITP(I)
 1061  CONTINUE
         TANGENTN=TANGENTN+1
         GOTO 899
         ENDIF
   99  JJ=JJ+1
         IF(JJ.LE.INPT) GOTO 799
         CALL GLOB(ELD2,GSN2,GSS2,TDVR,JITE2,JITP2,DVR3,EXMX3,EXMY3,MAXS,GSN3,GSS3,JITE3,JITP3,UEJJ,DETT,GLOBK2)
         IF(DETT.LE.0.0)THEN
         GOTO 999
         ELSE
         ENDIF
         DO 504 I=1,INPT
         DEXMX(I)=ABS(EXMX3(I)-EXMX2(I))
         DEXMY(I)=ABS(EXMY3(I)-EXMY2(I))
  504  CONTINUE
         MAXEMX=DEXMX(1)
         MAXEMY=DEXMY(1)
         DO 505 I=1,INPT
         MAXEMX=MAX(MAXEMX,DEXMX(I))
         MAXEMY=MAX(MAXEMY,DEXMY(I))
  505  CONTINUE
         IF(UPDATEN.LE.9)THEN
         IF (MAXEMX.LE.CONVERMX.AND.MAXEMY.LE.CONVERMY) THEN
          PRINT*,' THE CALCULATION CAN MOVE TO THE NEXT LOAD LEVEL'
         DO 515 J=1,INPT
         DVR2(J,1)=TDVR(J,1)
         DVR2(J,2)=TDVR(J,2)
         DVR2(J,3)=TDVR(J,3)
  515  CONTINUE
         GOTO 999
         ELSE
         PRINT*,'OVERALL CONVERGENCE IS NOT SATISFIED YET'
         UPDATEN=UPDATEN+1
         DO 513 I=1,INPT
         ELD1(I)=ELD2(I)
         EXMX1(I)=EXMX2(I)
         EXMY1(I)=EXMY2(I)
         DVR1(I,1)=TDVR(I,1)
         DVR1(I,2)=TDVR(I,2)
         DVR1(I,3)=TDVR(I,3)
         EXMX2(I)=EXMX3(I)
         EXMY2(I)=EXMY3(I)
         DO 514 J=1,TOT
         GSN1(I,J)=GSN3(I,J)
         GSS1(I,J)=GSS3(I,J)
         JITE1(I,J)=JITE2(I,J)
         JITP1(I,J)=JITP2(I,J)
  514  CONTINUE
  513  CONTINUE
         GOTO 699
         ENDIF
         ELSE
         GOTO 999
         ENDIF
  999  END
!***********
         SUBROUTINE INTERLOAD(TEMPD,BSTRN,BSTRES,ST,UPLOAD,ITE,ITP,USTRN,STRESS,NPLASTIC)
         IMPLICIT NONE
         INTEGER DD,DE,DK,TOT,NH1,NV1,NH2,NV2,NH4,NV4,NE1,NE2,NE4,I,BCT
         PARAMETER(DD=42,DK=42,DE=2000)
         REAL*8 W1,T1,D2,T2,W4,T4,YB,B1,ST(3)
         REAL*8 X(DE),Y(DE),AD(DE),BSTRN(DE),BSTRES(DE)
         INTEGER ITE(DE),ITP(DE),NPLASTIC
         REAL*8 UPLOAD(3),STRESS(DE),USTRN(DE),MAXUSTR(2),UE(4)
         REAL*8 TEMPD,RTYE, SIGMARC, RTSIGMAY, SIGMAY, YE,PTMR,STRNTH,EPSILONY,CS,KS
         COMMON/M1/ W1,T1,D2,T2,W4,T4,YB,NH1,NV1,NH2,NV2,NH4,NV4
         COMMON/M2/ RTYE,SIGMARC,RTSIGMAY
         COMMON/M6/ BCT, PTMR,CS
```

```
      NE1=NH1*NV1
      NE2=NH2*NV2*2
      NE4=NH4*NV4
      TOT=NE1+NE2+NE4
      CALL TEMP(TEMPD,SIGMAY,YE,STRNTH,EPSILONY)
      UPLOAD(1)=0.0
      UPLOAD(2)=0.0
      UPLOAD(3)=0.0
      CALL TSTRAIN(TEMPD,BSTRN,BSTRES,ST,ITE,ITP,STRESS,USTRN,NPLASTIC,MAXUSTR,UE)
      CALL SEC(X,Y,AD)
      DO 100 I=1,TOT
      UPLOAD(1)=UPLOAD(1)-STRESS(I)*SIGMAY*AD(I)
      UPLOAD(2)=UPLOAD(2)+STRESS(I)*SIGMAY*Y(I)*AD(I)
      UPLOAD(3)=UPLOAD(3)-STRESS(I)*SIGMAY*X(I)*AD(I)
100   CONTINUE
      END
!***********************************************************************
      SUBROUTINE TANGENTSIFF(TEMPD,ST1,ITE,ITP,FT,ST2,ICRAMER)
!The subroutine is used to calculate the deformation vector by using tangent stiffness method.
      IMPLICIT NONE
      INTEGER INPT,TOT,ICRAMER,DD,DK,DE,I,J
      REAL*8 W1,T1,D2,T2,W4,T4,YB
      INTEGER NH1,NV1,NH2,NV2,NH4,NV4,NE1,NE2,NE4
      PARAMETER(DD=42,DK=42,DE=2000)
      INTEGER ITE(DE),ITP(DE),NPLASTIC,BCT
      REAL*8 ST1(3),STRESS(DE),USTRN(DE),ST2(3)
      REAL*8 X(DE),Y(DE),STR(DE),AD(DE)
      REAL*8 Q1,Q2,Q3,Q4,Q5,Q6,Q7,Q8,Q9,F1,F2,F3,FT(3)
      REAL*8 DX1(3),DETST1,DETST2,DETST3,DETCR
      REAL*8 YE,SIGMARC,SIGMAY,MAXUSTR(2),EPSILONY
      REAL*8 TEMPD,STRNTH,RTYE,RTSIGMAY,UE(4),PTMR,CS,KS
      COMMON/M1/ W1,T1,D2,T2,W4,T4,YB,NH1,NV1,NH2,NV2,NH4,NV4
      COMMON/M2/ RTYE,SIGMARC,RTSIGMAY
      COMMON/M6/ BCT,PTMR,CS
      NE1=NH1*NV1
      NE2=NH2*NV2*2
      NE4=NH4*NV4
      TOT=NE1+NE2+NE4
      ICRAMER=0
      CALL TEMP(TEMPD,SIGMAY,YE,STRNTH,EPSILONY)
      Q1=0.0
      Q2=0.0
      Q3=0.0
      Q4=0.0
      Q5=0.0
      Q6=0.0
      Q7=0.0
      Q8=0.0
      Q9=0.0
      CALL SEC(X,Y,AD)
      DO 103 I=1, TOT
      Q1=Q1-AD(I)*ITE(I)
      Q2=Q2-Y(I)*AD(I)*ITE(I)
      Q3=Q3+X(I)*AD(I)*ITE(I)
      Q4=Q4+Y(I)*AD(I)*ITE(I)
      Q5=Q5+Y(I)**2*AD(I)*ITE(I)
      Q6=Q6-Y(I)*X(I)*AD(I)*ITE(I)
      Q7=Q7-X(I)*AD(I)*ITE(I)
      Q8=Q8-X(I)*Y(I)*AD(I)*ITE(I)
      Q9=Q9+X(I)**2*AD(I)*ITE(I)
103   CONTINUE
      F1=FT(1)/YE
      F2=FT(2)/YE
      F3=FT(3)/YE
      DETCR=Q1*(Q5*Q9-Q6*Q8)-Q2*(Q4*Q9-Q6*Q7)+Q3*(Q4*Q8-Q5*Q7)
      DETST1=F1*(Q5*Q9-Q6*Q8)-Q2*(F2*Q9-Q6*F3)+Q3*(F2*Q8-Q5*F3)
      DETST2=Q1*(F2*Q9-Q6*F3)-F1*(Q4*Q9-Q6*Q7)+Q3*(Q4*F3-F2*Q7)
      DETST3=Q1*(Q5*F3-F2*Q8)-Q2*(Q4*F3-F2*Q7)+F1*(Q4*Q8-Q5*Q7)
      IF (DETCR.EQ.0.0) THEN
      ICRAMER=1
      GOTO 99
      ENDIF
      DX1(1)=DETST1/DETCR
      DX1(2)=DETST2/DETCR
      DX1(3)=DETST3/DETCR
      ST2(1)=ST1(1)+DX1(1)
      ST2(2)=ST1(2)+DX1(2)
      ST2(3)=ST1(3)+DX1(3)
```

```
 99  END
!*******************************************************************
    SUBROUTINE TSTRAIN(TEMPD,BUSTRN,BUSTRES,ST,ITE,ITP,STRESS,USTRN,NPLASTIC,MAXUSTR,UE)
!This subroutine is to calculate the total strain in each element.
    IMPLICIT NONE
    INTEGER I,J,K,JJ,KK, NH1,NV1,NH2,NV2,NH4,NV4,NE1,NE2,NE4
    INTEGER INPT,TOT,DE,DD
    PARAMETER (DD=42,DE=2000)
    REAL *8 W1,T1,D2,T2,W4,T4,YB,HB
    REAL*8 EL,YE,SIGMARC,SIGMAY,EPSILONY
    REAL*8 X(DE),Y(DE),STR(DE),AD(DE),A,IX,IY,IXY,SX,SY
    REAL*8 ST(3),STRN(DE),USTRN(DE),STRESS(DE)
    INTEGER ITE(DE),ITP(DE),NPLASTIC,BCT
    REAL*8 PUSTRN(DE),NUSTRN(DE),BPUSTRN,BNUSTRN,MAXUSTR(2)
    REAL*8 BUSTRN(DE),BUSTRES(DE),UE(4),DL
    REAL*8 TEMPD,STRNTH,SIGMAP,SIGMAU,RTYE,RTSIGMAY,PTMR,CS,KS
    COMMON/M1/ W1,T1,D2,T2,W4,T4,YB,NH1,NV1,NH2,NV2,NH4,NV4
    COMMON /M2/ RTYE,SIGMARC,RTSIGMAY
    COMMON/M4/ INPT,EL,HB
    COMMON/M6/ BCT, PTMR,CS
    NE1=NH1*NV1
    NE2=NH2*NV2*2
    NE4=NH4*NV4
    TOT=NE1+NE2+NE4
    CALL TEMP(TEMPD,SIGMAY,YE,STRNTH,EPSILONY)
    CALL SEC(X,Y,AD)
    CALL RESIDUALSTRESS(STR)
    A=W1*T1+D2*T2*2+W4*T4
    DO 701 I=1, TOT
    STRN(I)=ST(1)+ST(2)*Y(I)-ST(3)*X(I)+STR(I)/YE
    USTRN(I)=STRN(I)/EPSILONY
    IF(ABS(USTRN(I)).GE.ABS(BUSTRN(I)))THEN
    IF(USTRN(I).GE.1.0D0)THEN
    STRESS(I)=1.0
    ITE(I)=0
    ITP(I)=1
    ELSEIF(USTRN(I).LE.-1.0D0)THEN
    STRESS(I)=-1.0
    ITE(I)=0
    ITP(I)=1
    ELSE
    STRESS(I)=USTRN(I)
    ITE(I)=1
    ITP(I)=0
    ENDIF
    ELSEIF(ABS(USTRN(I)).LT.ABS(BUSTRN(I)))THEN
    STRESS(I)=(USTRN(I)-BUSTRN(I)+BUSTRES(I))
    ITE(I)=1
    ITP(I)=0
    ELSE
    ENDIF
701 CONTINUE
    NPLASTIC=0
    DO 702 I=1,TOT
    IF ( ITP(I).EQ.1)THEN
    NPLASTIC=NPLASTIC+1
    ELSE
    ENDIF
702 CONTINUE
    MAXUSTR(1)=USTRN(1)
    MAXUSTR(2)=USTRN(TOT)
    END
!***********************************************************
    SUBROUTINE GLOB(ELD,GSN,GSS,DVR,JITE,JITP,DVR1,EXMX1,EXMY1,MAXS,GSN1,GSS1,JITE1,JITP1,UEJJ,DETT,GLOBK)
!The subroutine program is to solve goverment equations using the former load level stiffness matrix.
    IMPLICIT NONE
    INTEGER INPT,NR,NH1,NV1,NH2,NV2,NH4,NV4,TOT,DD,DK,DE,NE1,NE2,NE4
    INTEGER I,J,JJ,K
    REAL*8 ELD(6),DELAPTH
    REAL*8 P,MBX,MBY,MTX,MTY
    REAL*8 W1,T1,D2,T2,W4,T4,YB,B1,EL,H,PYE,DELX,DELY,HB,YBAR1,YBAR2
    PARAMETER(DD=42,DK=42,DE=2000)
    REAL*8 U0(DD),V0(DD),U(DD), V(DD)
    REAL*8 A,IX,IY,IXY,SX,SY,KBX,KBY,KTX,KTY
    REAL*8 YE,SIGMAY,SIGMARC,SIGMART,PY,MXYY,MYYY
    REAL*8 ALP1(DD),ALP2(DD),ALP3(DD),ALP4(DD),ALP5(DD),ALP6(DD)
    REAL*8 GAM1(DD),GAM2(DD),GAM3(DD),GAM4(DD),GAM5(DD),GAM6(DD)
    REAL*8 AE(DD),SXE(DD),SYE(DD),IXE(DD),IYE(DD),IXYE(DD),IX1,IX23,IX4
```

```
REAL*8 X(DE),Y(DE),AD(DE),Z(DD)
REAL*8 PRE(DD),MXRE(DD),MYRE(DD),PP(DD),MXP(DD),MYP(DD),STR(DE)
REAL*8 N1(DD,DD),N2(DD,DD),N3(DD,DD),N4(DD,DD),N5(DD,DD),N6(DD,DD)
REAL*8 NA6(DD,DD),NG6(DD,DD),FX(DD),FY(DD)
REAL*8 WA(DK,DK),WAV(DK,DK),WF(DK,1),GLOBK(DK,DK)
REAL*8 DELTA(DK,1),DELTAU(DD),DELTAV(DD)
REAL*8 STRESS(DE),USTRN(DE)
REAL*8 DELTAVB(DD),DELTAUB(DD),THETAP,MBXP,MTXP,MBYP,MTYP
REAL*8 VSLOP(DD),USLOP(DD),MAXUSTR(2),MAXS(DD,2)
REAL*8 GSN(DD,DE),GSS(DD,DE),BSTRN(DE),BSTRES(DE),GSN1(DD,DE),GSS1(DD,DE)
REAL*8 JURN(DD,DE),JSTRESS(DD,DE),UE(4),UEJJ(DD,4)
REAL*8 TEMPD,RTYE,RTSIGMAY,PTMR,STRNTH,EPSILONY
REAL*8 PTH(DD),MXTH(DD),MYTH(DD)
REAL*8 DVR1(DD,3),DVR(DD,3),DVRJJ(3),EXMX1(DD),EXMY1(DD),BVRJJ(3),DETT
INTEGER JITE1(DD,DE),JITP1(DD,DE),JITE(DD,DE),JITP(DD,DE),ITE(DE),ITP(DE),NPLASTIC
INTEGER BCT
REAL*8 REMBY, REMTY, REMBX, REMTX, DL
REAL*8 SPRINGSRAIN(DD),PTOT(DD)
REAL*8 MPYT(DD),MPYB(DD),MPY(DD),CS, KS
COMMON/M1/ W1,T1,D2,T2,W4,T4,YB,NH1,NV1,NH2,NV2,NH4,NV4
COMMON/M2/ RTYE,SIGMARC,RTSIGMAY
COMMON/M3/ KBX,KBY,KTX,KTY,DELX,DELY
COMMON/M4/ INPT,EL,HB
COMMON/M5/ THETAP
COMMON/M6/ BCT,PTMR,CS
NE1=NH1*NV1
NE2=NH2*NV2*2
NE4=NH4*NV4
NR=2*INPT
TOT=NE1+NE2+NE4
YBAR1=(W1*T1*T1/2+D2*T2*(T1+D2/2)*2+W4*T4*(T1+YB+T4/2))/(W1*T1+D2*T2*2+W4*T4)
YBAR2=YB+T1-YBAR1
A=W1*T1+D2*T2*2+W4*T4
IX1=W1*T1**3/12+W1*T1*(YBAR1-T1/2)**2
IX23=(T2*D2**3/12+D2*T2*(D2/2+T1-YBAR1)**2)
IX4=W4*T4**3+W4*T4*(YB+T1-YBAR1+T4/2)**2
IX=IX1+2*IX23+IX4
IY=T1*W1**3/12+T4*W4**3/12+(D2*T2**3/12+D2*T2*(W4/2+T2/2)**2)*2
IXY=SQRT(IX*IY)
TEMPD=68
CALL TEMP(TEMPD,SIGMAY,YE,STRNTH,EPSILONY)
KS=CS*A*YE/EL
H=EL/(INPT-1)
P= ELD(1)
MBX=ELD(2)
MTX=ELD(3)
MBY=ELD(4)
MTY=ELD(5)
CALL TEMP(ELD(6),SIGMAY,YE,STRNTH,EPSILONY)
MBXP=KBX*THETAP
MTXP=KTX*THETAP
MBYP=KBY*THETAP
MTYP=KTY*THETAP
H=EL/(INPT-1)
DO 1001 I=1,INPT
Z(I)=(I-1)*H
1001 CONTINUE
PYE=4.0D0*ATAN(1.0D0)
DO 1002 I=1,INPT
U0(I)=DELX*DSIN(Z(I)/EL*PYE)
V0(I)=DELY*DSIN(Z(I)/EL*PYE)
1002 CONTINUE
CALL SEC(X,Y,AD)
CALL RESIDUALSTRESS(STR)
DO 801 I=1,INPT
DELTAVB(I)=-DVR(I,2)
DELTAUB(I)=DVR(I,3)
801 CONTINUE
CALL INTEGRALCOEFFICIENT (N1,N2,N3,N4,N5,N6)
CALL MULTIPLICATION (N6,DELTAVB,INPT,INPT,1,VSLOP)
CALL MULTIPLICATION (N6,DELTAUB,INPT,INPT,1,USLOP)
JJ=1
3333 IXYE(JJ)=0.0
IXE(JJ)=0.0
IYE(JJ)=0.0
SYE(JJ)=0.0
SXE(JJ)=0.0
AE(JJ)=0.0
```

```
        PRE(JJ)=0.0
        MXRE(JJ)=0.0
        MYRE(JJ)=0.0
        PP(JJ)=0.0
        MXP(JJ)=0.0
        MYP(JJ)=0.0
        PTH(JJ)=0.0
        MXTH(JJ)=0.0
        MYTH(JJ)=0.0
        DO 1030 I=1,TOT
        STRESS(I)=GSS(JJ,I)*SIGMAY
        ITE(I)=JITE(JJ,I)
        ITP(I)=JITP(JJ,I)
1030 CONTINUE
        DO 1004 I=1,TOT
        AE(JJ)=AE(JJ)+AD(I)*ITE(I)
        SYE(JJ)=SYE(JJ)+AD(I)*X(I)*ITE(I)
        SXE(JJ)=SXE(JJ)+AD(I)*Y(I)*ITE(I)
        IXYE(JJ)=IXYE(JJ)+AD(I)*X(I)*Y(I)*ITE(I)
        IXE(JJ)=IXE(JJ)+AD(I)*Y(I)**2*ITE(I)
        IYE(JJ)=IYE(JJ)+AD(I)*X(I)**2*ITE(I)
        PRE(JJ)=PRE(JJ)+AD(I)*STR(I)*ITE(I)
        MXRE(JJ)=MXRE(JJ)+AD(I)*STR(I)*Y(I)*ITE(I)
        MYRE(JJ)=MYRE(JJ)+AD(I)*STR(I)*X(I)*ITE(I)
        PP(JJ)=PP(JJ)+AD(I)*STRESS(I)*ITP(I)
        MXP(JJ)=MXP(JJ)+AD(I)*STRESS(I)*Y(I)*ITP(I)
        MYP(JJ)=MYP(JJ)+AD(I)*STRESS(I)*X(I)*ITP(I)
1004 CONTINUE
        IF(BCT.EQ.1)THEN
        PTH(JJ)=0.0
        MXTH(JJ)=0.0
        MYTH(JJ)=0.0
        ELSEIF(BCT.EQ.2)THEN
        PTH(JJ)=YE*STRNTH*AE(JJ)
        MXTH(JJ)=YE*STRNTH*SXE(JJ)
        MYTH(JJ)=YE*STRNTH*SYE(JJ)
        ELSEIF(BCT.EQ.3)THEN
        SPRINGSRAIN(JJ)=STRNTH-KS*EL*STRNTH/(YE*AE(JJ)+KS*EL)
        PTH(JJ)=YE*SPRINGSRAIN(JJ)*AE(JJ)
        MXTH(JJ)=YE*SPRINGSRAIN(JJ)*SXE(JJ)
        MYTH(JJ)=YE*SPRINGSRAIN(JJ)*SYE(JJ)
        ELSE
        ENDIF
        ALP1(JJ)=IXYE(JJ)*AE(JJ)-SXE(JJ)*SYE(JJ)
        ALP2(JJ)=AE(JJ)*IXE(JJ)-SXE(JJ)**2
        GAM1(JJ)=-SYE(JJ)**2+IYE(JJ)*AE(JJ)
        GAM2(JJ)=-SYE(JJ)*SXE(JJ)+IXYE(JJ)*AE(JJ)
        ALP3(JJ)=AE(JJ)*(P+PTH(JJ))/YE
        GAM3(JJ)=AE(JJ)*(P+PTH(JJ))/YE
        ALP4(JJ)=-AE(JJ)*KBX/YE
        ALP5(JJ)=AE(JJ)*KTX/YE
        GAM4(JJ)=-AE(JJ)*KBY/YE
        GAM5(JJ)=AE(JJ)*KTY/YE
        JJ=JJ+1
        IF(JJ.LE.INPT) GOTO 3333
        CALL INTEGRALCOEFFICIENT (N1,N2,N3,N4,N5,N6)
        DO 1005 I=1,INPT
        DO 1005 J=1,INPT
        NA6(I,J)=ALP3(I)*N3(I,J)+ALP4(I)*N4(I,J)+ALP5(I)*N5(I,J)
        ALP6(I)=-AE(I)/YE*((P+PTH(I))*V0(I)-MXRE(I)-MXP(I)+Z(I)/EL*(MTX-MBX)+MBX+MXTH(I))
        NG6(I,J)=GAM3(I)*N3(I,J)+GAM4(I)*N4(I,J)+GAM5(I)*N5(I,J)
        GAM6(I)=AE(I)/YE*(-(P+PTH(I))*U0(I)+MYRE(I)+MYP(I)-MBY-Z(I)/EL*(MTY-MBY)+MYTH(I))
1005 CONTINUE
        DO 1006 I=1,INPT
        FX(I)=-SXE(I)/YE*(PP(I)+PRE(I)+P+PTH(I)-PTH(I))+ALP6(I)
        FY(I)=-SYE(I)/YE*(PP(I)+PRE(I)+P+PTH(I)-PTH(I))+GAM6(I)
1006 CONTINUE
        DO 1007 I=1,NR
        IF(I.LE.INPT) THEN
        WF(I,1)=FX(I)
        ELSE
        WF(I,1)=FY(I-INPT)
        ENDIF
1007 CONTINUE
        DO 1008 I=1,INPT
        DO 1008 J=1,INPT
        IF(I.EQ.J)THEN
        WA(I,J)=ALP2(I)+NA6(I,J)
```

```
      ELSE
      WA(I,J)=NA6(I,J)
      ENDIF
1008  CONTINUE
      DO 1009 I=1, INPT
      DO 1009 J= INPT+1, NR
      IF (I.EQ.(J-INPT)) THEN
      WA(I,J)=ALP1(I)
      ELSE
      WA(I,J)=0.0
      END IF
1009  CONTINUE
      DO 1010 I=INPT+1,NR
      DO 1010 J=1, INPT
      IF ((I-INPT).EQ.J) THEN
      WA(I,J)=GAM2(I-INPT)
      ELSE
      WA(I,J)=0.0
      ENDIF
1010  CONTINUE
      DO 1011 I= INPT+1, NR
      DO 1011 J=INPT+1, NR
      IF (I.EQ.J) THEN
      WA(I,J)=GAM1(I-INPT)+NG6(I-INPT,J-INPT)
      ELSE
      WA(I,J)=NG6(I-INPT, J-INPT)
      ENDIF
1011  CONTINUE
      DO 0402 I= 1,NR
      DO 0402 J=1,NR
      GLOBK(I,J)=WA(I,J)
0402  CONTINUE
      CALL FINDDET(WA,NR,DETT)
      IF(DETT.GT.0.0)THEN
      CALL INVERT(WA,NR,WAV)
      ELSE
      GOTO 66
      ENDIF
      CALL MULTIPLICATION (WAV,WF,NR,NR,1,DELTA)
      DO 1016 I=1,INPT
      DELTAU(I)=DELTA(I+INPT,1)
      DELTAV(I)=DELTA(I,1)
1016  CONTINUE
      CALL MULTIPLICATION (N3,DELTAU,INPT,INPT,1,U)
      CALL MULTIPLICATION (N3,DELTAV,INPT,INPT,1,V)
      CALL MULTIPLICATION (N6,DELTAV,INPT,INPT,1,VSLOP)
      CALL MULTIPLICATION (N6,DELTAU,INPT,INPT,1,USLOP)
      DO 1041 I=1,INPT
      DVR1(I,2)=-DELTAV(I)
      DVR1(I,3)=DELTAU(I)
      DVR1(I,1)=(-P-PTH(I)-PRE(I)-PP(I)+PTH(I)+YE*SXE(I)*DELTAV(I)+YE*SYE(I)*DELTAU(I))/(YE*AE(I))
      EXMX1(I)=YE*(SXE(I)*DVR1(I,1)-IXYE(I)*DELTAU(I)-IXE(I)*DELTAV(I))+MXP(I)+MXRE(I)-MXTH(I)
      EXMY1(I)=YE*(-SYE(I)*DVR1(I,1)+IXYE(I)*DELTAV(I)+IYE(I)*DELTAU(I))-MYP(I)-MYRE(I)+MYTH(I)
1041  CONTINUE
      JJ=1
88    DO 1040 I=1,TOT
      BSTRN(I)=GSN(JJ,I)
      BSTRES(I)=GSS(JJ,I)
1040  CONTINUE
      BVRJJ(1)=DVR1(JJ,1)
      BVRJJ(2)=DVR1(JJ,2)
      BVRJJ(3)=DVR1(JJ,3)
      CALL TSTRAIN(TEMPD,BSTRN,BSTRES,BVRJJ,ITE,ITP,STRESS,USTRN,NPLASTIC,MAXUSTR,UE)
      DO 1042 I=1,TOT
      JITE1(JJ,I)=ITE(I)
      JITP1(JJ,I)=ITP(I)
      GSN1(JJ,I)=USTRN(I)
      GSS1(JJ,I)=STRESS(I)
1042  CONTINUE
      MAXS(JJ,1)=MAXUSTR(1)
      MAXS(JJ,2)=MAXUSTR(2)
      UEJJ(JJ,1)=UE(1)
      UEJJ(JJ,2)=UE(2)
      UEJJ(JJ,3)=UE(3)
      UEJJ(JJ,4)=UE(4)
      JJ=JJ+1
      IF(JJ.LE.INPT) GOTO 88
66    END
```

```fortran
!**********************************************************************
      SUBROUTINE TEMP(TEMPF,SIGMAY,YE,STRNTH,EPSILONY)
      IMPLICIT NONE
      REAL*8  SIGMAY, YE,RTSIGMAY,RTYE,SIGMARC
      REAL*8 TEMPF,TEMPC,STRNTH,EPSILONY
      COMMON/M2/ RTYE,SIGMARC,RTSIGMAY
      TEMPC=(TEMPF-32)*5/9
      IF(TEMPC.LT.750)THEN
      STRNTH=0.000012*TEMPC+0.000000004*TEMPC**2-0.0002416
      ELSEIF(TEMPC.LE.860.AND.TEMPC.GE.750)THEN
      STRNTH=0.011
      ELSEIF(TEMPC.LE.1200.AND.TEMPC.GE.860)THEN
      STRNTH=0.00002*TEMPC-0.0062
      ELSE
      ENDIF
      IF(TEMPC.LT.100)THEN
      YE=RTYE*1.0
      ELSEIF(TEMPC.LT.500.AND.TEMPC.GE.100)THEN
      YE=RTYE*(-0.001*TEMPC+1.1)
      ELSEIF(TEMPC.LT.600.AND.TEMPC.GE.500)THEN
      YE=RTYE*(-0.0029*TEMPC+2.05)
      ELSEIF(TEMPC.LT.700.AND.TEMPC.GE.600)THEN
      YE=RTYE*(-0.0018*TEMPC+1.39)
      ELSEIF(TEMPC.LT.800.AND.TEMPC.GE.700)THEN
      YE=RTYE*(-0.0004*TEMPC+0.41)
      ELSEIF(TEMPC.LT.1200.AND.TEMPC.GE.800)THEN
      YE=RTYE*(-0.000225*TEMPC+0.27)
      ELSEIF(TEMPC.GE.1200)THEN
      YE=RTYE*0.0
      ELSE
      ENDIF
      IF(TEMPC.LT.400)THEN
      SIGMAY=RTSIGMAY*1.0
      ELSEIF(TEMPC.LT.500.AND.TEMPC.GE.400)THEN
      SIGMAY=RTSIGMAY*(-0.0022*TEMPC+1.88)
      ELSEIF(TEMPC.LT.600.AND.TEMPC.GE.500)THEN
      SIGMAY=RTSIGMAY*(-0.0031*TEMPC+2.33)
      ELSEIF(TEMPC.LT.700.AND.TEMPC.GE.600)THEN
      SIGMAY=RTSIGMAY*(-0.0024*TEMPC+1.91)
      ELSEIF(TEMPC.LT.800.AND.TEMPC.GE.700)THEN
      SIGMAY=RTSIGMAY*(-0.0012*TEMPC+1.07)
      ELSEIF(TEMPC.LT.900.AND.TEMPC.GE.800)THEN
      SIGMAY=RTSIGMAY*(-0.0005*TEMPC+0.51)
      ELSEIF(TEMPC.LT.1200.AND.TEMPC.GE.900)THEN
      SIGMAY=RTSIGMAY*(-0.0002*TEMPC+0.24)
      ELSEIF(TEMPC.GE.1200)THEN
      SIGMAY=RTSIGMAY*0.0
      ELSE
      ENDIF
      EPSILONY=SIGMAY/YE
      END
!****************************************************
      SUBROUTINE RESIDUALSTRESS (STR)
! The program is to calculate the residual stress
      IMPLICIT NONE
      INTEGER NH1,NV1,NH2,NV2,NH4,NV4,TOT,I,DE,NE1,NE2,NE4
      PARAMETER (DE=2000)
      REAL*8 STR(DE),C1,C2,SIGMART,SIGMARC,YE,SIGMAY,EPSILONY
      REAL*8 W1,T1,D2,T2,W4,T4,YB,X(DE),Y(DE),AD(DE),YBAR1,YBAR3,W2
      REAL*8 TEMPD,TALPHA,RTYE,RTSIGMAY
      COMMON/M1/ W1,T1,D2,T2,W4,T4,YB,NH1,NV1,NH2,NV2,NH4,NV4
      COMMON /M2/ RTYE,SIGMARC,RTSIGMAY
      CALL SEC(X,Y,AD)
      NE1=NH1*NV1
      NE2=NH2*NV2*2
      NE4=NH4*NV4
      TOT=NE1+NE2+NE4
      W2=W4+2*T2
      YBAR1=(W1*T1*T1/2+D2*T2*(T1+D2/2)*2+W4*T4*(T1+YB+T4/2))/(W1*T1+D2*T2*2+W4*T4)
      YBAR3=D2+T1-YBAR1
      C1=(T1*W1+T4*W4+2*T2*D2)/(T1+T4+2*T2)/(2+SIGMARC/SIGMART+SIGMART/SIGMARC)
      C2=SIGMARC/SIGMART*C1
      SIGMART=SIGMARC*2.5D0
      DO 200 I=1,TOT
      IF(SIGMARC.EQ.0.0)THEN
      STR(I)=0.0
      ELSE
      IF(I.LE.NE1)THEN
```

```fortran
      IF(X(I).LE.(-W1/2+C1+C2).AND.X(I).GT.(-W1/2))THEN
      STR(I)=-(SIGMARC+SIGMART)/(C1+C2)*(X(I)+W1/2)+SIGMART
      ELSEIF(X(I).GT.(-W1/2+C1+C2).AND.X(I).LE.(W1/2-C1-C2))THEN
      STR(I)=-SIGMARC
      ELSEIF(X(I).LE.(W1/2).AND.X(I).GT.(W1/2-C1-C2))THEN
      STR(I)=(SIGMARC+SIGMART)/(C1+C2)*(X(I)-W1/2)+SIGMART
      ELSE
      ENDIF
      ELSEIF(I.GT.NE1.AND.I.LE.(NE1+NE2))THEN
      IF(Y(I).LE.(-YBAR3+C1+C2).AND.Y(I).GT.(-YBAR3))THEN
      STR(I)=-(SIGMARC+SIGMART)/(C1+C2)*(Y(I)+YBAR3)+SIGMART
      ELSEIF(Y(I).LE.(YBAR1-T1-C1-C2).AND.Y(I).GT.(-YBAR3+C1+C2))THEN
      STR(I)=-SIGMARC
      ELSEIF(Y(I).LE.(YBAR1-T1).AND.Y(I).GT.(YBAR1-T1-C1-C2))THEN
      STR(I)=(SIGMARC+SIGMART)/(C1+C2)*(Y(I)-YBAR1+T1)+SIGMART
      ELSE
      ENDIF
      ELSEIF(I.GT.(NE1+NE2))THEN
      IF(X(I).LE.(-W4/2+C1+C2).AND.X(I).GT.(-W4/2))THEN
      STR(I)=-(SIGMARC+SIGMART)/(C1+C2)*(X(I)+W4/2)+SIGMART
      ELSEIF(X(I).LE.(W4/2-C1-C2).AND.X(I).GT.(-W4/2+C1+C2))THEN
      STR(I)=-SIGMARC
      ELSEIF(X(I).LE.W4/2.AND.X(I).GT.(W4/2-C1-C2))THEN
      STR(I)=(SIGMARC+SIGMART)/(C1+C2)*(X(I)-W4/2)+SIGMART
      ELSE
      ENDIF
      ELSE
      ENDIF
      ENDIF
200   CONTINUE
      END
!*****************************
      SUBROUTINE SEC(X,Y,AD)
      IMPLICIT NONE
      INTEGER NH1,NV1,NH2,NV2,NH4,NV4,NE1,NE2,NE4,TOT,I,L,LY,DE
      PARAMETER(DE=2000)
      REAL*8 W1,T1,D2,T2,W4,T4,YB,YBAR1,YBAR2,X(DE),Y(DE),AD(DE),W2
      REAL*8 XXB(DE),YYB(DE),ADB(DE)
      COMMON/M1/ W1,T1,D2,T2,W4,T4,YB,NH1,NV1,NH2,NV2,NH4,NV4
      NE1=NH1*NV1
      NE2=NH2*NV2*2
      NE4=NH4*NV4
      TOT=NE1+NE2+NE4
      W2=W4+2*T2
      YBAR1=(W1*T1*T1/2+D2*T2*(T1+D2/2)*2+W4*T4*(T1+YB+T4/2))/(W1*T1+D2*T2*2+W4*T4)
      YBAR2=YB+T1-YBAR1
      DO 101 I=1,TOT
      IF (I.LE.NE1) THEN
      L=INT((I-1)/NH1)
      X(I)=(-W1/2+(I-L*NH1)*W1/NH1-W1/(2*NH1))
      Y(I)=(YBAR1-L*T1/NV1-T1/2/NV1)
      AD(I)=(W1/NH1)*(T1/NV1)
      ELSE IF((I.GT.NE1).AND.(I.LE.(NE1+NE2))) THEN
      L=INT((I-NE1-1)/NH2)
      LY=INT((I-NE1-1)/(2*NH2))
      IF (MOD(L,2).EQ.0) THEN
      X(I)=(-W2/2+(I-NE1-L*NH2)*T2/NH2-T2/2/NH2)
      Y(I)=(YBAR1-T1-LY*(D2/NV2)-D2/(2*NV2))
      AD(I)=((D2)/NV2)*(T2/NH2)
      ELSE
      X(I)=(W2/2-T2+(I-NE1-L*NH2)*T2/NH2-T2/2/NH2)
      Y(I)=(YBAR1-T1-LY*(D2/NV2)-D2/(2*NV2))
      AD(I)=((D2)/NV2)*(T2/NH2)
      END IF
      ELSEIF (I.GT.(NE1+NE2)) THEN
      L=INT((I-NE1-NE2-1)/NH4)
      X(I)=(-W4/2+(I-NE1-NE2-L*NH4)*W4/NH4-W4/(2*NH4))
      Y(I)=(-YBAR2-T4-L*T4/NV4-T4/(2*NV4))
      AD(I)=(W4/NH4)*(T4/NV4)
      ENDIF
      XXB(I)=X(I)/(W1/2)
      YYB(I)=Y(I)/YBAR1
101   CONTINUE
      END
!*********************************************************
      SUBROUTINE INTEGRALCOEFFICIENT (N1,N2,N3,N4,N5,N6)
      IMPLICIT NONE
      INTEGER INPT,I,J,DD
```

```fortran
      PARAMETER (DD=42)
      REAL*8 N1(DD,DD),DN(DD,DD),N2(DD,DD),N3(DD,DD),N4(DD,DD),N5(DD,DD),N6(DD,DD)
      REAL*8 H, Z(DD),EL,HB
      COMMON/M4/ INPT,EL,HB
      H=EL/(INPT-1)
      DO 313 I=1,INPT
      Z(I)=(I-1)*H
313   CONTINUE
      DO 301 I =1,INPT
      DO 301 J= 1,INPT
      DN(I,J)=0.0
301   CONTINUE
      DO 302 I=4,INPT
      IF (MOD(I,2) .EQ. 0.0) THEN
      DN(I,I-1)=5.0
      DN(I,I)=8.0
      DN(I,I+1)=-1.0
      ELSE
      DN(I,I-2)=-1.0
      DN(I,I-1)=8.0
      DN(I,I)=5.0
      END IF
302   CONTINUE
      DO 303 I =1,INPT
      DO 303 J= 1,INPT
      N1(I,J)=0.0
      N2(I,J)=0.0
      N3(I,J)=0.0
      N4(I,J)=0.0
303   CONTINUE
      N1(2,1)=5.0
      N1(2,2)=8.0
      N1(2,3)=-1.0
      N1(3,1)=4.0
      N1(3,2)=16.0
      N1(3,3)=4.0
      DO 304 I=4,INPT
      DO 304 J=1,INPT
      N1(I,J)=N1(I-1,J)+DN(I,J)
304   CONTINUE
      CALL MULTIPLICATION(N1,N1,INPT,INPT,INPT,N2)
      DO 307 I= 1,INPT
      DO 307 J=1,INPT
      N3(I,J)=(H/12)**2*(N2(I,J)-Z(I)*N2(INPT,J)/EL)
307   CONTINUE
      DO 309 J=1,INPT
      N4(I,J)=(H/EL/12)**2*(Z(I)-EL)*N2(INPT,J)
309   CONTINUE
      DO 311 I=1,INPT
      DO 311 J=1,INPT
      N5(I,J)=Z(I)*(H/12*N1(INPT,J)-(H/12)**2*N2(INPT,J)/EL)/EL
311   CONTINUE
      DO 314 I= 1,INPT
      DO 314 J=1,INPT
      N6(I,J)=H/12*N1(I,J)+(-HB*H/12*N1(INPT,J)-(H/12)**2*N2(INPT,J))/(EL+2*HB)
314   CONTINUE
      END
!**********************************************************
      SUBROUTINE MULTIPLICATION(A,B,M,L,N,C)
      IMPLICIT NONE
      INTEGER M,L,N,I,J,K,DK
      PARAMETER (DK=42)
      REAL*8 A(DK,DK),B(DK,DK),C(DK,DK)
      DO 401 I=1,M
      DO 402 J=1,N
      C(I,J)=0.0
      DO 403 K=1,L
      C(I,J)=C(I,J)+A(I,K)*B(K,J)
403   CONTINUE
402   CONTINUE
401   CONTINUE
      END
!**********************************************************
      SUBROUTINE INVERT(CB,N,C)
      IMPLICIT NONE
      INTEGER J,I,N,K,IJ,JI,JK,JP,JQ,JR,IZ,KI,KJ,IK,KK,NK,KOUNT,DK
      PARAMETER(DK=42)
      REAL*8 C(DK,DK),A(2000),L(2000),M(2000),D,CB(DK,DK)
```

```
      REAL*8 BIGA,HOLD
      DO 300 J=1,N
      DO 300 I=1,N
      C(I,J)=CB(I,J)
300   CONTINUE
      KOUNT=0
      DO 200 J=1,N
      DO 200 I=1,N
      KOUNT=KOUNT+1
      A(KOUNT)=C(I,J)
200   CONTINUE
      D=1.0
      NK=-N
      DO 80 K=1,N
      NK=NK+N
      L(K)=K
      M(K)=K
      KK=NK+K
      BIGA=A(KK)
      DO 20 J=K,N
      IZ=N*(J-1)
      DO 20 I=K,N
      IJ=IZ+I
10    IF(ABS(BIGA)-ABS(A(IJ))) 15,20,20
15    BIGA=A(IJ)
      L(K)=I
      M(K)=J
20    CONTINUE
      J=L(K)
      IF(J-K) 35,35,25
25    KI=K-N
      DO 30 I=1,N
      KI=KI+N
      HOLD=-A(KI)
      JI=KI-K+J
      A(KI)=A(JI)
30    A(JI)=HOLD
35    I=M(K)
      IF(I-K) 45,45,38
38    JP=N*(I-1)
      DO 40 J=1,N
      JK=NK+J
      JI=JP+J
      HOLD=-A(JK)
      A(JK)=A(JI)
40    A(JI)=HOLD
45    IF(BIGA) 48,46,48
46    D=0.0
      RETURN
48    DO 55 I=1,N
      IF(I-K) 50,55,50
50    IK=NK+I
      A(IK)=A(IK)/(-BIGA)
55    CONTINUE
      DO 65 I=1,N
      IK=NK+I
      HOLD=A(IK)
      IJ=I-N
      DO 65 J=1,N
      IJ=IJ+N
      IF(I-K) 60,65,60
60    IF(J-K) 62,65,62
62    KJ=IJ-I+K
      A(IJ)=HOLD*A(KJ)+A(IJ)
65    CONTINUE
      KJ=K-N
      DO 75 J=1,N
      KJ=KJ+N
      IF(J-K) 70,75,70
70    A(KJ)=A(KJ)/BIGA
75    CONTINUE
      D=D*BIGA
      A(KK)=1.0/BIGA
80    CONTINUE
      K=N
100   K=(K-1)
      IF(K) 150,150,105
105   I=L(K)
```

```fortran
      IF(I-K) 120,120,108
108   JQ=N*(K-1)
      JR=N*(I-1)
      DO 110 J=1,N
      JK=JQ+J
      HOLD=A(JK)
      JI=JR+J
      A(JK)=-A(JI)
110   A(JI)=HOLD
120   J=M(K)
      IF(J-K) 100,100,125
125   KI=K-N
      DO 130 I=1,N
      KI=KI+N
      HOLD=A(KI)
      JI=KI-K+J
      A(KI)=-A(JI)
130   A(JI)=HOLD
      GO TO 100
150   KOUNT=0
      DO 205 J=1,N
      DO 205 I=1,N
      KOUNT=KOUNT+1
      C(I,J)=A(KOUNT)
205   CONTINUE
      DO 350 J=1,N
      DO 350 I=1,N
      CB(I,J)=C(I,J)
350   CONTINUE
      RETURN
      END
!****************************************************************
      SUBROUTINE FindDet(WK, N,DETERMINANT)
      IMPLICIT NONE
      INTEGER I, J, K,N, L,DD,DE,DK
      PARAMETER (DD=42,DK=42,DE=2000)
      REAL*8 MATRIX(DK,DK),WK(DK,DK),DETERMINANT
      REAL*8 m, TEMP
      LOGICAL DetExists
1012  CONTINUE
      DO 70 I=1,N
      DO 80 J=1,N
      MATRIX(I,J)=WK(I,J)
80    CONTINUE
70    CONTINUE
      L = 1
      DO 10 K = L, N-1
      IF (MATRIX(K,K) .EQ. 0.0) THEN
      DetExists = .FALSE.
      DO 20 I = K+1, N
      IF (MATRIX(I,K).NE. 0.0) THEN
      DO 30 J = 1, N
      TEMP = matrix(i,j)
      matrix(i,j)= matrix(k,j)
      matrix(k,j) = TEMP
30    CONTINUE
      DetExists = .TRUE.
      I=-I
      EXIT
      ENDIF
20    CONTINUE
      IF (DetExists .EQV. .FALSE.) THEN
      DETERMINANT = 0.0
      RETURN
      END IF
      ENDIF
      DO 40 J = k+1, n
      m = matrix(j,k)/matrix(k,k)
      DO 50 I = k+1, n
      matrix(j,i) = matrix(j,i) - m*matrix(k,i)
50    CONTINUE
40    CONTINUE
10    CONTINUE
      DETERMINANT = I
      DO 60 I = 1, n
      DETERMINANT = DETERMINANT * matrix(i,i)
60    CONTINUE
      END
```

VITA

Name: Yanhong Zhao
Born: April 21, 1978
Place of birth: Jining City, Shandong Province, China
Permanent Address: Xingfuji Village, Yutun Town, Shizhong District, Jining City,
Shandong Province, China 272000

Yanhong Zhao was born to Shuyou Zhao and Jinying Pang and grew up in Jining City, Shandong Province, China. She completed her early education up to the high school in Jining City. In July, 2002, she received B. S. in Civil Engineering from Yantai University, China. Then she worked in the Department of Construction, Shandong Tractor Factory for about two years. Then she went back to school to pursue her master degree in Shandong Jianzhu University in September, 2002. After she received M.S. in Civil Engineering in July, 2005, she joined the Shandong Urban Construction Vocational College with a lecturer position where she worked from August, 2005 to January, 2006. In August, 2007, she joined Old Dominion University to pursue her Ph.D degree in Civil Engineering. The author is a member of Chi Epsilon. She is married to Changlong Zhu and they have two lovely daughters, Lingling and Lily.